NASA TM-86429

NASA Technical Memorandum 86429

NASA R&T FOR AEROSPACE PLANE VEHICLES - PROGRESS AND PLANS

S. C. DIXON

MAY 1985

NASA
National Aeronautics and
Space Administration

Langley Research Center
Hampton, Virginia 23665

SUMMARY

The U.S. had extensive programs in the late 1950's and 1960's aimed at various vehicles/missions requiring flight at hypersonic speeds. Due to accelerating costs and formidable technical challenges most of these programs were terminated, and except for the NASA Space Shuttle Program R&T for aerospace plane-type vehicles has been a low priority effort. In spite of this limited activity, mainly conducted by NASA, at the Langley Research Center, significant progress has been made in key technologies such as materials, structures, aerothermodynamics, hypersonic aerodynamics, and hypersonic airbreathing propulsion. In addition, advances have been made in more generic, but essential, areas such as active controls, flight computer hardware and software, and interdisciplinary analytical design methodology. These technology advancements coupled with the development of and experiences with the Space Shuttle now make feasible aerospace plane-type vehicles that meet the more demanding requirements of various DOD missions and/or an all-weather Shuttle II with reduced launch costs.

This paper reviews studies of technology needs and high payoff technologies, and the technology advancements in control-configured-vehicles, aerothermodynamics, aerothermal loads, and materials and structures. The emphasis will be placed on the highest payoff technologies of materials and structures including thermal-structural analysis and high temperature test techniques. Plans, in the sense of what remains to be done rather than firm program commitments, are also briefly discussed.

Page Missing in Original Document

INTRODUCTION

The National Aeronautics and Space Administration (NASA), and its predecessor agency the National Advisory Committee for Aeronautics (NACA), has worked the problems of high speed flight since the late 1940's. The U.S. had extensive programs in the 1950's and 1960's aimed at various vehicles and missions requiring flight at hypersonic speeds. Although most of these missions were of a military nature, civil programs such as supersonic and hypersonic transports were also studied. Early work by NACA in the structures area is summarized in Reference 1. Work on hypersonic transports during the 1950's and early 1960's is summarized in Reference 2. Due to accelerating costs and formidable technical challenges most programs were terminated, and except for the NASA Space Shuttle Program R&T, for aerospace plane type vehicles has been a low priority effort. In spite of this limited activity, mainly conducted by NASA at the Langley Research Center, significant progress has been made in key technologies such as materials, structures, aerothermodynamics, propulsion, structural heat transfer and hypersonic airbreathing propulsion (Refs. 3-10).

In addition, advances have been made in more generic, but essential, areas such as active controls (Ref. 11), flight computer hardware and software, and interdisciplinary analytical design methodology (Ref. 12). These technology advancements coupled with the development of and experiences with the Space Shuttle (Refs. 13 and 14) now make feasible aerospace plane type vehicles that meet the demanding requirements of various potential DOD missions and/or an all-weather Shuttle II with reduced launch costs.

The purpose of this paper is to review current technology needs and high payoff technologies, and to summarize technology advancements in aerothermodynamics, control-configured vehicles, aerothermal loads, and materials and structures. The emphasis will be placed on the highest payoff technologies of materials and structures including thermal-structural analysis and high temperature test techniques. Plans, in the sense of what remains to be done rather than firm program commitments, are also briefly discussed.

MISSION DRIVERS FOR AEROSPACE PLANE VEHICLES

The mission drivers for both orbit-on-demand and/or priority and rescue vehicles and advanced space transportation systems are shown. They share in common the need of low cost per launch, and quick turn around time. Significant drivers for the orbit-on-demand vehicle are time to launch and launch and landing site requirements. For advanced STS large payloads may be a requirement and thus cost per pound to LEO is a significant driver for this class of vehicle. More details for mission requirements may be found in Reference 15 for advanced STS and Reference 16 for orbit-on-demand vehicles.

MISSION DRIVERS FOR AEROSPACE PLANE VEHICLES

ORBIT-ON-DEMAND/PRIORITY & RESCUE

- TIME TO LAUNCH
- COST PER LAUNCH
- TURN AROUND TIME
- LAUNCH/LANDING SITE REQUIREMENTS

ADVANCED SPACE TRANSPORTATION SYSTEMS

- COST PER LAUNCH
- COST PER POUND PAYLOAD TO LEO
- TURN AROUND TIME

Figure 1

PRIMARY TECHNOLOGY DRIVERS FOR AEROSPACE PLANE VEHICLES

A number of studies, both in-house and contractual, have been sponsored by NASA over the years to assess technology requirements for advanced space transportation systems. Although mission requirements have changed somewhat over the years the key technologies have not (Refs. 17, 18, for example) as shown on Figure 2. Propulsion and materials and structures are always the highest two priority items for advanced technology work. Other areas needing work are aerothermodynamics, guidance and control, and automation.

Propulsion work tends to focus on developing a SSME - derivative advanced LOX/H2 engine, a reusable, high performance LOX/HC engine, and, more recently, air breathing hypersonic propulsion systems.

Materials and structures has a large agenda of work areas including lightweight structural design concepts, durable reusable TPS, cryo tank and cryo insulation materials for reuse, thermal management systems, for local high heating areas such as leading edges, nose caps, and regeneratively cooled propulsion structure. One of the difficulties in this area is the nebulous criteria for "durability" or a firm definition of "all weather" in defining reusability.

PRIMARY TECHNOLOGY DRIVERS FOR AEROSPACE PLANE VEHICLES

PROPULSION

- HIGH PRIORITY: AFTERNOON SESSION TO COVER
- ADVANCED LOX/H_2 ETO MAIN ENGINE (SSME) DERIVATIVE
- REUSABLE, HIGH PERFORMANCE LOX/HC ETO ENGINE
- HYPERSONIC AIRBREATHING PROPULSION ASSESSMENT

MATERIALS AND STRUCTURES

- HIGH PRIORITY: MAJOR PART OF THIS PRESENTATION
- LIGHTWEIGHT THERMOSTRUCTURAL DESIGN CONCEPTS
- ADVANCED COMPOSITE MATERIALS
- DURABLE REUSABLE TPS
- CRYO TANKAGE DESIGN

AEROTHERMODYNAMICS

- NONEQUILBRIUM CONVECTIVE HEATING WITH WALL CATALYSIS
- REAL-GAS AERO CHARACTERISTICS
- BOUNDARY-LAYER TRANSITION

GUIDANCE AND CONTROL

- ADAPTIVE G&C SYSTEMS DESIGN
- STABILITY AUGMENTATION, CONTROL CONFIGURATION DESIGN

AUTOMATION

- AUTOMATED CHECKOUT & COUNT DOWN
- STATUS MONITORING
- ON-ORBIT OPERATIONS

Figure 2

WINGED SSTO SUBSYSTEM/CENTER-OF-GRAVITY STUDIES

Figure 3 shows the application of the CCV design to a single-stage-to-orbit launch vehicle system. One problem of SSTO systems that has been identified is their very far aft center of gravities. These vehicles are essentially empty fuel tanks with a large mass of engines stuck on the rear. Flying these vehicles on entry generally requires tolerating a c.g. as far aft as 75% body length, or more. The little graph on the figure points this out and also shows that as the vehicle size is increased the aft c.g. problem gets worse. The figure shows single stage vehicles of about the Shuttle size have c.g.'s at about 72% while so-called heavy lift systems have c.g.'s as far aft as 76 to 78% body length. These c.g. locations will cause the vehicle to be unstable or control configured. The CCV photograph shows the technology advances that are required to fly the far aft c.g. vehicles as CCV designs. These include lighter thrust to weight ratio engines, high rate control vehicles to fly unstable, etc. More details are given in Reference 19.

WINGED SSTO SUBSYSTEM/CENTER—OF—GRAVITY STUDIES

C.G. CHARACTERISTICS

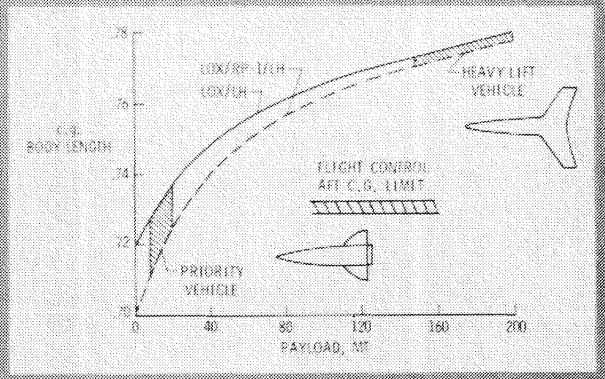

TECHNOLOGY AREAS STUDIED

- ADVANCED PROPULSION SYSTEMS
- CONTROL CONFIGURED DESIGN
- ADVANCED AVIONICS
- ENTRY TRAJECTORY/THERMAL STRUCTURES OPTIMIZATION
- EXTEND AFT C.G. RANGE FOR TRIM
- ALTERNATE FLIGHT CONTROL SCHEMES

Figure 3

AEROHEATING MODEL OF SHUTTLE ORBITER WITH TIP-FIN CONTROLLER

The large amount of data available for the Space Shuttle Orbiter makes it a good vehicle to use for study purposes although retrofitting the Orbiter with wing tip fin controllers is not presently cost effective. The 1.75 percent heat transfer model is shown in Figure 4. The trailing edge of the fin is split with the outboard section being the controller. The vertical tail on the Space Shuttle Orbiter is ineffective above an angle of attack of about 18 degrees at M = 3.5 during entry. When the vertical tail is ineffective, yaw control is obtained by using the reaction control system and the elevons which causes coupling between yaw and roll. Wing tip fin controllers reduce the coupling between the control modes. Some additional advantages of using wing tip fin controllers are a potential savings in weight, reduced use of the reaction control system below M = 7 and easier ground handling and space docking than with the vertical tail. Potential problem areas to be studied include aerodynamic heating and thermal protection systems design, particularly for the control surface and for the leading edge; crosswind landing capability; and the effect on flutter, vehicle dynamics, and energy management. The heating and aerodynamic and control characteristics results of the study are given in Reference 20 and 21.

AEROHEATING MODEL OF SHUTTLE ORBITER
WITH TIP-FIN CONTROLLER

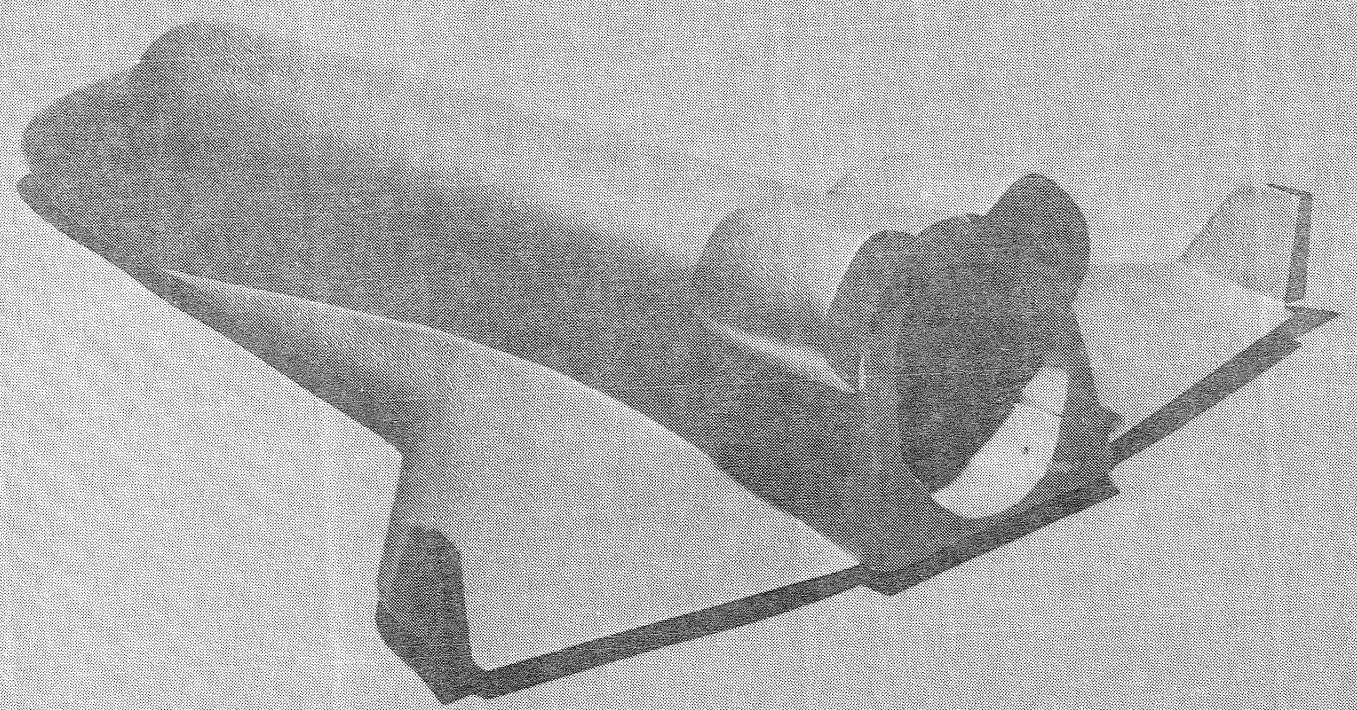

Figure 4

ADVANTAGES OF TIP-FIN CONTROLLERS

Figure 5 points out the advantages of the tip-fin, controllers over the current Shuttle system. First the tip fin controller provides control effectiveness at Mach numbers from 7 to landing where the vertical tail with rudder, because it is shielded by the wing, does not become effective until Mach numbers below 2. Analyses at Langley have shown a potential weight savings for the tip fin controller of approximately 2400 pounds. Part of this is in the vehicle structure and part is in RCS fuel savings. The tip fin does provide an opportunity to decouple the controls, that is, have a single surface for each function (roll, yaw, and pitch). This would provide a much simplified overall control system . More details are given in Reference 20.

ADVANTAGES OF TIP-FIN CONTROLLERS

- ELIMINATES RCS BELOW M = 7
- POTENTIAL WEIGHT SAVINGS OF 2400 #
- DECOUPLES ROLL AND YAW CONTROL
- EASIER GROUND HANDLING AND DOCKING WITH NO VERTICAL TAIL

Figure 5

RESULTS OF TIP-FIN STUDY FOR SHUTTLE ORBITER

Figure 6 presents the results of the Langley tip-fin controller study. During the study 6-D entry simulations showed that the orbiter with tip-fin controllers could be flown over the entire entry with responses very similar to those of the conventional orbiter. Wind tunnel results coupled with analyses have shown the aerodynamic heating environment is within the capability of existing materials (carbon-carbon and RSI). These analyses also demonstrated feasibility with existing technology thermo-structures design, and identified a potential weight savings of 2400 pounds. Details of this study are given in References 20 and 21.

RESULTS OF TIP-FIN STUDY FOR SHUTTLE ORBITER

- FLIGHT CONTROL ANALYSES SHOW THAT THE ORBITER WITH TIP-FIN CONTROLLERS IS CONTROLLABLE WITH RESPONSES SIMILAR TO THOSE OF THE ORBITER NOMINAL ENTRY.

- THE AEROHEATING TEMPERATURES ARE WITHIN THE CAPABILITY OF RSI AND CARBON-CARBON.

- THE RESULTS OF THE THERMO-STRUCTURES ANALYSES HAVE DEMONSTRATED FEASIBILITY WITH EXISTING TECHNOLOGY.

- POTENTIAL WEIGHT SAVINGS FOR THE TIP-FIN CONTROLLER WITH THE VERTICAL TAIL REMOVED OF 2400 POUNDS IDENTIFIED.

Figure 6

THE APPROACH - - A 3 LEGGED STOOL
AEROTHERMODYNAMICS DYNAMICS R&T

Computational work emphasizes the development of new techniques and solution methods for CFD as well as the utilization of existing methods for specific applications. Codes are divided into two categories: benchmark calculation methods for which a premium is placed on rigor, and engineering codes which emphasize computational speed. These engineering codes frequently must be "calibrated" by comparing to the benchmark calculations. Both wind-tunnel and flight tests are necessary in verifying the accuracy of computational codes, in developing techniques for extrapolating to other flight conditions, and in assessing the importance of real-gas effects since those effects are present in the flight data but usually not in the wind-tunnel results. Thus the program is characterize as a 3 legged stool - all three "legs" are needed if it is to be useful.

THE APPROACH - - A 3 LEGGED STOOL

AEROTHERMODYNAMICS R & T

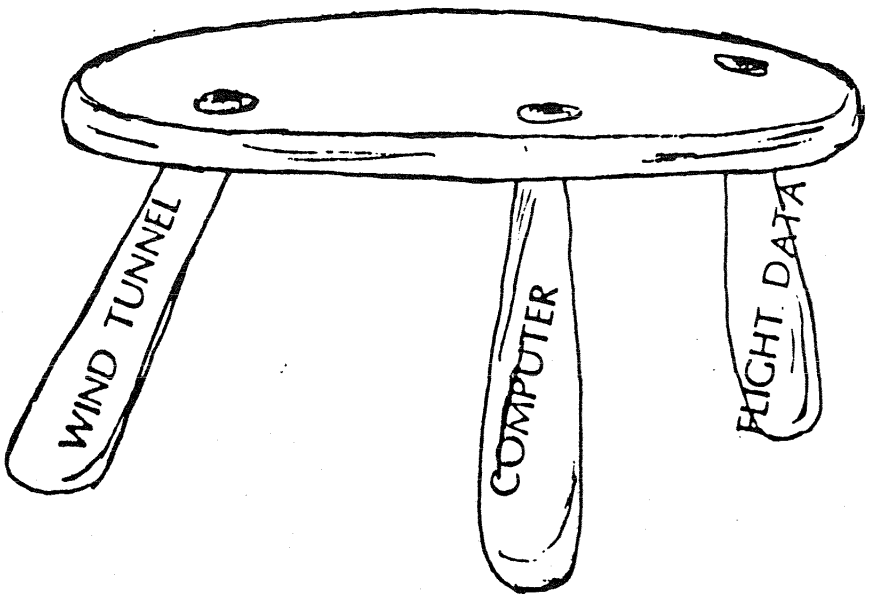

Figure 7

CFD METHODS FOR THREE-DIMENSIONAL FLOW

Early work in CFD utilized only axisymmetric codes because of their relative simplicity and because the primary application was for bodies of revolution such as the planetary probes. This left the analyst in a rather poor position to compute flows over advanced space transportation systems or AOTV concepts. So for the last 3 or 4 years, primary emphasis has been on developing and verifying three-dimensional flow capability. A three-pronged effect is illustrated in figure 8. The inviscid-plus boundary-layer method is the tried and true classical approach and has certain computational advantages. The inviscid code called HALIS (High Alpha Inviscid Solution, Ref. 22 was developed to handle the Shuttle, including high angles of attack where much of the forebody flow might be subsonic. This code has been highly successful but saturated the computational capability at NASA Langley until the recent acquisition of the VPS32. A companion approximate boundary-layer method was developed to couple with the inviscid solutions. This code, A3DBL (Axisymmetric Analog Three-Dimensional Boundary Layer, Reference 23, ignores the local crossflow and thus treats each spot on the surface as though it were a segment of a cone at zero angle of attack. Nevertheless, it has been shown to be quite accurate for most situations.

The viscous-shock layer method differs from a PNS code in that only terms of the order of $1/RE^2$ are retained. It is a very valuable method because it retains the intrinsic viscous nature of the flow, and yet is computationally quite rapid. The method is described in References 24. The code VSL81 is described in Reference 25 and 26. VSL84 (Ref. 27) has extensive modifications (including some very important error corrections), and the code does a good job for the Shuttle under-surface. The viscous-shock-layer method cannot march through a region of embedded subsonic flow. Either because of this or because of high gradients around the leading edge, some of the computational planes must be dropped. After dropping these planes, it is only able to compute the inboard portion of the wing.

The parabolized Navier Stokes code generally in use is the one described in Reference 28. A number of improvements have been made in the code (Ref. 29), including developing a new starting code for the nose solution.

CFD METHODS FOR THREE-DIMENSIONAL FLOW

- INVISCID + BOUNDARY LAYER

  HALIS, AA3DBL } HAMILTON & WEILMUENSTER

- THREE-DIMENSIONAL VISCOUS SHOCK LAYER

  VSL81 -- LEWIS (VPI)

  VSL84 -- THOMPSON

- PARABOLIZED NAVIER STOKES

  PNS -- GNOFFO

Figure 8

ORBITER EXPERIMENTS PROGRAM

Figure 9 shows the list of orbiter (OEX) aerothermodynamics experiments. The Langley experiments of SEADS, SUMS, and SILTS are presently scheduled to fly in November of this year. ACIP has flown on OV-102 and OV-99 from the beginning and has been the primary data source for aerodynamic performance assessment. These experiments are described in Reference 30. Tile-gap heating and catalytic-surface effects were very successful experiments on the 102 vehicle. The Aerodynamic Instrumentation Package will provide for the hooking up of certain thermocouples and pressure transducers to supplement the SILTS information on the leeside. Initial results from these experiments are given in Reference 13.

ORBITER EXPERIMENTS PROGRAM

AEROTHERMODYNAMICS EXPERIMENTS

ACRONYM	TITLE	SPONSORING CENTER
SEADS	SHUTTLE ENTRY AIR DATA SYSTEM	LANGLEY
SUMS	SHUTTLE UPPER ATMOSPHERE MASS SPECTROMETER	LANGLEY
ACIP	AERODYNAMIC COEFFICIENT IDENTIFICATION PACKAGE	JOHNSON
SILTS	SHUTTLE INFRARED LEESIDE TEMPERATURE SENSING	LANGLEY
AIP	AERODYNAMIC INSTRUMENTATION PACKAGE	LANGLEY
TGH	TILE GAP HEATING	AMES
CSE	CATALYTIC SURFACE EFFECTS	AMES

Figure 9

SHUTTLE INFRARED LEESIDE TEMPERATURE SENSING (SILTS)

The SILTS experiment has modified a commercially available infrared camera and mounted it in a pod at the tip of the vertical tail. It will alternately view the fuselage surface and the left wing through two windows in the pod. This cycle is repeated at 10 Hz. SILTS will provide heating data on the leeside of the orbiter where current CFD codes are not as effective due to the very complex nature of the flow.

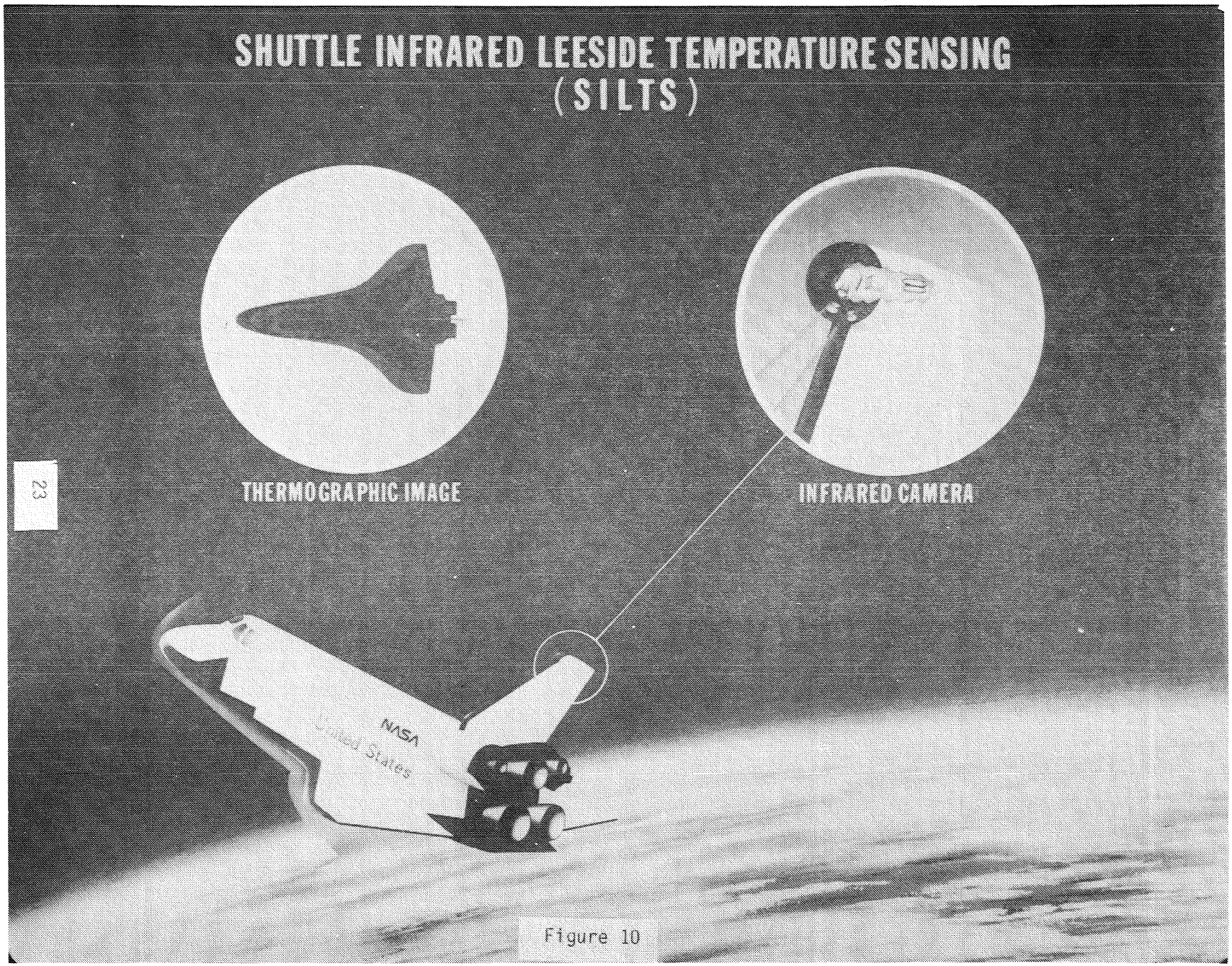
SHUTTLE INFRARED LEESIDE TEMPERATURE SENSING
(SILTS)
THERMOGRAPHIC IMAGE
INFRARED CAMERA
NASA
United States

Figure 10

BOUNDARY-LAYER TRANSITION CRITERION

A transition criterion ($R\theta/M_e$) computed at the experimentally determined STS transition locations is shown as a function of the respective normalized axial transition lengths in Figure 11. R is the momentum thickness Reynolds number based on local conditions and M_e is the local Mach number. The limited STS-1 results (Ref. 21) are included also. Over the first 30% of the shuttle, the STS-1 and STS-2 (Ref. 32) results are in good agreement and a transition criterion value of approximately 290 would be representative. The transition criterion for STS-2 conditions has been computed by both the approximate (Ref. 33) and local swept-cylinder (Ref. 34) techniques and the results are in generally good agreement over the shuttle length.

Ground-test transition results computed in the same parametric form by Goodrich (Ref. 35) are represented also in Figure 11. The ground-test data yield a peak value in $R\theta/M_e$ of about 225. Note that while the present techniques (Refs. 33, 34) were not used to recompute the ground-test results, flight transition Reynolds numbers tend to be greater than ground-test results on similar bodies (Refs. 36-38).

BOUNDARY-LAYER TRANSITION CRITERION

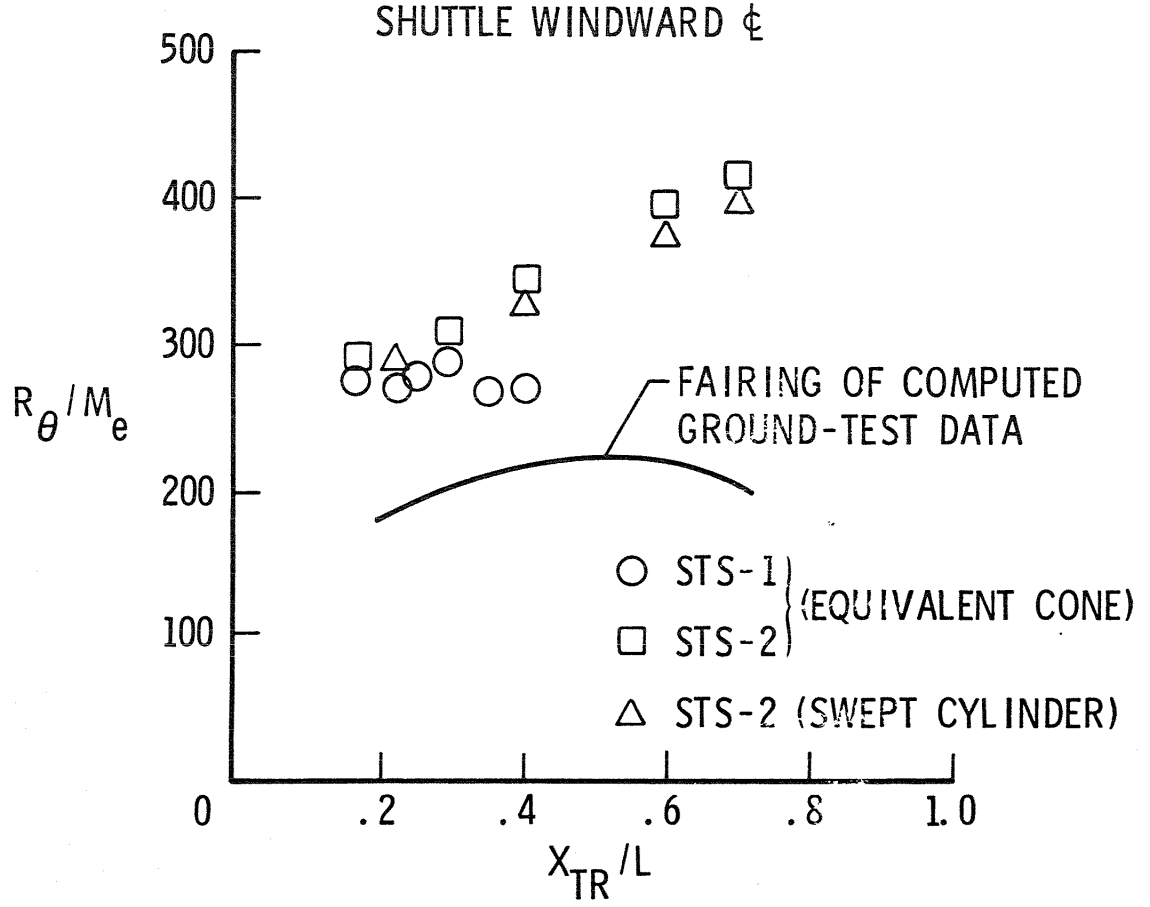

Figure 11

HEATING DISTRIBUTION ALONG WINDWARD SYMMETRY PLANE OF SHUTTLE ORBITER

A comparison of the predicted and measured heat-transfer distributions along the windward centerline for Mach 9.15 and 34.8° angle of attack on the STS-2 trajectory is shown in Figure 12. The three-dimensionaal VSL prediction is generally within 10 percent of the measured values which, in this case, exhibit a fair amount of scatter. The decrease in heating to the windward centerline surface around the 50 percent axial location is evident in the computational results although the data scatter precludes any statement about measured distributions. The centerline heating from the three-dimensional VSL prediction was compared against an axisymmetric VSL solution and an approximate solution (Ref. 39) both of which employ "equivalent" hyperboloid geometry to model the Shuttle windward centerline. The axisymmetric solutions predict a smooth distribution of heat transfer, and are within 10 percent of the flight data and the present three-dimensional calculation.

Due to the limitations of the code, it is only able to compute the inboard portion of the wing. Although not shown, the comparison with the limited flight data is fair, and not as good as the comparison shown in Figure 12.

HEATING DISTRIBUTION ALONG WINDWARD SYMMETRY PLANE OF SHUTTLE ORBITER

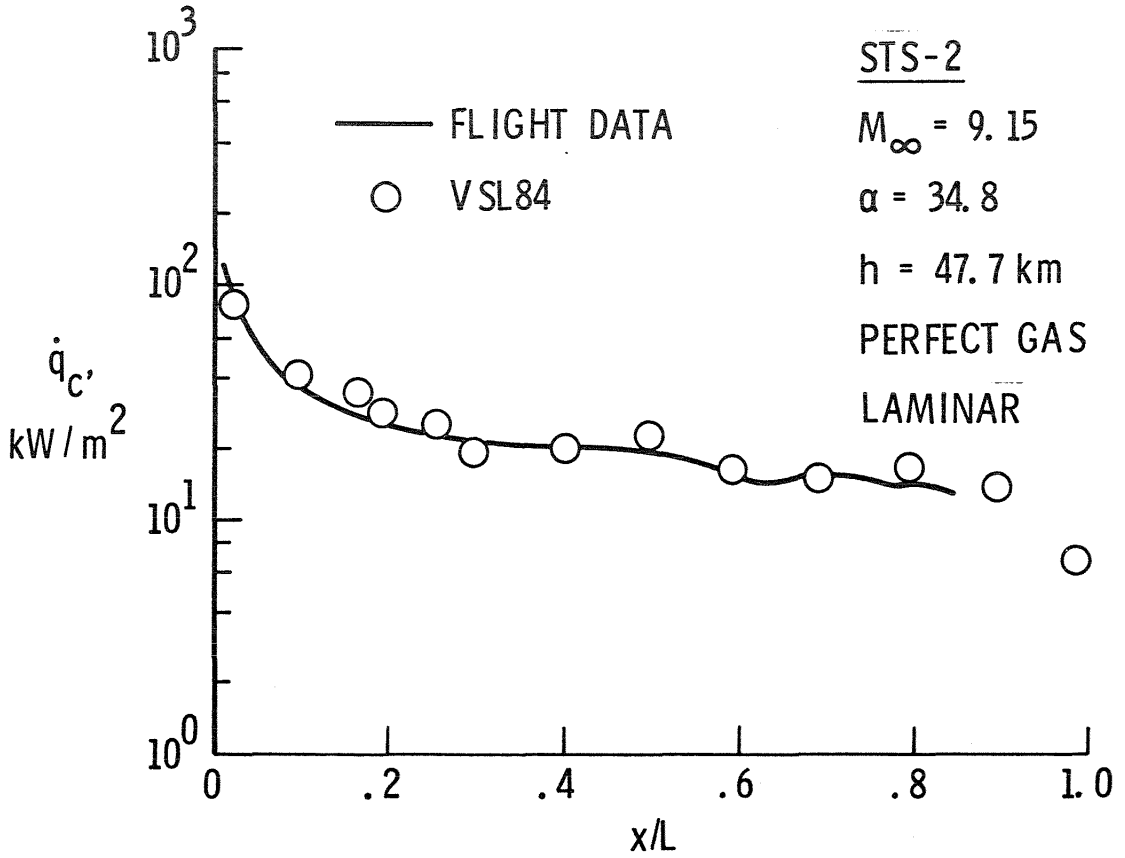

Figure 12

COMPARISON OF MEASURED AND PREDICTED HEATING FOR LAMINAR FLOW OVER A BENT BICONIC

Comparisons of measured and predicted heating distributions for a bent biconic (from Ref. 40) are shown in Figure 13 for the conditions shown on the figure. These results, both experimental and analytical, correspond to a model surface temperature of 80°F. In general, the PNS code of Reference 28 predicted windward heating to within 10 percent. Agreement between prediction and measurement was poorer on the leeward side where the PNS code under predicted heating up to 25 percent. The different trends in measured leeward heating distributions due to the change in Reynolds number were qualitatively predicted by the PNS code. Since this code was exercised only for laminar flow, this qualitative agreement implies the leeward flow was laminar for both values of Reynolds number. One possible reason for the PNS code tending to under predict measured heating is this code does not account for downstream influences propagating upstream through the subsonic portion of the boundary layer. There is evidence that failure to include this effect will yield values of heating that are too low. All things considered, the PNS code provides a reasonably accurate prediction of the heating distributions on the present biconics in Mach 10 air.

COMPARISON OF MEASURED AND PREDICTED HEATING FOR LAMINAR FLOW OVER A BENT BICONIC

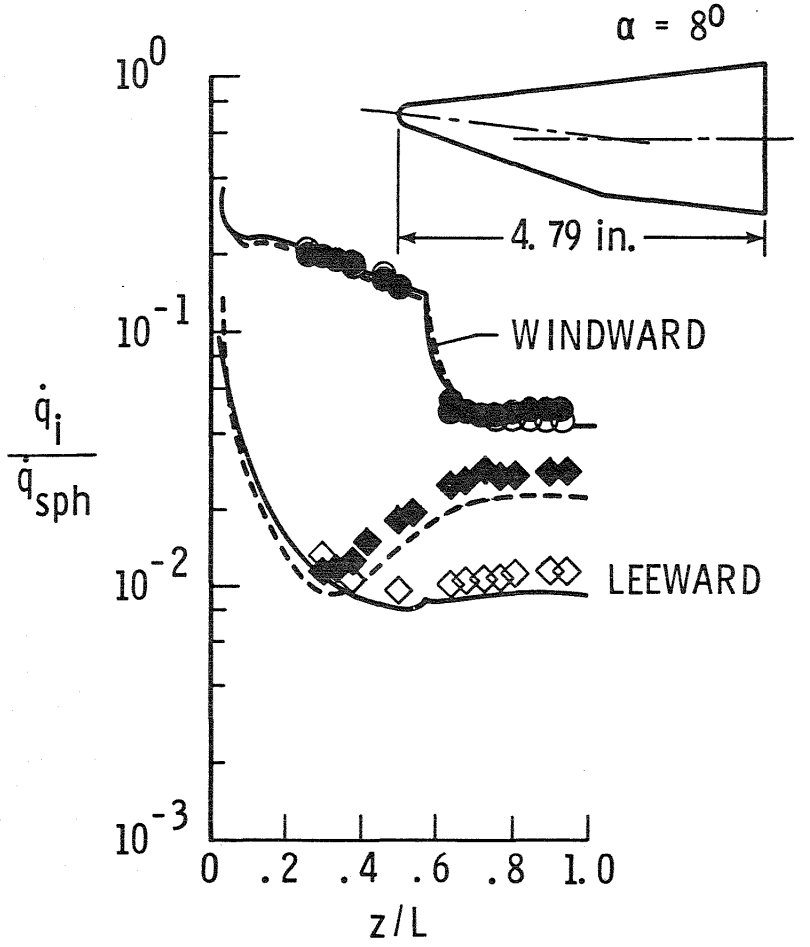

PREDICTED (PNS CODE)

	M_∞	$R_{\infty,L}$
———	9.9	2.5×10^5
- - - - -	10.2	9.4×10^5

MEASURED

	θ, deg	M_∞	$R_{\infty,L}$
○	180	9.9	2.5×10^5
●	180	10.2	9.4×10^5
◇	0	9.9	2.5×10^5
◆	0	10.2	9.4×10^5

Figure 13

SHUTTLE FLIGHT DATA ANALYSIS RESULTS

The completion of the first and second flights of the space Shuttle Orbiter has given aerodynamicists the first opportunity to test their prediction skills over diverse flight conditions. The performance predictions were in excellent agreement with flight performance above Mach 1; however, drag was over predicted at the subsonic Mach numbers (Ref. 41)

The trim characteristics were predicted adequately in the Mach range of 2 to 10; however, above Mach 10 and below Mach 2, the predictions were less than satisfactory. Analysis results of the STS-2 maneuvers during entry indicate the hypersonic trim discrepancy is due to an error in prediction of the basic vehicle pitching moment (Ref. 41) and not an error in prediction of the elevon and body flap effectiveness.

Flight-derived aerodynamic heat-transfer data for the Orbiter leeside centerline and wing surfaces have been compared with appropriate ground test results. Heat-transfer rates to these surfaces in flight are very low, in general less than 1% of the 1 ft radius sphere reference value (5-10% of windward side heating rates). Flight heating levels are, in general, less than those which are inferred from the ground test results. This result is apparently due to laminar-to-turbulent transition of the flow in the separated region having occurred at a much larger Reynolds number in flight than in the wind tunnel. When the state (laminar/turbulent) of the separated flow is the same both in flight and in the wind tunnel, the levels of heat transfer expressed in the form of Stanton number are comparable (Ref. 42)

Computational methods have been developed to predict the three-dimensional nonequilibrium flowfield past the windward side of the Space Shuttle Orbiter, and numerical solutions have been obtained for different flight conditions. The governing equations take into account the finite-rate chemical reactions of multicomponent ionizing air. A general nonorthogonal computational grid system is used to treat the nonaxisymmetric geometry. The methods solved the viscous nonequilibrium flows over the entire Shuttle windward surface in reasonable computing times. The computational results show good agreement compared to the STS-2 flight data (Ref. 43)

A generalized PNS code and a time-dependent blunt-body code have been used successfully to compute the complete flow around the Space Shuttle Orbiter forebody at two different flow conditions. The good agreement between the computational results and the experimental data proves the effectiveness of the generalized PNS solver (Ref. 44). The complex flow structure that develops near the wing-body region is predicted reasonably well by the generalized PNS solver. It is believed that an improved grid will permit the computation to continue to the aft portion of the shuttle.

Computation of the wing region should be possible if the flow outside of the boundary layer is supersonic, and there is evidence that this is the case. Regions of reversed axial flow remain a problem.

SHUTTLE FLIGHT DATA ANALYSIS RESULTS

AERO CHARACTERISTICS:

- GENERALLY WELL PREDICTED BY TUNNEL DATA
  - EXCEPTIONS: - HYPERSONIC PITCH ANOMALY
  - SUBSONIC C_D
- FLIGHT CONTROL GOOD OVERALL
  - EXCEPTIONS: - FCS/NAV COUPLING
  - TRANSONIC TRIM

HEATING:

- WINDWARD ℄ HEATING GENERALLY WELL PREDICTED
  - NON-CATALYTIC WALL EFFECTS ABOVE 67 KM
  - EQUILIBRIUM BELOW 67 KM
- TRANSITION CONSISTENT WITH SMOOTH WALLS
- SEMI-EMPIRICAL THEORY DEVELOPED FOR LEESIDE ℄
- LOCALIZED, OFF-℄ (STREAKS, SIDEWALLS) NOW BEING ANALYZED

<u>BIG QUESTIONS</u>

- REAL GAS EFFECTS ON AERO?
- TRANSITION FRONT MOVEMENT?
- OFF-℄ LOCALIZED HEATING?

Figure 14

SUMMARY - AEROTHERMODYNAMICS

The completion of several flights of the Space Shuttle Orbter has given aerothermodynamicists the opportunity to test their prediction skills over diverse flight conditions. Flight-derived aerodynamic heat-transfer data for the Orbiter leeside centerline and wing surfaces have been compared with appropriate ground test results. Flight heating levels are, in general, less than those which are inferred from the ground test results. This result is apparently due to laminar-to-turbulent transition of the flow in the separated region having occurred at a much larger Reynolds number in flight than in the wind tunnel. When the state (laminar/turbulent) of the separated flow is the same both in flight and in the wind tunnel, the levels of heat transfer expressed in the form of Stanton number are comparable. Although the Orbiter configuration is in no way similar to the Apollo entry capsule, it is interesting to note that these results are consistent with those previously observed for the Apollo capsule. the flight/wind tunnel data comparisons confirm the appropriateness of the Orbiter thermal protection system design approach which utilized wind tunnel results applied directly at flight conditions to define the flight leeside aerothermodynamic environment.

Computational methods have been developed to predict the three-dimensional nonequilibrium flowfield past the windward side of the Space Shuttle Orbiter, and numberical solutions have been obtained for different flight conditions. The methods solved the viscous nonequilibrium flows over the entire Shuttle windward surface in reasonable computing times. The computational results show good agreement compared to flight data.

A generalized PNS code and a time-dependent blunt-body code have been used successfully to compute the complete flow around the Space Shuttle Orbiter forebody at different flow conditions. The good agreement between the computational results and the experimental data proves the effectiveness of the generalized PNS solver. The complex flow structure that develops near the wing-body region is predicted reasonably well by the generalized PNS solver.

Computation of the wing region should be possible if the flow outside of the boundary layer is supersonic, and there is evidence that this is the case. Regions of reversed axial flow remain a problem.

Future analytical efforts will include comparisons with Shuttle flight data and improved methods to account for viscous interactions and nonequilibrium chemistry. More, better, and different types of flight data will be obtained in future flights using the SILTS, SEARS, SUMS and AIP OEX experiments. Comparisons of flight and wind tunnel data will continue, and the overall improed understanding of various aerothermodynamics phenomena will permit more intelligent use of wind tunnels in the future.

SUMMARY - AEROTHERMODYNAMICS

ANALYSIS

- EXPLORING RANGE OF APPLICABILITY OF CFD CODES
  - PNS
  - VISCOUS-SHOCK-LAYER
  - INVISCID-PLUS BOUNDARY LAYER
  - GOOD COMPARISONS WITH WINDWARD CENTER LINE FLIGHT DATA OVER COMPLETE VEHICLE
  - GOOD COMPARISONS WITH LEEWARD CENTER LINE FLIGHT DATA OVER FORWARD PORTION

- MORE ATTENTION TO HIGH-ALTITUDE EFFECTS IN FUTURE
  - VISCOUS INTERACTION
  - NONEQUILIBRIUM CHEMISTRY

EXPERIMENT

- EXPECT MORE AND BETTER FLIGHT DATA
  - SILTS
  - SEADS
  - SUMS
  - AIP

- CONTINUED USE OF WIND TUNNELS
  - DATA BASE FOR GENERIC CONFIGURATIONS
  - SPECIFIC TESTS FOR INDENTIFIED CONFIGURATIONS

Figure 15

ENTRY VEHICLE TECHNOLOGY ISSUES

NASA is conducting technology and systems studies of an Entry Research Vehicle (ERV), a potential new initiative in the late 1980's. The ERV would be carried to orbit in the Shuttle Orbiter payload bay. As shown in Figure 16, technology issues addressed by the ERV include atmospheric uncertainties, maneuvering entry/synergetic plane change, aerodynamic and aeroheating data for verification of prediction techniques, advanced guidance and navigation, and advanced TPS and thermostructures concepts.

ENTRY VEHICLE TECHNOLOGY ISSUES

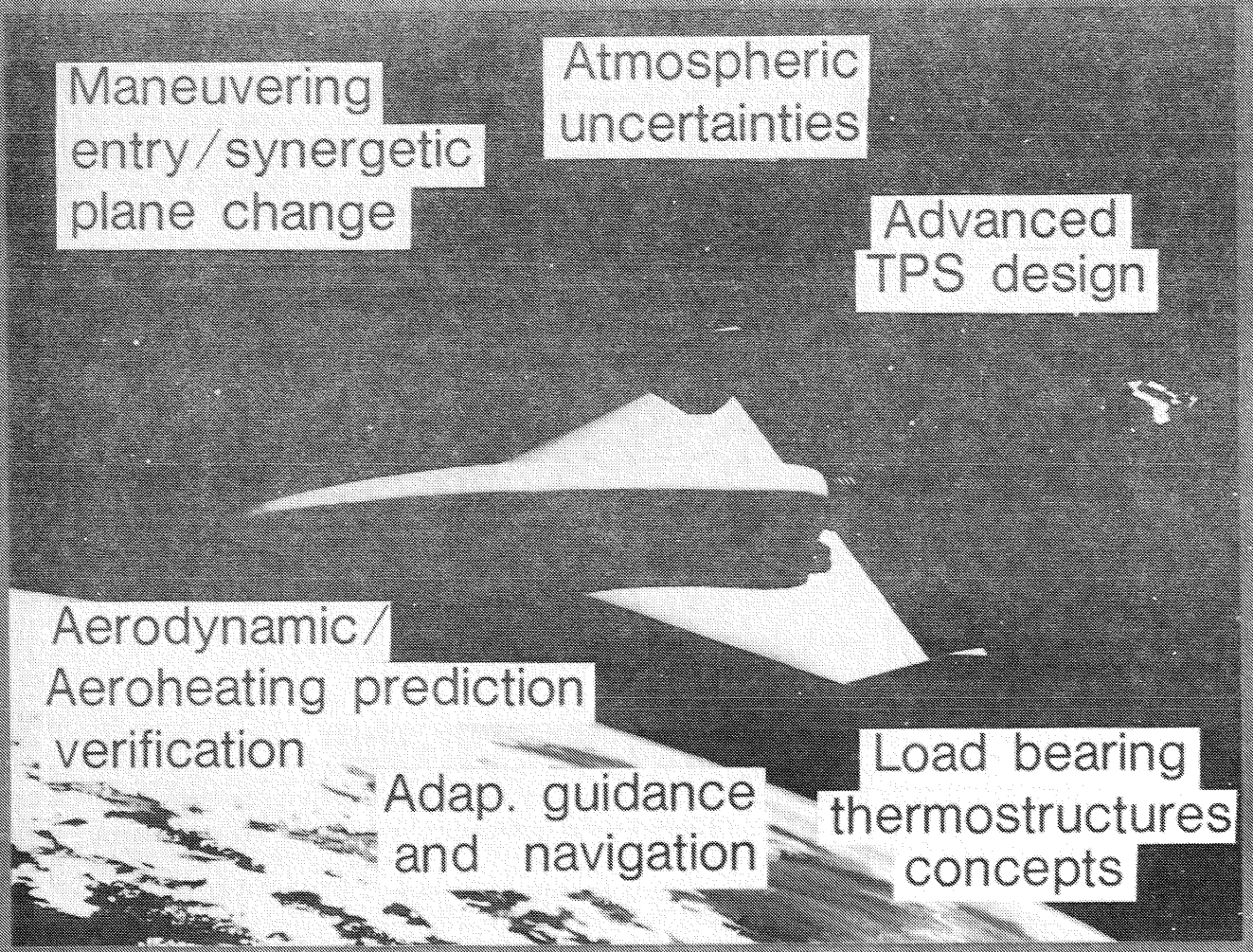

Figure 16

TECHNOLOGY ASSESSMENTS REVEAL STRUCTURES R&T GOALS FOR AEROSPACE PLANE TYPE VEHICLES

A number of technology assessments have revealed the significant challenges facing the materials and structures communities for aerospace plane type vehicles. Briefly stated, systems studies reveal a need for a 25 percent reduction in structural mass compared to the current Space Shuttle Orbiter, and a factor of five increase in mission life. In addition, for some missions the performance requirements are such that higher maximum use temperatures and overall heat loads must be accommodated; generally maximum use temperature is the limiting factor on desired performance. Also, for reduced operational cost and mission flexibility reusable containment of cryogenic LOX and LH2 and durable, long life surface structures are required. These requirements dictate that loads be known to an accuracy never before required to reduce margins of safety, and that the structural concepts designer wring out every ounce of nonoptimum structure. Such requirements dictate a large data base on aerothermal loads and accurate and efficient structural and heat transfer analysis codes. In addition, test facilities, techniques and instrumentation must be provided to verify analysis codes, advanced lightweight concepts, and overall structural performance.

TECHNOLOGY ASSESSMENTS REVEAL STRUCTURES R & T GOALS FOR AEROSPACE PLANE TYPE VEHICLES

- 25 PERCENT MASS REDUCTION
- FACTOR OF 5 OR MORE INCREASE IN MISSION LIFE
- INCREASE IN MAX USE TEMPERATURE (THE HIGHER, THE BETTER)

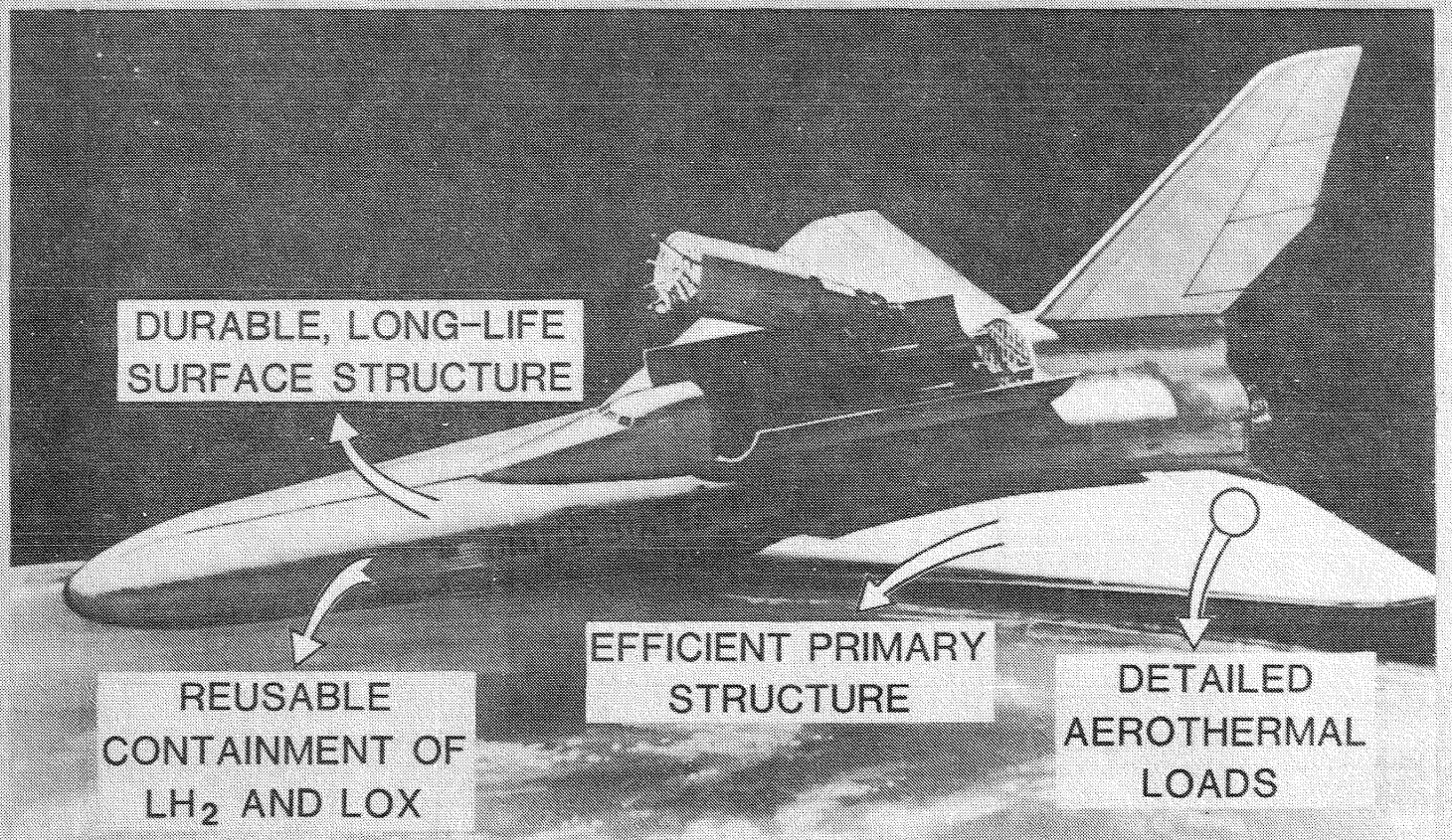

Figure 17

MATERIALS AND STRUCTURES RESEARCH AREAS

Figure 18 gives an outline for the rest of this paper. Work on ceramics will be presented as a part of the overall effort on Thermal Protection Systems (TPS). Also covered under TPS is heat-pipe-cooled structures (leading edge) and actively cooled structural panels. Primary structures will include work on graphite/polyimide (GR/PI) composites, titanium, superalloy and carbon-carbon components.

MATERIALS AND STRUCTURES RESEARCH AREAS

- MATERIALS
  - COMPOSITES
  - TITANIUM
  - SUPERALLOYS
  - CARBON-CARBON
  - CERAMICS
- STRUCTURES
  - AEROTHERMAL LOADS
  - THERMAL-STRUCTURAL TEST AND ANALYSIS
  - CONCEPTS: DESIGN, FAB, AND TEST
    - TPS
    - CRYO TANKS
    - PRIMARY STRUCTURE
    - AIR BREATHING PROPULSION

Figure 18

TIME-TEMPERATURE-STRESS CAPABILITIES OF COMPOSITE MATERIALS

High temperature composite materials have the potential of significantly reducing the weight of future high speed vehicle structures. However, implementation of the material into vehicle usage is contingent upon demonstrating its airworthiness when exposed to the long-time high speed flight service environment. The primary objective of the research of reference 45 was to establish the time-temperature-stress characteristics and capabilities of five classes of high temperature composite materials to determine their suitability for advanced supersonic technology consideration. The systems studied were B/EP, G/EP, B/PI, G/PI, and B/Al.

Figure 19 is a schematic diagram, that shows the principal elements of the work. The baseline properties are typical mechanical properties for each of the composites, and these properties were generated in sufficient detail so that any changes in them due to repeated loading and thermal or environmental aging could be measured and reported. Fatigue life was measured before and after various load and temperature histories. The materials' creep behavior was measured early in the program in order to fully evaluate filamentary composites of this type. The aging characteristics of the material were measured at various temperatures. A limited study of moisture exposure effects was included for the resin matrix materials. However, with this exception, moisture effects were deliberately avoided by use of standard bakeout procedures prior to the various tests conducted during the program. The added costs of including moisture effects to each of the test areas was beyond the scope of the overall program.

The tests that were conducted on the composite systems were baseline tensile, notched tensile, compressive, shear, and fracture; environmental and thermal aging; constant amplitude fatigue, creep and creep rupture; and both accelerated and real-time flight simulation testing using totally random fatigue loading. Phase I (Ref. 45) of the two-phase program included the baseline, fatigue, and creep determinations and all the aging and flight simulation studies up through 10,000 hours of cumulative exposure. The baseline, constant amplitude fatigue, and creep tests characterized the composite materials and form a basis for comparison with the post-exposure test results. The baseline tests were also used to set the test conditions for the short-term exposures (100 and 200 hours, random fatigue at temperature). The short-term service history tests were performed to generate wearout analysis model data, and to set the stress levels for the long-term service history tests. Finally, the long-term tests provide data on the effect of 10,000 and 50,000-hour simulated supersonic flight service on residual properties of the composites. The thermal aging and the environmental aging exposures are concurrent with the service history tests.

TIME–TEMPERATURE–STRESS CAPABILITIES OF COMPOSITE MATERIALS

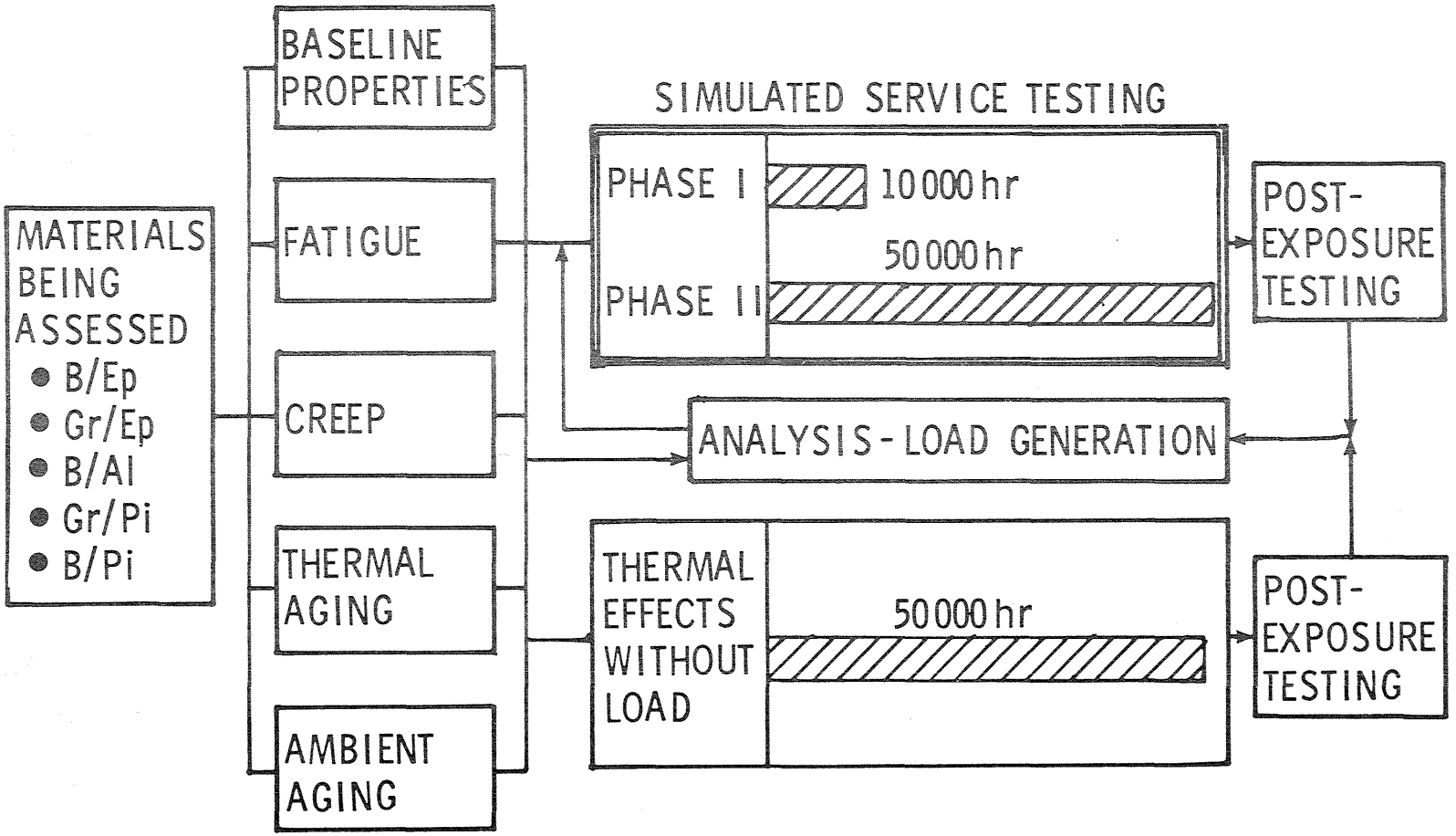

Figure 19

PHASE I CONCLUSIONS

G/EP (A-S/3501) and B/EP (B/5505) should be limited to temperatures lower than 212°F for cumulative exposures greater than 10,000 hours because of:

1. Early flight simulation test failures (due to compressive loading and thermal cycling combined with oxidation induced matrix degradation).

2. Loss of residual strength during flight simulation and thermal aging exposures (due to oxidation induced matrix degradation).

3. Moisture effects on elevated temperature strength (due to matrix degradation).

G/PI (HT-S/710) should be limited to 450°F for exposures greater than 10,000 hours because of:

1. Loss of residual tensile strength during thermal aging (due to oxidation induced matrix degradation).

2. Loss of residual strength, primarily matrix dominated, during flight simulation exposure (due to combined compressive and thermal stressing in conjunction with oxidation induced matrix degradation).

B/Al (B/6061) should be limited to 450°F for exposures greater than 10,000 hours because of:

1. Loss of residual tensile strength during thermal aging (due to interface diffusion induced fiber degradation). Some loss in strength can occur at temperatures as low as 350°F.

2. High temperature fatigue effects (matrix surface cracking and oxidation).

3. Loss of residual strength during flight simulation exposure (due to interface diffusion induced fiber degradation, matrix surface cracking, and oxidation).

B/PI (B/P 105 A) is not suitable for this application because of severe matrix degradation during thermal aging and short-term flight simulation exposures at 450°F.

PHASE I CONCLUSIONS

MATERIAL	MAXIMUM TEMPERATURE TESTED	MAXIMUM TEMPERATURE TO SURVIVE 10,000 HR	REMARKS
G/EP (A-S/3501)	450 K (350° F)	394 K (250° F)	MATRIX DEGRADATION
B/EP (B/5505)	450 K (350° F)	394 K (250° F)	MATRIX DEGRADATION
B/AL (B/6061)	728 K (850° F)	450 K (350° F)	FIBER DEGRADATION MATRIX OXIDATION
G/PI (HT-S/710)	561 K (550° F)	505 K (450° F)	MATRIX DEGRADATION
B/PI (B/P105A)	MATERIAL WAS DROPPED EARLY IN PROGRAM DUE TO VERY POOR PERFORMANCE		

Figure 20

CASTS - FABRICATION DEVELOPMENT COMPONENTS

Development of fabrication procedures and specification for Gr/PI composites utilizing NR150B2, PMR-15, LARC-160 and THERMID 600 polyimide matrix materials is described in NASA CP 2079, Graphite/Polyimide Composites, 1979. Prepreg specification, cure and post cure cycles, manufacturing methods applicable for building full scale structural components and nondestructive inspection procedures were included in the effort. Items shown in Figure 21 were built to demonstrate the fabrication technology. Flat laminates up to 0.125 in thick and 2 x 4 ft in area, chopped fiber moldings, honeycomb core sandwich panels, skin-stringer panels and a built-up component such as a body flap segment were fabricated utilizing each of the four matrix materials. Mechanical fasteners, secondary bonding and cocuring were evaluated for fabricating joints in Gr/PI structures.

Both in-house NASA Langley and contract efforts were used to develop fabrication technology. The in-house effort focused on PMR-15 and LARC-160 Gr/PI composites. Paper 3 of NASA CP 2079 reports preliminary accomplishments. Separate contracts were awarded to develop fabrication procedures for each of the four Gr/PI composites. Papers 4, 6, 7, and 12 in NASA CP 2079 report on the initial contract efforts.

The capability to fabricate structural components has been demonstrated with Gr/PMR-15 composite.

CASTS FABRICATION DEVELOPMENT COMPONENTS

0.6 m x 1.2 m LAMINATES
(2 ft x 4 ft)

.76 mm (0.030 in.) THICK
1.52 mm (0.060 in.) THICK
3.18 mm (0.125 in.) THICK

CHOPPED FIBER MOLDING

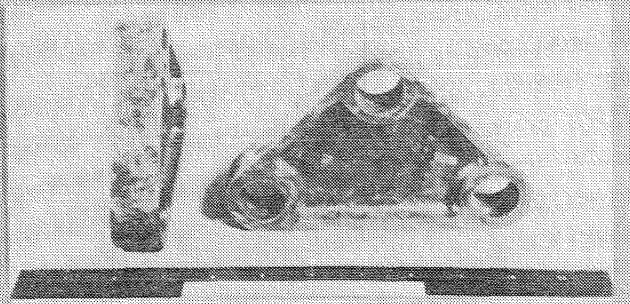

HONEYCOMB CORE PANEL

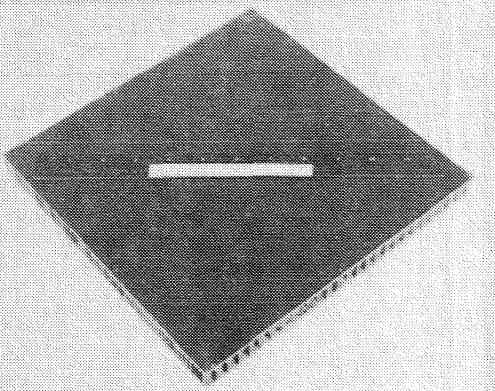

SKIN - STRINGER PANELS

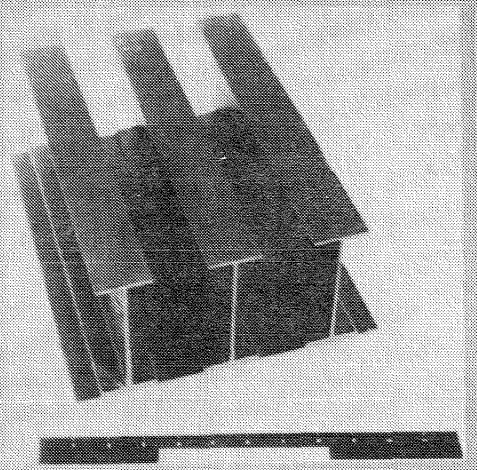

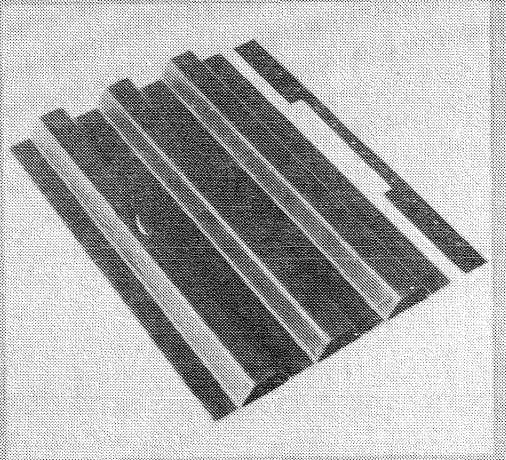

AFT BODY FLAP COMPONENT

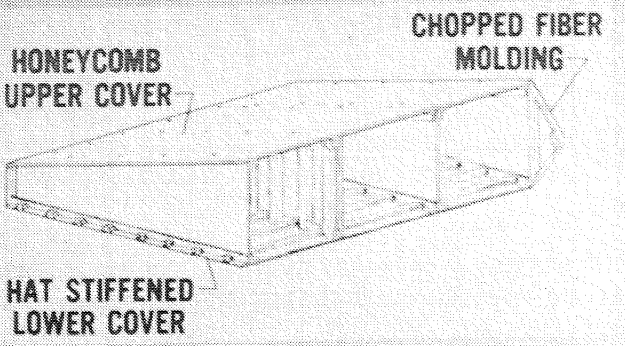

Figure 21

APPLICATION OF CREEP PREDICTION TECHNIQUE TO TPS PANELS

Early Shuttle system studies indicated that creep could become a significant factor in the design and performance of metallic TPS. The requirements for the Shuttle TPS were in sharp contrast to most previous experiences in the area of creep prediction. For example, the Shuttle TPS is subjected to multiple, complex missions of combined thermal and pressure loads. Furthermore, TPS designs generally were fabricated from thin-gage material less than 0.005 inch thick, where the effects of oxidation on creep could be pronounced. In addition, the Shuttle TPS deflection criteria limited allowable creep strains to 1%, a range where measurement and prediction capability were not well established.

By 1972, several experimental programs had been conducted to assess creep prediction capability on simple tensile specimens subjected to simulated mission cycles. Results for various materials indicated that creep predictions were not good (by factors of 2 or more) and, more importantly, predicted strains were unconservative.

As a result of these early experiments, an extensive experimental and analytical creep investigation was conducted on candidate TPS materials (Ref. 46). This program evaluated both the steady-state and cyclic creep behavior of four alloys in their sheet from: Ti-6Al-4V, Rene' 41, L-605, and TD Ni-20Cr. Comparison of test and predictions (which used a strain-hardening rule) for titanium were good, and results for L-605 were excellent. The results for Rene' 41 and TD Ni-20Cr did not show such good agreement with differences on the order of 40-50%. Although this is not good agreement, it is significantly better than the capability that existed in 1972.

To extend the prediction capability obtained from tensile specimens to more complex TPS heatshields, panel segments (2.5" x 12.4") were tested. In order to predict creep deflections resulting from complex stress distributions in the built-up panel, a computer program was developed which incorporates the basic cyclic correlation equations and hardening rules to calculate panel creep strains and deflections as a function of time. An example of the prediction capability for panel segments of L-605 is shown in Figure 22. The panels were subjected to simulated Shuttle mission cycles, including continuously varying temperature and pressure loads. The lower part of the figure compares the measured and predicted creep deflections of the panel midpoint as a function of the number of simulated mission cycles. The agreement between the predicted deflection and the results from the two panels is considered good. For the four materials investigated, the agreement between calculated and test midpoint deflections of the panel segments was comparable to the prediction capability for the elemental specimens.

The results of the panel segment test suggest that, if the tensile cyclic creep behavior of a material can be characterized, then the creep deflection predictions can be made for thin-gage sheet structures subjected to complex cyclic thermal and bending loads. The current prediction capability, although not perfect, is considered adequate for design of metallic TPS panels that are sized by cyclic creep deformation criteria.

APPLICATION OF CREEP PREDICTION TECHNIQUE TO TPS PANELS
L-605 (COBALT ALLOY)

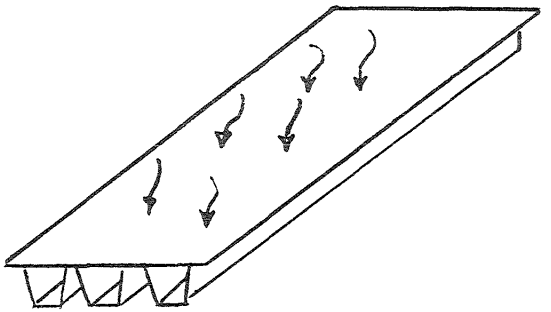

TPS PANEL SEGMENT

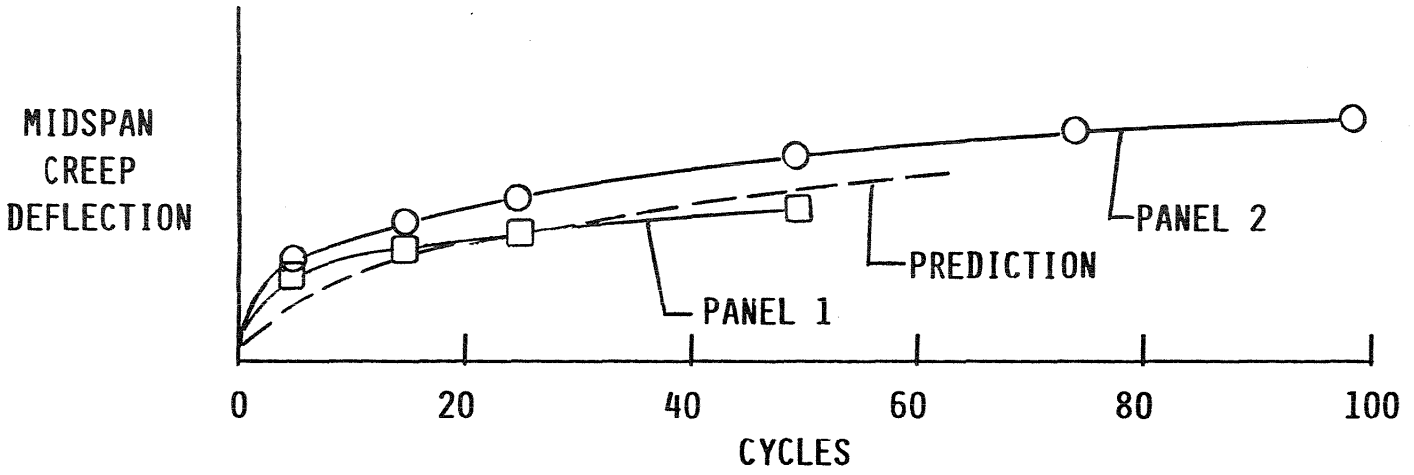

Figure 22

CREEP STRENGTH OF HAYNES 188 SHEET

Early in the Shuttle technology program creep strength was identified as a possible design constraint for metallic TPS and studies were initiated to improve the creep strength of HS 188 (a Cobalt base TPS candidate material). These studies (Ref. 47) have led to the improvements in the low-strain creep strength of HS 188 sheet shown in Figure 23. The figure shows that with advanced themomechanical processing the creep strength (1% strain in 1000 H) of the material is increased approximately 50% over the complete temperature range of interest, or, alternatively, design life has been increased by an order of magnitude for a constant stress level. These improvements were obtained using an advanced thermomechanical processing procedure that severely cold-works the sheet material prior to a high-temperature (2100°F) solution anneal. This processing does not significantly degrade other mechanical or physical properties. It remains to be seen if the creep properties of precipitation-hardening nickle base alloys, such as Rene' 41, can also be improved by advanced thermomechanical processing.

CREEP STRENGTH OF HAYNES HS 188 SHEET

1% CREEP STRAIN IN 1000 HOURS

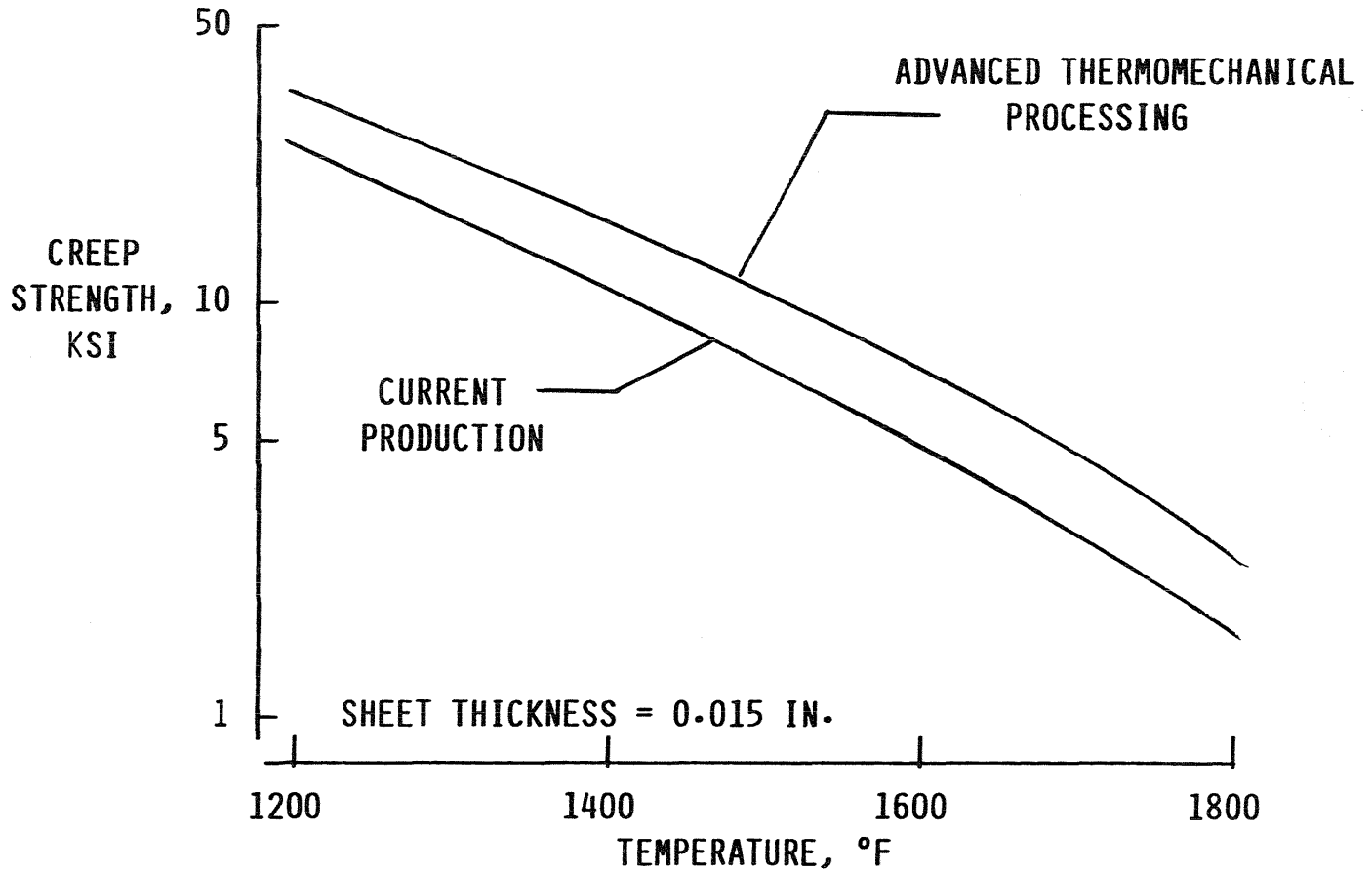

Figure 23

MECHANICAL PROPERTIES OF RENE' 41 AFTER TPS EXPOSURE

Nickel-base superalloys have been the focus of strong interest for heat shield applications because of their potential for forming high-emittance oxides on exposure to elevated temperatures (Ref. 48). Figure 24 shows results from a thermal fatigue test of a flightweight Rene' 41 panel which define the residual mechanical characteristics of Rene' 41 after exposure to simulated TPS service conditions. The panel was similar in design to the one used in a study of a radiative and actively cooled panel (Refs. 49, 50). The heat shield consisted of corrugation-stiffened, beaded-skin, Rene' 41 panels backed by a thin layer of high-temperature insulation contained within stainless steel foil packages to seal against water ingress. The heat shield was fabricated from 0.010 inch Rene' 41 beaded outer skin spotwelded to a 0.010 inch Rene' 41 corrugated inner skin. Two heat shield panels, joined at the center with a slip joint, were attached to structural plates at the far ends. The edges of the heat shields were attached to the structural plate by bolts through slotted holes which permitted longitudinal movement of the panels. The figure shows the nominal thermal-fatigue test cycle. The panel was exposed to 20,000 thermal cycles using radiant heaters. The maximum surface temperature of the panel was 1450°F and the minimum temperature of the corrugated skin was 200°F.

Examination of the panel after the 20,000 cycles revealed no buckling of the skins, a decrease in panel width of 0.10 inch, cracks developed from the elongated holes, and additional wear at the elongated holes which were enlarged while the bolts were worn.

Subsize tensile specimens conforming to the recommended practice of ASTM E-8 (Ref. 51) were machined from the corrugated skins of the fatigue panel at the conclusion of the thermal-fatigue tests. The figure shows a comparison of room temperature tensile strength and tensile elongations of Rene' 41 as received in the aged condition. The most significant result shown is the large reduction in tensile elongation of specimens from the exposed panels compared to the tensile elongation of Rene' 41 in the aged condition. Specimens from the thermal-fatigue panel failed at six percent strain. The yield strength was increased somewhat and the ultimate stress was essentially not affected. These changes were related to changes in microstructural changes that occurred during the thermal-fatigue exposure (Ref. 52).

MECHANICAL PROPERTIES OF RENE′ 41 AFTER TPS EXPOSURE

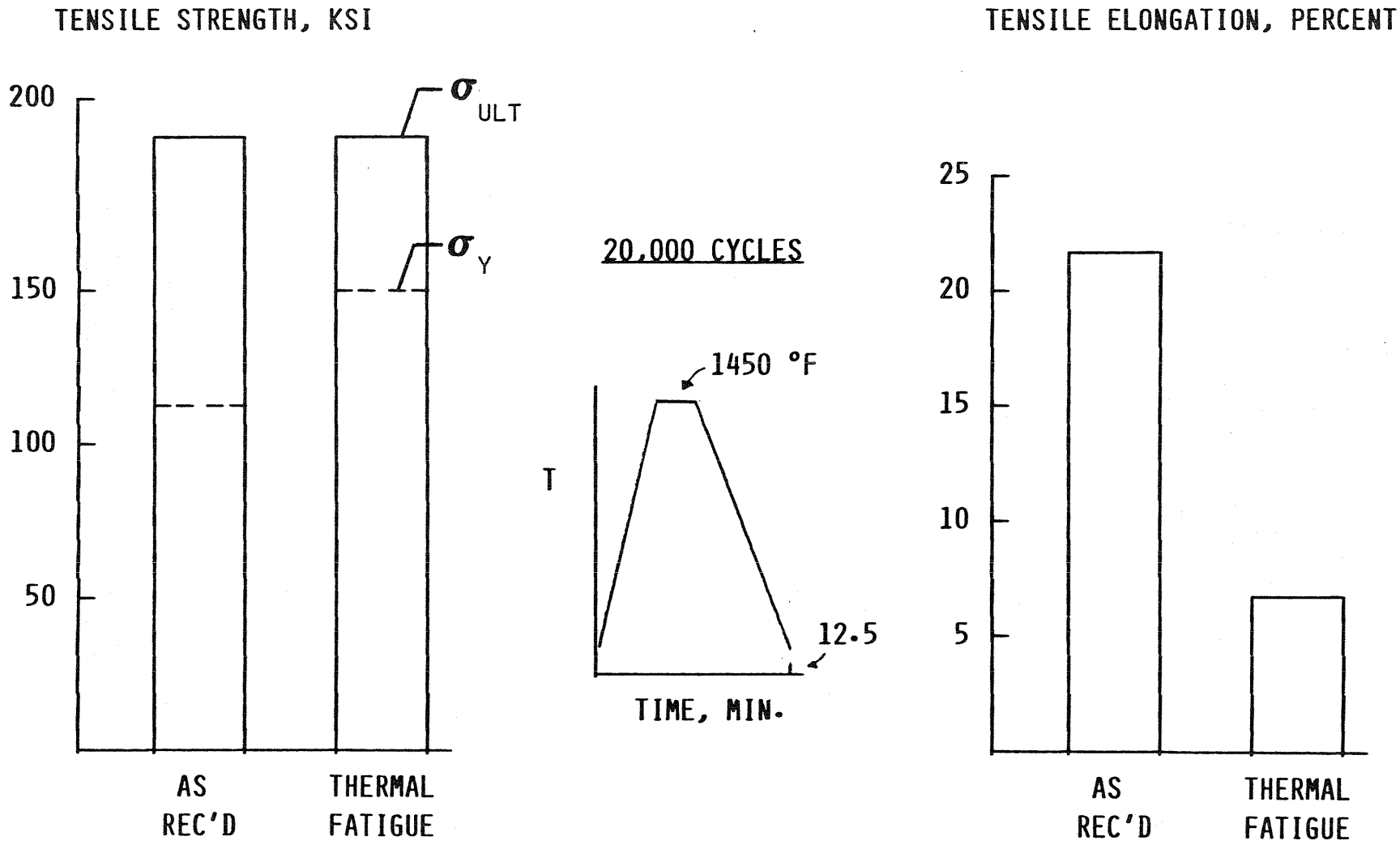

Figure 24

VARIATION IN REENTRY TEMPERATURE WITH EMITTANCE/CATALYSIS OF SURFACE

Superalloys in metallic Thermal Protection System (TPS) applications must have good high temperature strength and resistance to dynamic oxidation, have a high emittance, and have a low catalytic activity to the recombination of dissociated oxygen and nitrogen that exist in reentry environments. Two alloys of potential interest for TPS applications are Inconel 617 and MA 956. Inconel 617, which is a nickel-chromium superalloy, has been shown to meet the high temperature strength, oxidation resistance and high emittance criteria for use in TPS applications (Ref. 53-55). MA 956, which is an oxide dispersion strengthened, iron base superalloy, also has good high temperature strength and very good oxidation resistance (Ref. 56), but it has a relatively low emittance. The catalytic activity of Inconel 617 and MA 956 exposed to reentry heating conditions is thought to be high due to the presence on the exposed surface of naturally occurring oxides of metals which tend to catalyze the recombination reactions of dissociated oxygen and nitrogen. The TPS reentry environment contains substantial concentrations of these species.

Figure 25 shows the variation of surface equilibrium temperature as a function of surface recombination efficiency (catalysis) for a range of emittance from 0.5 to 0.9 for the conditions shown on the figure. MA 956 and Inconel 617 are shown over an estimated range of emittance and surface recombination efficiency. For the conditions shown on the figure, the MA 956, with an emittance of 0.5 - 0.6, is seen to reach a temperature of about 2700°F, and the inconel 617, with an emittance of 0.75 - 0.85, is seen to reach a temperature of about 2400°F. These temperatures exceed the maximum use temperatures of these materials, thus coatings that will reduce catalicity without decreasing emissivity are needed. The Langley Research Center is conducting work in this area with a target for the equilibrium temperature of 2000°F. This goal requires a coating with a value of surface recombination efficiency in the transition range from oxides to glasses.

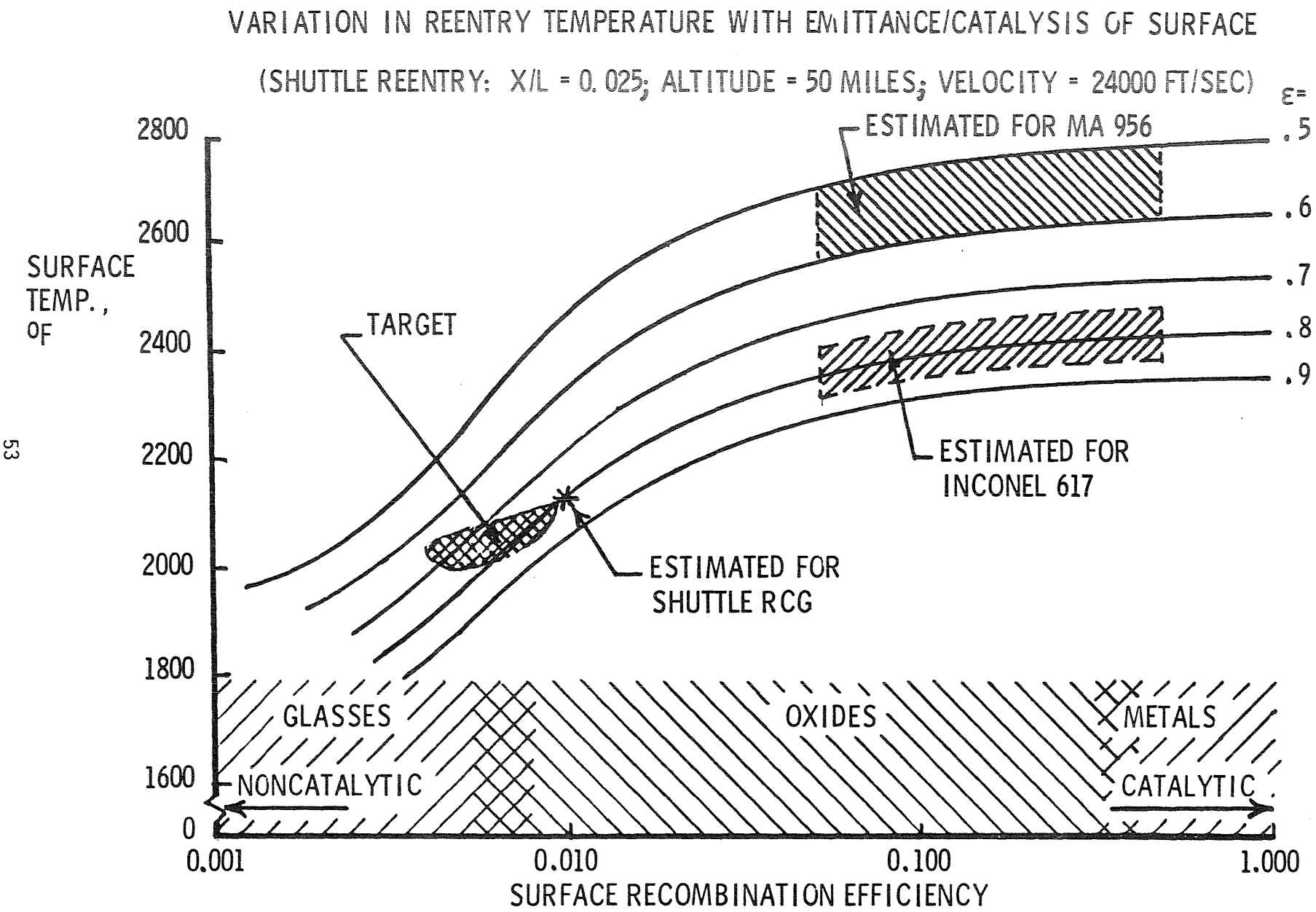
VARIATION IN REENTRY TEMPERATURE WITH EMITTANCE/CATALYSIS OF SURFACE
(SHUTTLE REENTRY: X/L = 0.025; ALTITUDE = 50 MILES; VELOCITY = 24000 FT/SEC)
ε=
ESTIMATED FOR MA 956
.5
.6
.7
.8
.9
SURFACE TEMP., °F
2800
2600
2400
2200
2000
1800
1600
0
TARGET
ESTIMATED FOR INCONEL 617
ESTIMATED FOR SHUTTLE RCG
GLASSES
OXIDES
METALS
NONCATALYTIC
CATALYTIC
0.001
0.010
0.100
1.000
SURFACE RECOMBINATION EFFICIENCY

Figure 25

COATINGS REDUCE CATALYSIS OF SUPERALLOYS

Superalloys in metallic thermal protection system (TPS) applications must have good resistance to dynamic oxidation, have a high emittance, and have low catalysis to the recombination of dissociated oxygen and nitrogen. A number of superalloys have been found to have good oxidation and/or emittance characteristics; however, the naturally occurring oxides of most metals tend to catalyze the recombination of oxygen and nitrogen. Two alloys of interest are Inconel 617 and MA 956.

Inconel 617 ha a high-temperature emittance greater than 0.8 under simulated reentry conditions; however, MA 956 has a low emittance (about 0.55) and very high resistance to oxidation. The low emittance of MA 956 results from Al_2O_3 that forms at the surface, shielding the alloy from oxidation.

Chemical vapor deposited coatings have been successfully applied to statically oxidized Inconel 617 and MA 956 superalloys by reacting silane and borane in the presence of hydrogen gas (Ref. 57). The coatings were formulated to have a high emittance and a low catalysis. Results from simulated reentry testing of coated specimens indicated the coated MA 956 has both increased emittance and low catalysis and the coated Inconel 617 has low catalysis after 5 hours (30 cycles) of exposure at 2000°F.

The figure shows the effect of the coating of MA 956 for the $q = 16$ BTU/ft$_2$-sec exposure conditions is to reduce the surface temperature by 525°F compared to the uncoated MA 956. The effect of the coating of Inconel 617 is about half that for MA 956 because of interaction of the coating and alloy oxide and because the high emittance of Inconel 617 is not improved by the coating.

COATINGS REDUCE CATALYSIS OF SUPERALLOYS

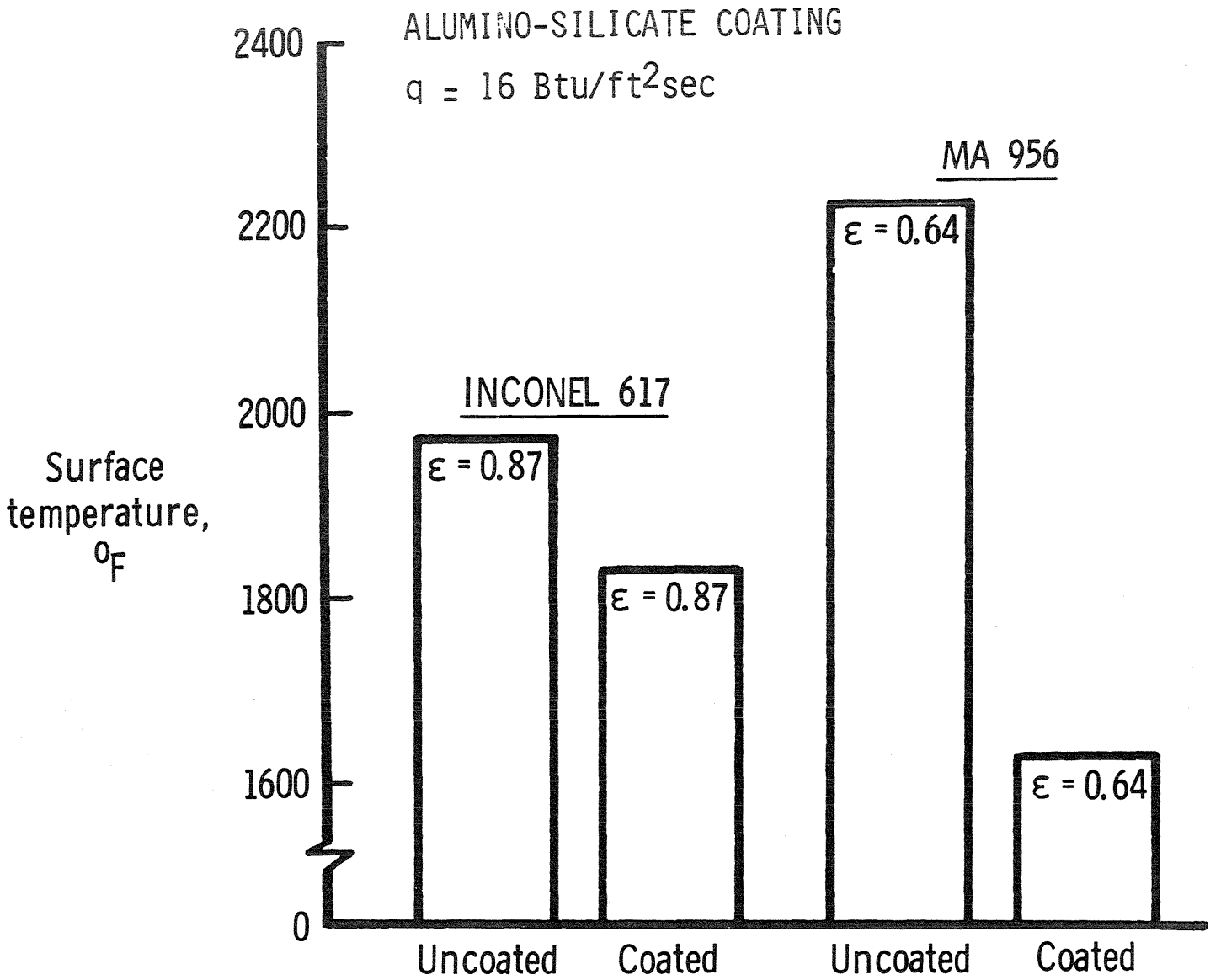

Figure 26

STRENGTH EFFICIENCY OF VARIOUS MATERIALS

The effect of temperature on the ratio of tensile strength to density for several classes of high-temperature materials is shown in figure 27. The major advantage of carbon-carbon materials for high-temperature applications is that they do not lose strength as the use temperature is increased. This is in contrast to other structural materials such as superalloys and ceramics.

This figure shows three levels of carbon-carbon strength efficiency. The first, labeled Shuttle material, is the strength level of the RCC material used in the Shuttle thermal protection system. Even though this material is made with low-strength carbon fibers, its strength efficiency is superior to both superalloys and ceramics at temperatures above 1800°F. Recent research has led to the development of an advanced carbon-carbon (ACC) that is twice as strong as the RCC. This material is currently being evaluated by a number of laboratories. The ACC material is made up using woven carbon cloth. If unidirectional carbon fiber tapes are interplied with woven cloth to create a hybrid ACC, its strength in at least one direction can be increased to 50,000 psi or more. Research on hybrid ACC is just beginning. More details are give in Reference 58.

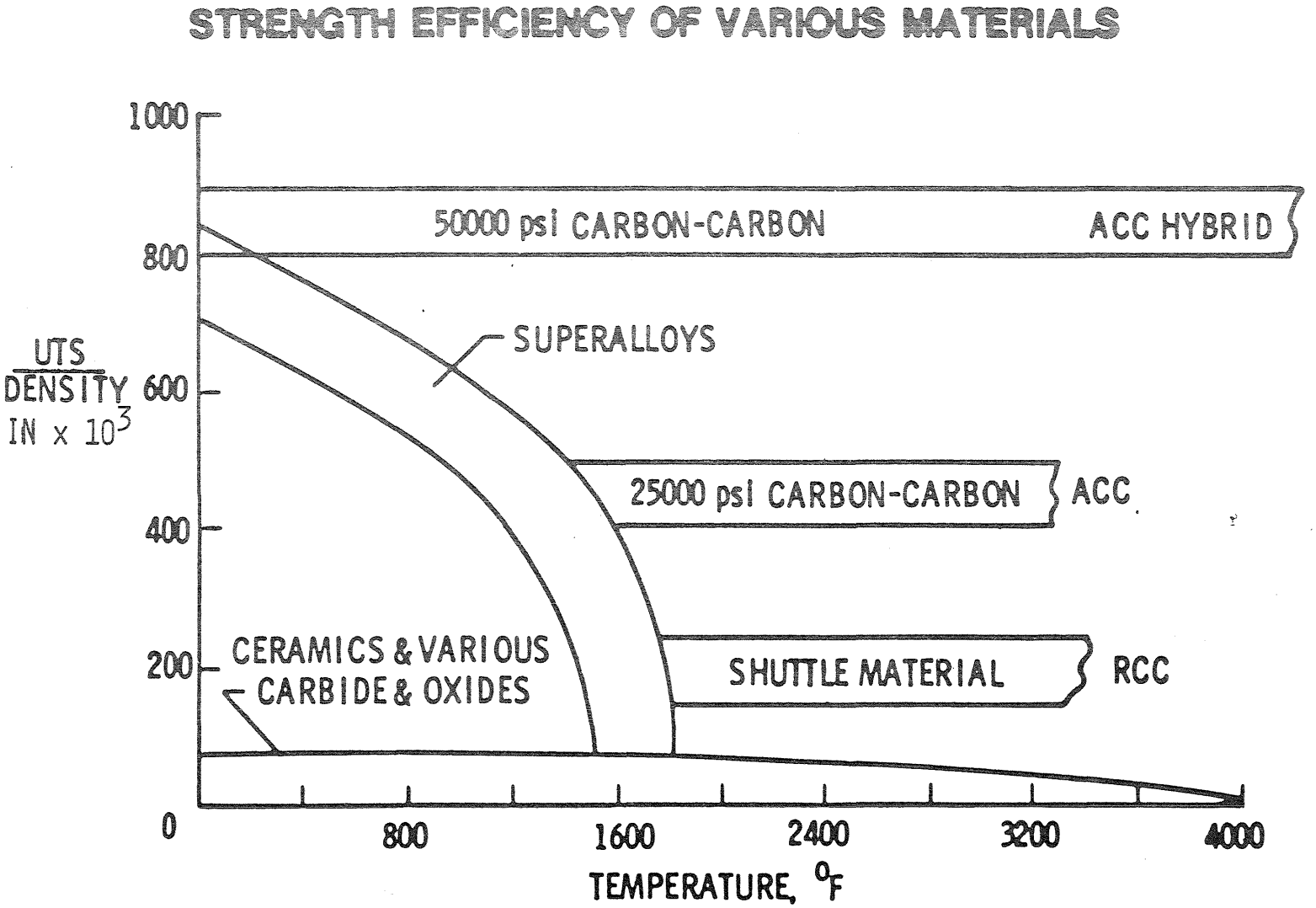
STRENGTH EFFICIENCY OF VARIOUS MATERIALS
1000
800
600
400
200
0
UTS / DENSITY IN x 10^3
50000 psi CARBON-CARBON
ACC HYBRID
SUPERALLOYS
25000 psi CARBON-CARBON
ACC
CERAMICS & VARIOUS CARBIDE & OXIDES
SHUTTLE MATERIAL
RCC
800
1600
2400
3200
4000
TEMPERATURE, °F

Figure 27

CARBON-CARBON SURFACE IMPACT DAMAGE

Front surface damage due to impact (Ref. 59) is shown in Figure 28 for coated carbon-carbon material containing 18 plys of T-300 eight harness satin weave fabric layed up in alternating 0 and 90 degree orientations. Front and back surfaces of the specimens were conversion coated to a depth of about 1.5 plys with silicon carbide followed by a tetreathyl orthosilicate high temperature sealer and a low temperature sealer. The specimens were impacted with a 0.50 inch diameter aluminum projectile at various velocities. The specimens were clamped between aluminum plates with 2.5 in. diameter holes in front and back as shown. The aluminum plates were supported by a massive backstop and the specimen impacted at its center. The projectile was propelled by a compressed air operated gun. The velocity of the projectile was controlled by varying the air pressure and was determined by measuring the time required for the projectile to traverse two light beams located 6.0 inches apart at the end of the gun barrel.

Front surface damage area is shown as a function of (qualitative) impact energy for three energy levels. At the lower impact energy level, front surface damage is characterized by a slight spherical indentation in the material coating with a diameter considerably less than the projectile diameter. At the high energy level, the front surface damage consists of a spherical indentation and a local loss of coating. At the intermediate impact energy level, the damage is only slightly greater than that obtained for the low impact energy levels. Projecting the curve given for the three impact levels to a zero damage area results in a threshold energy level for front surface damage. Back surface damage for the low impact energy levels consist of coating cracks and is less severe than the front surface damage. At the higher impact energy levels, back surface damage is characterized by spallation of the coating and is equal to or more severe than the front surface damage.

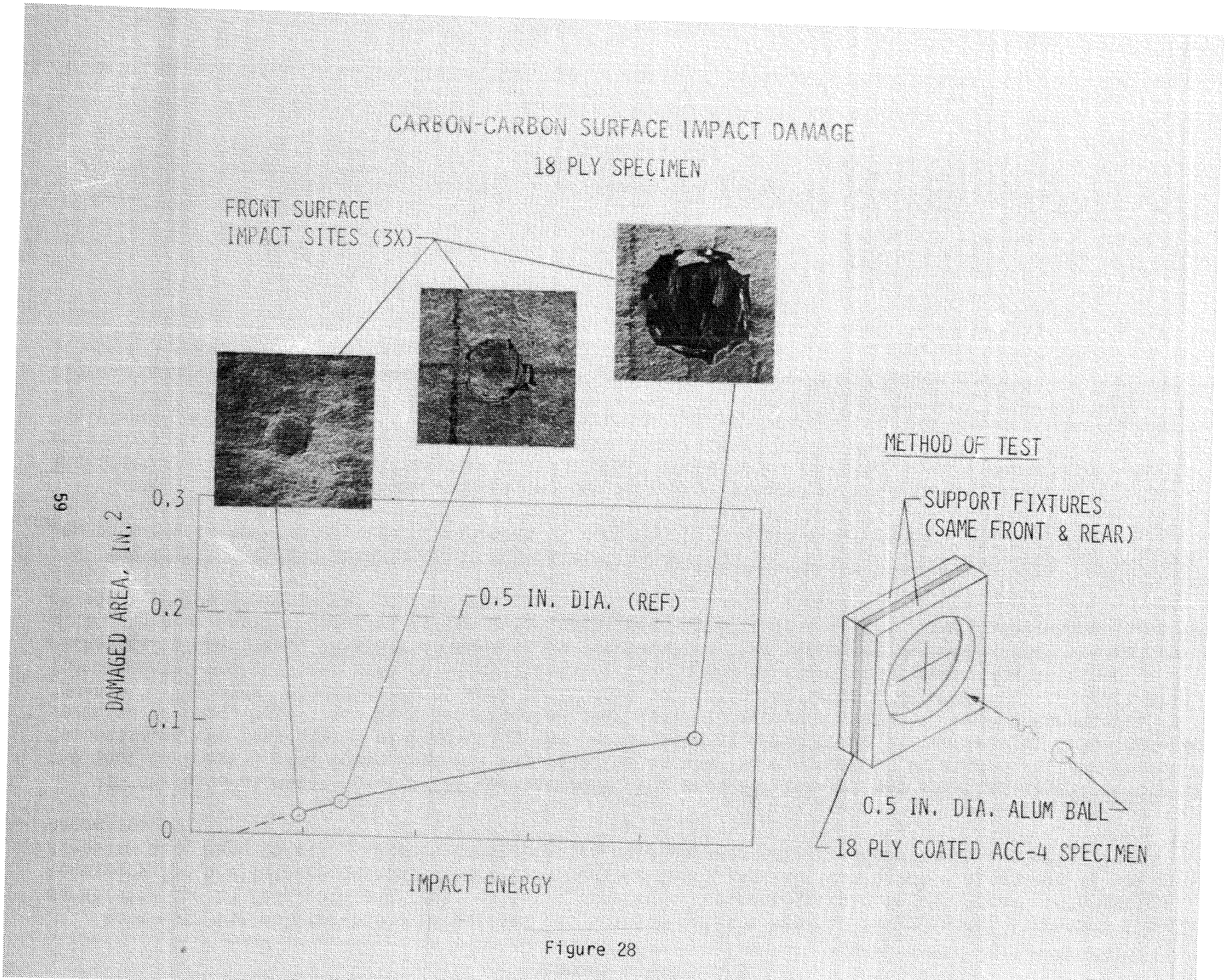
CARBON-CARBON SURFACE IMPACT DAMAGE
18 PLY SPECIMEN
FRONT SURFACE
IMPACT SITES (3X)
DAMAGED AREA, IN.2
0.3
0.2
0.1
0
0.5 IN. DIA. (REF)
IMPACT ENERGY
METHOD OF TEST
SUPPORT FIXTURES
(SAME FRONT & REAR)
0.5 IN. DIA. ALUM BALL
18 PLY COATED ACC-4 SPECIMEN

Figure 28

SUMMARY - MATERIALS

Work with the polymer-based composites has pointed out the need to fully assess long-term structural durability and to fabricate and test realistic structural components to gain the "real" information necessary for preliminary design. Short time tensile tests and fabrication of flat panels is not an adequate data base to allow serious consideration of a polymer matrix composite to typical flight hardware.

In the area of metallics for TPS applications, the state-of-the-art has advanced significantly since the Shuttle Phase B time frame when RSI was selected as the TPS of choice. Work on creep prediction has demonstrated the feasibility of predicting the performance of complicated, flight-weight TPS. More work needs to be done, but it has been demonstrated that cyclic creep prediction of complex structures is "doable." The major significance of work to improve the creep performance of H-188 was the fact that the improvements were obtained with no alloy chemistry change and no significant reduction in other mechanical properties. This should suggest to the industry that there are probably other superalloys which can have their properties tailored for particular applications by the "smart" development and use of advanced thermomechanical processing.

The feasibility and advantages of non-catalytic coatings for metallic TPS, have been demonstrated. The task now is to complete the development of durable, high emittance, non-catalytic coatings.

Carbon-carbon composites are an exciting new family of structural materials. Recently ACC hybrid architectures have been demonstrated with tensile strengths up to 100 psi. From a materials point-of-view there is still a great deal to learn about processing science, oxidation protection, impact resistance, and a host of other issues. As more potential applications for ACC appear, more resources for R&T will be devoted to this exciting class of materials. As our understanding, particularly microstructure/property relationships, increases ACC will become a full-fledged member of the aerospace structural materials community.

SUMMARY - MATERIALS

- CASTS PROGRAM DEMONSTRATED FEASIBILITY OF G/PI STRUCTURES
- REFINED STATE-OF-THE-ART FOR CREEP OF METALLICS FOR TPS DEVELOPMENTS
- DURABLE, HIGH EMITTANCE, NON-CATALYTIC COATINGS FOR METALLIC TPS ARE FEASIBLE
- CARBON/CARBON COMPOSITES ARE A PROMISING NEW FAMILY OF MATERIALS

Figure 29

DETAILED AEROTHERMAL ENVIRONMENT IN SHUTTLE GAPS UNKNOWN AT INITIATION OF PHASE B, 1972 STUDIES

The Langley Research Center initiated a program in detailed aerothermal loads in the late 1970's. The rationale for this program is illustrated on Figure 30. There are detailed, generic surface irregularities such as gaps and protuberances that will exist on most high speed vehicles, yet there was no systematic exploration of the flow disturbances and augmented heating caused by such irregularities. For example, as shown on Figure 30, for the high Mach number flow encountered by the orbiter there was one reference in the open literature on heating in gaps similar to the gaps between the Shuttle tiles, no published work relevant to the gaps between the split elevons, and only two documents relating to the flow environment of a wing-elevon-cove region. This lack of data led to excessive cost and delays in component development for the Shuttle project. Urgent requests for tests and analysis disrupted ongoing research and development efforts and resulted in "reaction to crises" type studies. The Shuttle experience was not an exception, but is the rule all to familiar to project managers of previous and on-going high speed vehicle projects. Since such surface irregularities can be anticipated and defined in a generic sense, a combined experimental and analytical program is in progress to provide a data base and prediction/extrapolation technique for use in design of future high speed vehicles.

DETAILED AEROTHERMAL ENVIRONMENT IN SHUTTLE GAPS UNKNOWN AT INITIATION OF PHASE B 1972

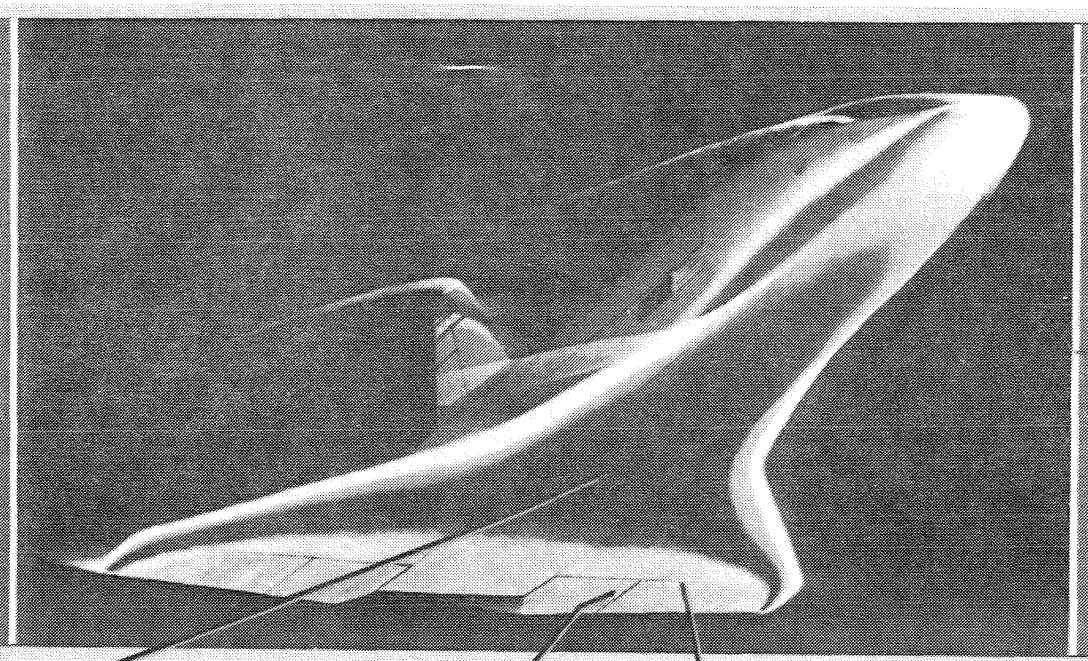

TILE GAPS	SPLIT ELEVON CHORDWISE GAP	WING ELEVON GAP SPANWISE GAP
1970 WIETING TND 5908	NONE	1968 HAMILTON & DEARING NASA TN D4686 1968 DEARING & HAMILTON NASA TN D4911

- EXCESSIVE COST & DELAY IN PROJECT
- DISRUPTED RESEARCH & CAUSED SCRAMBLE TO DEFINE ENVIRONMENT

Figure 30

FLOW ANGULARITY EFFECTS ON TILE/GAP IMPINGEMENT HEATING

Previous aerothermal tests on Shuttle type tiles in the LaRC 8' HTT (Ref. 60, 61) identified the effects of boundary layer and gap geometry on the impingement heating rate on the tile's forward face at the end of the longitudinal gap aligned with the flow ("T" gap). However, more detailed heating data was needed to define the overall tile heating at various flow angles for Shuttle tile certification. Reference 62 extended the previous effort to include the effect of impingement heating on the upstream tile corner due to flow angularity with respect to the longitudinal gap. Flow angles include 0, 15, 30, 45, and 60 degrees. In addition, the effects of boundary layer state and thickness, Reynolds number, and gap width on localized heating, which affects tile coating and overall heating which effects the structural integrity, were studied.

In order to obtain the desired heating detail, a highly instrumented thin-wall metallic tile was tested in the 8' HTT as shown in the tile array in the figure. A special technique was used to fabricate the thin-wall tile (Ref. 63).

Preliminary results indicating flow angularity effects for laminar and turbulent boundary layers on the peak impingement heating for a gap width of 0.070" are shown in Figure 31. The heating rates are nondimensionalized to the theoretical flat plate value. For laminar flow, the impingement heating at the upstream corner and at the end of the "T" gap are relatively constant for $\Lambda < 453°$. For $\Lambda > 45°$, the increased heating probably reflects increasing flow in the uninterrupted gap as the gap becomes more closely aligned with the flow. For turbulent flow the behavior of the heating at the corner is very similar to that of the laminar flow. However, impingement heating at the end of the "T" gap is significantly higher at $\Lambda = 0°$ but reduces with flow angle. Typically for turbulent flow, the heating at $\Lambda = 45°$ was 1.25 times the flat plate value, which correlates well with the Shuttle rule-of-thumb design guideline of increasing heating by 20 percent to account for the effects of the tile gaps.

FLOW ANGULARITY EFFECTS ON TILE/GAP IMPINGEMENT HEATING

TEST APPARATUS IN 8FT HTST

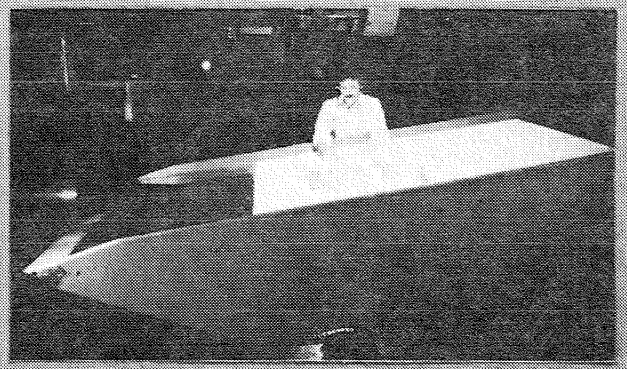

TILE/GAP MODEL

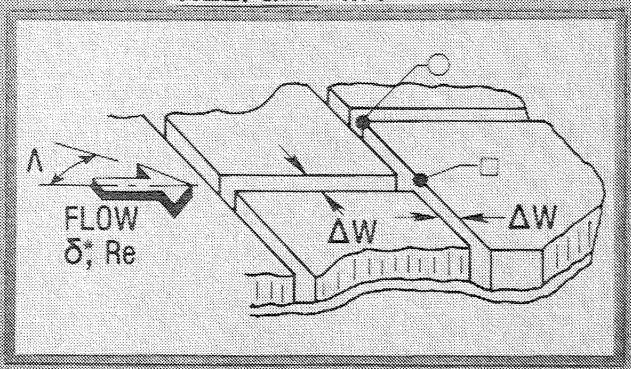

LAMINAR HEATING

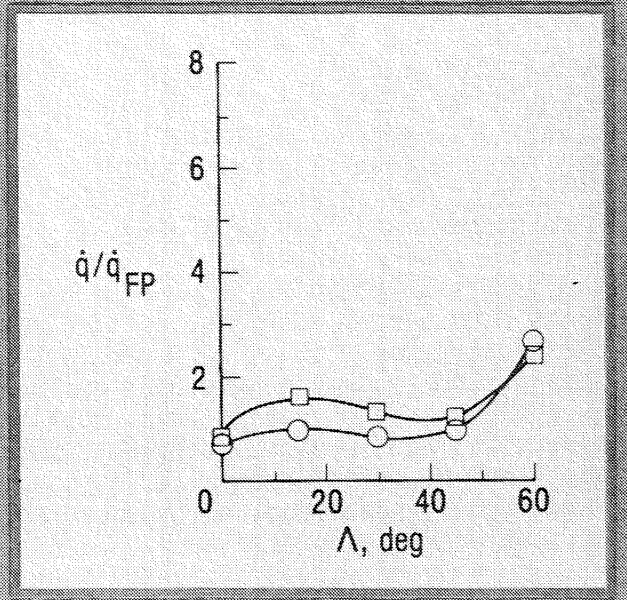

TURBULENT HEATING

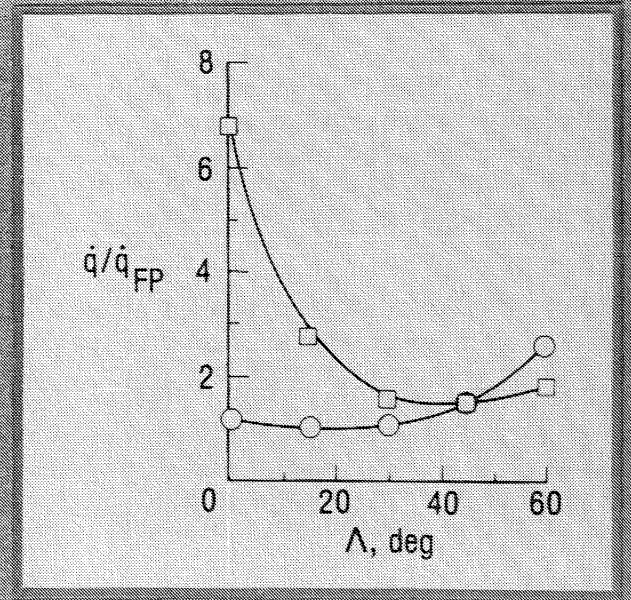

Figure 31

CHINE TILE-GAP HEATING MODEL

The application of reusable surface insulation tiles on the Shuttle has introduced local flow disturbances associated with the gaps between tiles. The effects of these disturbances and the resulting flow penetration into the tile gaps has been studied extensively on flat surfaces (Ref. 60-62). Important parameters including gap width and length and flow angularity have been identified, and the effects on localized and total heat loads have been evaluated. Similar studies are needed for curved surfaces where natural pressure gradients occur that would cause greater flow ingestion into the tile gaps and augment the aerothermal loads. For the Shuttle, many of the tile gaps are filled to circumvent this problem, but this practice costs in weight and labor. The actual aerothermal loads associated with tile gaps on the chine with higher surface pressure gradients need to be defined to serve as a data base for future thermal protection system designs.

The Curved Surface Test Apparatus, CSTA, has been developed as a test bed for the Langley 8-Foot High Temperature Tunnel. The CSTA is representative of the forward portion of a lifting body and the complex, three-dimensional flow field around this body has been defined experimentally and anaytically (Ref. 64). An extensive array of simulated tiles has been designed and fabricated that covers the aft portion of one side of the CSTA shown in Figure 32 sitting on the floor next to the rest of the model which is mounted on a work table. Three thin-wall, metallic heat-transfer tiles, one for the small radius chine and two for the large radius chine, will be located adjacent to solid tiles instrumented with pressure orifices to determine the aerothermal effects in the tile gaps.

The Chine Tile-Gap Heating Model fabrication was completed in FY 84 and aerothermal tests in the 8' HTT are scheduled for early FY 86. During the interim, the application of additional newly developed instrumentation that will help characterize flow in the gaps is being investigated.

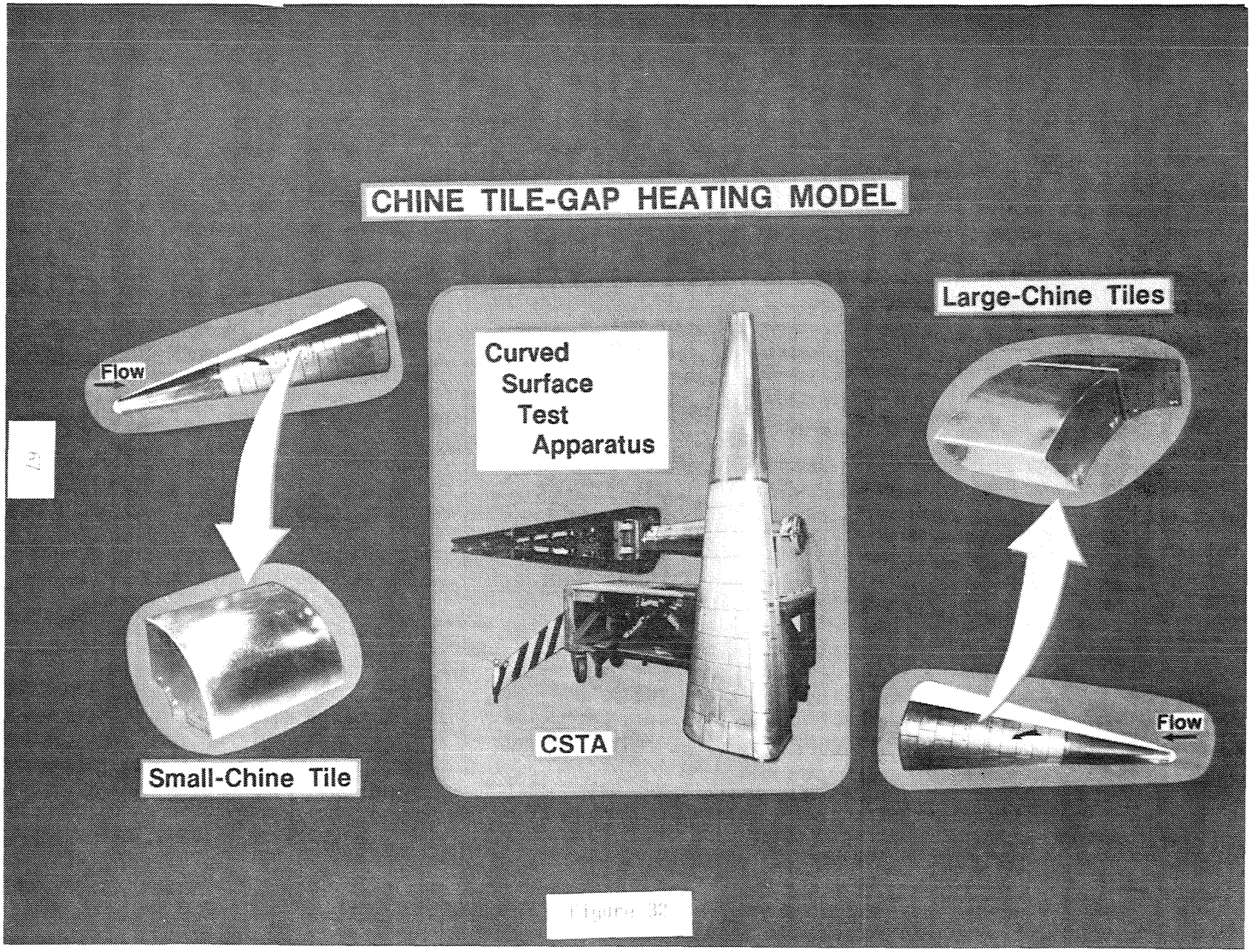
CHINE TILE-GAP HEATING MODEL
Flow
Small-Chine Tile
Curved
Surface
Test
Apparatus
CSTA
Large-Chine Tiles
Flow

AEROTHERMAL TEST OF WING-STUB/ELEVON JUNCTION

The Shuttle Orbiter is designed with split, wing elevons which require dynamic seals along the hinge line and at the stub enclosures to prevent ingestion of aerodynamically heated gases. Also, cross-flow around the edges of the deflected elevons could produce excessive heating loads to the chordwise gaps of the stub enclosures and the elevon side walls. Since complex flow effects between elevons are not amenable to proven analytical techniques, an experimental investigation was initiated to determine aerodynamic heating flux distributions at the wing-stub/elevon junction. The original Shuttle baseline design for the TPS of the elevon sidewalls assumed a sidewall heating equal to windward surface heating of the elevon for laminar and turbulent flow. Therefore, the original TPS for the elevon gap was HRSI tile. Tests at NASA Ames of a scale model in laminar flow indicated gap heating 136% of the corresponding elevon heating. Assuming the same relationship for turbulent flow, the TPS of the elevon gap was changed to an ablator.

In order to obtain results for turbulent flow the split elevon model shown in figure 33 was tested in the NASA Langley 8-Foot High Temperature Tunnel with a turbulent boundary layer on the wing and elevon. A full-scale model was required for tests to establish reasonable flow boundary layers ahead of the junction and the proper flow regime within the narrow chordwise gaps and between elevons. The flow pattern between elevons was studied, and the pressure and heat load was determined within the chordwise gaps formed by adjacent elevons and by the stub fairing which separates the elevons. Model angle of attack, elevon deflection angle, and gap width were varied. Heating in the gaps was generally proportional to windward surface heating and inversely proportional to gap width. Maximum heating between the elevons was 30 percent of the heating on the windward elevon surface for a wide elevon gap (Ref. 65).

During the first five Shuttle flights the ablation in the elevon gaps was less than expected (Ref. 66). Accordingly, prior to STS-5, the lefthand side installation was replaced with tiles. Post flight inspection revealed no evidence of inboard tile overheating; however, the outboard tiles along the tile edge were glazed and the surface was rough because of melting and overheating. The increased heating is attributed to gap fillers which extend out of the tile gaps, resulting in a localized disturbed flow (Ref. 66). HRSI tiles have been used for all subsequent flights.

AEROTHERMAL TEST OF WING–STUB/ELEVON JUNCTION

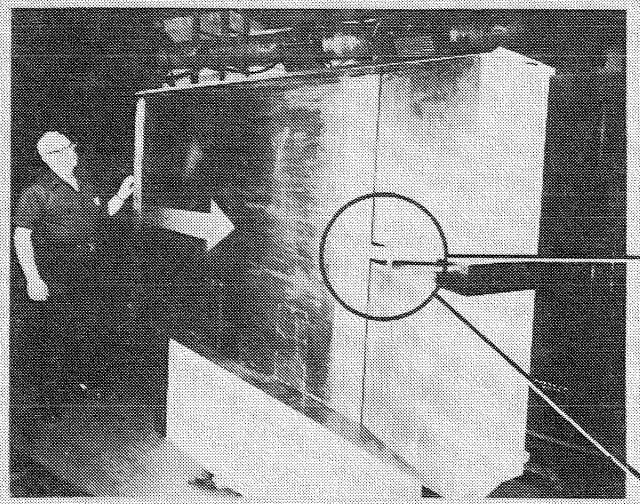

SPECIALIZED TEST APPARATUS

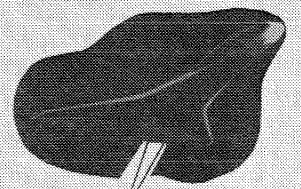

CHORDWISE GAPS

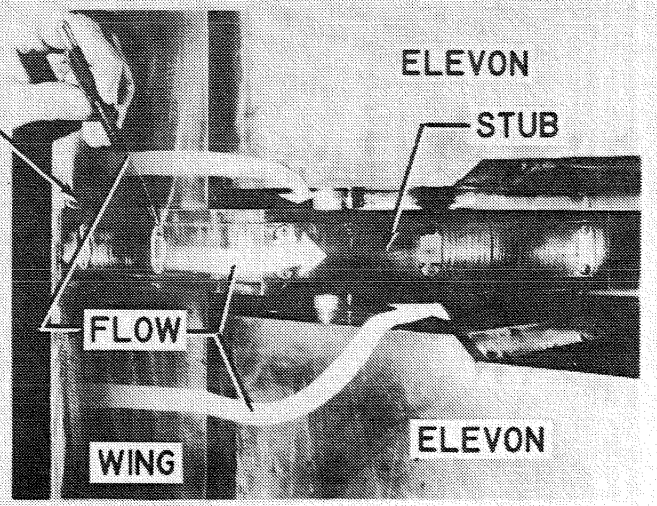

WING STUB DETAILS

- EXPERIMENTAL HEAT FLUX LESS THAN THAT ASSUMED FOR DESIGN

Figure 33

UNSEALED WING-ELEVON COVE HEATING CHRACTERISTICS AT M = 6.8 FOR SEPARATED FLOW ON WING

An extensive investigation was conducted at a free-stream Mach number of 6.8 in the Langley 8' HTT to define effects of laminar flow separation on aerodynamic heating in a leaking cove of a full-scale representation of the wing-elevon juncture (Fig. 34) on the Space Shuttle Orbiter (Ref. 67). The investigation is part of an on-going effort to collect information on the nature of cove flow for use in formulating a method for predicting the thermal response of an unsealed cove structure for winged reentry vehicles (Ref. 68, 69).

The extent of flow separation was varied by changing the cove seal leak gap (0 to 0.5 inch), elevon deflection (15° to 35°), and free-stream unit Reynolds number (0.4×10^6 to 1.4×10^6 per ft.). Pressure and cold-wall heating-rate distributions were obtained along the wing, cove, and elevon surfaces shown on the simplified cross-sectional view at the upper right for an angle of attack of 5°.

Three typical heating-rate distributions present heating rates referenced to the wing value for laminar attached flow at the cove entrance for various flow separation distances obtained with 12.5- and 50-percent leaks (0.06- and 0.25-inch gaps) and elevon deflections of 15° and 25° at a free-stream unit Reynolds number of 0.4×10^6 per ft. When laminar flow separation occurs near the cove entrance, wing heating rates under the separated boundary layer decrease sharply from equivalent attached-flow values, and cove heating rates diminish from the cove entrance by an order of magnitude. Increasing the elevon deflection angle extends the length of flow separation, and, as shown by the rising wing heating rates, the separated laminar boundary layer transitions to turbulent flow ahead of the cove entrance. Consequently, cove heating rates are an order-of-magnitude greater than for purely laminar flow separation at the same cove seal leak gap. However, if the leak gap increases sufficiently, boundary-layer suction can force the separated boundary layer to reattach, in which event cove heating rates approximate the level of heating for laminar flow separation. As indicated, the agreement between test data and calculated values is good. Calculations for cove heating were obtained using a simple 1-D math model (Ref. 70) which assumed laminar developing channel flow. Scatter of cove data about the predicted distribution results from abrupt changes in flow path and cove area which are not accounted for by the constant-area channel-flow math model.

UNSEALED WING-ELEVON COVE HEATING CHARACTERISTICS AT M=6.8 FOR SEPARATED FLOW ON WING

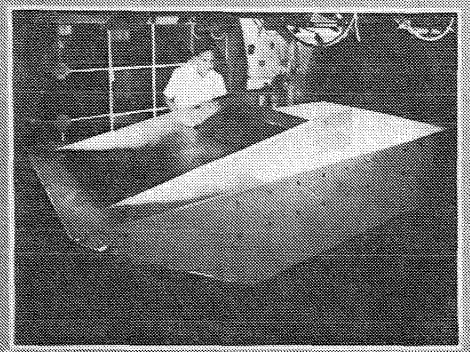

TEST APPARATUS IN 8 ft HTST

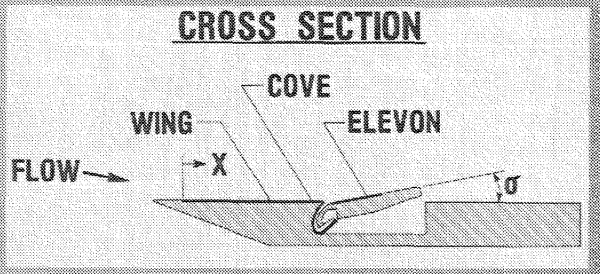

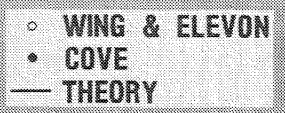

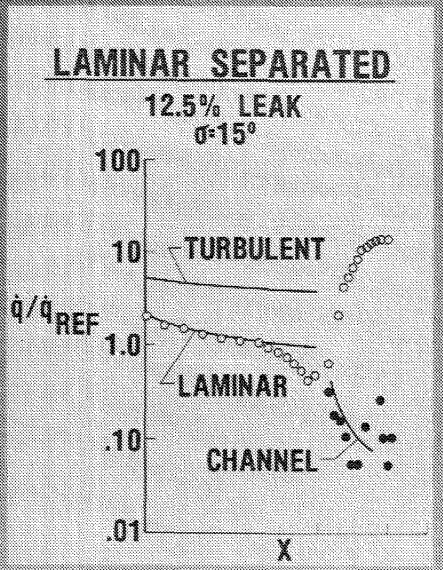

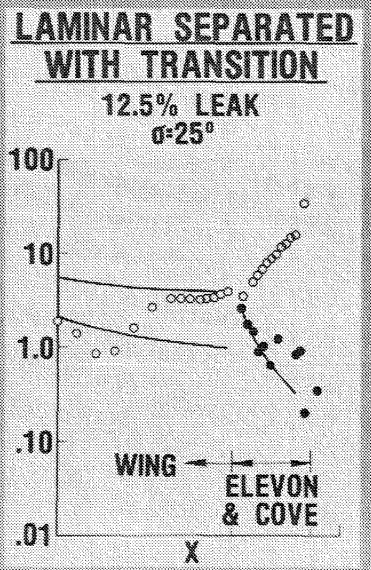

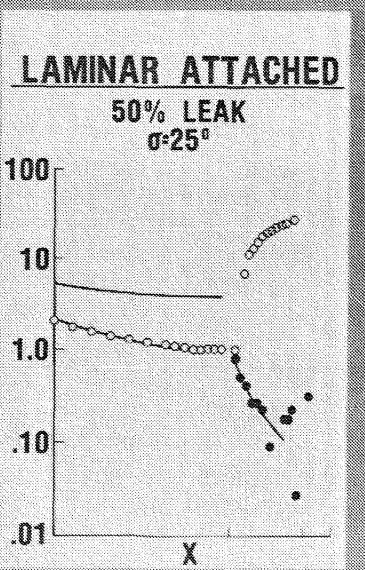

Figure 34

NASA DRYDEN FLIGHT LOADS RESEARCH FACILITY

The Flight Loads Research Facility (FLRF) is a unique national facility which has the capabiliy for testing structural components and complete vehicles under the combined effects of loads and temperatures, as described in Reference 71 and illustrated in Figure 35. The FLRF is also used for calibration and evaluation of flight loads instrumentation under the conditions expected in flight. The facility provides close support of flight to flight program planning by permitting structural-integrity testing, instrumentation calibration, ground vibration tests, mass property testing, and the analysis of unexpected problems in the course of research vehicle flights.

Major improvements to the facility are being implemented or planned. These include a new data acquisition and control system of both thermal and mechanical loads (in progress), and acquisition of additional load frame test machines with increased capacity (up to 500K lb) (planned). The following future capabilities are currently under study:

CAPABILITY	DESCRIPTION
Cryogenics	Investigation and development of test capabilities to liquid hydrogen temperatures using a combination of LN_2 and LHE.
Vacuum Chamber	Develop test capabilities for combined heat, load, cryogenic, and vacuum of medium sized (desk size) specimens.
Very High Temperatures	Expand envelope and develop test capabilities for radiant testing at temperatures in the range of 3000 - 4000 Deg. F.
Measurement Technology	Investigation and development of temperature and strain measurement technology at temperature extremes.

NASA DRYDEN FLIGHT LOADS RESEARCH FACILITY

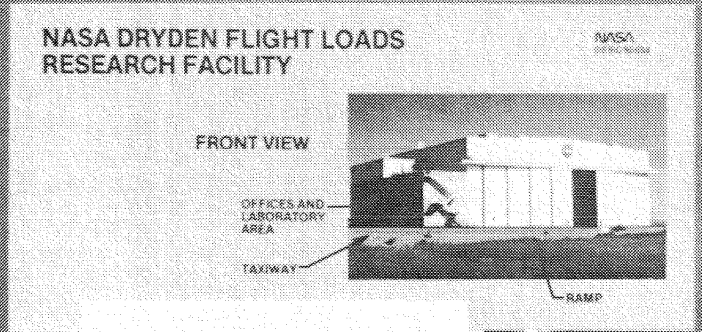

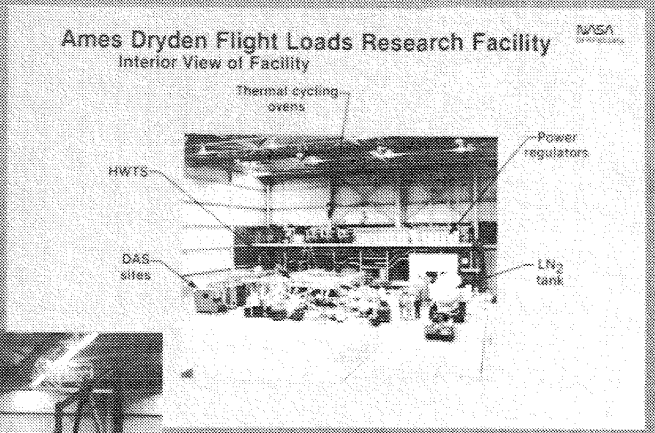

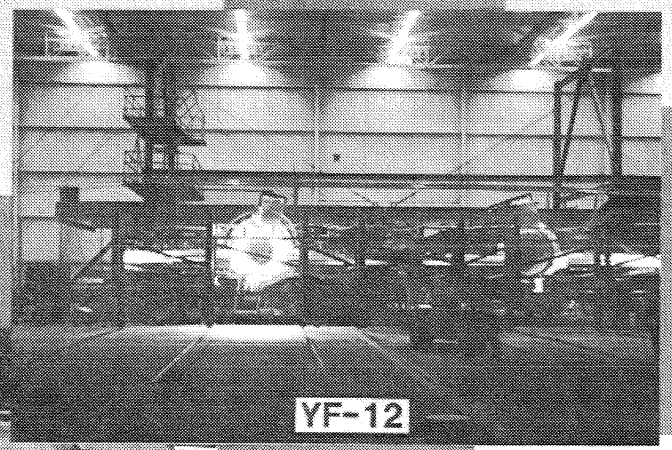

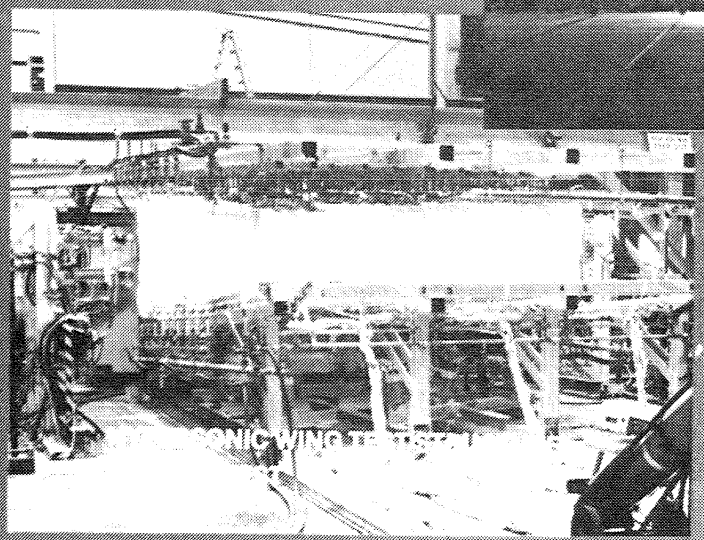

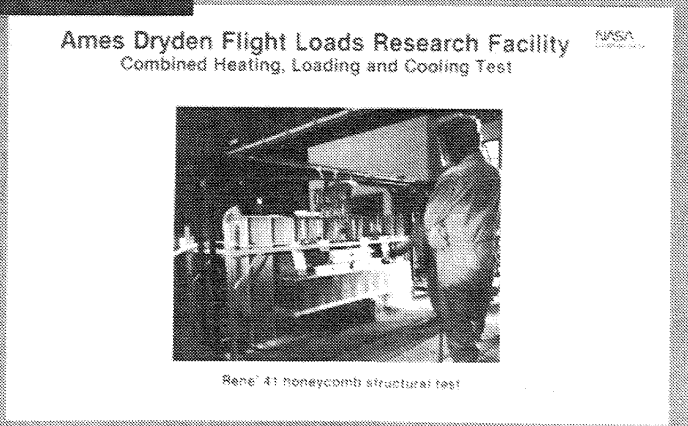

Figure 35

NEED FOR LARGER STRUCTURAL HEAT TRANSFER MODEL FOR ON-ORBIT THERMAL CALCULATIONS

Shuttle experience has shown that the design of large structures for the hostile re-entry environment taxes the capabilities of existing thermal and structural analysis methods. The overall thermal model of the Shuttle Orbiter (Fig. 36) consists of 118 three-dimensional, lumped-parameter local models each having about 200 nodes. Temperatures are computed in each of the local models indicated by the shaded areas and interpolated to obtain temperatures in the unmodeled regions. About 90 percent of the temperatures used in stress calculations were obtained by interpolation. Examination of analysis requirements indicated that certain complicating factors such as long transients, nonlinear material characteristics and radiation (including view factors) calculations were primarily responsible for the excessive resources required for the analysis. To determine the times of occurrence of the critical combinations of thermal and mechanical internal loads, it is necessary to inspect temperature-time histories from the thermal analyses. This procedure, while somewhat standard for analysis of such complicated structures, constitutes a tedious, laborious, and expensive task. For future vehicles with potentially higher structural temperatures, longer heat pulses, and more closely integrated thermal and structural functions than the current Shuttle, the analysis problems will be magnified.

Although in the past the thermal and structural functions of thermostructural concepts have been analyzed separately and interactive effects have been handled approximately, advances in optimization processes (Ref. 12) portend the development of effective integrated thermostructural analysis (Ref. 72-74) and design capability. With such capability, the selection of optimum structural systems for a future space transportation system can be enhanced at an early stage in the design process.

With regard to the Shuttle Orbiter calculations, there was some uncertainty and uneasiness associated with the use of interpolation. Thus NASA Dryden was asked to develop more detailed thermal models to provide a check on the interpolated values. Typical results for a complete cross-section are shown on Figure 36. As can be seen, there were significant differences which led to underpredicted (unconservative) thermal stresses. Consequently, NASA has undertaken a coordinated effort to develop improved thermostructural analysis techniques. These improvements will include: 1) methods to automate the more tedious aspects of generating thermal models; 2) faster solution techniques for large-order matrix equations governing nonlinear, transient heat transfer; 3) methods of automating the determination of the times at which the critical combinations of thermal and mechanical internal loads occur; and 4) improved modeling procedures to reduce model size. This effort will also include the verification of procedures through comparison with experimental results obtained from large representative structural components. A variety of papers providing a status report on efforts to improve thermostructural analysis techniques were presented at a recent symposium (Ref. 10).

NEED FOR LARGER STRUCTURAL HEAT TRANSFER MODEL

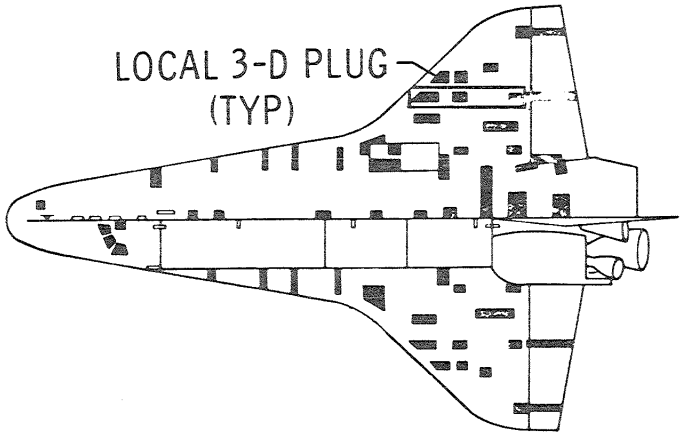

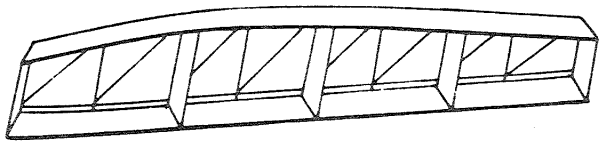

- PLUG MODELS/SMEARED TEMPERATURES
- COMPLETE CROSS-SECTION MODEL

- COMPARISON OF SPAR AND SMEARED TEMPERATURES

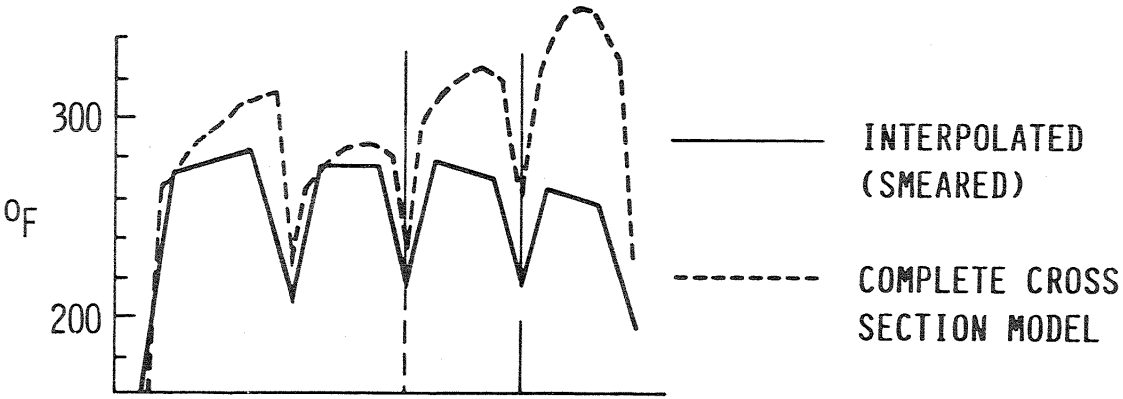

CHORDWISE TEMPERATURE DISTRIBUTION

Figure 36

STUDY OF THERMAL MATH MODEL SIZE REQUIREMENTS

The SPAR (Ref. 75) finite element reentry heat transfer analysis of the Space Shuttle Orbiter was started by using the most simple model and gradually extended to more complex models. Three wing segments, one entire left wing, and one fuselage cross section were selected for setting up the SPAR finite element models. A total of nine models were set up, and the four shown on Figure 37 are listed below:

1. 1-Dimensional model for WS 240 Bay 3
2. 2-Dimensional model for entire WS 240
3. 3-Dimensional model for entire WS 240
4. 3-Dimensional model for the entire left wing

The 1-D model for WS 240 Bay 3 was set up concurrently with a finite difference model for comparison of the structural temperatures obtained from the finite element and the finite difference methods. The results of the two methods turned out to be quite close. Figure 38 shows the structural temperatures at the lower and upper skins of WS 240 Bay 3 predicted from different SPAR thermal models. Notice that the 1-D model gives the highest skin temperatures because of neglecting the existance of both the spar webs and the trusses. The 2-D model gives intermediate skin temperatures because the spar webs were modeled. The 3-D model gives the most accurate (lowest) skin temperatures because the heat flow through the spar webs and the trusses were taken into account. The structural temperatures predicted from the complete wing model (Fig. 37), even though it has relatively coarse elements, turned out to be quite close to those predicted from the 3-D model of WS 240. The next step is to refine the complete wing model so that more accurate temperature distributions can be obtained. However, more complex computations for the three dimensional view factors for the internal radiation are expected.

STUDY OF MATH MODEL SIZE REQUIREMENTS

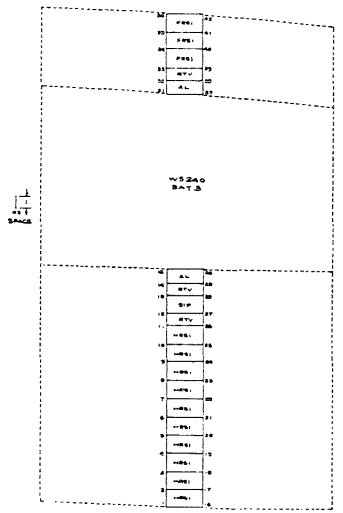

1-D
WBS 240 BAY 3

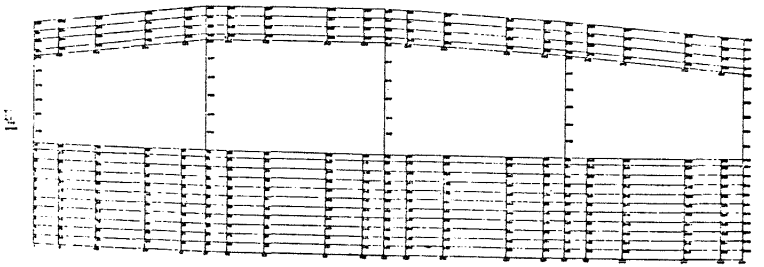

2-D
WBS 240

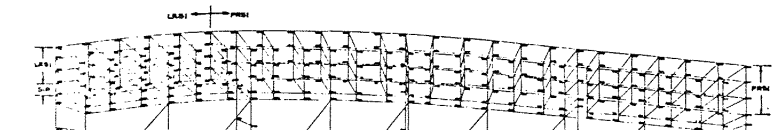

3-D
WBS 240

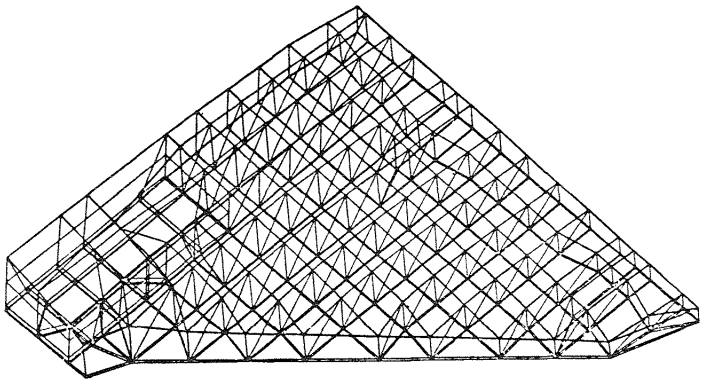

COMPLETE WING

Figure 37

Page Missing in Original Document

EFFECTS OF MATH MODEL SIZE ON CALCULATED TEMPERATURE HISTORIES

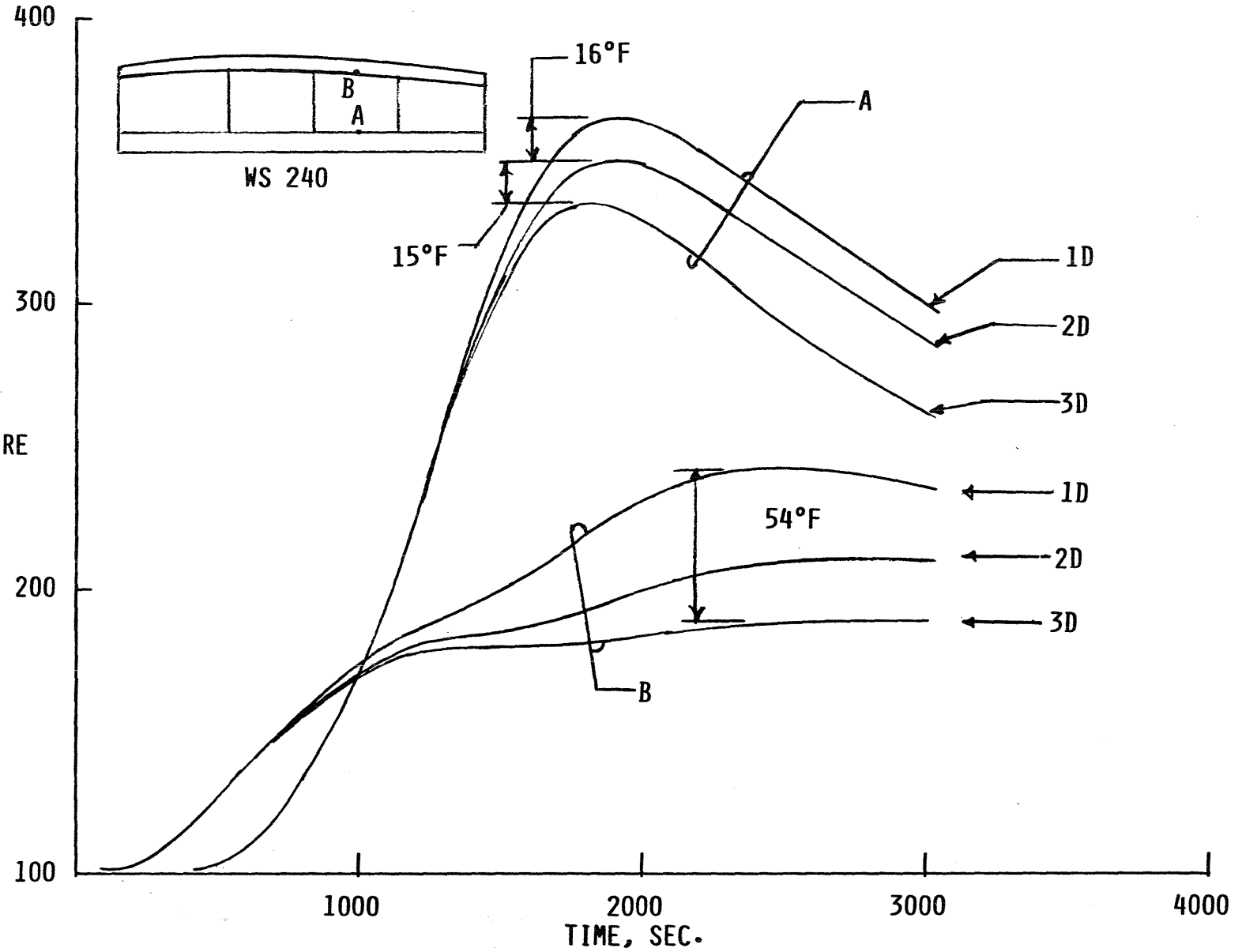

Figure 38

EFFECTS OF INTERNAL CONVECTION

The WS 240 3-D model (see Fig. 37) was used in studying the effect of internal free convection on the structural temperatures. Figure 39 shows the STS-5 flight measured temperature at the lower and upper skin of WS 240 Bay 2 compared with the SPAR predicted values with and without internal free convection. Notice that the agreement between the flight data and the SPAR predictions is fairly good and that the effect of internal free convection is not insignificant. However, the analyis still overpredicts the measured temperatures on the lower skin after touchdown and on the upper skin from 900 sec. after entry to just prior to touchdown. The discrepacy for the lower skin could be due to forced convection, which is difficult to model accurately. The discrepancy for the upper skin is not understood.

EFFECTS OF INTERNAL CONVECTION

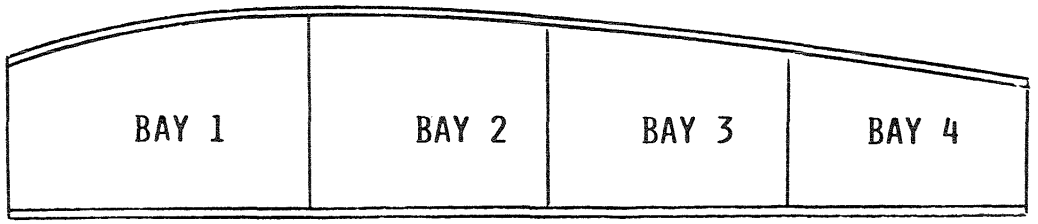

0 COMPLETE CROSS-SECTION MODEL

——— SPAR, WITH NATURAL CONVECTION

------- SPAR, WITHOUT NATURAL CONVECTION

o FLIGHT DATA

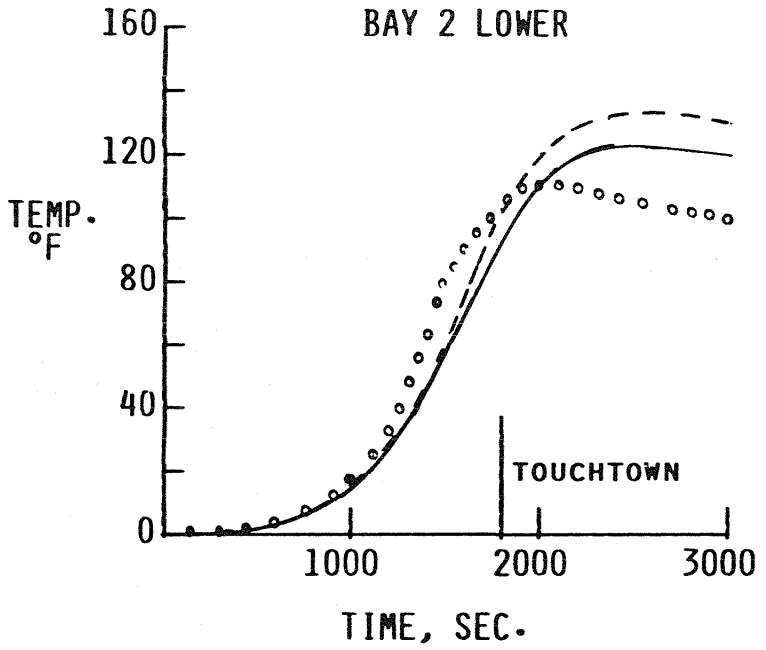

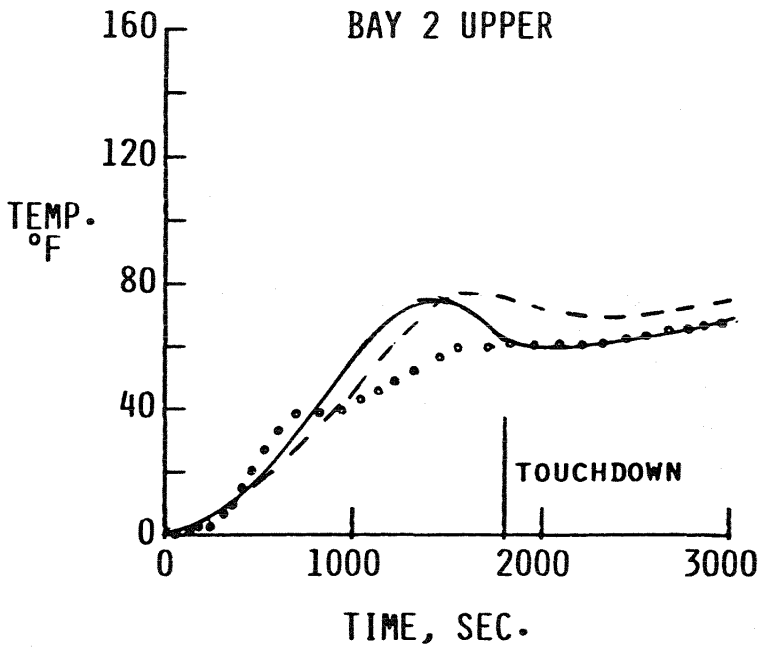

Figure 39

COMPARATIVE WEIGHTS OF INSULATED AND HOT STRUCTURES FOR VARIOUS STRUCTURAL MATERIALS VS. LOAD INTENSITY

The method of Reference 76 allows the optimization of a simple insulation-structure system based on a one-dimensional transient thermal analysis, prescribed inplane loads, and a prescribed surface temperature history. The results shown in Figure 40 were obtained by this method for a variety of insulation and structural materials. The material properties are based on the temperature expected for the loads applied (that is, low temperatures for ascent conditions, etc.). The figure shows that hot structures of such materials as Rene 41, advanced carbon-carbon, and a hybrid carbon-carbon provide the lowest weight system for the load range covered, which is typical of the loads encountered by aerospace plane type vehicles; for higher loads the results suggest that insulated composites would become competitive. Obviously, if the flight conditions are such that the maximum use temperature of the hot structures are exceeded, then insulated structures will be required. Thus NASA Langley has been conducting research on efficient TPS and structural concepts to provide designers options for both hot and insulated structures for future high speed vehicles.

COMPARATIVE WEIGHTS OF INSULATED AND HOT STRUCTURES FOR VARIOUS STRUCTURAL MATERIALS VS. LOAD INTENSITY

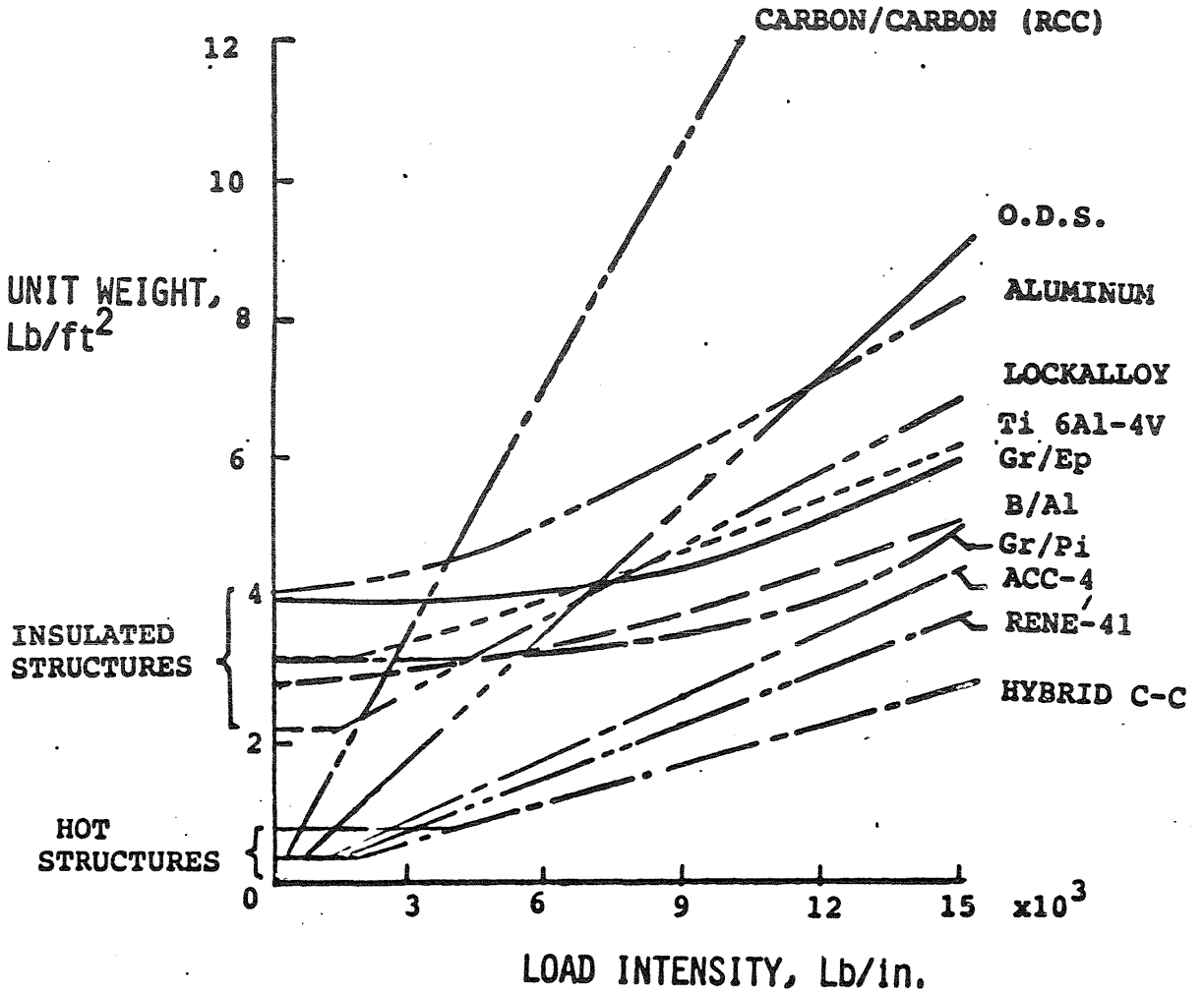

Figure 40

BASELINE SHUTTLE TPS MATERIALS

The heat shield requirements for an advanced space vehicle during entry will depend upon its configuration and desired flight capabilities. These requirements will be more demanding (i.e., greater toughness and/or temperature capability) and different from those defined for the current Shuttle Orbiters. The baseline Shuttle thermal protection system is composed of several materials as shown on Figure 41 including reinforced carbon-carbon (RCC), low-temperature reusable surface insulation (LRSI), flexible reusable surface insulation (FRSI), gap fillers, advanced flexible reusable surface insulation (AFRSI), and high-temperature reusable surface insulation (HRSI). The properties and capabilities of these materials define their location and degree of application on each orbiter. Research into improving the capabilities of these materials for use on an advanced vehicle has continued.

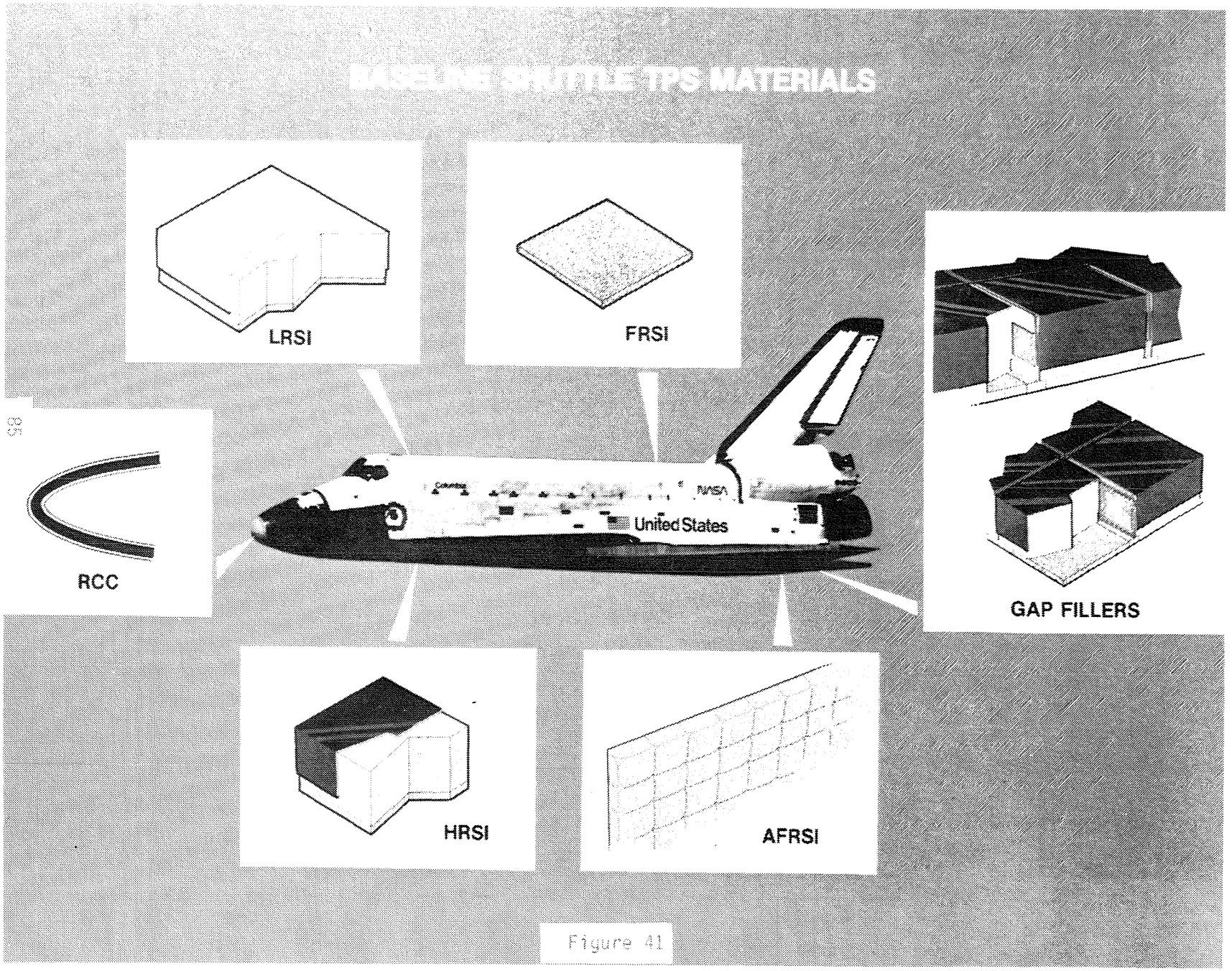
BASELINE SHUTTLE TPS MATERIALS
LRSI
FRSI
GAP FILLERS
RCC
NASA
United States
HRSI
AFRSI

Figure 41

CERAMIC TPS DESCRIPTION

The primary insulation used to protect up to 70 percent of the Space Shuttle Orbiter's exterior surface on reentry is an externally attached, rigidized fibrous silica, designated LI-900 (9 lb/ft^3 density) or LI-2200 (22 lb/ft^3 density), which has been machined into tiles approximately 6 to 8 in. square. These tiles, together with a strain isolation material, make up the High or Low Temperature Reusable Surface Insulation (HRSI or LRSI) systems. The tiles are bonded to the strain isolation pad (SIP) which in turn is bonded to the orbiter aluminum alloy skin structure using a silicon based room temperature vulcanizing (RTV-560) adhesive (Fig. 42). The SIP is required to isolate the tiles from strains due to thermal expansion of the orbiter structure and skin deflections due to aerodynamic loads. The majority of the strips of filler bar bond only to the aluminum substructure, and not to the RSI, thus providing a SIP vent path during ascent. In selected areas, the tiles are also bonded to the filler bars to distribute loads over a larger area, reducing the stress on highly loaded tiles. The RCG coating on the sides of the tile does not extend to the filler bar. Thus some uncoated surface allows the porous tile to vent.

The SIP and filler bar is a felted mat of Nomex fibers. The majority of tese fibers are oriented in the plane of the mat. Others are normal (transverse) to the plane of the mat. The transverse fibers hold the mat together and transfer loads from the tile to the skin. Tension failures of HRSI test tiles at unexpectedly low stress levels have been attributed to the stress concentrations in the RSI at these transferse fibers. To redistribute the stresses in the RSI, a tile densification procedure has been implemented in which the density near the bondline is increased to increase local strength.

CERAMIC TPS DESCRIPTION

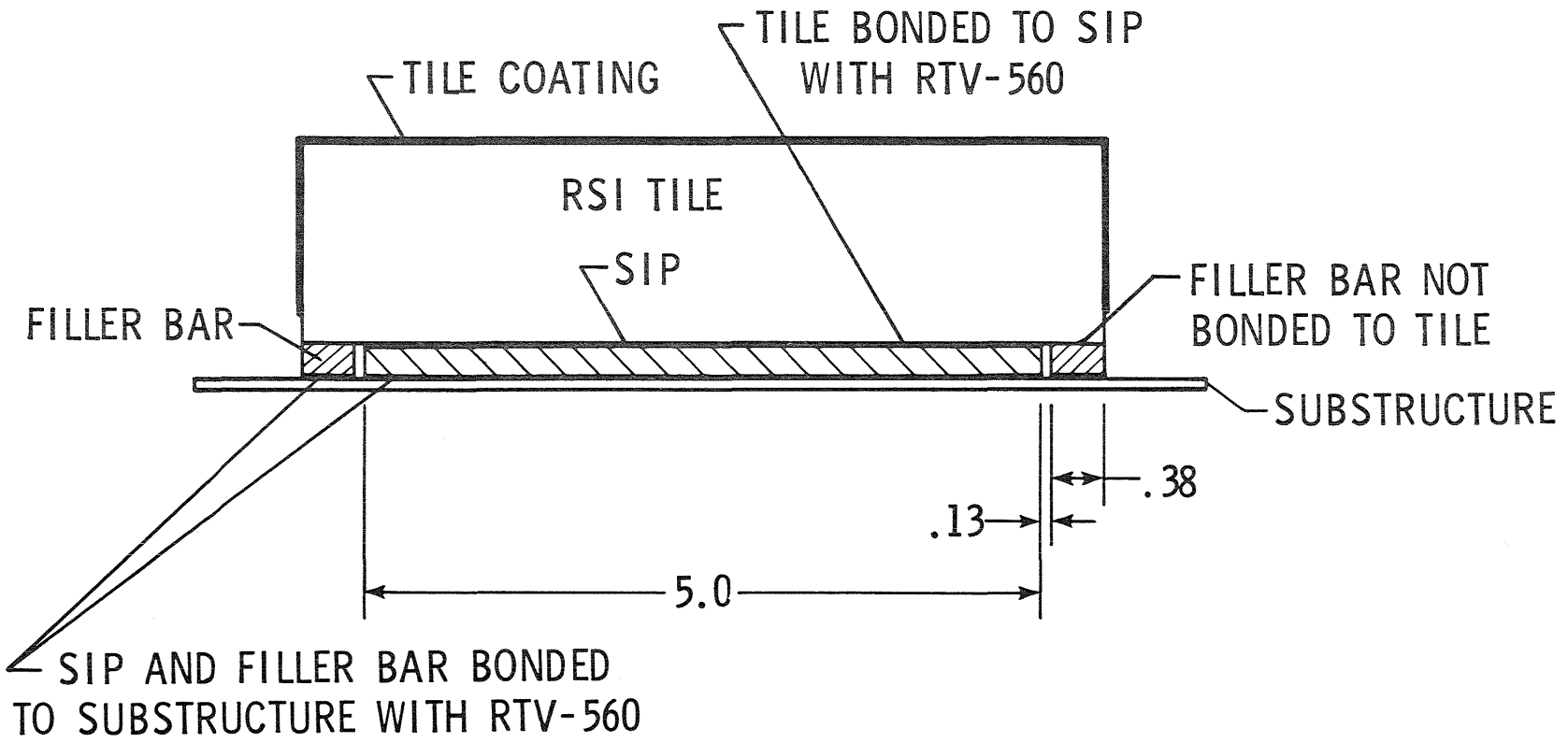

Figure 42

PHOTOMICROGRAPHS OF SIP

Results of an investigation on the microstructure of the SIP were reported in Reference 77 and typical photomicrographs from that report are shown in Figure 43. The low magnification view of the uncoated SIP face reveals a pattern of dimples. The highly magnified view shows that the dimples are locations of transverse bundles of nomex fibers. Also shown is a cross-section view of the SIP and the orientation of the transverse bundles through the SIP thickness. The RTV adhesive transfer coating was developed to aid in bonding the SIP to the RSI tile. However, not all the transverse fibers are securely locked into the transfer coat. The transverse fiber bundles are not perpendicular to the plane of the SIP and thus the SIP material has a preferred orientation and a shear-extension coupling. Transverse fiber bundles also introduce stress concentrations (Ref. 78) which cause premature failures in the tile at the RSI/SIP interface. A process for densifying the faying surface of the tile has been developed which greatly increases the strength of the SIP/tile system (Refs. 79, 80).

PHOTOMICROGRAPHS OF SIP

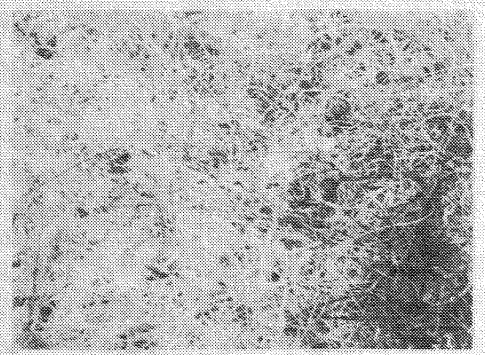

0.04 in.

UNCOATED SIP FACE, 13×

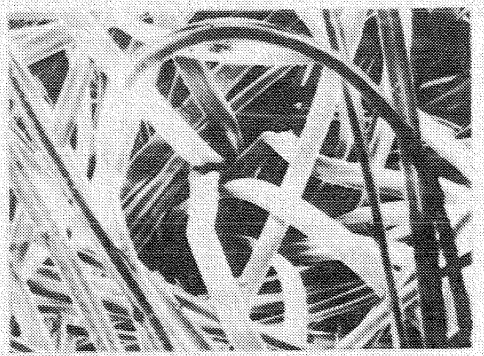

0.002 in.

DIMPLE IN SIP FACE, 425×

RTV TRANSFER COATING

TRANSVERSE FIBER BUNDLE

0.06 in.

CROSS-SECTION OF SIP, 120×

Figure 43

PHOTOELASTIC STUDY OF SIP LOAD TRANSFER TO RSI

The ceramic RSI/TPS, being highly brittle, has strain-to-failure performance considerably below the yield strain of aluminum, and a low coefficient of linear thermal expansion. Thermal and mechanical expansion and contraction of the aluminum skin would cause ceramic material bonded to it to crack. The Shuttle designers decided to protect the RSI from excessive strain in two ways. First, the ceramic insulation was placed on the aluminum in the form of individual tiles with side dimensions of the order of six inches or less. About 30,000 tiles of various sizes and shapes cover slightly over 70% of the Orbiter's exterior. Gaps between tiles permit them relative motion as the aluminum skin expands or contracts and as the substructure deforms causing skin-surface curvatures. The allowance for relative motion alone does not prove sufficient to protect the integrity of the ceramic material. A tile bonded directly to the structure will still crack as the aluminum skin under it expands locally or undergoes local lateral deformations. Some means must isolate the strain of the aluminum substructure from the tile. To do this, the tile was first bonded to a felt pad using an elastomeric, room-temperature-vulcanizing (RTV) silicone adhesive and then the tile and pad combination was bonded to the aluminum skin with the same adhesive. This strain-isolation pad (SIP), having very low shear and extensional moduli, protects the brittle ceramic material from deformations of the aluminum structure.

Initially, the loads expected on the TPS came well within the strength of RSI and SIP, but as the design of the Orbiter progressed, mission requirements became firmer, and load predictions became refined, it became obvious that the TPS would have to withstand loads higher than anticipated. Although they reduced margins of safety, the loads in most cases caused stresses within the strength of the RSI and the SIP as considered independently. However, tests of the RSI/RTV/SIP as a system revealed the group tensile strength to be less than the tensile strength of the individual components. This caused negative margins of safety over large areas of the Orbiter, and the TPS in certain areas did not have sufficient strength to survive the tensile loads of a single mission.

NASA-Langley conducted a photoelastic study (Ref. 78) to demonstrate that the reduced strength occurred because of the pad-transfer mechanisms of the SIP. A highly sensitive photoelastic material (giving optical signals proportional to the internal stress level when viewed under polarized light) was bonded to the SIP using RTV adhesive. Figure 44 shows the specimen loaded in tension and the resultant stress field for RSI bonded to SIP. The SIP/photoelastic-material interface exhibits discrete stress risers all along the interface. In contrast, the aluminum/photoelastic material interface shows only corner stress concentrations, caused by the differential stiffness of the materials. The stress concentrations measured at the SIP/photoelastic-material interface (as high as 1.9) account for the reduced strength of the SIP/RSI assemblage.

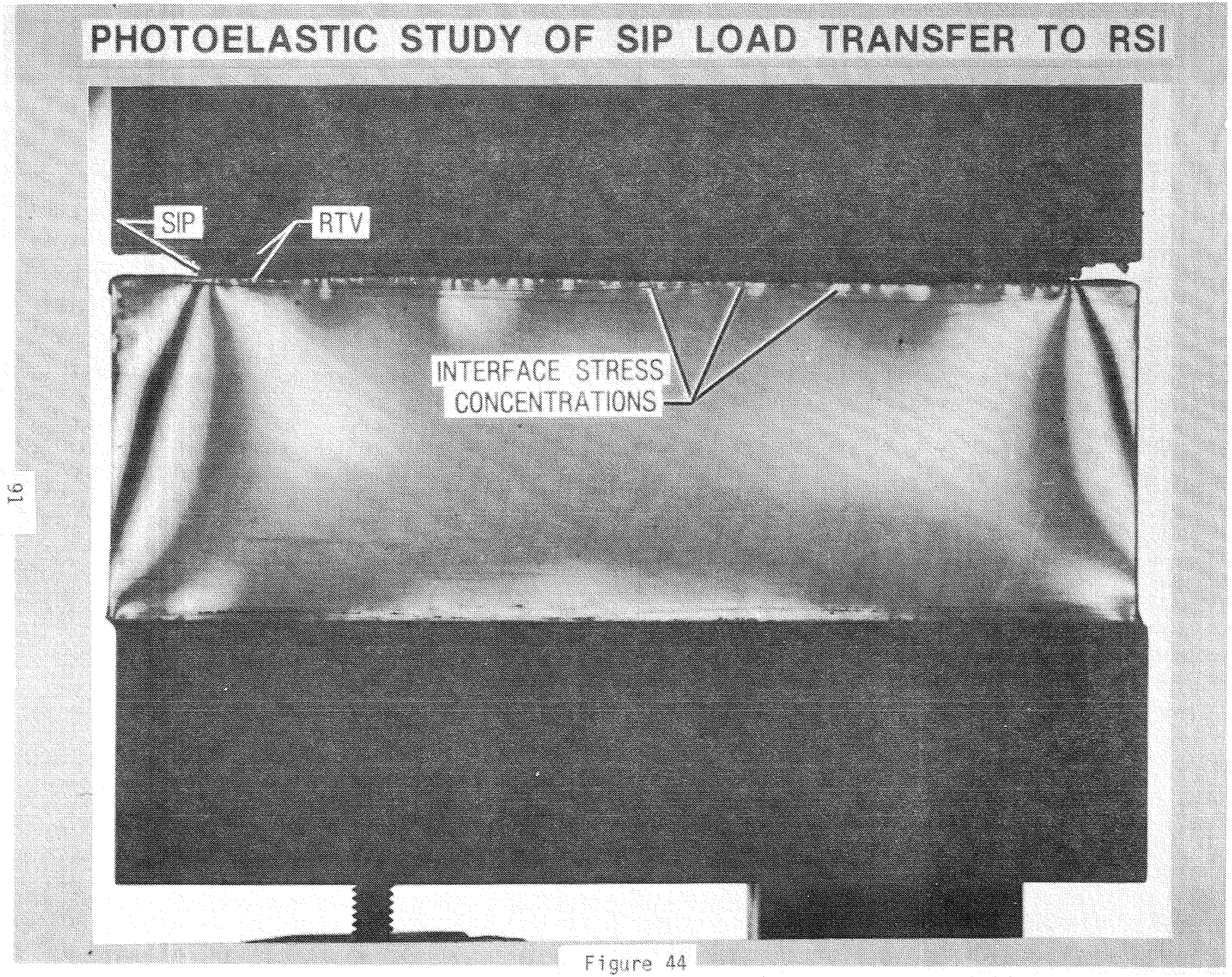
PHOTOELASTIC STUDY OF SIP LOAD TRANSFER TO RSI
SIP
RTV
INTERFACE STRESS
CONCENTRATIONS

Figure 44

CYCLIC FATIGUE BEHAVIOR OF 0.16 inch SIP/LI-900 TILE SYSTEM

A summary of the results of the cyclic fatigue tests of Reference 81 for the SIP/tile system are shown in Figure 45 for the 0.160 inch/LI-900 tile densified and undensified system. The stress levels are shown as a function of the number of fully reversed (R = 1) cycles to failure for the SPI/tile system. The dashed lines on each figure are a least squares fit of the test results where the intersection at one cycle (indicated by the filled symbols) is the mean static failure stress of at least 45 tests performed by Rockwell International, the prime contractor for the shuttle Orbiter. A small number of static tests were performed during the fatigue program of Reference 81 and results are plotted at the one cycle location.

Cyclic loading results in a relatively large reduction in the stress level that the SIP/tile systems can withstand for a small number of cycles. For example, the average static strength of the undensified tile system is reduced from 12.5 psi to 9 psi after a thousand cycles. The undensified tile systems have a SIP/tile interface failure mode. Densifying the faying surface of the RSI tile strengthens the SIP/tile interface sufficiently that cyclic loading failure occurs in the SIP due to complete failure or excessive elongation. Each load cycle result in slightly increased elongation of the SIP during the tension portion of the cycle until complete separation failure occurs. Mission failure due to excessive elongation may occur before complete separation.

For the densified tile system shown by the circle symbols in Figure 45, failure of the SIP was arbitrarily assumed to have occurred when the elongation between the maximum and minimum loads exceeded 0.25 inch. Once the total elongation reaches 0.25 inch, the specimen rapidly deteriorates under further load cycling until complete SIP separation failure occurs.

Densification of the faying surface increases both the static and fatigue strength of the SIP/tile system. The 0.160 inch thick SIP/LI-900 densified tile system at 10 psi has a mean lifetime of approximately 15,000 cycles whereas the same system undensified has an expected lifetime of only 100 cycles at the same stress level. However, even the densified tile systems have a relatively low fatigue life due to excessive elongation or complete failure of the SIP. Thus the full benefit of the increased static strength of the densified tile system is not achieved in fatigue. Also, since failure occurs due to SIP elongation, further improvements in the RSI tile strength alone will not result in any improvement in the total system fatigue strength.

CYCLIC FATIGUE BEHAVIOR OF 0.16 inch SIP/LI-900 TILE SYSTEM

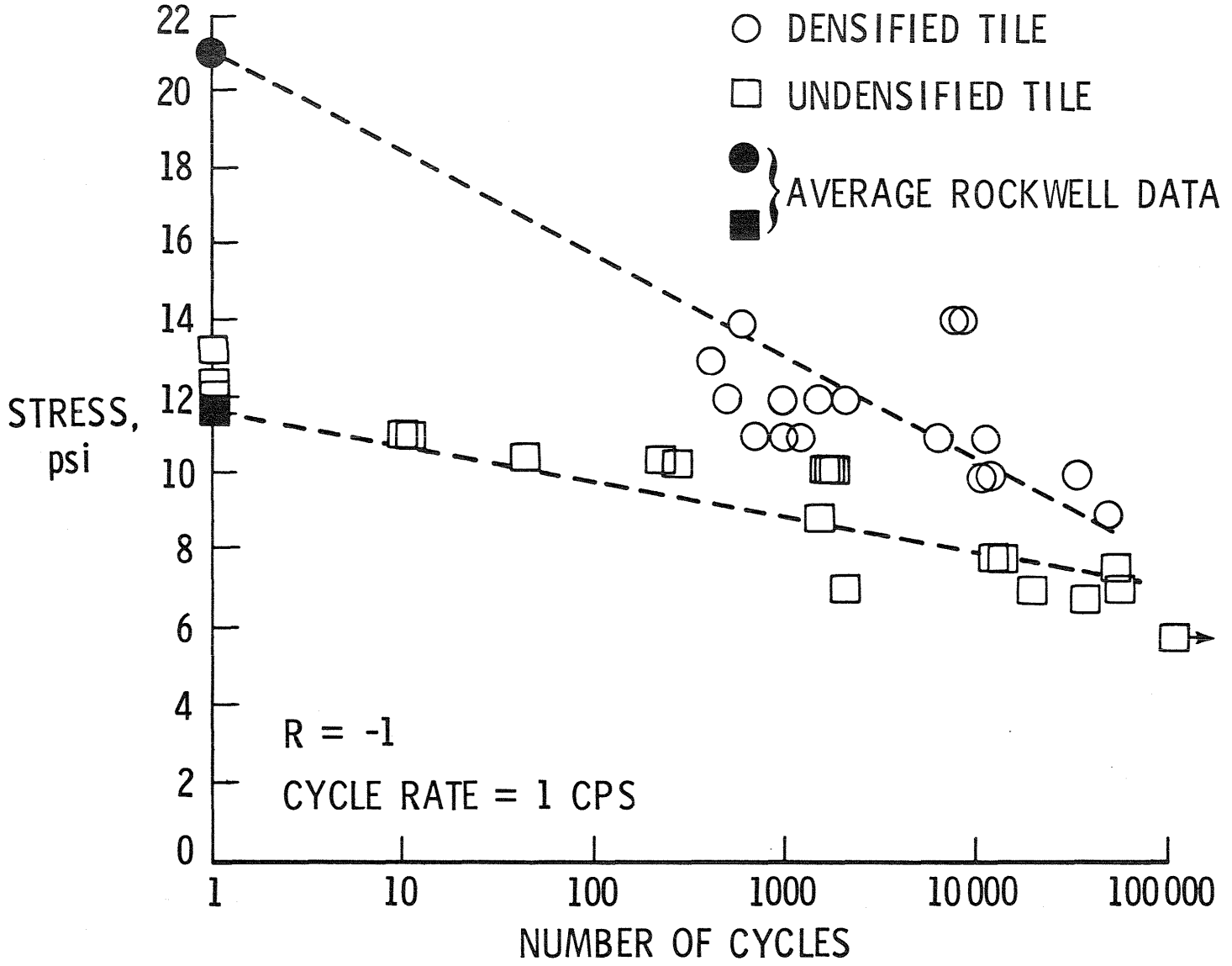

Figure 45

SIP SHOWS PERMANENT GROWTH DUE TO DYNAMIC RANDOM LOADS

The TPS tiles experience a variety of random vibrational loads during ascent. These include: main engine and solid rocket motor ignition overpressures during liftoff, substructure motions due to engine vibrations and aerodynamic loadings, direct acoustic pressure loads caused by boundary-layer noise, differential pressures due to shock passages, aerodynamic gradients and gust loads, and tile buffeting due to vortex shedding from connecting structure. The critical load conditions on the TPS during ascent are expected to occur between the time the orbiter reaches transonic speeds (approximately 40 seconds after liftoff) and the time the orbiter experience maximum dynamic pressure (approximately 65 seconds after liftoff). During this critical time, the TPS on the lower wing and mid-fuselage surfaces experience loads caused by substructure deformation, shock passage aerodynamic gradients which can cause a net tensile force and moment on the tiles, and random acoustic loads transmitted to the tiles from the orbiter base structure. Prior to the first flight, a series of random dynamic load tests were performed on undensified tiles to obtain a more realistic evaluation of the expected behavior of the TPS under simulated flight load conditions in the windward surface wing and midfuselage region. Results of those tests are reported in Reference 82.

Figure 46 contains a plot of the development of permanent growth of the SIP at the highest stressed corner as the dynamic test progressed. By the conclusion of the test, the SIP had a permanent extension at this corner equal to the initial thickness of the SIP (i.e., 100 percent increase in thickness). Figure 46 also presents a comparison of the applied stress vs. displacement measured during the ± 5 psi static uniform load tests performed before and after the dynamic test. The peak-to-peak measure of 0.052 in. is an indication of the degree to which the SIP has loosened. The tile failed during the final test-to-failure undensified region of the parent RSI material at an ultimate static load of 422 lb. This failure load was 70 percent greater than the original bond verification load.

If the load spectrum does represent actual flight conditions, the test data indicate that excessive SIP growth may occur within the operational lifetime of the orbiter. This mode of failure under random loading is benign if corrective action is taken during ground maintenance between flights. However, if loose tiles are not eventually replaced, several unacceptable consequences might result: (1) hot gas may be allowed to penetrate between tiles to the filler bar protecting the substructure, (2) chipping of the protective coating of the neighboring tiles may occur, and (3) disruption of the airflow could prematurely trip the boundary layer causing turbulent flow which would lead to an increase in downstream heating.

SIP SHOWS PERMANENT GROWTH DUE TO DYNAMIC RANDOM LOADS

- SIMULATED SHUTTLE ENVIRONMENT
  - SUBSTRATE DEFORMATIONS
  - TENSILE LOAD (AERO SHOCK)
  - VIBRATION OF SUBSTRATE
- POTENTIAL CHANGES IN GAP-STEP HEIGHT NOT A CONCERN

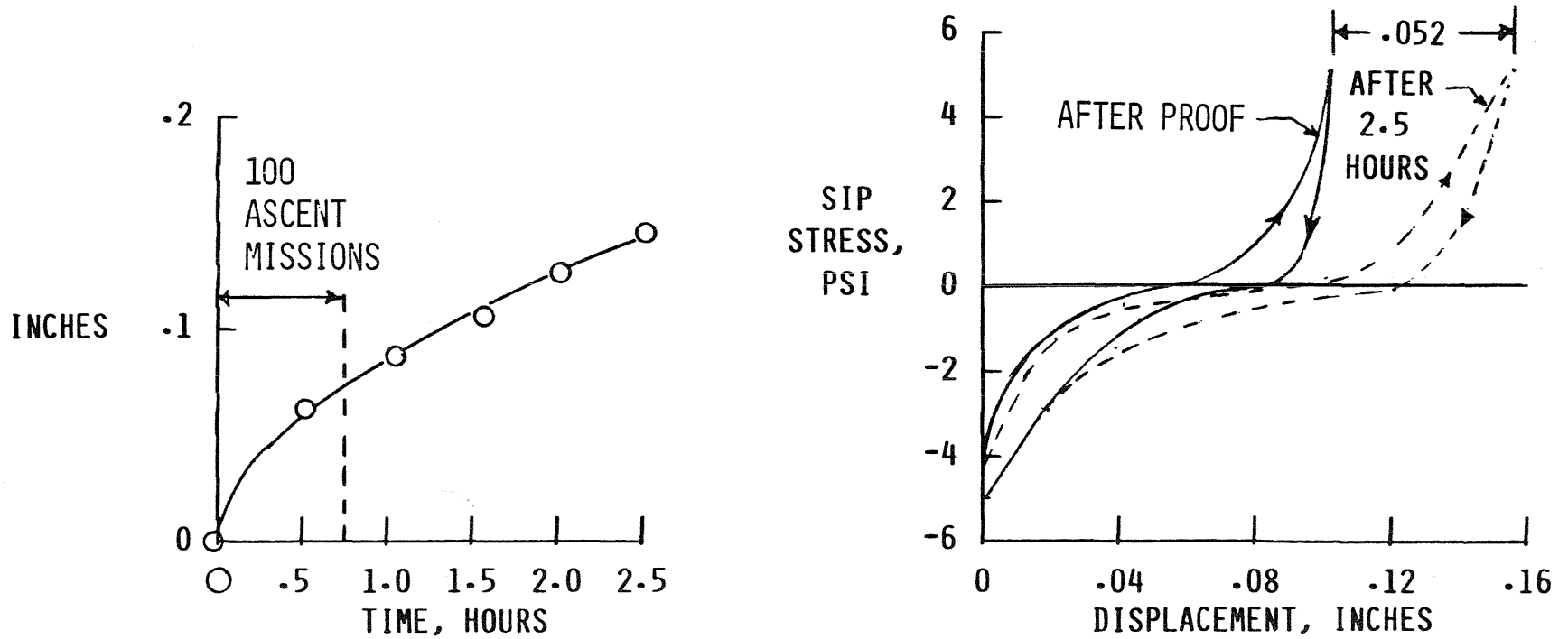

Figure 46

ADVANCED MATERIALS FOR FUTURE ATMOSPHERIC ENTRY VEHICLES

The NASA Ames Research Center has a long history of developments in ceramic insulations. As shown in Figure 47, their current work is focused primarily on tougher, more durable materials and higher maximum use temperatures. They are looking at both rigid (Fiberous Refactory Composite Insulation, FRCI) and flexible (tailorable advanced blanket insulation, TABI) insulations. The FRCI is tough enough that threaded nuts and bolts can be machined from it as illustrated on the figure.

The thermal protection system of the Orbiter Discovery, launched in August 1984, included Fibrous Refractory Composite Insulation (FRCI-12) for the first time. The new 12 lb/ft^2 density tile material replaced most of the LI-2200 (22 lb/ft^3 density) used on earlier orbiters (about 10% of the Shuttle silica tiles), saving 1000 pounds in structural weight. The new aluminoborosilicate material has a lower density and is stronger than earlier heat shield tile materials.

Nearly all of the 8000 white low temperature (LRSI) tiles and some of the coated Nomex felt (FRSI) blankets were also replaced on Discovery with 2300 Advanced Flexible Reusable Surface Insulation (AFRSI) quilts. These new flexible fibrous, silica quilts have been used in limited areas on previous orbiters, butDiscovery is the first to have most of the upper surface so covered. The AFRSI, with a new ceramic coating developed by Rockwell International Space Division, offers higher temperature capability than the FRSI, and improved durability, simplicity, and lower weight than the LRSI it is replacing.

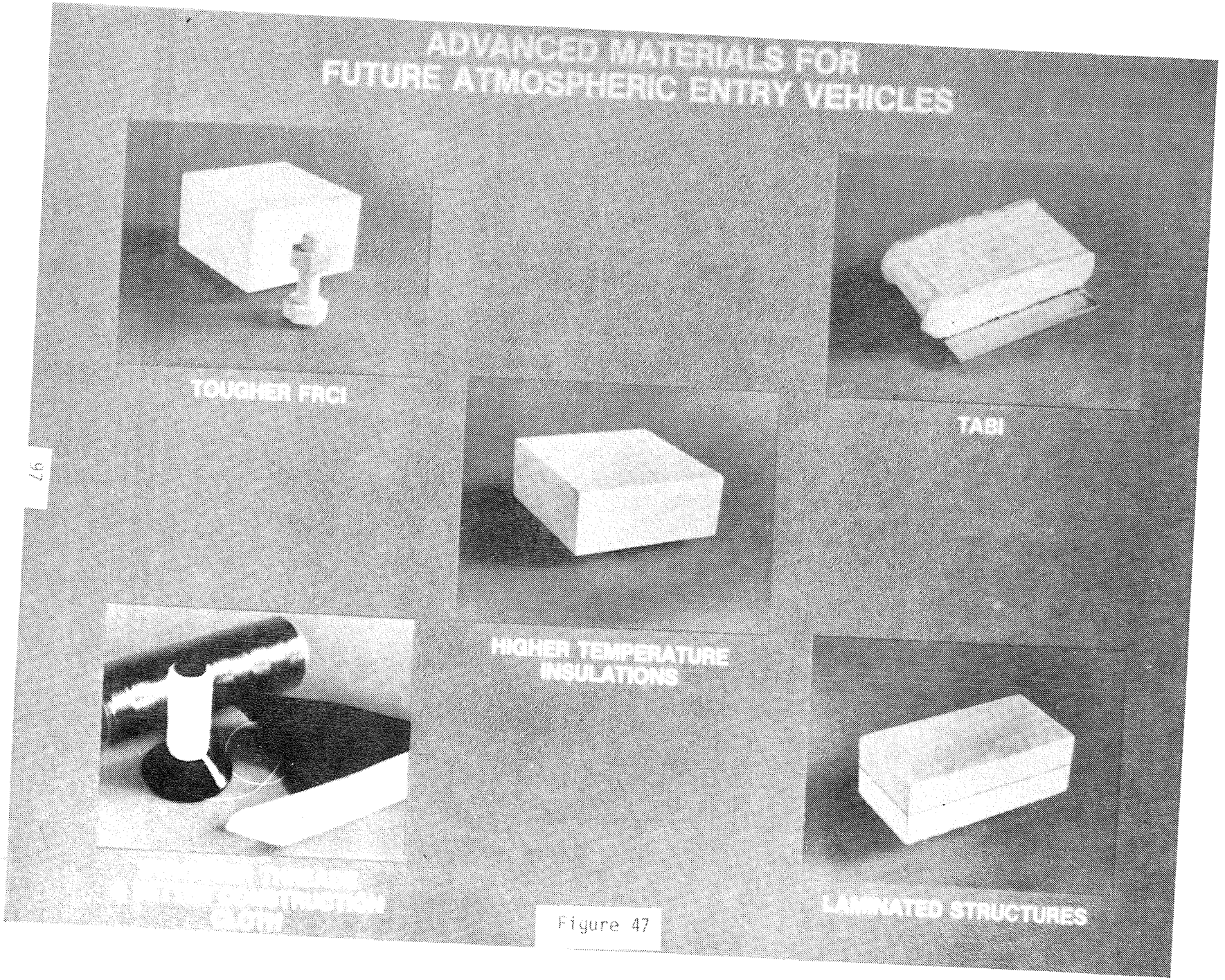
ADVANCED MATERIALS FOR
FUTURE ATMOSPHERIC ENTRY VEHICLES
TOUGHER FRCI
TABI
HIGHER TEMPERATURE
INSULATIONS
LAMINATED STRUCTURES

Figure 47

ADVANCED FLEXIBLE CERAMIC TPS

Figure 48 shows the various advanced flexible ceramic TPS currently under development at NASA Ames. The AFRSI is currently in use on the Shuttle Orbiters, but work continues on increasing surface toughness, weave geometry, and integral woven core structures. These systems offer great potential over the rigid and fragile LRSI that they are replacing on the Orbiters, and could find more extensive use as the maximum use temperature is increased. One difficulty in developing such materials for aerospace plane type vehicles is the lack of a definitive durability criteria that researchers can work towards.

ADVANCED FLEXIBLE CERAMIC TPS

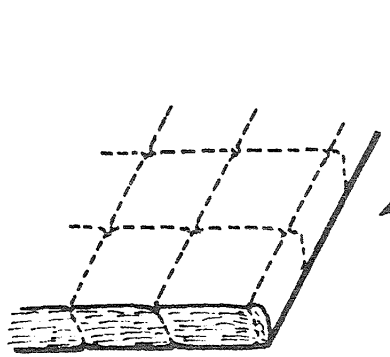

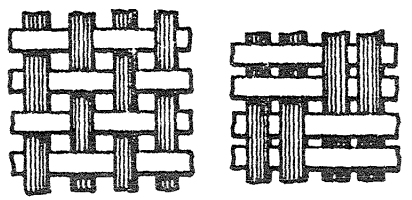

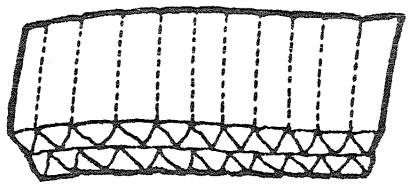

ADVANCED CERAMIC FABRICS/THREADS – ALUMINOBOROSILICATE; SILICON CARBIDE

ADVANCED FLEXIBLE REUSABLE SURFACE INSULATION (AFRSI)

TAILORABLE ADVANCED BLANKET INSULATION (TABI)

RESEARCH IN PROGRESS

SURFACE TOUGHENING
- CERAMIC COATINGS
- SOL/GEL TECHNOLOGY
- HYDROPHOBIC COATINGS

WEAVE GEOMETRY STUDIES
- THERMAL OPTICAL AND CATALYTIC EFFECTS
- MECHANICAL PROPERTIES

INTEGRAL WOVEN CORE STRUCTURES
- DESIGN STUDIES
- THREADLESS, INTEGRAL CONSTRUCTION
- DENSITY, INSULATIVE PROPERTIES

Figure 48

CERAMIC THERMAL PROTECTION SYSTEM TECHNOLOGY PROJECTIONS

Figure 49 shows the NASA Ames projections of material temperature capability for multiple reuse that could be expected by 1990. For the rigid RSI a modest but very useful increase in temperature from 2700°F to 3000°F is projected. For the flexible insulations significant increases from 1200°-1800°F to 1800°-2500°F are projected. If obtained, these insulations could have significant impact on future designs. For high density materials such as carbon-carbon and Sic/Sic they again project significant improvements from 2800°-3200°F to 3800°-4000°F. If these high temperatures are obtained designers will have much more freedom in vehicle performance since many proposed missions, which are now temperature limited, could obtain significant performance improvements.

CERAMIC THERMAL PROTECTION SYSTEM TECHNOLOGY PROJECTIONS

MATERIAL TEMPERATURE CAPABILITY, °F — MULTIPLE REUSE

MATERIAL	CURRENT	1990 TECHNOLOGY
RIGID REUSABLE SURFACE INSULATION LI-2200, FRCI, HTP	2700	3000
FLEXIBLE SURFACE INSULATION AFRSI, TABI	1200-1800	1800-2500
HIGH DENSITY CERAMIC COMPOSITES RCC, ACC, SiC/SiC	2800-3200	3800-4000

Figure 49

ORBITER DIRECT-BOND APPLICATIONS AND POTENTIAL WEIGHT SAVINGS

Savings of 25 to 30 percent of the total structure/TPS weight can be realized where 600°F structural allowable graphite/polyimide (GR/PI) is used (Ref. 83). In comparison to the baseline aluminum structure (350°F structural allowable), GR/PI has reduced TPS requirements and the FRCI TPS tiles can be bonded directly to the GR/PI substrate because of the greater strength of the FRCI and thermal compatability and the greater strength-to-density and stiffness-to-density ratios of the advanced composite materials. TPS weight can be reduced significantly by using the 600°F structural allowable of GR/PI and the direct-bond fibrous refractory composite insulation (FRCI) tile concept. The potential weight savings associated with advanced composite application to the Space Shuttle Orbiter are also summarized in Figure 50. These potential weight savings total 15,178 pounds: 4,544 pounds for retrofittable structures and 10,634 pounds for block change or non-retrofittable structures (Ref. 44).

The retrofittable structures identified for future structural weight reduction applications with advanced composite and direct-bond RSI include the vertical tail, body flap, elevon, main landing-gear door, wing leading edge, and nose cap. Block change structures identified for composite materials with direct-bond RSI applications include the wing, and forward, mid and aft fuselages.

ORBITER DIRECT-BOND APPLICATIONS AND POTENTIAL WEIGHT SAVINGS

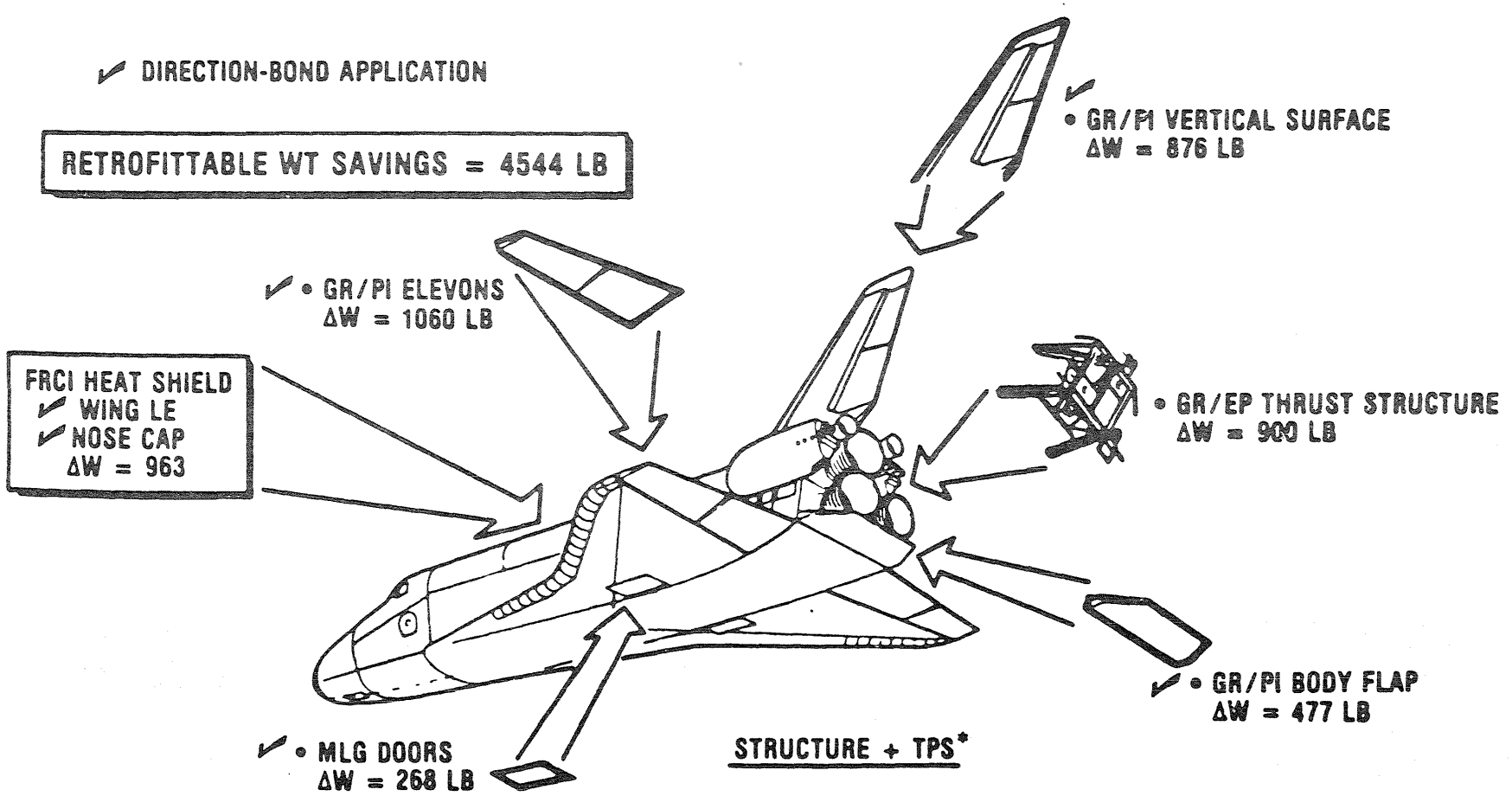

Figure 50

ESTIMATED WEIGHT SAVINGS FOR DIRECT-BOND RSI ON GR/PI STRUCTURE

Structural weight reduction and orbiter performance gain can be realized by taking advantage of the large strength-to-weight and stiffness-to-weight ratios of advanced composites and the increased strength of FRCI TPS. The weight savings associated with the advanced structure/TPS concept for typical areas on the lower surface of the orbiter are compared to the baseline in Figure 51. The feasibility of direct-bond FRCI TPS tile on GR/PI structure is based on structure/TPS thermal compatibility (i.e., the similarity of thermal expansion coefficients for small thermal stresses), sufficient structural stiffness to preclude RSI tile fracture caused by out-of-plane structural deflection, and the availability of a high-temperature (650°F), room temperature curing adhesive. The large stiffness-to-weight ratio of the GR/PI composite allows a lightweight structure design with the required stiffness, and GR/PI's low coefficient of thermal expansion is compatible with that of the ceramic tile.

Because of the higher strength of FRCI TPS and the higher stiffness of GR/PI, the use of a larger tile permits an additional weight decrease compared to the baseline as a result of reducing tile gaps and gap heating (less aeroheating). Additional details are given in reference 85.

ESTIMATED WEIGHT SAVINGS FOR DIRECT-BOND RSI ON GR/PI STRUCTURE

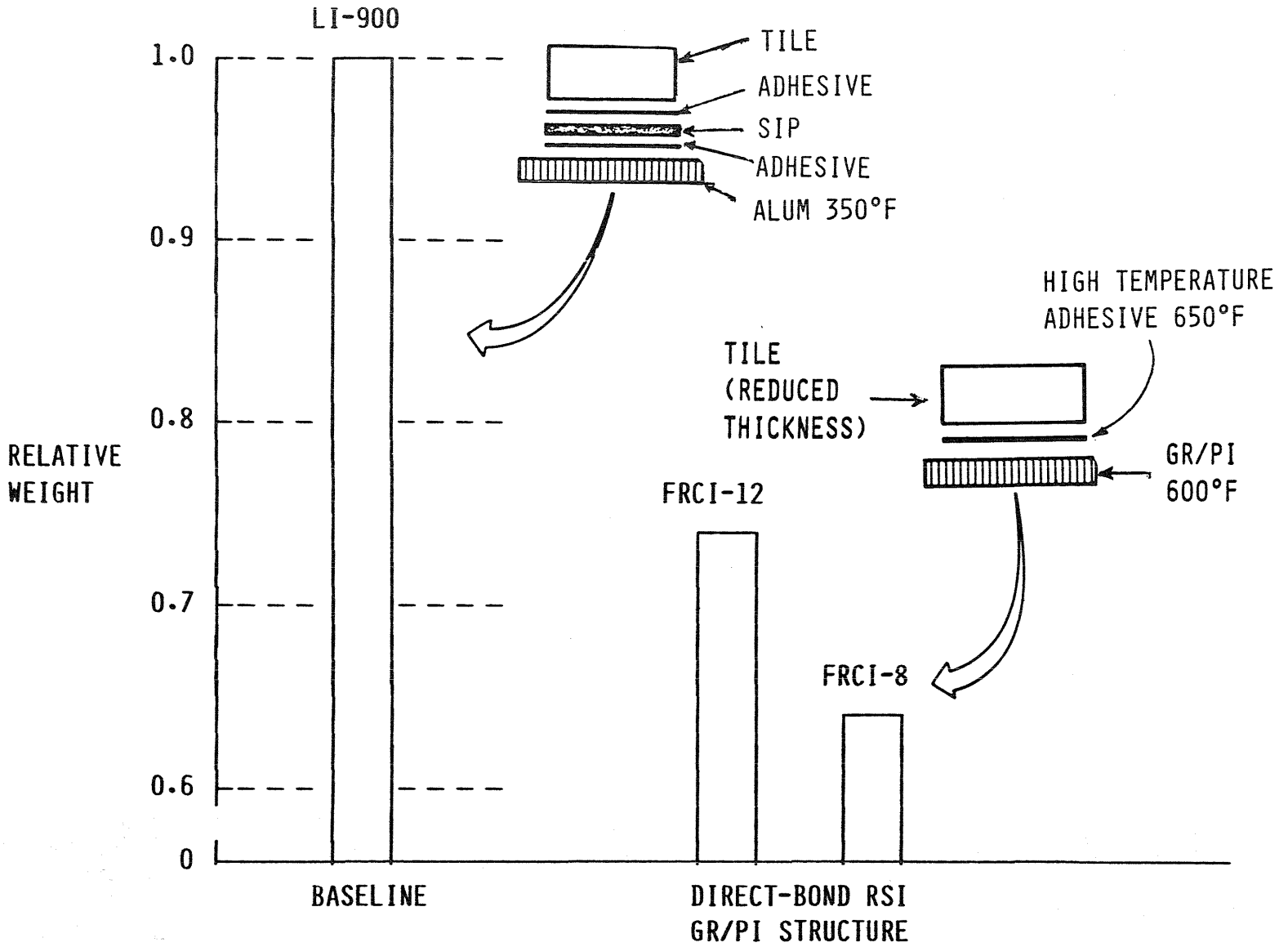

Figure 51

WHAT PROBLEMS MUST BE SOLVED?

The problems to be solved, as might be expected, are the problems currently being worked: increased durability and temperature capability. Both rigid and flexible systems need improved durability against handling damage and particle and rain impact. The flexible ceramics also need better resistance to aeroacoustics and aerothermo environments. Increased temperature capability will probably always be a goal of material scientists.

WHAT PROBLEMS MUST BE SOLVED

- RIGID CERAMICS
  - DURABILITY
    - PARTICLE AND RAIN IMPACT
    - HANDLING DAMAGE
  - INCREASED TEMPERATURE CAPABILITY
- FLEXIBLE CERAMICS
  - DURABILITY
    - AEROACOUSTICS
    - AEROTHERMO ENVIRONMENTS
    - HANDLING DAMAGE
    - PARTICLE AND RAIN IMPACT
  - INCREASED TEMPERATURE CAPABILITY

Figure 52

METALLIC TPS CIRCA 1972

Figure 53 shows a partially disassembed metallic TPS CIRCA 1972, the year the decision was made to use RSI on the shuttle orbiter. As can be seen from the figure, the metallic systems were complex with many parts, such as foil packages for the fibrous insulation (life of such packages are still an unresolved problem today), and were heavy compared to the RSI systems. But many test programs (Refs. 86-88) demonstrated their durability; hence work has continued with a goal to achieve simplicity, reduce weight, and eliminate short-life components.

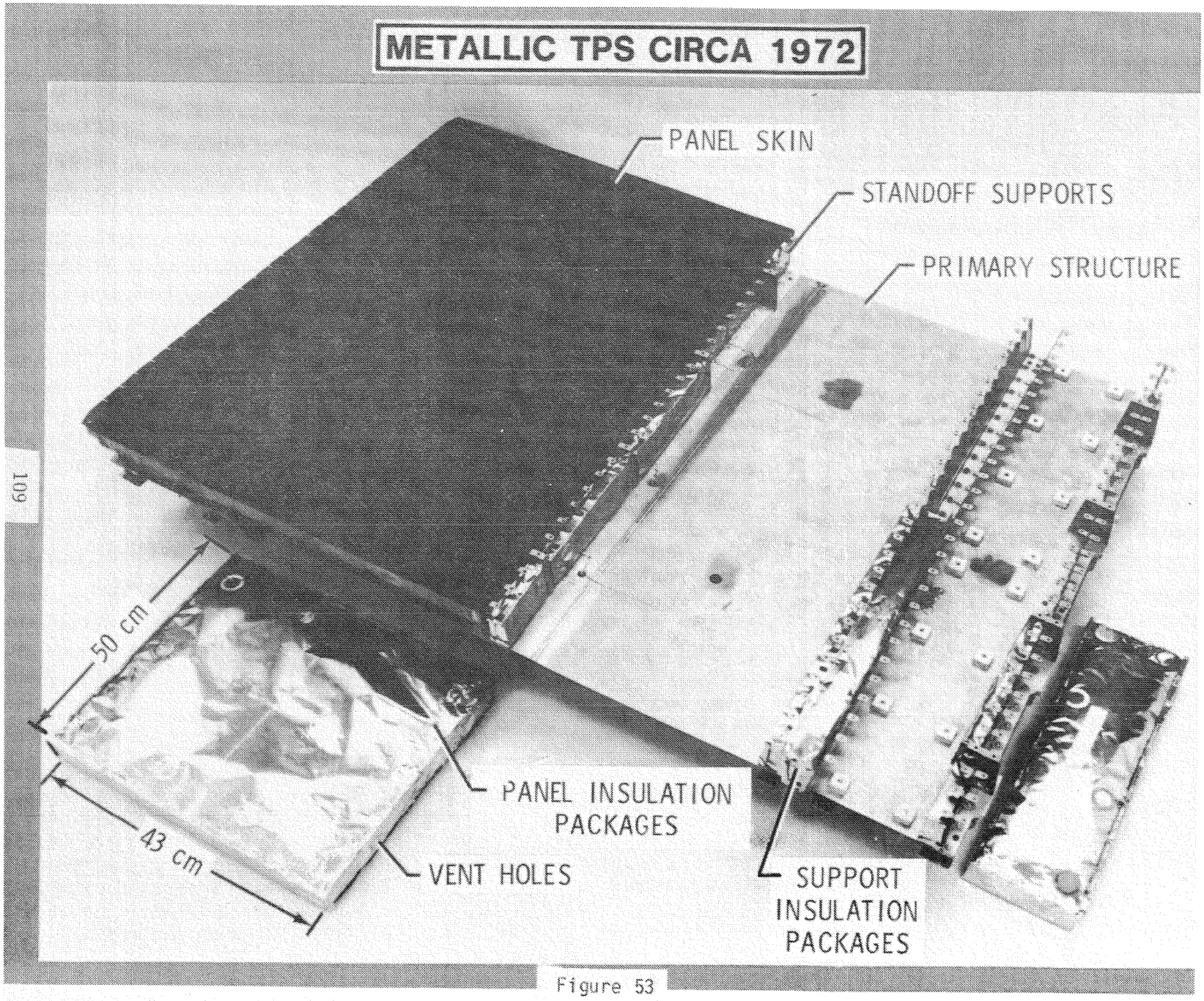
METALLIC TPS CIRCA 1972
PANEL SKIN
STANDOFF SUPPORTS
PRIMARY STRUCTURE
50 cm
43 cm
PANEL INSULATION PACKAGES
VENT HOLES
SUPPORT INSULATION PACKAGES

Figure 53

METALLIC AND CARBON-CARBON TPS CONCEPTS

Although the Reuseable Surface Insulation (RSI) currently used on the Space Shuttle is an excellent insulation, it may not be durable enough for aerospace plane applications. Figure 54 summarizes a program to develop a more durable Thermal Protection System (TPS) using metallic concepts for temperatures from 700°F to 2000°F and using Advanced Carbon-Carbon (ACC) above 2000°F. The goals of the program are to develop TPS that have durable surfaces, are mechanically attached, have covered gaps between panels to reduce gap heating, and are mass competitive. The graph in the figure shows that the durable TPS concepts indicated by the symbols are mass competitive with RSI indicated by the cross-hatched area.

METALLIC AND CARBON-CARBON TPS CONCEPTS

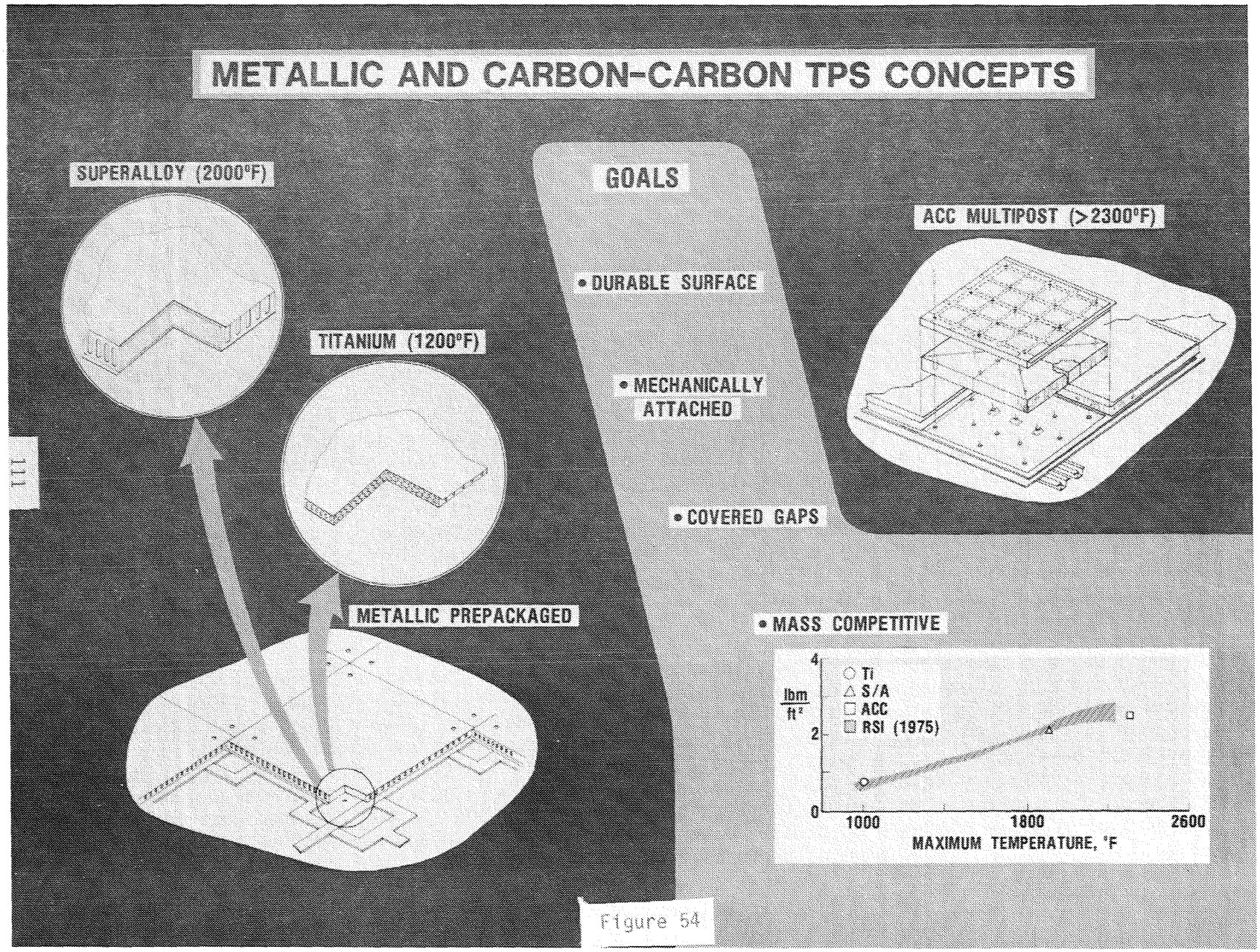

Figure 54

METALLIC TPS CONCEPTS

The two TPS concepts identified in Figure 54 are also shown in more detail in Figure 55. The two metallic prepackaged concepts are discrete panels that have a strip of RTV-covered Nomex felt beneath the perimeter of each panel to prevent hot gas flow beneath the panels. The titanium multiwall concept (maximum surface temperature < 1200°F) consists of layers of dimpled titanium foil Liquid Interface Diffusion (LID)* bonded together at the dimples with a flat foil sheet sandwiched between each dimpled sheet. The superalloy honeycomb concept (maximum surface temperature < 2000°F) consists of an Inconel 617 honeycomb outer surface panel, layered fibrous insulation, and a titanium honeycomb inner surface panel. The edges of the two metallic concepts are covered with beaded closures to form discrete panels nominally 12 inches square. The titanium multiwall and superalloy honeycomb panels are described in detail in References 89 and 90 respectively.

The two types of attachments shown in Figure 55 can be applied to either of the TPS concepts. The bayonet-clip attachment, shown with the titanium multiwall concept, consists of two clips and a metal tab (bayonet) LID bonded to the lower surface of the panel. One clip is mechanically attached to the vehicle surface, and one clip is LID bonded to the lower surface of an adjacent panel. Thus, a single bayonet attaches a corner from each of two adjacent panels. The through panel fastener, shown with the superalloy honeycomb concept, consists of a thin-walled cylinder through the panel that allows access to a bolt which fastens the panel corner to the vehicle structure. The cylinder which contains fibrous insulation, is covered with an Inconel 617 threaded plug. These fasteners are described in detail in Reference 90.

*Proprietary joining process of Rohr Industries.

METALLIC TPS CONCEPTS

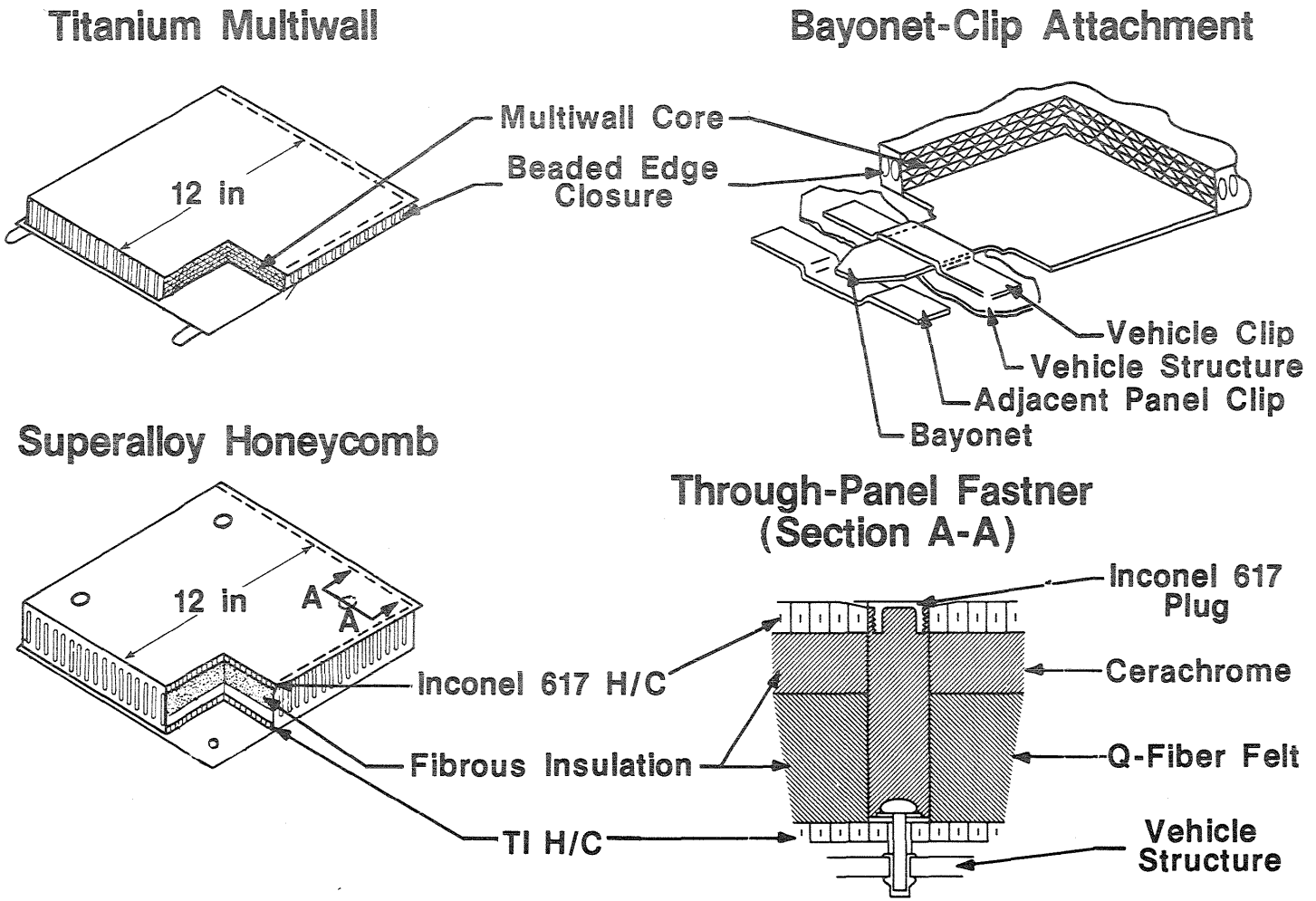

Figure 55

INTERACTION OF DISCIPLINES - EXAMPLE FOR METALLIC TPS DEVELOPMENT

Figure 56 shows the highly interdisciplinary nature of the design process for TPS, which really are systems requiring a systems approach to successful design. Starting with a concept, illustrated here by a prepackaged superalloy honeycomb concept (Ref. 90), the designer needs to consider material performance such as surface emittance and catalysis, fabrication developments, and various environmental tests such as aerothermal and launch site contamination, durability to resist impact, and lightning strike, etc. Since a metallic TPS will have a wavy surface, or as in the example, deform into a pillowed surface, such surface roughness effects on loads and heating must be determined. The product of such research should be verified concepts (where verified can mean different things to researchers and project personnel), and verified analytical design and fabrication methods.

INTERACTION OF DISCIPLINES — EXAMPLE FOR METALLIC TPS DEVELOPMENT

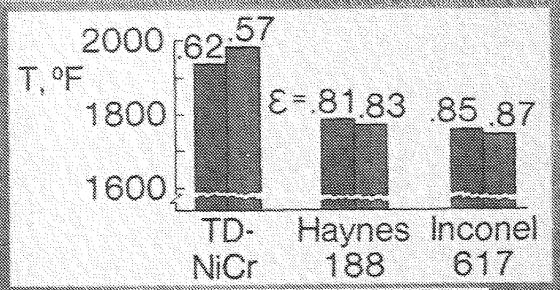

Emittance Evaluation

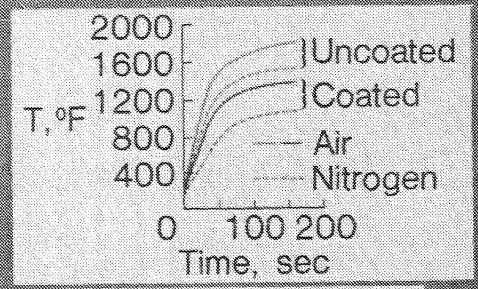

Catalytic Coatings

Superalloy Honeycomb

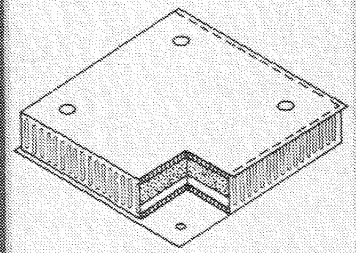

Conceptual Design

Needs

Needs

Needs

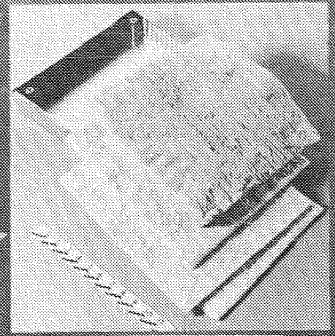

Fabrication

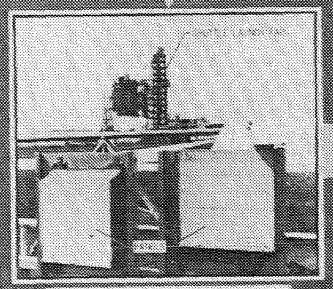

Launch Site Environment

Verified Concepts and Design & Fab. Methods

Product

Aerothermal Environment

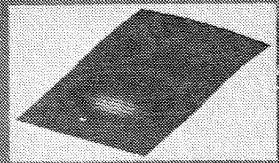

Loads on Pillowed Surface

Figure 56

VERIFICATION TEST FACILITIES

NASA test facilities at Johnson Space Center (JSC), Kennedy Space Center (KSC), and Langley Research Center (LaRC) are being used for verification tests of the concepts. Figure 57 summarizes the types of tests, shows representative test facilities, and identifies the NASA Centers where the tests have been conducted.

TPS test models were exposed to combined temperature and pressure conditions to obtain thermal response characteristics of the concepts using thermal/vacuum test facilities at JSC, KSC, and LaRC. These facilities consist of radiant heaters enclosed in an environmental chamber. One of the facilities, the JSC facility, is shown in the figure. The heater system, which is suspended over the test model, is mounted in a boiler-plate Apollo-command-module test chamber that is evacuated by a mechanical vacuum pump. The heater consists of electrically heated graphite elements enclosed in a fixture box purged with gaseous nitrogen. One side of the fixture box is a columbium susceptor plate which radiates heat to the test model.

Dynamic response of metallic TPS concepts was evaluated by shaker-table vibration tests and by acoustic exposure in a sound chamber at JSC and a progressive wave facility at LaRC. The acoustic levels were representative of those experienced during Space Shuttle lift-off. The LaRC facility, shown in Figure (b), used air modulation to generate the noise which propagates through a horn to the test section. The test panels were attached to the side wall of the test section. (An ACC test model was also exposed to thermal vacuum tests in this facility. Graphite heaters are added to the test section side wall opposite the test panel to provide radiant heating capability.)

Environmental tests to assess water retention and the effects of atmospheric contamination on metallic TPS are being conducted near the Space Shuttle NASA launch site at KSC as shown in Figure (c). Additional water retention tests are being conducted with a wind/rain machine at JSC.

Lightning strike tests, shown in (d), were conducted at LaRC to determine how much damage lightning impact caused on the metallic panels. The facility operates by charging a bank of capacitors and rapidly discharging the capacitors to a grounded test model. The maximum capability of the facility is a peak current of 100 kA and an action integral of 0.25×10^6 A^2-sec.

The metallic TPS concepts were tested in the LaRC 8-Foot High Temperature Tunnel (8' HTT) and the ACC concept was tested in the LaRC 20-MW Aerothermal Arc Tunnel to evaluate the performance of the concepts in an aerothermal environment. The upper portion of (e) shows an array of metallic TPS panels in the 8' HTT, and the lower portion of the figure shows an ACC model in the arc tunnel. Details of these investigations are given in Reference 91 and in subsequent figures.

NASA
L-84-5719

VERIFICATION TEST FACILITIES

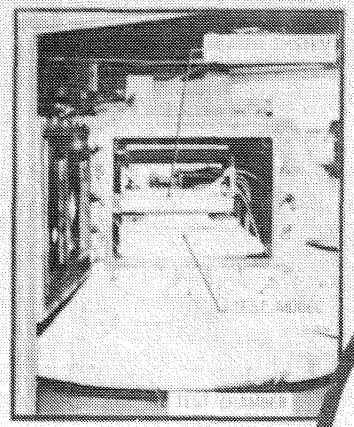

a) Thermal / Vacuum
(JSC-KSC-LaRC)

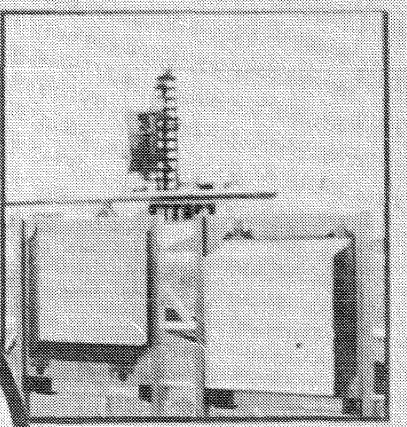

c) Environmental
(KSC-JSC)

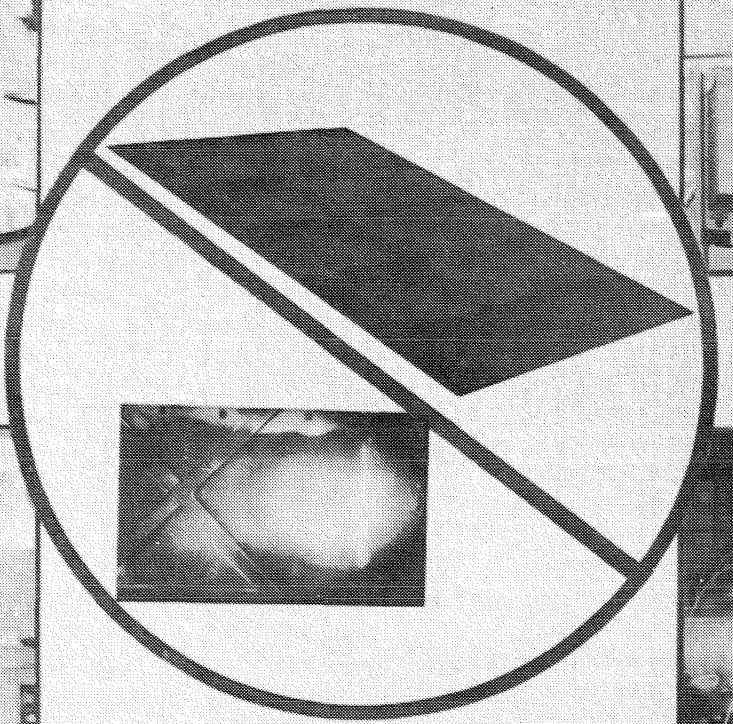

e) Aerothermal
(LaRC)

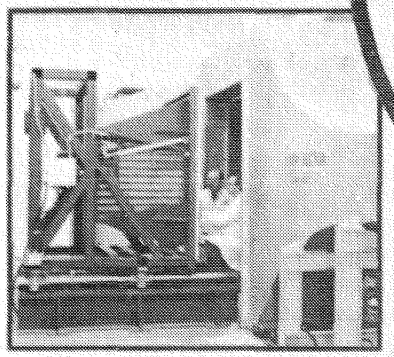

b) Vibration and Acoustic
(LaRC-JSC)

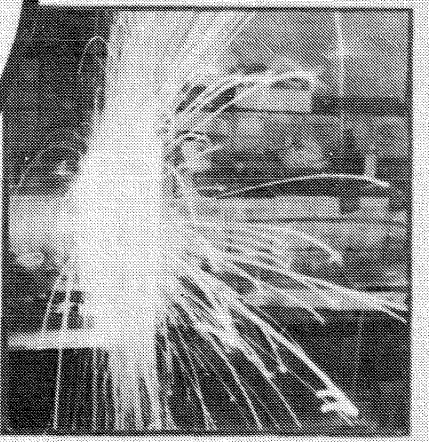

d) Simulated Lightning
(LaRC)

Figure 57

RADIANT CYCLIC TESTS - HEATING DISTRIBUTIONS THROUGH MODELS

A two-tile array of multiwall tiles and a comparable area of low-temperature reusable surface insulation (LRSI-LI 900) were subjected to cyclic radiant heat in the Johnson Space Center Building 13 Radiant Heating Facility. The purpose of these tests was to evaluate the cyclic thermal performance of the multiwall and to provide a direct comparison with the performance of the insulation system currently employed on the Shuttle Orbiter. Both insulation systems were mounted on aluminum plates representative of the local thermal mass of the Shuttle structure. The thickness of the multiwall tiles was designed for the thermal requirements at body point 3140, but the thickness of the LRSI tiles was 60% greater than that required for thermal design (which was 0.128 in.) because of Shuttle Orbiter outer mold-line fairing requirements. Even so, the multiwall tiles were thicker because the conductivity of multiwall is higher than the conductivity of LI-900. The total mass of the multiwall system was 9% greater than the LRSI system. The tiles were subjected to 25 temperature and pressure cycles representative of conditions at body point 3140 during trajectory 14414.1C, the baseline design trajectory for the Shuttle.

Typical results for the two insulation systems are shown in Figure 58. The performance of the insulation systems appears to be the same since the peak structural temperature beneath each system is the same. Each maintained the primary structure well below the maximum allowable temperature of 350°F. The results indicate that the thermal design of the multiwall system is conservative since it performed in the same way as the LRSI system which was 60% thicker than that required to meet the thermal requirements.

There was no significant change in the thermal performance of either system over the entire 25 cycles. Except for a slight curling of the overhanging edge between multiwall tiles and flaking of the thermal paint on the multiwall tiles which was unintentionally not cured before testing, there were no ill effects despite the fact that the insulations had been exposed to elevated temperatures for over 17 h.

RADIANT CYCLIC TESTS - HEATING DISTRIBUTIONS THROUGH MODELS

(TESTS 1 TO 25)

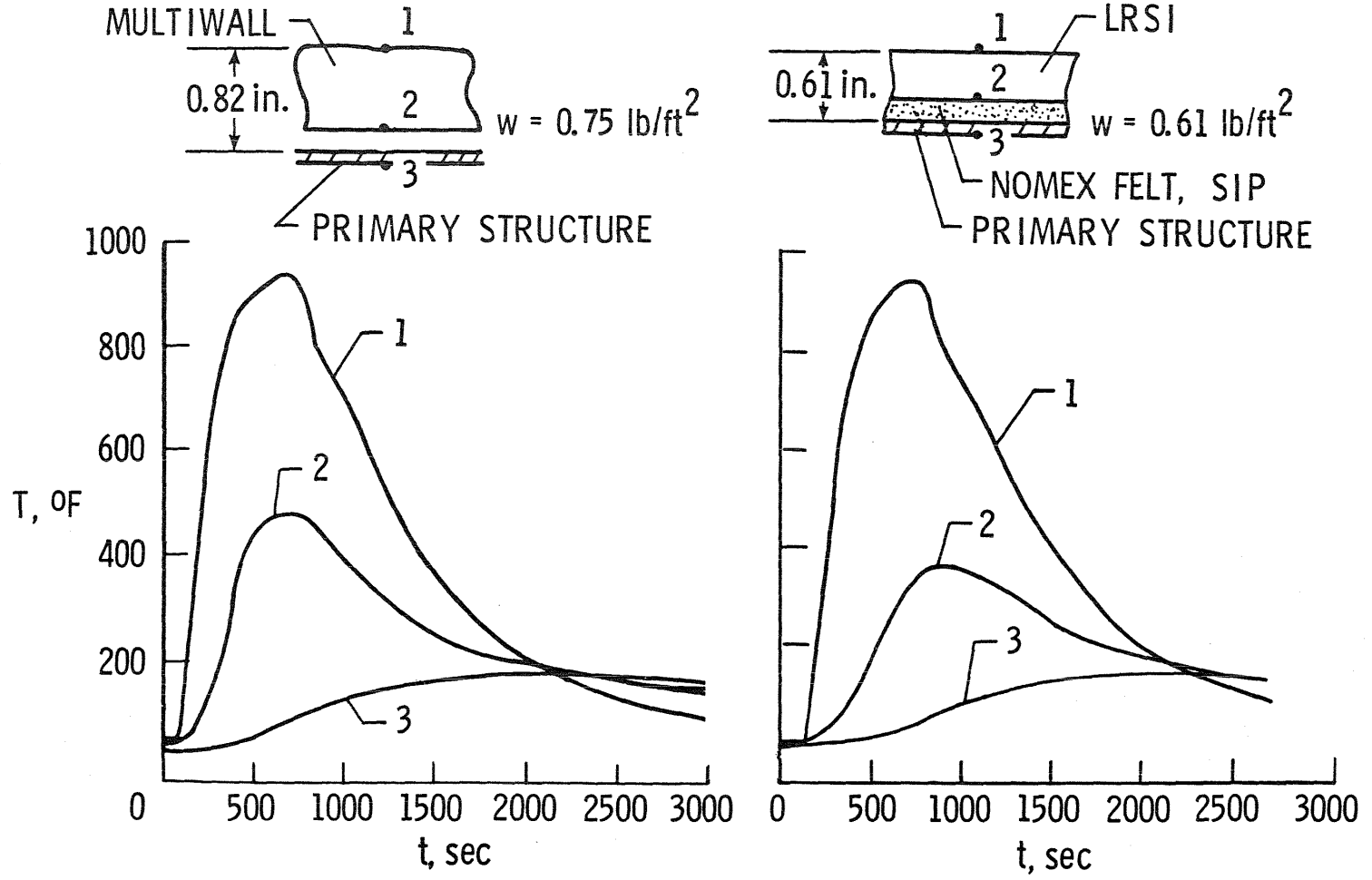

Figure 58

DAMAGE FROM ACOUSTIC TESTS OF SUPERALLOY HONEYCOMB

Both the titanium multiwall and the superalloy honeycomb concepts were exposed to acoustic environment in a sound chamber at JSC operating at an overall sound pressure level (OASPL) of 161 dB and in a progressive wave facility at LaRC operating at 159 dB. The spectrums were representative of the launch sound environment for the Space Shuttle. The 2-panel arrays tested at JSC had bayonet-clip attachments and were exposed to sound for 15 minutes which is representative of about 25 missions with a scatter factor of 4. The single panels tested at LaRC had through-panel fasteners and were tested for 60 minutes which corresponds to about 100 missions with a scatter factor of 4.

In both types of tests, no damage occurred to the titanium multiwall panels. However, the superalloy honeycomb panels did sustain some damage in each type of test. Figure 59 shows an edge view of one of the superalloy honeycomb panels tested in the JSC sound chamber. Prior to the test, the overhanging lip along the right half of the panel edge shown was bent down (in a pattern which fits a human hand), and some buckling along the bottom edge of the side closure occurred. Additionally, as pointed out in the figure, this edge was not properly supported by Nomex felt. All other edges were supported by a 1-inch wide strip of Nomex felt as specified in the concept design. During the tests, numerous cracks occurred on the bottom edge of this side closure. Since no other side closures on the two panels suffered any damage during the tests, the cracks probably occurred due to the handling damage and lack of felt support on the damaged edged.

One side closure of the single superalloy honeycomb panel tested in the LaRC progressive wave facility was buckled in shipment. The panel was judged to be acceptable for vibration tests since the damage was limited to only one edge. Upon completion of the vibration tests with no visable damage, the panel was exposed to the acoustic load for 60 minutes. After the first 15 minutes, small cracks at the bottom of the buckled side closure were noticed. These cracks were monitored during the remaining exposure, but negligible growth occurred. A typical crack is shown in the figure. Since the only edge to experience these cracks during tests was on the side damaged in shipment, the cracks that developed were probably due to the shipping damage.

Since the titanium multiwall panels showed no damage from the acoustic tests, and the only cracks developed on the superalloy honeycomb panels both at JSC and LaRC occurred in areas which had suffered handling damage prior to the tests, it appears that both concepts will survive sonic envionments as high as 161 dB. However, additional acoustic tests may be required to remove the uncertainty.

DAMAGE FROM ACOUSTIC TESTS OF SUPERALLOY HONEYCOMB

a) Tested in JSC Sound Chamber

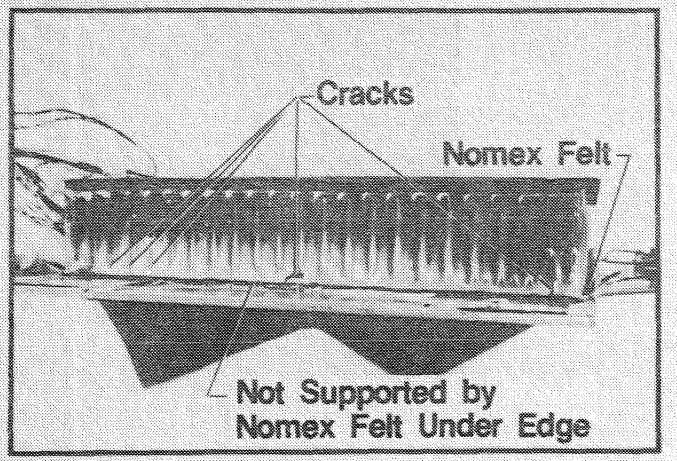

b) Tested LaRC Progressive Wave Facility

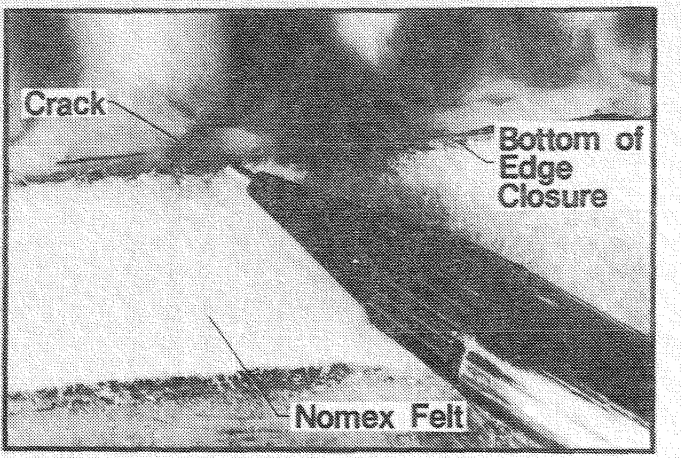

Figure 59

SIMULATED LIGHTNING STRIKE ON METALLIC TPS

A titnaium multiwall panel and a superalloy honeycomb panel were exposed to simulated lightning strikes as shown in Figure 60. The strike on the titanium multiwall resulted in a conical hole through all the layers of the panel with a hole of approximately 1/8 inch diamter in the lower surface (see Fig. 60). However the damage to the superalloy honeycomb panel was limited to the Inconel surface. A spot the size of a dime was indented as though it were hit with a ballpeen hammer. In addition, the face sheet was burned away locally, exposing two of the honeycomb cells. The intensity of these strikes (100 kA) meets the Space Shuttle criteria for lightning strikes on acreage surfaces (Ref. 92).

SIMULATED LIGHTNING STRIKES ON METALLIC TPS

TITANIUM MULTIWALL

SUPERALLOY HONEYCOMB

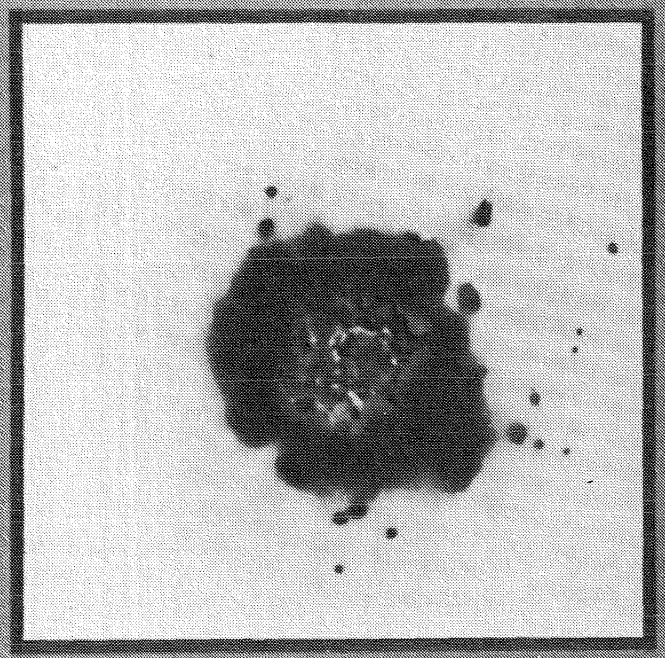

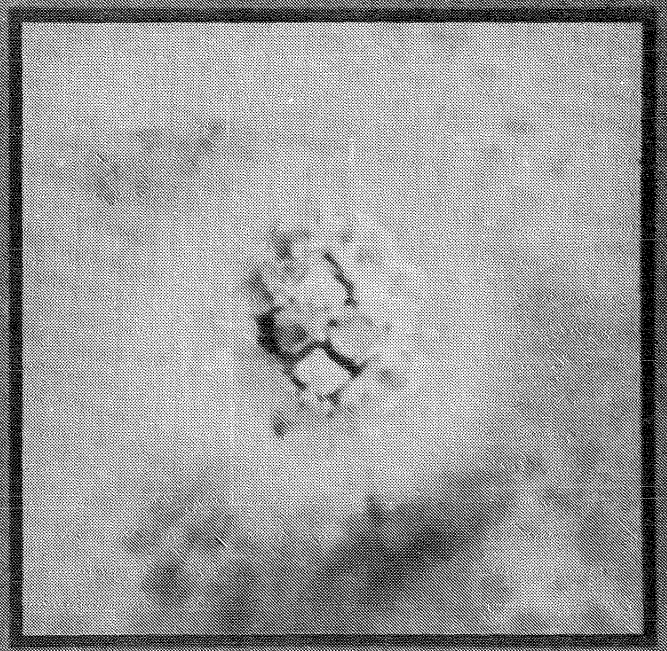

1 in.

100 kA

100 kA

Figure 60

METALLIC TPS ARRAYS FOR 8-FT HTT TESTS

A titanium multiwall array and a superalloy honeycomb array were fabricated for radiant and aerothermal tests in the 8' High Temperature Tunnel (HTT) at LaRC. These arrays, shown in Figure 61, consisted of 20 panels and were configured to fit a standard panel holder used in the 8' HTT. The panel holder has an opening, 60 in. x 42.5 in., and can accept test-specimen thicknesses up to about 12 inches. Since the standard metallic TPS panel is 12 inches square and the panel holder is 42.5 inches wide, panels approximately 6 inches wide were used to close out the array.

The panels, which had vertical beaded edge closures, were installed such that two of their edges were parallel to the flow direction. This installation is considered a "worst case" orientation of the panel with respect to the flow.

METALLIC TPS ARRAYS FOR 8-FT HTST TESTS

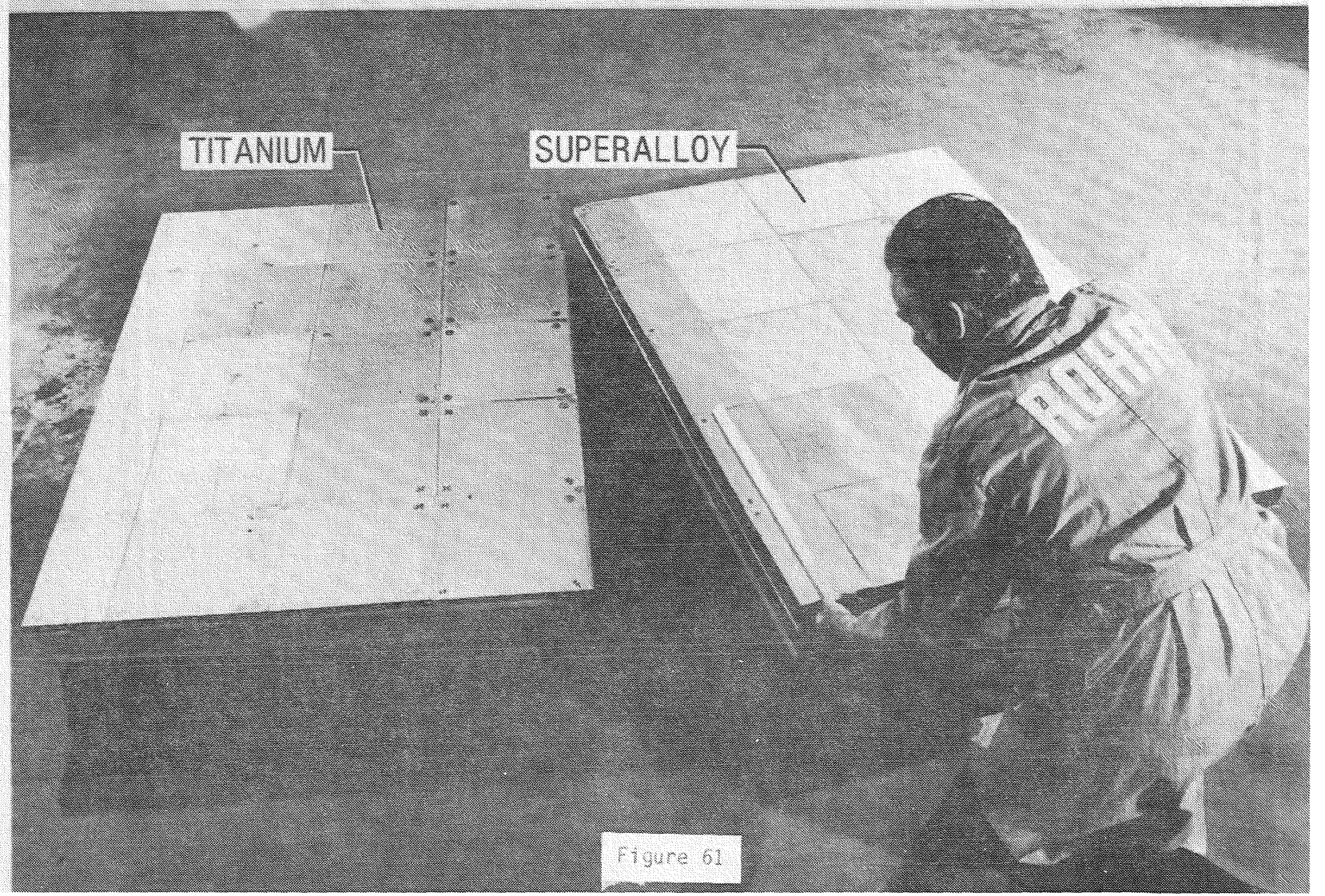

Figure 61

SCHEMATIC OF LANGLEY 8-FOOT HIGH-TEMPERATURE TUNNEL

Figure 62 shows a schematic view of the major components of the 8' HTT which is a "blow-down" tunnel. The model is held in a pod beneath the test section and covered by radiant heaters which not only preheat the model but also protect the model from tunnel start-up and shut-down loads. After the model is preheated and the tunnel is started, the radiant heaters are turned off and retracted by hydraulic actuators. The model is then rapidly inserted into the 8-foot diameter test stream by a hydraulically-operated 15-ton elevator which raises the model to the test position in approximately 1 second. For shutdown, the procedure is reversed. The total aerothermal test duration is up to two minutes depending on test conditions. Details of test techniques are given in Reference 93.

SCHEMATIC OF LANGLEY 8-FOOT HIGH-TEMPERATURE TUNNEL

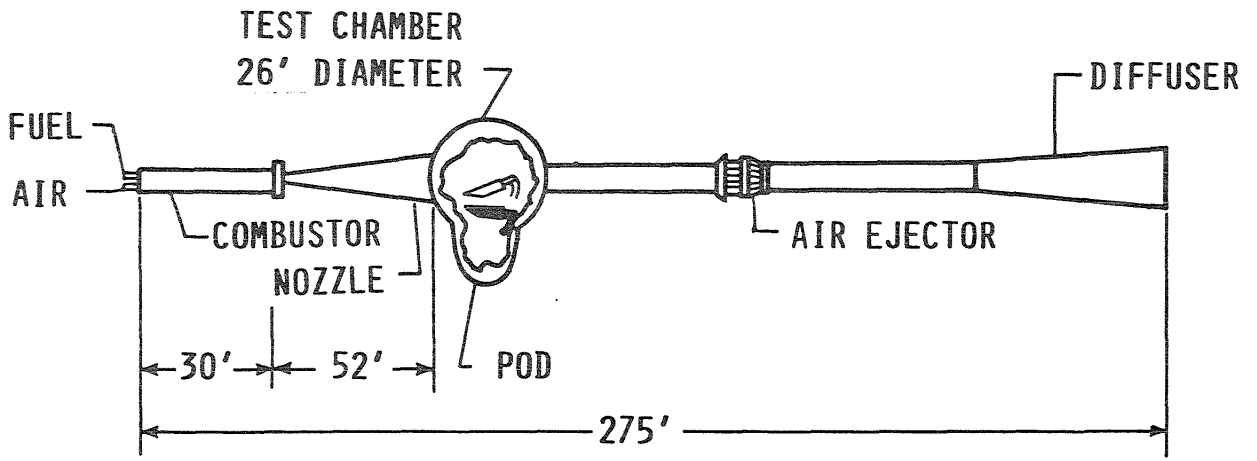

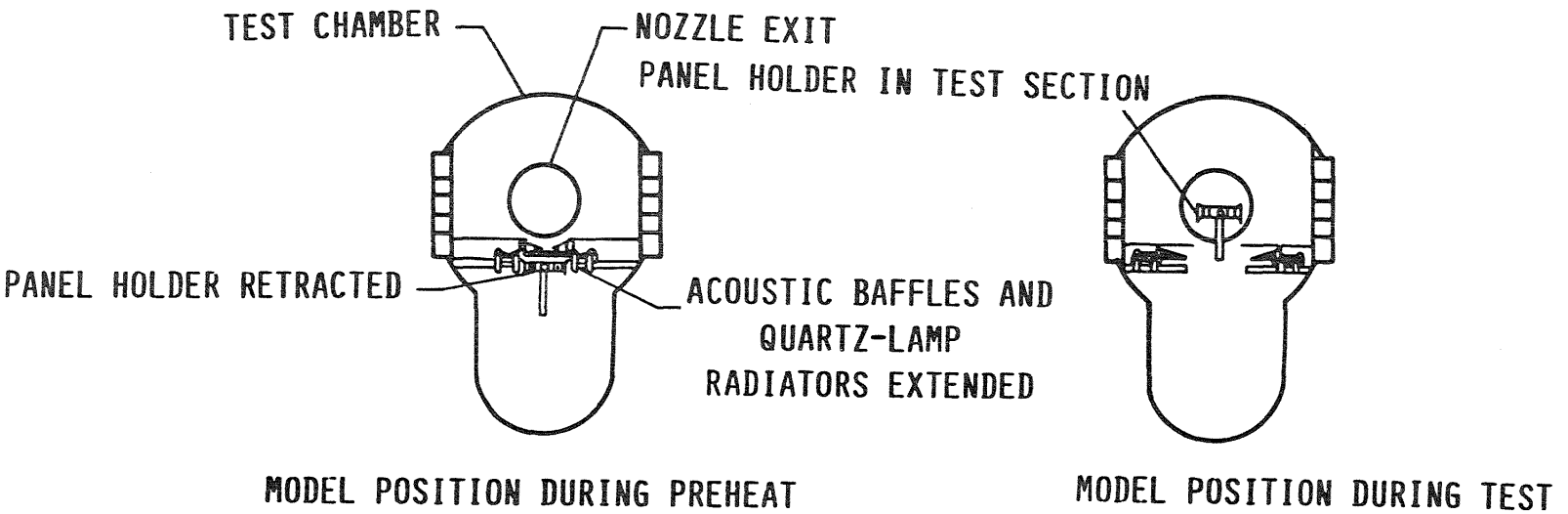

Figure 62

MAXIMUM GAP TEMPERATURES WITH AND WITHOUT FLOW

A nine-tile array of first generation multiwall tiles (Ref. 88) was fabricated and subjected to radiant heating tests and combined radiant-heating/aerothermal tests in the Langley Research Center 8-ft High-Temperature Tunnel (HTT) (Ref. 94). The array was attached to an aluminum panel that was representative of the thermal mass of the Shuttle structure. The tiles were skewed 30° to the direction of flow and were staggered to avoid long, continuous gaps between tiles. In a typical test, the array was radiantly heated before being inserted into the aerothermal environment of the tunnel. Flow conditions in the tunnel simulated the maximum temperature conditions associated with the trajectory 14414.1C entry temperature profile. In addition to the heating environment, the wind tunnel imposed an acoustical load of 163 dB which was slightly higher but similar in frequency content to the design conditions expected at the reference body point.

During the initial radiant heating tests, significant debonding occurred between the top face sheet and the underlying dimpled sheet. The debonding occurred mainly on the edge tiles which were partially restrained from thermal growth by the ceramic surface of the panel holder which surrounded the wind-tunnel array. Therefore, it is felt that unrealistic boundary conditions greatly contributed to the debonding problem. Surface debonding was repaired by spot welding (the tiles were not removed from the panel holder for repairs) and the array was subjected to seven radiant-heating tests and eight combined radiant-heating/aerothermal tests which included a total aerothermal exposure time of 294 s.

The aerothermal tests showed no evidence of localized convective heating in the gaps between tiles due to hot-gas ingress. Figure 63 shows typical maximum temperature distributions down to the edge of a tile where gap flow would impinge if it were present. The temperatures are normalized by the average of the maximum surface temperature T_s measured at the two locations shown. Comparison of the maximum temperatures for radiant heating only with temperature from the aerothermal tests indicate an absence of any significant hot-gas ingress.

Detailed inspection of the disassembled array revealed curling of the overhanging edge and five hairline cracks, all of which were on one of the boundary tiles which was adjacent to the ceramic surface of the panel holder.

These tests identified minor design changes to be incorporated in future designs to improve the fabrication and structural performance of the bonded joints. These changes include (1) slightly larger contact nodes, (2) alignment of tiles in an unstaggered manner to allow edge deflections of adjacent tiles to be more compatible, (3) use of stronger Ti 6Al-2Sn-4Zr-2Mo alloy in place of Ti 6Al-4V, and (4) a vertical edge closure to allow bonding fixtures to improve contact of the bond joints in the overhang region and to avoid interference between panels due to thermal deformations (Ref. 95).

MAXIMUM GAP TEMPERATURES WITH AND WITHOUT FLOW

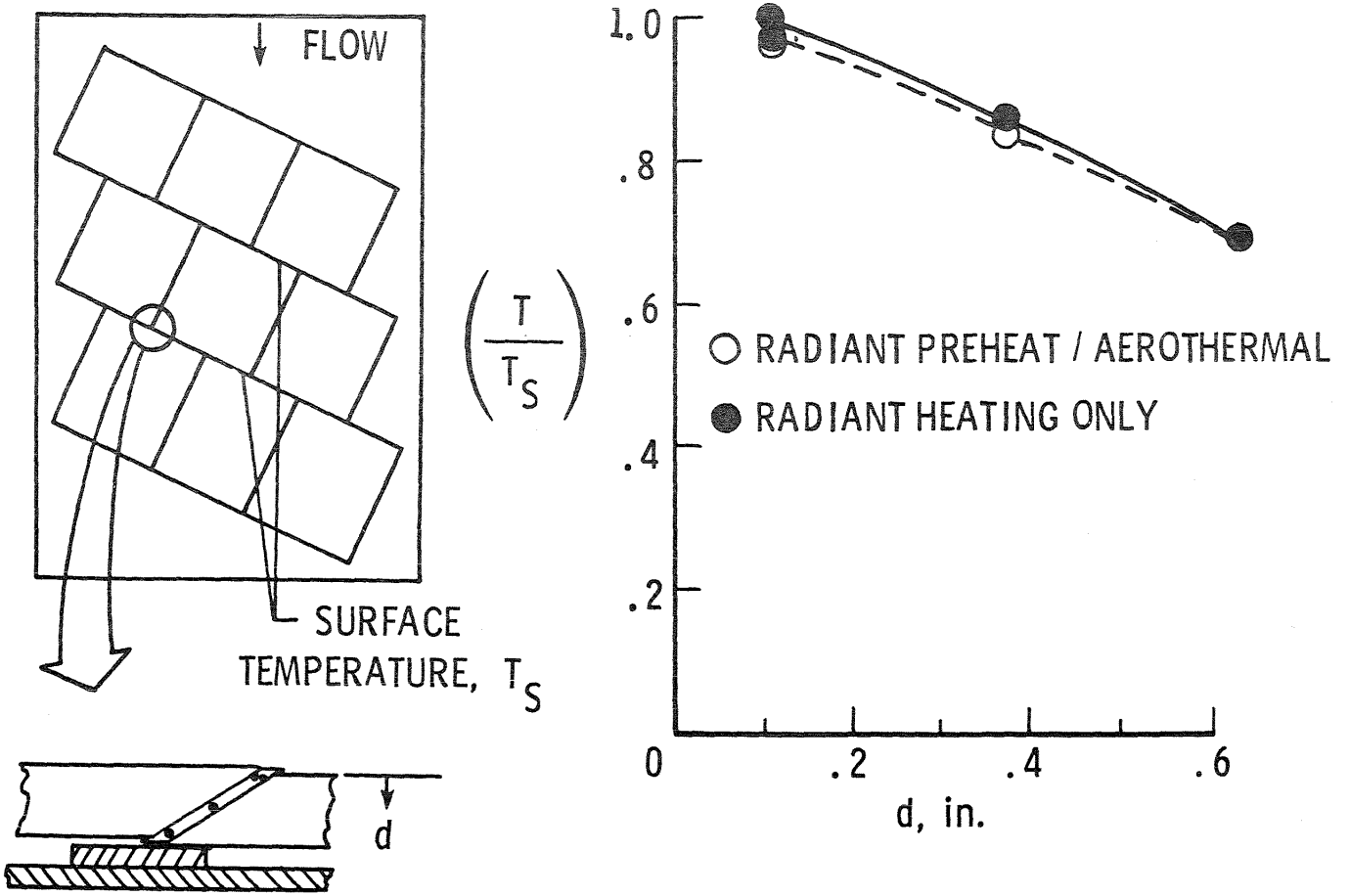

Figure 63

EFFECT OF AEROTHERMAL EXPOSURE ON GAP TEMPERATURE

One of the objectives of the aerothermal tests was to determine if temperatures in the gaps between panels would be increased by exposure to the flow. Such an increase would indicate that the panel edge overlap which covers the gap is not adequate by itself to prevent gap heating when the flow is parallel to the gap. As previously mentioned, tests of an array of 1st generation titanium multiwall panels indicated that flow did not occur in the gaps when the panels were oriented 30° to the flow (Ref. 94).

Surface temperatures and temperatures at the bottom of the gap are shown in Figure 64 for both 20-panel arrays. The dashed curves show temperatures during a 200 second portion of an aerothermal test when the array was inserted into the tunnel stream. The solid curves show temperatures recorded at the same locations and time intervals during a static radiant heating test. At the time interval shown, the surface and gap temperatures of the titanium multiwall model were at equilibrium. When the model was inserted into the flow, negligible temperature perturbation occurred at the bottom of the gap thus indicating no additional gap heating occurred.

Although the surface of the superalloy honeycomb panel reached equilibrium, the temperature at the bottom of the gap, was still approaching equilibrium when the radiant heaters were turned off and the model was inserted into the flow. Immediately after the superalloy model was inserted into the flow, the temperature at the bottom of the gap increased to a level considerably greater than it was before the tunnel started. This high, quick temperature rise indicates that hot gases flow in the gaps between panels. Thus, when the edges of the superalloy panels were parallel to the flow, the overlapping edges do not provide an adequate seal. Superalloy honeycomb panels may be more susceptible to gap heating because the gap is much larger than the gap between titanium multiwall panels. Consequently, when thermal expansion closes the top of the gap, the bottom of the gap remains partly open because it is much cooler.

EFFECT OF AEROTHERMAL EXPOSURE ON GAP TEMPERATURE

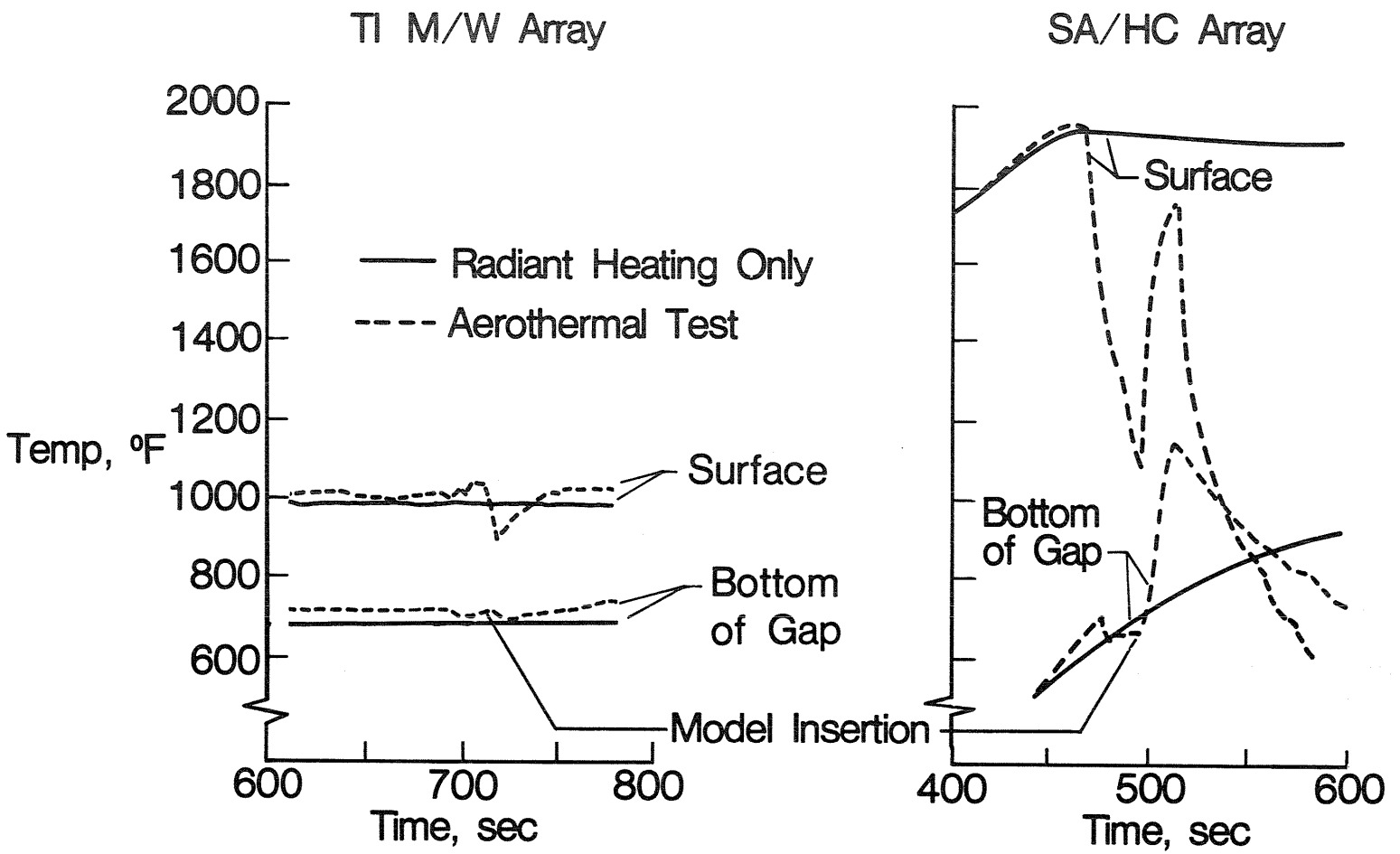

Figure 64

INTENTIONAL SURFACE DAMAGE TO SA/HC 20-PANEL ARRAY

The original test plan for the 20 panel arrays included aerothermal tests with the lightning damaged panel included in the array. The lightning-damaged titanium multiwall panel was unchanged by the aerothermal test. Furthermore, a negligible increase in temperature (less than 10°F) occurred on the backside of the panel at the area of damage. Thus, lightning damage of the titanium multiwall concept does not appear to be a design concern.

The lightning-damaged superalloy honeycomb panel could not be installed into the array in a timely manner; therefore, panels already in the array were damaged to simulate the lightning damage. Figure 65 shows the types of damage inflicted on the panels. The two rows of panels in the foreground of the figure, which were coated with a ceramic non-catalytic coating (Ref. 96) were the panels that received the damage. (The dark panels in the background were coated with a high temperature, high emittance paint.)

INTENTIONAL SURFACE DAMAGE TO SA/HC 20-PANEL ARRAY

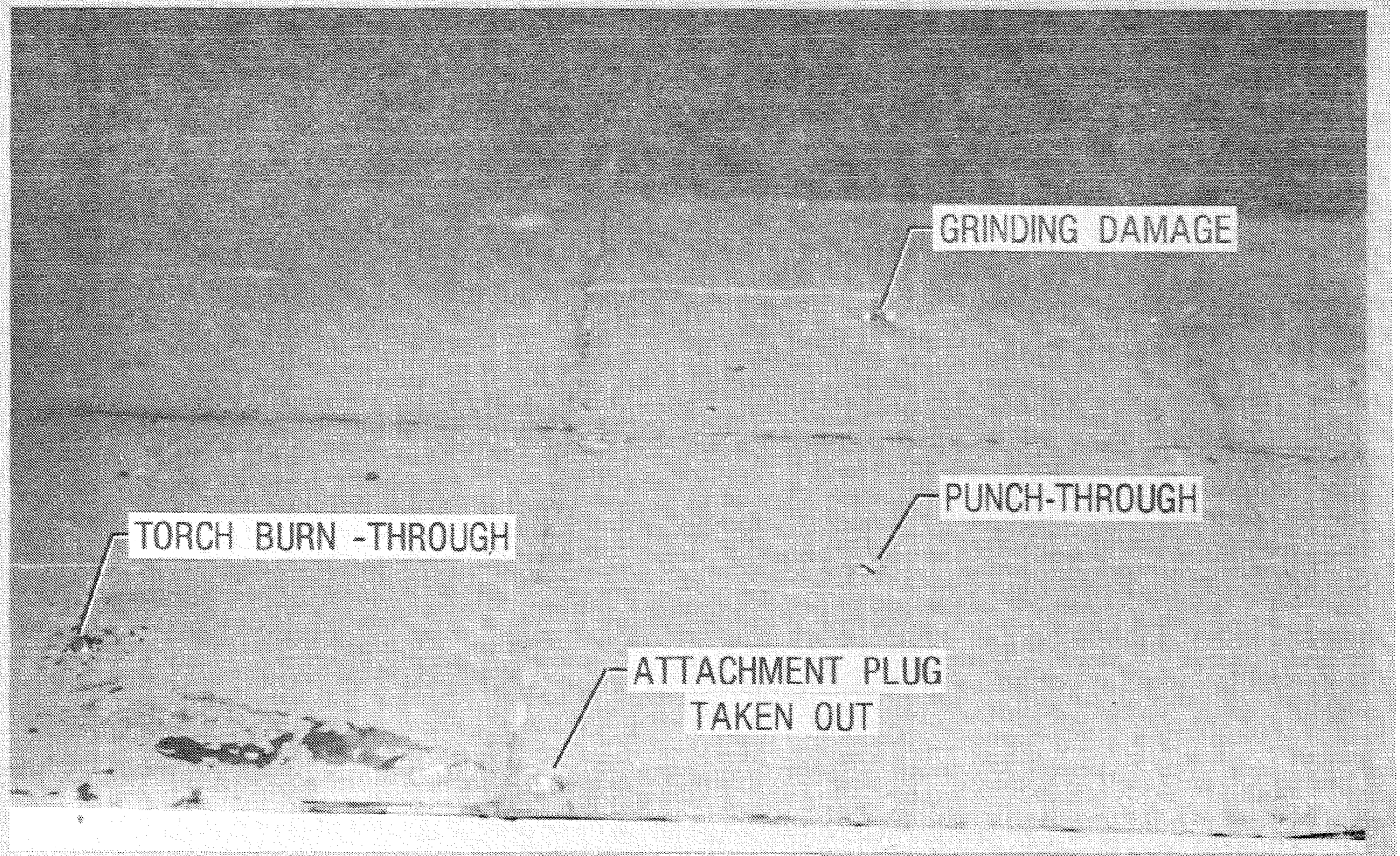

Figure 65

SA/HC 20-PANEL ARRAY IN 8' HTT

Figure 66 was made from a frame of movie film taken during the last aerothermal test of the superalloy honeycomb 20-panel array in the 8' HTT. The only light used to expose the film was that radiating from the model which was at a temperature of about 1850°F. The thermal deflections of the heated model resulted in panel "pillowing" which causes slightly higher temperatures to occur on the upstream side than on the downstream side of the individual panels. The greater brightness (and higher temperature) of the right-hand side of the array (looking downstream) is caused by the lower emittance of the panels with the non-catalytic coating.

Several hot spots can be seen where the face sheet buckled and delaminated from the honeycomb core. This damage occurred early in the test program when fiberglass curtains, used to protect surrounding structure from radiation from the quartz heaters, melted and fell on the panels. The buckles and delaminations did not propagate during the balance of the test program. A hot spot was caused by the torch burn-through shown on the previous figure. The other two damaged locations and the open attachment hole did not appear to cause any significant overheating. Bent up gap covers also showed up as hot spots since they protrude into the air flow. The gap covers in the rear of the model were in contact with the rigid glassrock which surrounded the array and were deformed when the panels bowed thermally. The gap-cover hot-spot that occurred at the intersection of four panels was probably caused by thermal bowing interference between panels with different attachments. This was the only intersection where a bayonet-clip-attached panel overhung a panel with through-panel attachments.

Post-test inspection of the array was not possible because, at the end of this test, part of the panel holder broke loose and caused the tunnel to "unstart." The strong shock wave (10 psi pressure rise in about 0.2 seconds) passing through the test section completely destroyed the array of panels.

SA/HC 20-PANEL ARRAY IN 8' HTT

RUN20

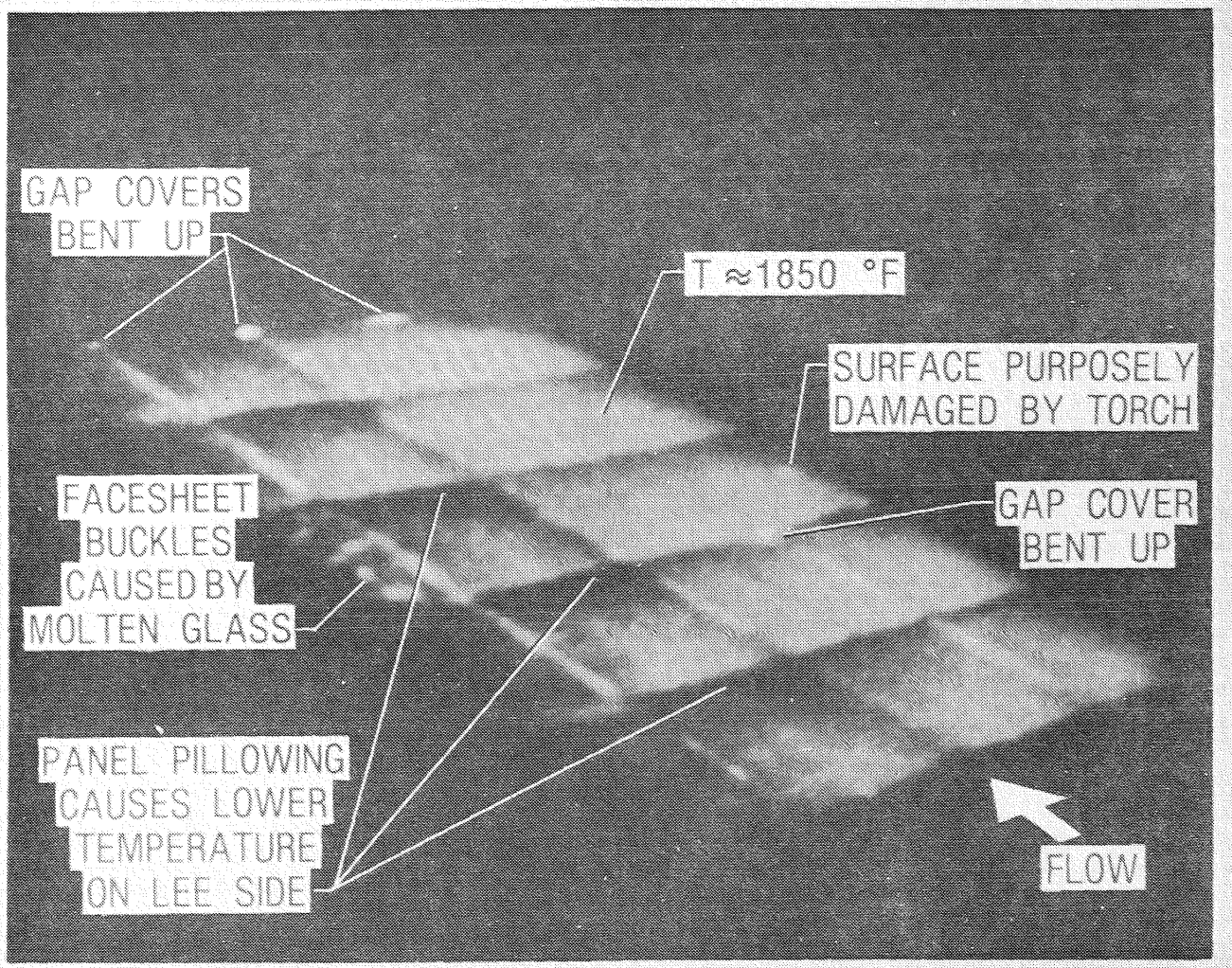

Figure 66

CURVED SUPERALLOY HONEYCOMB TPS PANELS

Even though much of the surface of Shuttle-type vehicles is flat or nearly flat, some locations, such as the chine areas, are necessarily curved. The fabrication of curved TPS panels often presents complexities not encountered in fabricating flat panels, and the design of curved panels must include large surface pressure gradients and factors contributing to thermal stress which are normally not important in the design of flat TPS.

A curved titanium multiwall panel has been fabricated to demonstrate that the multiwall concept will lend itself to curved panels (Ref. 97), and an array of curved superalloy panels has been fabricated for aerothermal tests to evaluate their performance in a high-surface-pressure gradient environment. The curved 20-panel array shown in Figure 67 will be installed into the cavity of the Curved Surface Test Apparatus (CSTA), so that the surface of the array will be flush with the surface of the CSTA. The array will be instrumented with thermocouples and pressure sensors and tested in the LaRC 8' HTT to determine if heating occurs in the gaps between panels. Metal tabs, one of which is identified on the single panel in the figure, are located at the corner intersections of the panels to block flow in the gaps. All of the panels are attached with through-panel fasteners. These tests are planned for May-June, 1985.

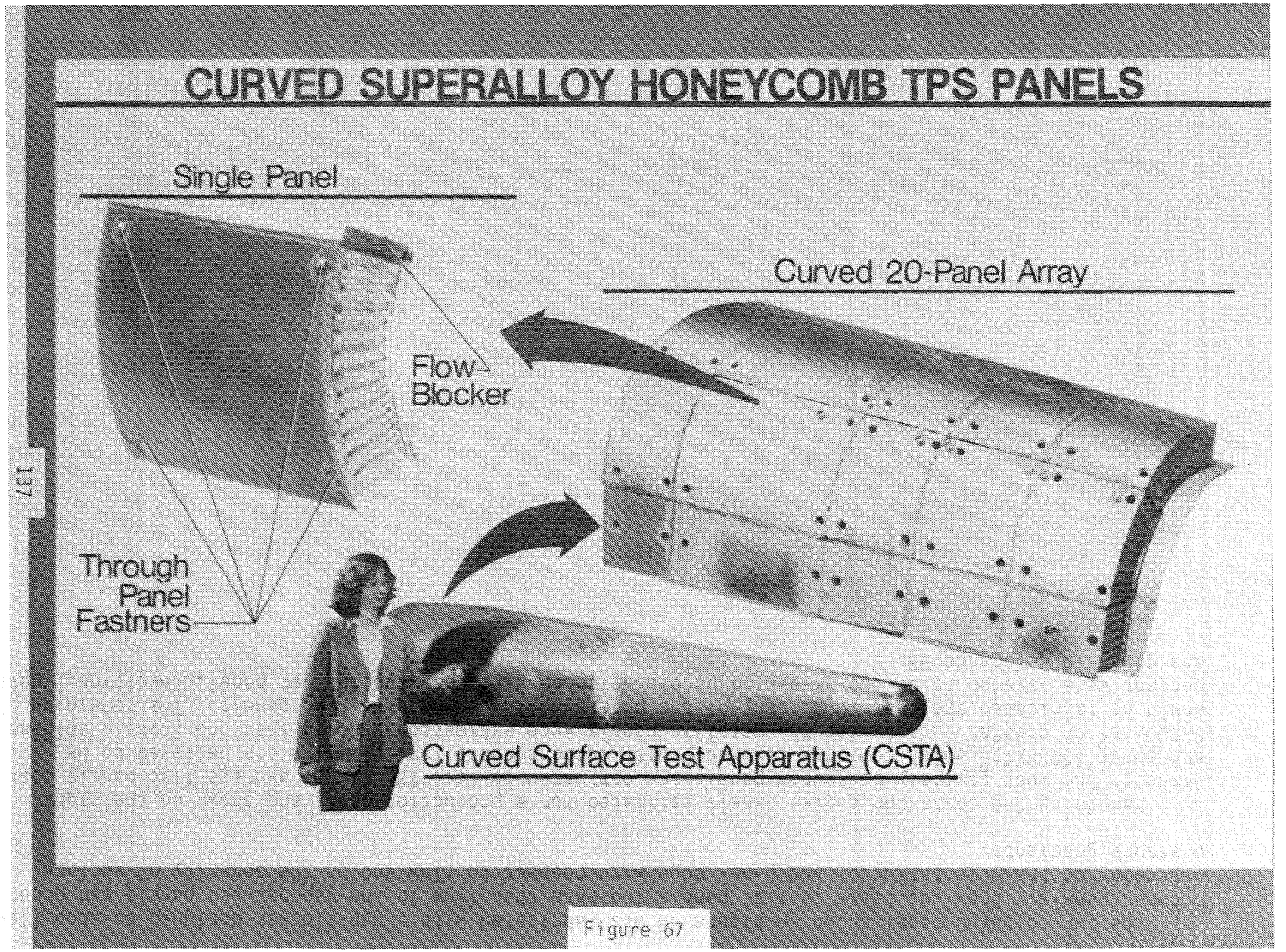
CURVED SUPERALLOY HONEYCOMB TPS PANELS
Single Panel
Curved 20-Panel Array
Flow Blocker
Through Panel Fastners
Curved Surface Test Apparatus (CSTA)

Figure 67

CURVED SUPERALLOY HONEYCOMB PANEL

The curved SA/HC panel shown in Figure 68 was fabricated with a gap blocker designed to stop flow between panels. Previous tests of flat panels indicate that flow in the gap between panels can occur depending on the orientation of the panel edge with respect to flow and on the severity of surface pressure gradients.

Manufacturing costs for curved panels estimated for a production basis are shown on the right. Although the most severely contoured panels are estimated to cost $\$2800/ft^2$, average flat panels costs are about $\$2000/ft^2$ which compares favorably with current costs for RSI which are believed to be $\$2000/ft^2$ or greater. Costs for the metallic panels were estimated assuming that one Shuttle shipset would be fabricated and that 70 percent of the panels would be one-of-a-kind panels. The remaining 30 percent were assumed to be two-of-a-kind panels which require less tooling per panel. Additional details are given in Reference 98.

CURVED SUPERALLOY HONEYCOMB PANEL

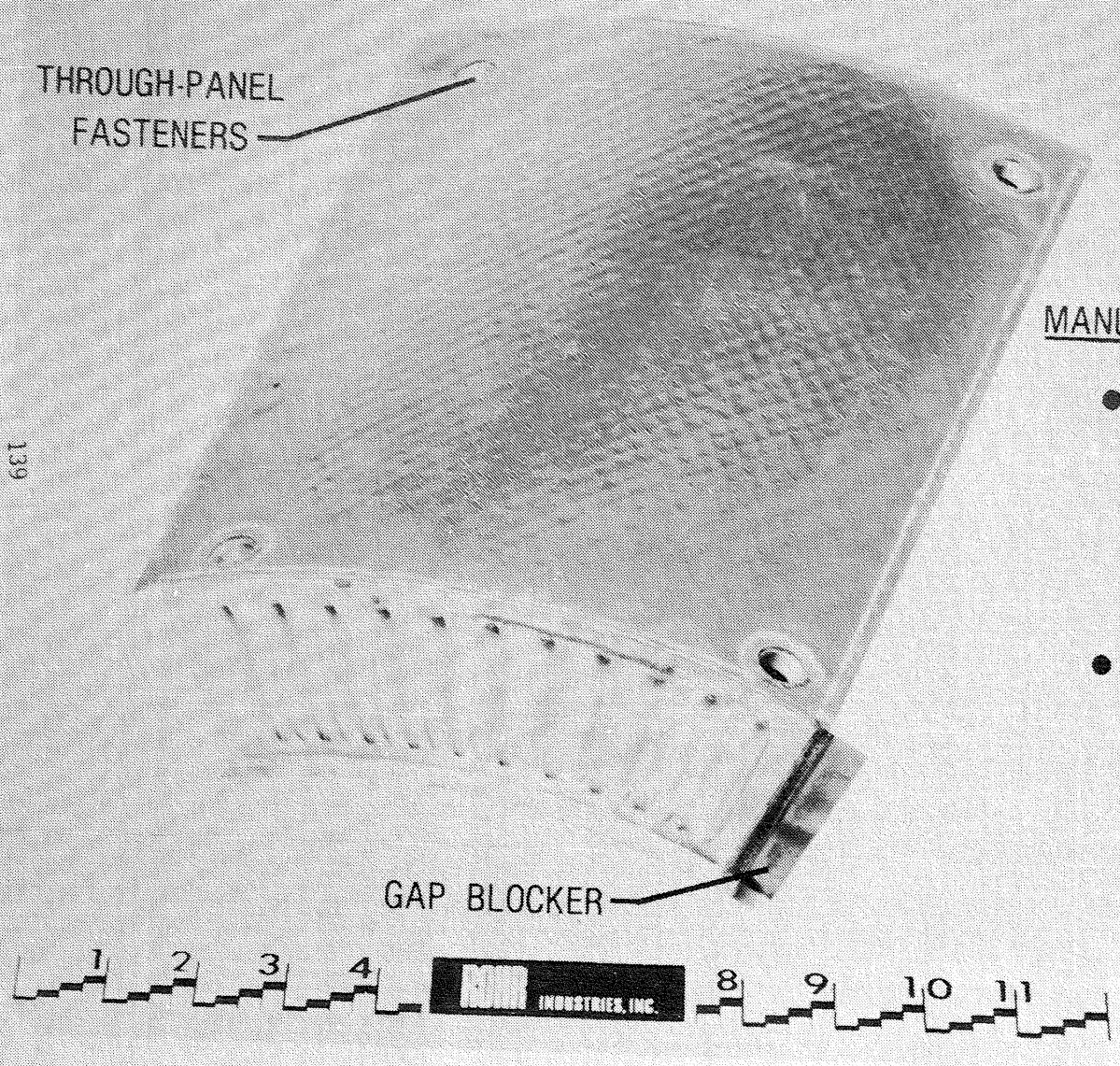

MANUFACTURING COST (ROHR)

- $2800/ft^2 — MOST SEVERE CONTOUR

ASSUMPTIONS

- 1 SHUTTLE SHIPSET
  - 70% 1-OF-A-KIND
  - 30% 2-OF-A-KIND

Figure 68

PROPOSED TPS TEST MODEL FOR INTERSECTING SURFACES

Figure 69 shows a sketch of the curved surface test apparatus (Ref. 64), CSTA, fitted with boiler plate wing calibration surfaces. This configuration has been designed but not fabricated. Once built and calibrated it will be modified to accept TPS panels for the intersecting fuselage and wing surfaces. Metallic TPS for such areas are likely as the equilibrium surface temperatures should be in the range (<2000F) where metallic TPS are lighter than all TPS concepts (Ref. 99). Design of an air tight (no hot gas ingress) metallic system for such an area is a challenge that apparently has not been previously addressed, at least not to the level of aerothermal environmental tests of flightweight hardware.

PROPOSED TPS TEST MODEL FOR INTERSECTING SURFACES

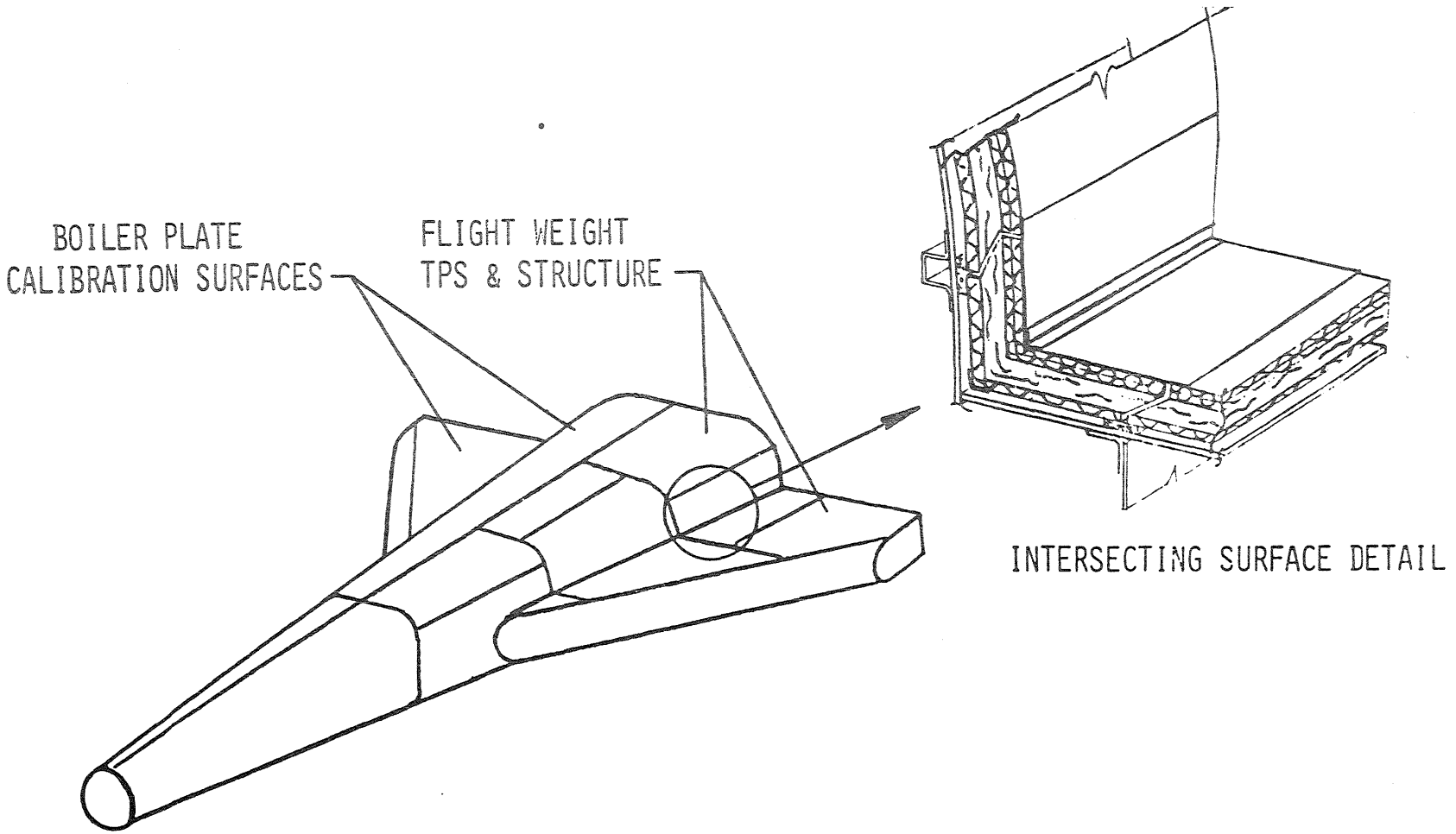

Figure 69

METALLIC TPS - SUMMARY

The results from a variety of verification tests indicate that metallic TPS concepts are viable over a temperature range from 700°F to 2000°F and are mass competitive with the current RSI thermal protection used on the shuttle. The disciplines considered for the verification tests include thermal and aerothermal performance, vibration and acoustic exposure, and exposure to simulated lighting strikes.

In an R&T generic-concept development program, limiting the disciplines to be studied and limiting the depths of study within each discipline is an arbitrary decision based on a trade-off between information desired and resources available. The adequacy of test environments selected today to represent environments for tomorrow's applications is a continual concern. For example, the perceived need to demonstrate the ability of metallic TPS to withstand wind and rain will require selecting a generic all-weather criteria which may not satisfy the needs of tomorrow's application. Another need is to study the thermal and aerothermal performance of curved metallic TPS including the study of thermal stress which becomes increasingly important as curvature increases. The potential to extend the temperature range of metallic TPS to about 2300°F exists by using higher temperature ODS materials.

Intersecting surfaces with concave curvature may have stress and deflection characteristics different from convex-curved surfaces. The list of possible study subjects goes on beyond surface erosion, but the items become less important in identifying critical "go or no go" characteristics of the concepts, and this can be left to be addressed by those applying the concept to a specific application.

METALLIC TPS - SUMMARY

ACCOMPLISHMENTS

- METALLIC TPS MASS COMPETITIVE WITH CURRENT SHUTTLE RSI TPS DEMONSTRATED FOR TEMPERATURES UP TO 2000°F
  - THERMAL/AEROTHERMAL
  - VIBRATION
  - ACOUSTIC
  - LIGHTNING STRIKE

NEEDS

- ESTABLISH ALL-WEATHER CRITERIA AND DEMONSTRATE ABILITY TO MEET IT
- DETERMINE THERMAL AND AEROTHERMAL PERFORMANCE OF CURVED METALLIC TPS INCLUDING THERMAL STRESS CHARACTERISTICS
- EXTEND METALLIC TPS TO 2300°F
- EVALUATE TPS CONCEPTS FOR INTERSECTING SURFACES
- SURFACE EROSION

Figure 70

ADVANCED CARBON-CARBON MULTIPOST STANDOFF TPS CONCEPT

The Advanced Carbon-Carbon (ACC) multipost concept (maximum surface temperature > 2000°F) shown in Figure 71 consists of a rib-stiffened ACC sheet attached to the vehicle primary structure by posts with fibrous insulation packaged in a ceramic cloth between the ACC panel and the vehicle structure. (Venting and waterproofing of the insulation package is a problem not studied in this investigation.) The surface of the single ACC panel is nominally 36 inches square. The ACC multipost concept is described in detail in Reference 100, and fabrication of the ACC test model discussed herein is described in Reference 101.

ADVANCED CARBON-CARBON MULTIPOST STANDOFF TPS CONCEPT

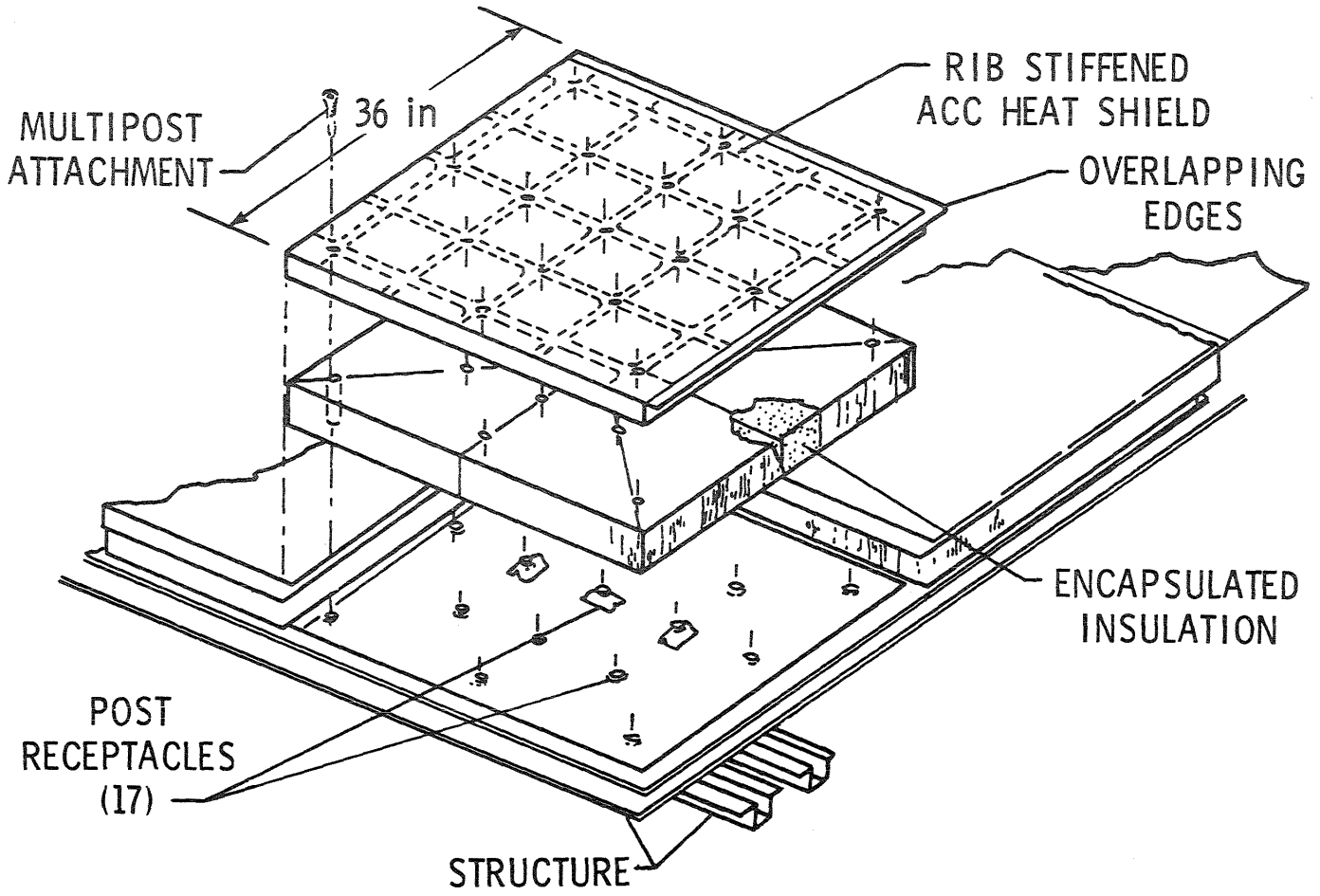

Figure 71

ACC MULTIPOST TPS TEST ARTICLE

The same 1 ft. by 2 ft. test model, Figure 72, that was subjected to the thermal vacuum tests was also subjected to aerothermal tests. The model is shown in Figure 73 installed in the LaRC 20-MW Aerothermal Arc Tunnel. The model was mounted in a water-cooled holder at 15° angle of attack to the stream with a 6-inch transition section between the nozzle and the model. Conditions were selected which gave a 2300°F surface temperature on the front of the model. Figure 54 shows the model in the test stream. Only light being radiated from the model was used to expose the film.

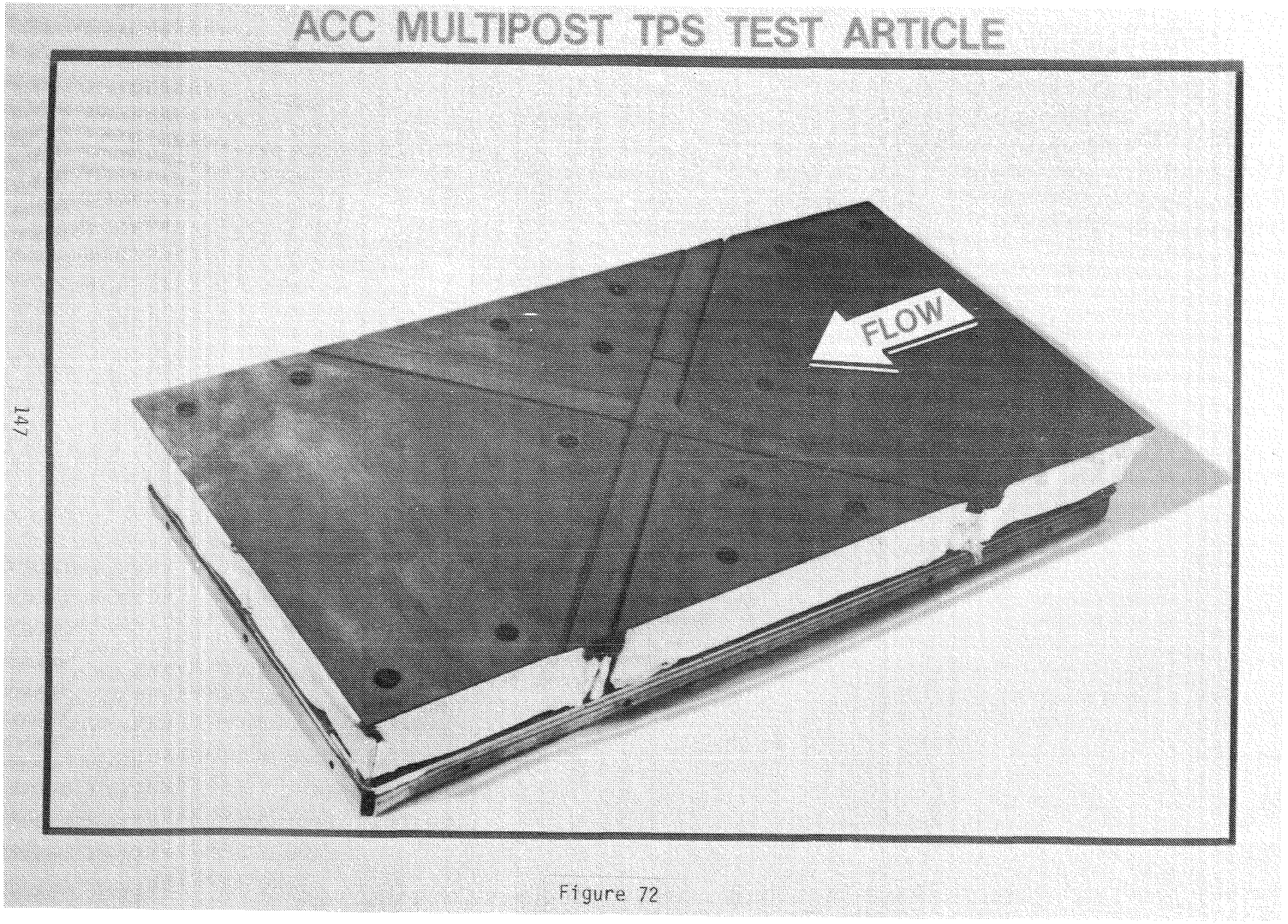

Figure 72

Page Missing in Original Document

ACC MULTIPOST TPS IN ARC-TUNNEL

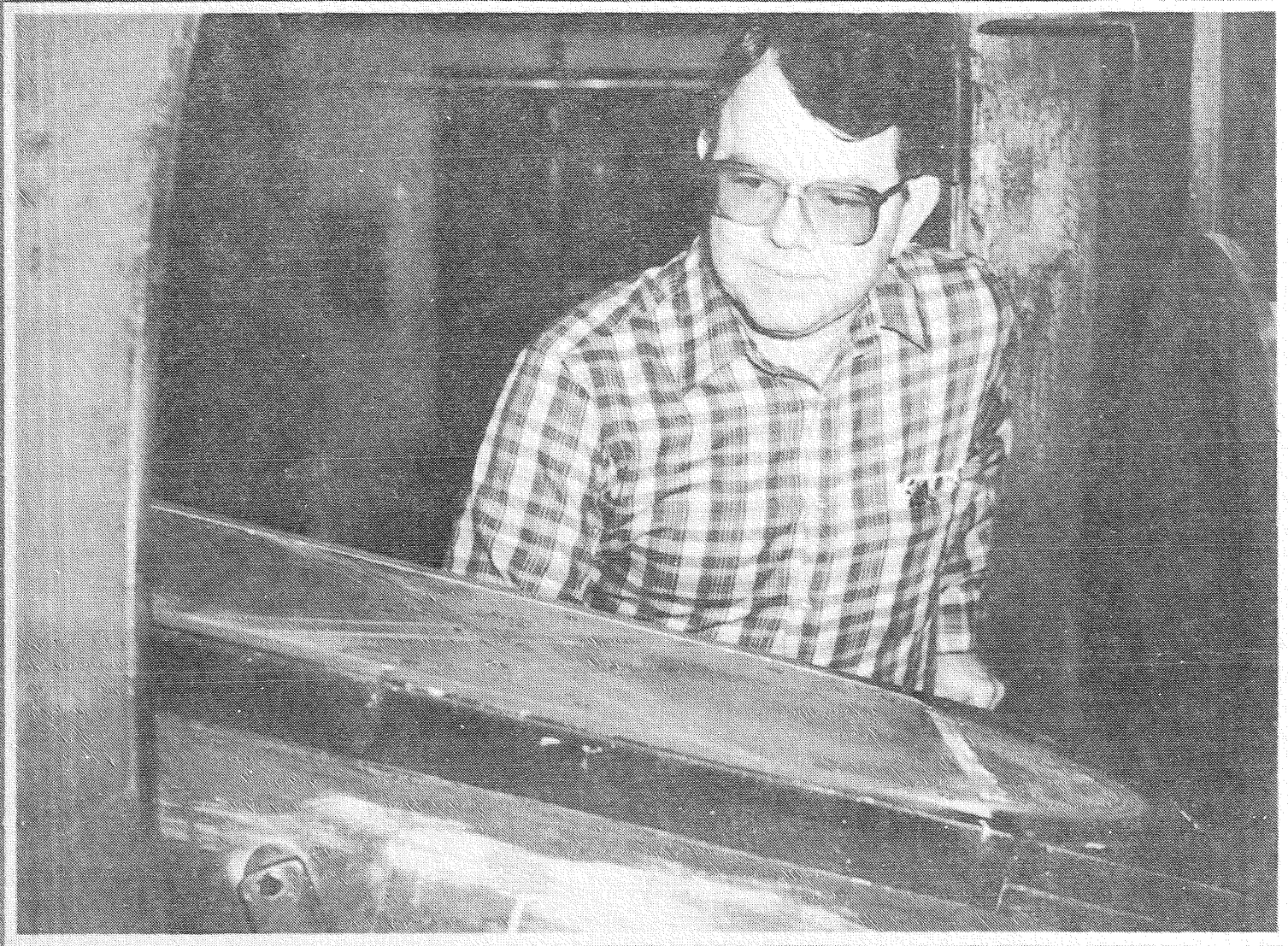

Figure 73

EFFECT OF AEROTHERMAL EXPOSURE ON GAP TEMPERATURE-ACC MULTIPOST

A comparison of temperatures obtained during the arc-tunnel tests with those obtained during a thermal/vacuum test is shown in Figure 74. The temperature was measured at the center of the model where pieces of 4 separate panels intersect. Thermocouples placed at locations 1, 2, and 3 measured the temperature at the ACC skin, at 1/3 of the depth of the model, and at the bottom of the model, respectively. The tunnel condition resulted in a surface temperature (1) nearly 100°F less than that obtained during the thermal/vacuum test. However, the temperature measured at (2) during the arc-tunnel test was not less than that obtained during the thermal vacuum test, indicating that slight heating due to flow occurred in the gap region where one panel overlaps another. A local design change may be required if this preliminary conclusion is sustained by additional test results and if the heating is found to be significant. The lower teperature measured on the aluminum plate during the tunnel test was typical of other locations and probably reflects a larger heat-sink effect caused by a water-cooled holder which was not used in the thermal/vacuum tests.

The ACC model was not damaged by either the thermal/vacuum or arc-tunnel tests. The only change in appearance occurred during the arc-tunnel tests when erosion of copper electrodes caused an orange-colored copper deposit on part of the model surface.

EFFECT OF AEROTHERMAL EXPOSURE ON GAP TEMPERATURE-ACC MULTIPOST

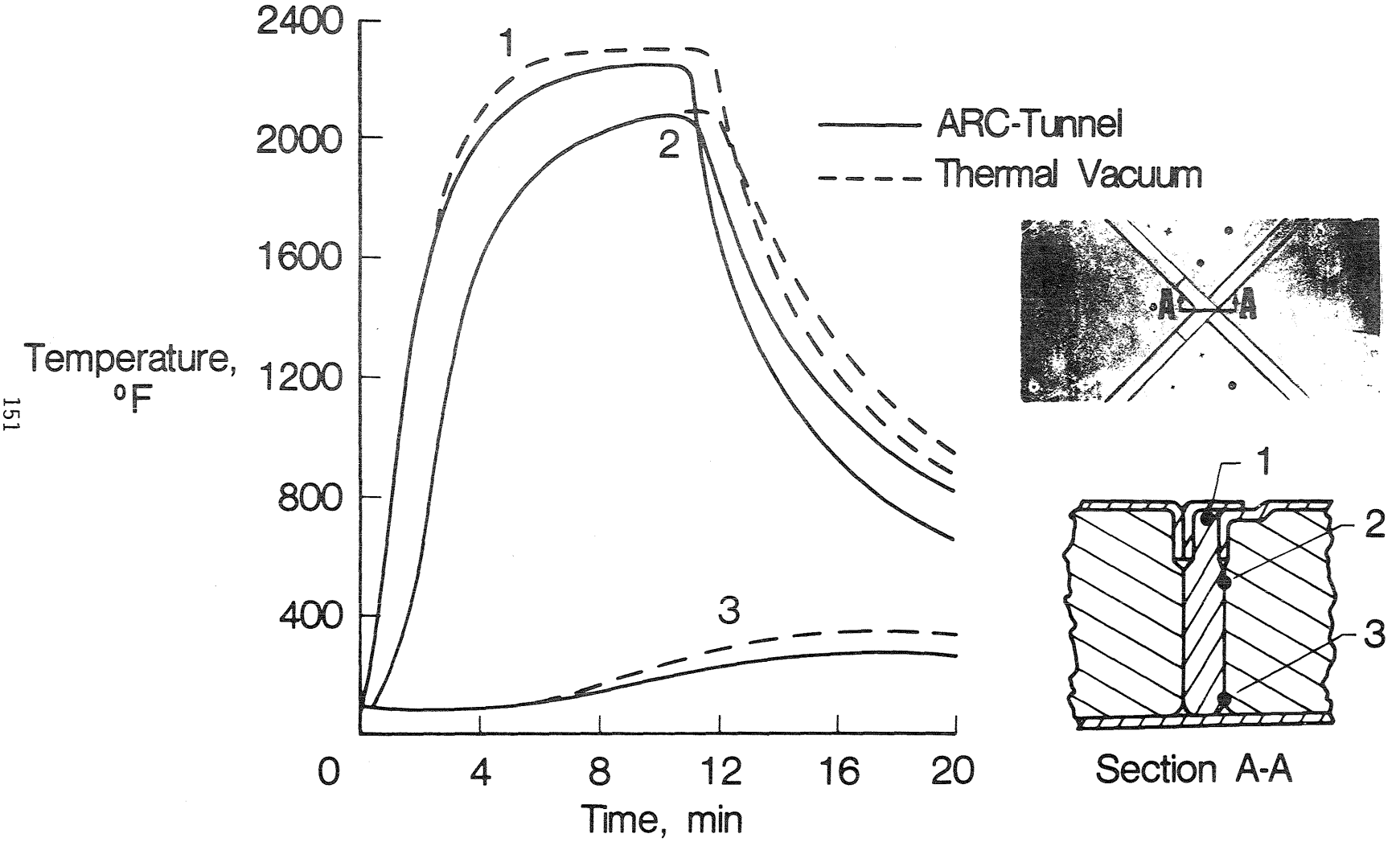

Figure 74

SUMMARY - ACC TPS

Advanced carbon-carbon is a promising material for acreage TPS applications at high temperatures. A multipost concept has been built and subjected to limited radiant heating and arcjet aerothermal tests with surface temperatures up to 2300°F. The specific concept that was tested may need a design change to prevent hot gas engress at panel joints. The material is subject to oxidation and thus must be coated. Tests have shown that impact damage of the coatings may be a problem. Materials research suggests use temperatures of 3000°F should be achieveable now, 3500°F in the near term, and 4000°F may be obtainable. The complex process required to make coated carbon-carbon makes these TPS concepts very expensive.

SUMMARY - ACC TPS

- MULTIPOST CONCEPT FOR ACERAGE APPLICATIONS SURVIVED REPEATED THERMAL EXPOSURES TO 2300° F

- ARCJET TESTS SUGGEST JOINT-SEAL DESIGN CHANGE MAY BE REQUIRED

- IMPACT DAMAGE TO COATINGS MAY BE A PROBLEM

- MATERIALS RESEARCH SUGGESTS HIGHER USE TEMPERATURES POSSIBLE
  - 3000° F, NOW
  - 3500° F, NEAR TERM
  - 4000° F, MAYBE

- WILL BE EXPENSIVE

Figure 75

HEAT-PIPE-COOLED LEADING EDGE ATTRACTIVE CONCEPT FOR HIGH-SPEED VEHICLES

Analytical studies have indicated that heat pipes could be incorporated in wing-leading edge structure to reduce peak stagnation temperatures and temperature gradients. A heat-pipe-leading edge could be constructed of durable superalloy metals instead of carbon-carbon, ablative, or coated refractory metals.

To investigate the concept a 1/2-scale feasibility test model representing a 6-inch span of the Shuttle Orbiter wing leading edge was fabricated. The model consisted of 12 sodium-filled Hastelloy X heat pipes whose performance was investigated in a series of radiant heating and aerothermal tests (see Fig. 76). Results of these tests are presented in References 102 and 103. A total of 34 radiant heat tests and 8 aerothermal tests indicate that the model was very durable and able to withstand overdesign heating and pressure loads. Results also indicated that a simple analysis method could accurately predict heat pipe startup and steady-state performance. As shown in Figure 76, peak temperatures were reduced by 1050°R to a level compatible with superalloy metals; also, temperature gradients and associated thermal stresses were eliminated.

Continued studies (Ref. 104) have led to a lighter weight configuration. It consists of a panel with a smooth 0.020 in. outer skin and a corrugated 0.016 in. inner skin. The two skins would be pre-formed to the contour of a leading edge, lined with screen wicking, and then longitudinally seam welded together, resulting in 0.5 in. diameter D-shaped channels running in a chordwise direction. The D-shaped heat pipe cross-section was determined to be optimum from the standpoint of structural weight--1.9 lb/ft^2, approximately 44% lighter than the circular cross-section previously investigated. This weight reduction makes the heat-pipe-cooled leading edge weight-competitive with the carbon-carbon design currently on the shuttle, for example, and enhances its utility for stagnation heating areas of future high speed vehicles.

HEAT-PIPE-COOLED LEADING EDGE ATTRACTIVE CONCEPT FOR HIGH SPEED VEHICLES

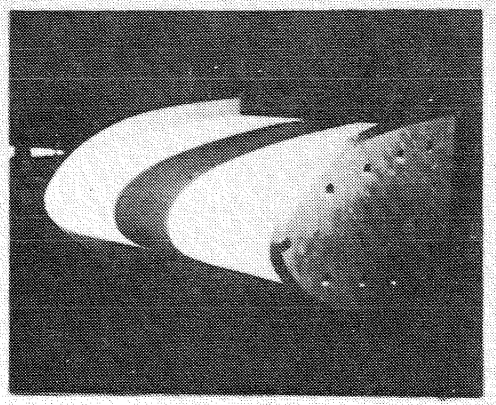

AEROTHERMAL TESTS IN LaRC 8'-HTST

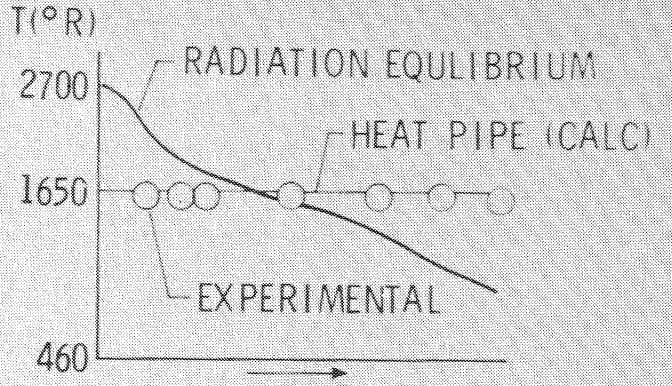

STEADY-STATE TEMP. DIST.

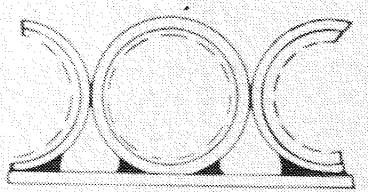

ORIGINAL

17 kg/m^2
(3.4 llm/ft^2)

REVISED
DESIGN CONCEPT

9.3 kg/m^2
(1.9 llm/ft^2)

REVISED DESIGN

- REDUCES T_{MAX} AND ΔT
- DURABLE
- MASS AND COST COMPETITIVE WITH CARBON-CARBON

Figure 76

ACTIVELY COOLED AIRFRAME STRUCTURES

For hypersonic aircraft to become a practical reality, techniques must be developed for the design and fabrication of low-mass, airframe structures that can withstand repeated and prolonged exposure to the severe aerodynamic heating encountered in hypersonic flight. The advancement of structural technology for this hostile flight regime has been the objective of continuing coordinated research at the NASA Langley Research Center.

In 1966, Heldenfels (Ref. 2) reviewed the structural prospects for hypersonic vehicles. Emphasis then was on hydrogen fuel-cooled structures for engines and passive hot structures of high temperature materials for airframes. Predicated on prospects of hydrogen fueled scramjets with low cooling requirements (Ref. 105), Becker, in 1970 (Ref. 106) proposed convectively cooled airframe structures of conventional low-temperature, low-mass materials (e.g., aluminum) that used the hydrogen fuel as the ultimate heat sink for all cooling requirements. The basic concept, uses a closed-loop secondary cooling circuit with liquid coolant flowing through passages to the surface structure to transport the absorbed aerodynamic heating to a heat exchanger where the heat is rejected the cryogenic hydrogen fuel flowing to the engine.

Although early studies recognized problems in matching the instantaneous aerodynamic heat load with the heat sink capacity of the hydrogen fuel flowing to the engines and proposed partial heat shielding to reduce the absorbed heat load, both system studies (Ref. 107-112) and hardware studies (Refs. 113-114) following the lead of Becker, concentrated on bare cooled structures with high level-cooling. Recent studies (Refs. 115-117) have yielded a better understanding of the significance of heat sink matching and the mass penalties associated with high-level cooling.

To complement the system studies a series of design and fabrication studies has produced three structural panels for thermal structural testing. The test structures include a shielded panel and two bare panels of different construction. All panels were designed for the same environment. Additionally, each panel was designed for a life of 10 000 hours and 20 000 fully reversed limit load cycles. The panels differed in both structural and cooling concepts but each used aluminum as the structural material and a 60/40 glycol water mixture as a coolant. The heat shielded configuration features a corrugation stiffened Rene'41 heat shield and an adhesively bonded honeycomb sandwich structure with half round coolant tubes. One of the bare configurations uses an adhesively bonded stiffened-skin structure with redundant, counter-flow, quarter-ellipse coolant tubes; the other uses a brazed plate-fin sandwich with adhesively bonded stiffeners for both the structure and cooling passages. Additional characteristics and features of the concepts are presented in Reference 113 and complete details of the shielded panel design and fabrication are presented in Reference 117.

ACTIVELY COOLED AIRFRAME STRUCTURES

SYSTEM STUDIES

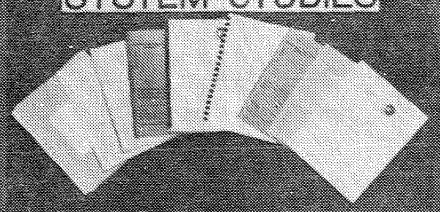

ACTIVE COOLING
WITH H_2 HEAT SINK--
AN ATTRACTIVE STRUCTURAL CONCEPT

PRACTICAL AIRFRAMES FOR HYPERSONIC FLIGHT

STRUCTURAL DESIGN STUDIES

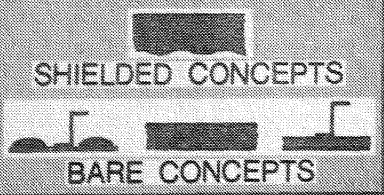

SHIELDED CONCEPTS

BARE CONCEPTS

SPECIMEN FATIGUE TESTS

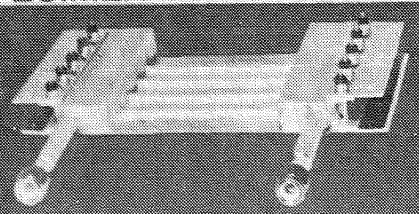

STRUCTURAL CONCEPT VERIFICATION

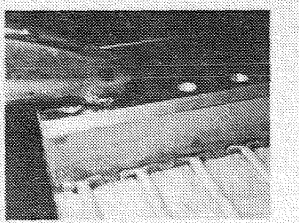

FABRICATION
DEVELOPMENT

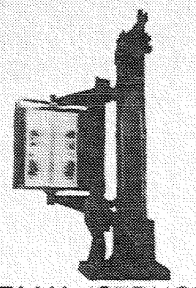

THERMAL/STRUCTURAL
TESTS

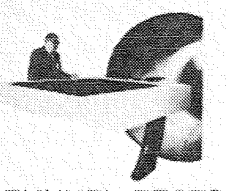

WIND TUNNEL TESTS

Figure 77

RADIATIVE-ACTIVELY COOLED PANEL TEST RESULTS

As described in Reference 49 and 50, and shown in Figure 78, a flightweight radiantly and actively cooled panel (RACP) was subjected to thermal/structural tests representing design flight conditions for a Mach 6.7 transport and off-design conditions simulating flight maneuvers and cooling system failures. The 2- by 4-ft. RACP was designed to withstand a uniform heat flux of 12 Btu/ft^2-sec to a 300°F surface temperature and utilized Rene' 41 heat shields backed by a thin layer of high-temperature insulation to radiate away most of the incident heating. A 60-percent mass solution of ethylene glycol in water circulating through tubes next to the outer skin of an aluminum-honeycomb-sandwich structural panel absorbed the remainder of the incident heating (0.8 Btu/ft^2 -sec). A total of 32 tests exposed the RACP to 15 thermal cycles and multiple cycles of mechanical loading. The RACP successfully withstood 55 hr of radiant heating and 5000 cycles of uniaxial inplane limit loading of $\pm$1200 lb/in. Additionally, the RACP withstood off-design heating conditions for a simulated 2g maneuver from cruise conditions and simulated cooling system failures without excessive temperatures on the structural panel. Wind tunnel tests exposed the RACP to 15 aerothermal cycles for a total of 137 sec in a Mach 6.6 test stream. The RACP responded as predicted and survived the extensive aerothermal/structural testing imposed without significant damage to the stuctural panel, coolant leaks, or hot-gas ingress to the structural panel.

RADIATIVE-ACTIVELY COOLED PANEL TEST RESULTS

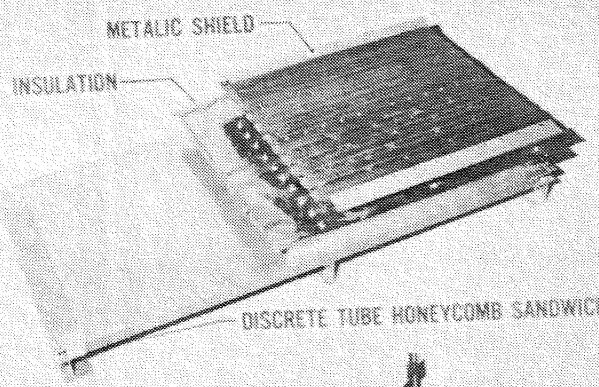

- 55 HOURS AT DESIGN HEATING CONDITIONS
- 65 THERMAL CYCLES
- 5000 LOAD CYCLES AT TEMPERATURE
- THERMAL AND STRUCTURAL PERFORMANCE WITHIN 10-PERCENT OF PREDICTED PERFORMANCE
- 132 SECONDS (TOTAL) IN M = 7 AEROTHERMAL ENVIRONMENT
- WITHSTOOD SIMULATED ABORT (COOLANT LOSS) HEATING TRAJECTORY
- NO EVIDENCE OF HOT GAS INGRESS OR STRUCTURAL FAILURE OR COOLANT LEAKS

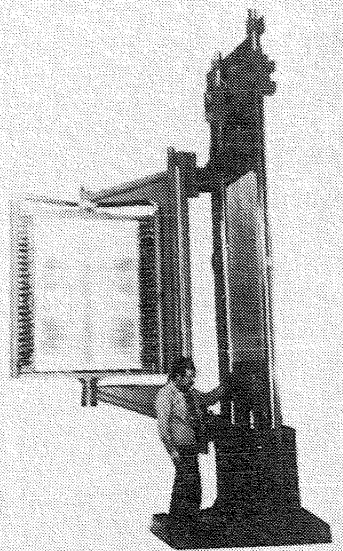

THERMAL/STRUCTURAL TESTS

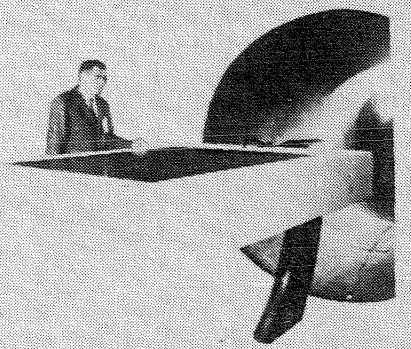

WIND TUNNEL TESTS

Figure 78

RACP RESPONSE TO ABORT HEATING

A failure mode for the RACP is total loss of coolant flow. One method to cope with this problem, predicated on early detection of loss of coolant flow, is to follow a load-factor limited trajectory which minimizes the heat load until flight speeds are decreased to values where aerodynamic heating is negligible. To determine the RACP response to such a procedure, the RACP was subjected to a heating cycle corresponding to the minimum-heat-load abort trajectory.

Shown in Figure 79 are temperature histories of the RACP response to the abort heating simulation for the heat shields and cooled panel. Average measured heat-shield and structural-panel temperatures are shown. Also shown for comparison are heat-shield and structural-panel temperature histories from a one-dimensional transient heat-transfer analysis for the abort heating profile starting at steady-state conditions. A calculated response for an unprotected aluminum panel is also shown. Maximum temperature for the RACP structural panel reached about 325°F, only 25°F above the panel maximum design temperature indicted by the tic mark on the ordinate. Thus, the RACP appears to tolerate the abort heating profile very well. By comparison an unprotected panel would very quickly reach temperatures where aluminum has virtually no strength.

RACP RESPONSE TO ABORT HEATING

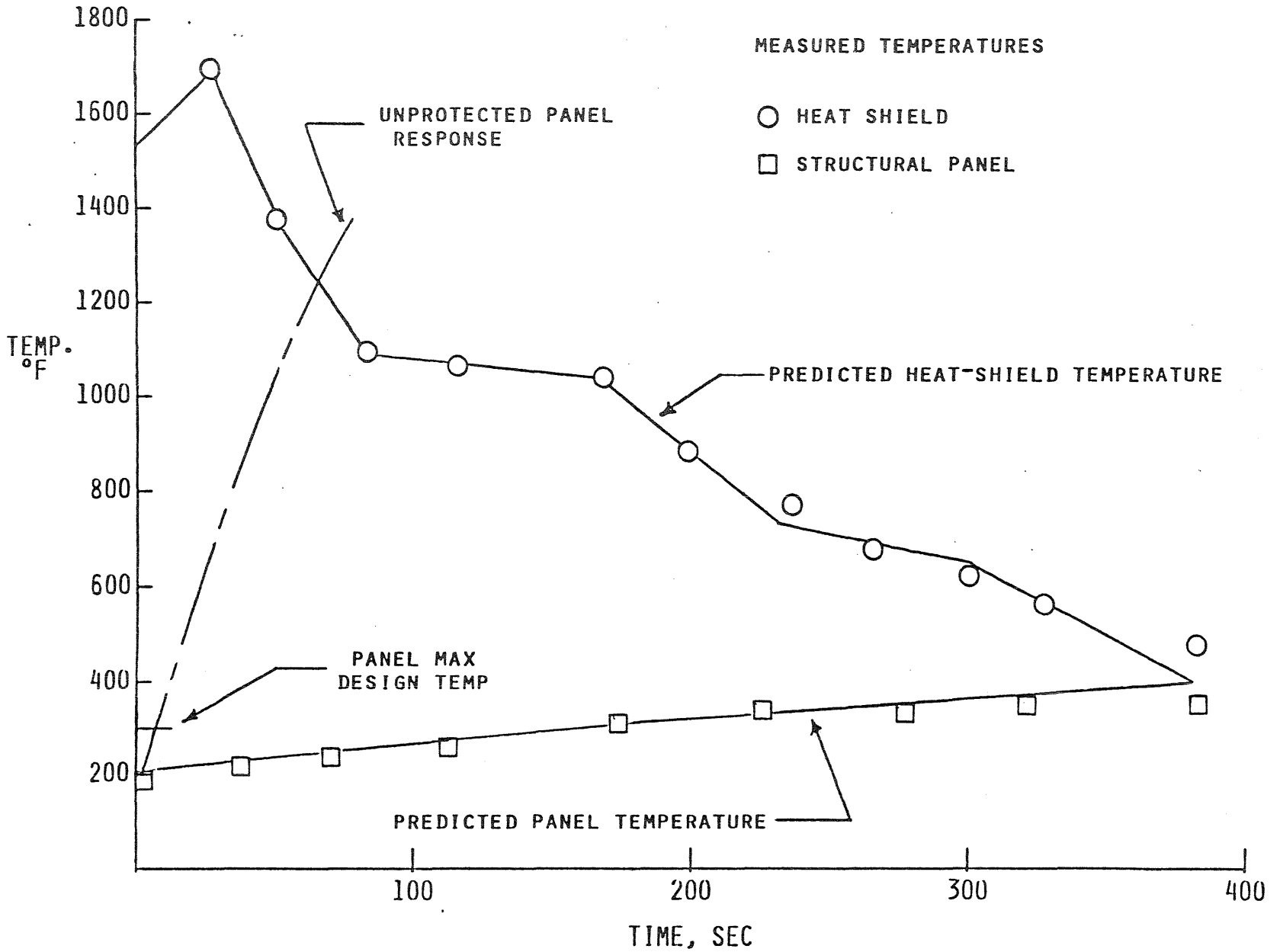

Figure 79

SUMMARY - ACTIVELY COOLED AIRFRAME STRUCTURE

Highlights of recent work on actively cooled airframe structure was presented in Figures 76-79. Heat pipe cooled structure is included in this category for a leading edge structure; a heat pipe cooled sandwich structure which was studied for scramjet applications is discussed in that section of the paper but the concept itself is very generic with broad applicability if weight competitive. Tests of a heat pipe cooled leading edge and subsequent design studies indicate such a concept is very attractive and deserving of more development.

Extensive work was done on actively cooled airframe structures in the 1970's, but little has been done since then. Systems studies revealed best concepts as a function of heat flux with coated concepts best for low values of heat flux. A radiative - actively cooled concept (cooled structure with a metallic TPS rejecting most of the heat input) was found to be the best for moderate values of heat flux. For very high values bare aluminum concepts where the coolant rejected virtually all of the heat input were best.

Systems studies identified actively cooled structure as attractive since it would be conventional aluminum structure. Design and in particular fabrication studies proved this to be incorrect; the structure was aluminum but not conventional. Major airframe manufacturers experienced fabrication problems, discovered a need for high conductivity adhesives, and also learned that the difficult task of designing joints is greatly increased for actively cooled concepts.

A radiative - actively cooled panel was subjected to radiant heating and cyclic mechanical loads as well as aerothermal loading and performed well and in the manner predicted. The metallic TPS used fibrous insulation encapsulated in metal foil, and the foil was found to have an unacceptable limited life; this problem has not been resolved. An obvious concern with an active system is what happens when it fails. Systems studies identified an abort trajectory that minimized heat load sufficiently to prevent structural temperatures from exceeding allowable values while the vehicle slowed to speeds where aeroheating is not a concern. Coolant to the panel was cut off during one test and the panel was subjected to the abort trajectory and performed as predicted.

No major show stoppers were found during the investigations and the biggest concern with this concept is the overall system complexities and the high reliability required. Since the mission studied was hypersonic cruise at Mach 6.7, applicability of the abort trajectory to an aerospace plane is doubtful.

SUMMARY OF ACTIVELY COOLED AIRFRAME STRUCTURE

- DEFINED BEST CONCEPTS
  - COATED FOR LOW HEAT FLUX
  - METALLIC TPS FOR MODERATE HEAT FLUX
  - BARE ALUMINUM FOR HIGH HEAT FLUX

- COOLED ALUMINUM STRUCTURE NOT TYPICAL AIRFRAME CONSTRUCTION
  - HAD FABRICATION PROBLEMS
  - NEED HIGH CONDUCTIVITY ADHESIVES
  - JOINTS ARE A PROBLEM

- TESTED RADIATIVE - ACTIVELY COOLED PANEL
  - GOOD, PREDICTABLE PERFORMANCE
  - FOIL ENCAPSULATING INSULATION HAD LIMITED LIFE
  - NO MAJOR SHOW STOPPERS FOUND

- OVERALL SYSTEM COMPLEXITIES MAJOR DESIGN CONCERN

Figure 80

CRYOGENIC TANKS FOR FUTURE STS

The only existing reusable Space Transportation System (STS), the Space Shuttle, employs an aluminum structure insulated from aerodynamic heating generated during ascent and entry by a reusable Thermal Protection System (TPS). The cryogenic fuel used by the shuttle is carried in the expendable external tank, but future systems designed for full reusability will undoubtedly carry their own cryogenic fuels internally. Consequently, structural design of new fully reusable systems must necessarily address problems associated with containment of cryogenic fuel as well as the conventional considerations of thermal protection and support of vehicle structural loads.

Both insulated and hot-structure design approaches have been studied. One such design approach (Ref. 18) is the hot-structure concept for a single-stage-to-orbit vehicle shown in Figure 81. This concept has followed the design philosophy of using the recently developed Space Shuttle main engines and striving for improvements in structural mass fraction. The concept is an integral tank/fuselage structure which combines the functions of fuel containment, thermal protection, and support of vehicle thrust and aerodynamic loads. The vehicle is designed for a low planform loading, which results in a higher altitude entry trajectory than that flown by the Shuttle Orbiter. This high-altitude, gliding entry results in maximum surface temperatures of only about 1400°F which are within the operating range for the nickel-base superalloy Rene' 41.

CRYOGENIC TANKS FOR FUTURE STS

HOT METALLIC STRUCTURE APPROACH

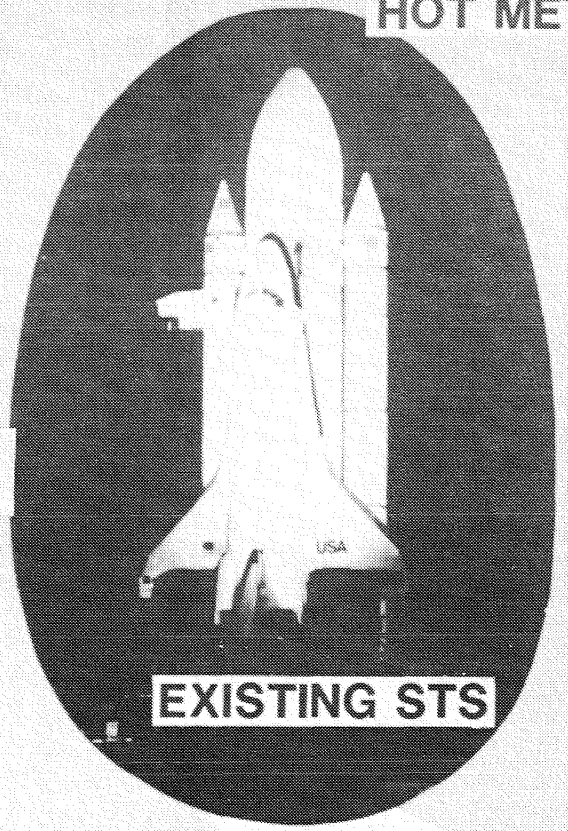

COMPLETE REUSABILITY

CRYOGENIC FUEL CONTAINMENT

LOWER WING LOADING
LOWER TEMP. TRAJECTORY

Figure 81

INTEGRAL TANK/FUSELAGE HOT STRUCTURE CONCEPT

The concept is an integral tank/fuselage structure which combines the functions of fuel containment, thermal protection, and support of vehicle thrust and aerodynamic loads. The vehicle is designed for a low planform loading, which results in a higher altitude entry trajectory than that flown by the Shuttle Orbiter. This high-altitude, gliding entry results in maximum surface temperatures of only about 1400°F which are within the operating range for the nickel-base superalloy Rene' 41.

The structure consists of a vacuum-sealed-cell honeycomb sandwich with the inner skin of the fuselage at temperature of -423°F due to exposure to the cryogenic fuel and the outer skin at a temperature of 400°F due to exposure to the boost aerothermal environment. These temperature gradients through the thickness of the sandwich during boost conditions produce large thermal stresses which must be accommodated in the design. The thermal stresses have been partially relieved by slotting the outer face sheet on the windward surface of the vehicle fuselage. These slots eliminate biaxial compression stress which would otherwise occur from thermal and pressure loads. (Transverse bending loads are low because LOX is carried in the wings.) The slots are approximately 0.030 in. wide and are sized to be nearly closed when the outer surface of the panel is heated to 1400°F. Pressure load in the noncircular section are carried by tension struts at each frame location (Fig. 82). Although Rene' 41 is required on the hotter, windward surface, a material with a better strength-to-weight ratio may be preferred on the cooler leeward surface to save weight. (The study of Ref. 18 considers using titanium honeycomb on this surface.)

Because the outer skin of the sandwich is slotted, the effect of these slots in the cryogenic environment during ground hold and boost and in the hypersonic environment during entry is a concern.

INTEGRAL TANK/FUSELAGE HOT STRUCTURE CONCEPT

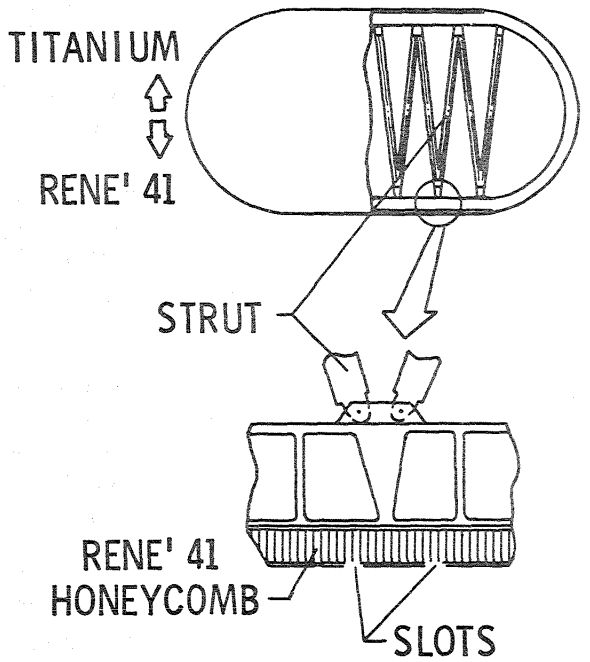

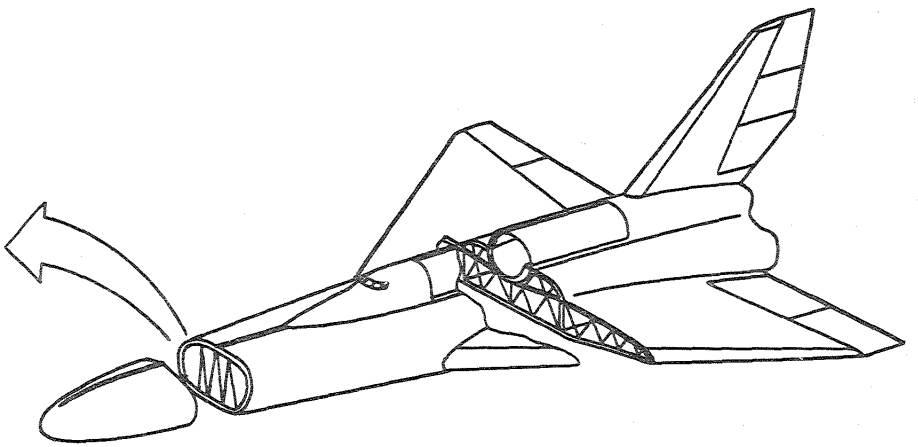

CONCERNS FOR RENE' 41 HONEYCOMB

- FABRICATION
- STRUCTURAL AND THERMAL PROPERTIES
- THERMAL STRESS DUE TO TEMPERATURE GRADIENTS
- EFFECTS OF CRYOPUMPING AND HOT GAS FLOW AT SLOTS

Figure 82

COMBINED LOADS TEST FIXTURE AND PANEL

Because thermal stresses are induced by an applied stain rather than an applied force, thermal stresses induced in the plastic range will be less than they would be for the same thermal strain in the elastic range. Furthermore, if the allowable deformation of a structure is large, and the structural stability is not critical, a benign type of failure may occur in which a large part of the thermal stresses are relieved at maximum loading (although significant residual stresses may remain after unloading). Therefore, it has been recommended that for critical conditions involving combined mechanical and thermal loads, the factor of safety used to arrive at ultimate load be applied only to the mechanical load and not to the thermally-induced component, regardless of how they are combined (Ref. 118). The use of lower load factors for thermal loads can result in higher allowable operating stresses for mechanical loads which will save mass. In addition, for a limited-life vehicle, these operating stresses may even be in the plastic range which can result in even greater mass saving.

A Rene' 41 honeycomb panel, 1 ft by 6 ft, was tested under combined thermal and bending loads at the NASA Dryden Flight Research Facility. The design and fabrication of the panel is documented in Reference 119. The purpose of these tests was to evaluate the life of a panel when exposed to cyclic combined thermal and mechanical stresses representative of high elastic stresses seen at a fuselage frame attachment.

The test apparatus and the test panel are shown in Figure 3. The slot down the center of the outer (hot) face sheet is as previously mentioned, necessary to reduce thermal stresses. The slot is approximately 0.030 in. wide and is sized to be nearly closed when the outer surface of the panel is heated to 1400°F. The panel was instrumented on both face sheets with thermocouples, strain gages and deflectometers.

Quartz lamp heaters were used to produce temperature histories representative of both boost and entry cycles. For safety reasons, the cryogenic temperature (-423°F for LH_2 fuel) required on the inner face sheet during the ascent cycle was represented by using LN_2 at -320°F. The use of LN_2 in place of LH_2 has only a small effect on the thermal strains which occur during the test. Nevertheless, hot surface temperatures were slightly increased to provide equivalent thermal strain levels to account for the small strain difference associated with using the warmer LN_2.

Mechanical loads representing fuel pressure loads were applied to the panel through the distribution system defined in the figure. Four line-load supports reacted the applied loads. The two internal reaction supports simulate the reaction forces which would result from fuselage frames reacting thermal and fuel pressure loads in a vehicle. The simulation is incomplete in that at these reaction points, the honeycomb core is exposed to compression rather than a net tension load, and the panel is not totally constrained from bowing in the transverse direction as it would be if it were continuously attached to a frame.

COMBINED LOADS TEST FIXTURE AND PANEL

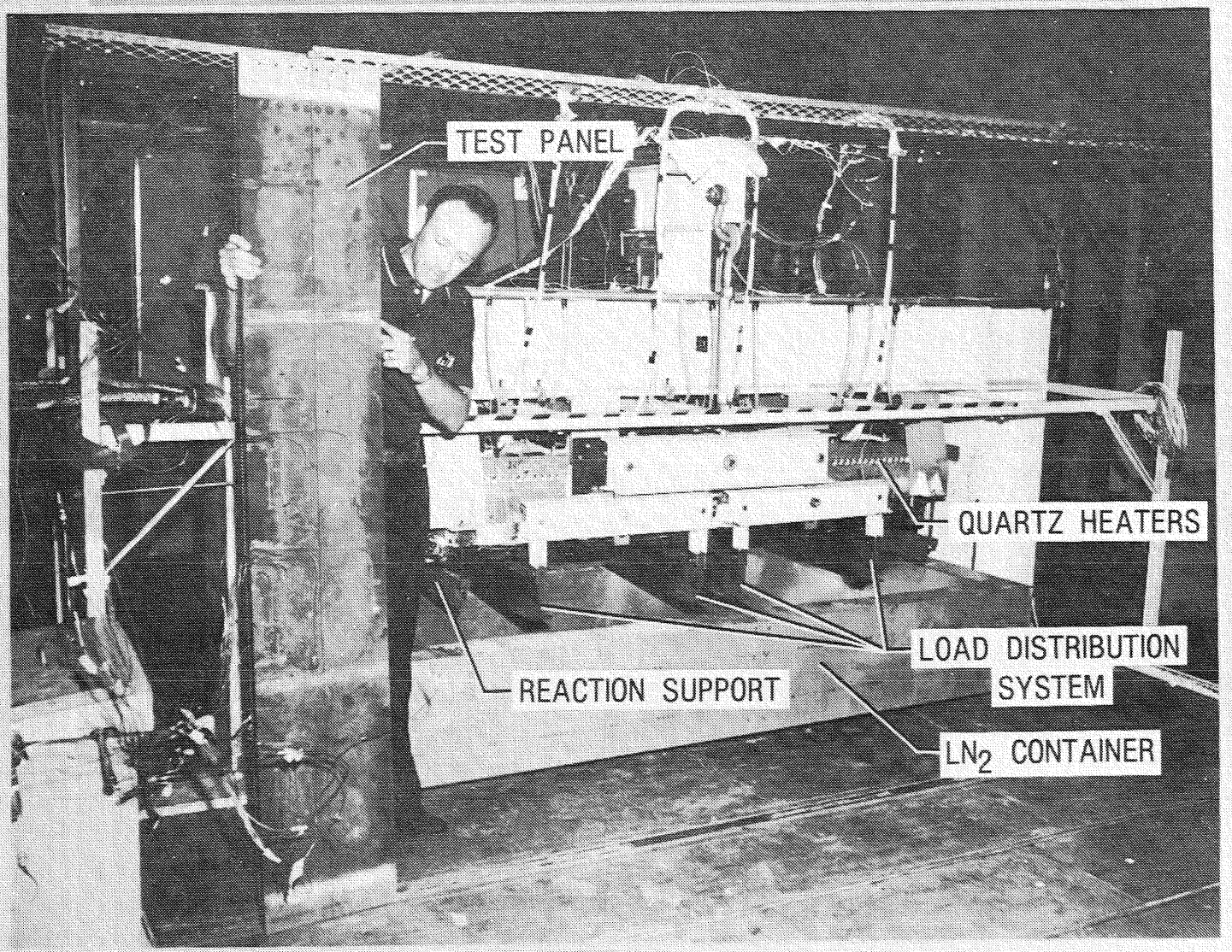

Figure 83

RENE' 41 HONEYCOMB PANEL STRAIN DISTRIBUTION DUE TO BOOST-TO-ORBIT THERMAL/MECHANICAL LOADS

The panel was exposed to mechanical load and thermal load separately prior to exposure to combined loads.

After the separate load tests, the panel was exposed to 500 boost cycles and 500 entry cycles by alternating between the type of tests in groups of 1, 49, 50, 100, 100, and 200. For each cycle, the mechanical load was held constant while the thermal load was applied. During the test program, lamps were adjusted and curtains added to achieve a more uniform temperature distribution on the hot surface, and the emission of the panel surface changed. The resulting changes in surface temperature distribution caused the maximum strains to vary slightly. The maximum compressive strains were between 60 and 80% of the proportional limit. After the first entry cycle, a small bow in the panel in the longitudinal direction was observed. This residual bowing gradually increased with additional exposure to entry cycles, but it was unaffected by additional boost cycles. No damage occurred as a result of the 500 boost and entry cycles, but the panel was left with a permanent center displacement of 0.58 in. over the length of 6 ft with the concave face on the hot side. A force of 210 lbf was required at each load point to elastically straighten the panel. The resulting residual tension stresses on the hot side were 10,400 psi at the support and 16,000 psi at the center of the panel. The cause of the bowing is not understood. A possible cause is a slight shrinkage of the hot face sheet which may occur during the 1400°F entry cycle exposure as a result of additional aging of the Rene' 41 material, but this has not been confirmed. (The panel was originally aged for 1 h at 1700°F and furnace cooled after a 1975°F braze cycle.)

Additional boost cycles (beyond 500) were imposed on the panel with increasing mechanical load until a failure was achieved during cycle 532. The panel failed prematurely by core crushing directly beneath an interior reaction support. This was a nonrepresentative failure mode because the test fixture placed the core in compression while the load pattern at a vehicle fuselage frame would place the core in tension. In addition, the failure is nonrepresentative because the reaction loads were concentrated over a small area to minimize the shading effect from the quartz lamps during heating cycles.

Representative strain data for the panel are shown in Figure 84 and are compared with a strain distribution calculated using the SPAR finite element structural analysis computer program (Ref. 75). Measured temperatures were used for the linear analysis. The figure shows results for the panel for the second boost cycle. The measured and calculated strains resulting from the combined thermal and mechanical loads are in good agreement. The strains on the hot and cold surfaces are different because the thickness of the hot face sheet for panel 1 was chem-milled to provide an increased thickness in the regions of the reactions. Additionally, the temperature distributions on the two surfaces were different. Temperatures on the LN_2 side were relatively constant since they were influenced by boiling against the specimen surface. The upper surface was hotter in the middle of the specimen than at the edges and at the supports. Additional details are given in Reference 120.

RENE'41 HONEYCOMB PANEL STRAIN DISTRIBUTION DUE TO BOOST-TO-ORBIT THERMAL/MECHANICAL LOADS

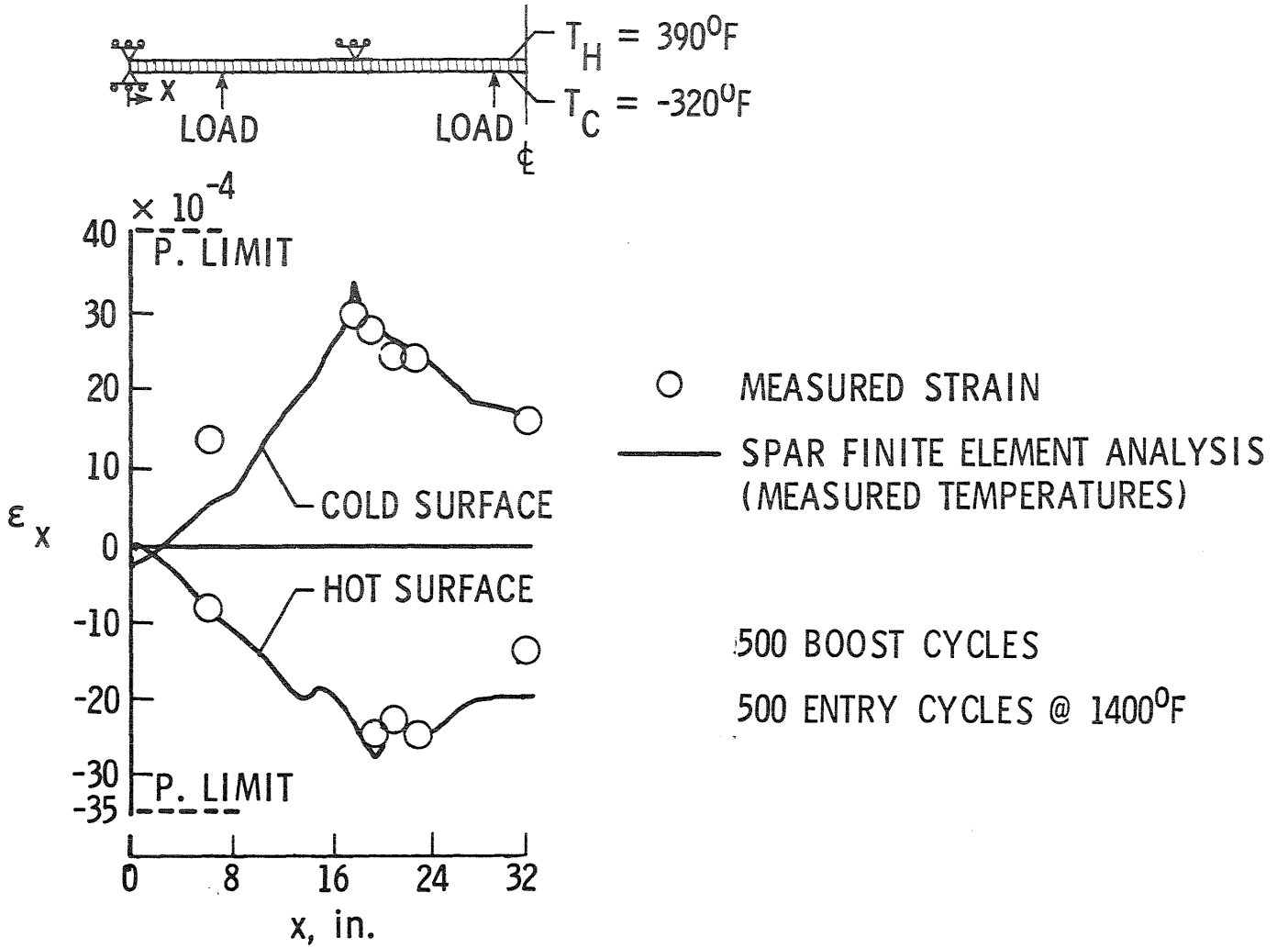

Figure 84

SLOTTED RENE' 41 HONEYCOMB EVALUATED IN LH_2/BOOST HEATING ENVIRONMENT

A panel was fabricated with several slots in the outer skin and tested to evaluate the effects of the slots in the boost environment. The panel was 21x25 1.2 in. in size. A frame was brazed to the inner skin on the panel centerline. The frame held the sandwich panel flat in the region of the centerline. Thus, the thermal stresses which occur in this region are representative of the thermal stresses that would exist in the integral fuselage structure of the vehicle studied in Ref. 18. About half the slots in the outer skin were open and half were covered with a 0.5-in.-wide strip of 0.010-in.-thick Rene' 41 electron beam welded to the skin along one side of the slot. The cover displays a technique which may be required to reduce high local heating to the sandwich during entry. The panel formed the bottom of a container which was partially filled with LH_2. The panel was supported in the container at the center frame and at each end of the panel. A 0.015-in. Hastalloy X seal was welded to the panel edge and to a frame at the bottom of the container. The schematic of the test fixture (Fig. 85) shows the container covered with foam insulation to minimize boiloff of LH_2. Quartz lamps were used to expose the panel to the boost heat cycle shown in the lower part of Figure 85. Hold times between cycles ranged from 10 min to 1 h during which cryodeposits accumulated on the panel surface and in the slots. Motion pictures were taken at 16 frames/s during the first cycle and at 1 frame every 6 s during all cycles. The panel was inspected after cycle 10 and cycle 30, and no damage to the panel was observed, although some cracking of the foam insulation around the container was noticed. After 36 cycles, a fire occurred in the test fixture but caused no damage to the panel. The cause of the fire was attributed to an undefined ignition source which could have ignited either gaseous hydrogen, which was leaking out at the lid-container interface, or the foam insulation in the presence of the liquid oxygen component of liquid air condensed in the cracks in the insulation. (The lid-container interface was not tightly sealed for fear that if the vent stack could not accommodate all LH_2 boiloff, a pressure greater than 1 psi might occur and damage the panel seal.) Completion of 36 cycles achieved all test goals except the demonstration of 100 cycles. The costs to repair the test fixture and continue testing compared with an assessment of the need for the remaining 64 cycles led to a decision to stop testing. The panel was examined visually and by x ray and c scan. Sections cut from the panel were examined by metallographic inspection. No structural damage was found.

During the hold times water frost was observed depositing on the -200°F panel surface, and temperatures less than -300°F measured during the tests indicated that liquid air formed in the regions of the core open to the atmosphere. There was no observable or measurable damage to the panel whether the outer skin slots were open or covered. However, the results indicate that additional attention must be given to sealing honeycomb core splices to prevent passage of air into the core from the slots. Without such sealing, considerable liquid oxygen may flow within the honeycomb structure. The results also show that a honeycomb core sandwich with a slotted outer skin integrally fixed to an inner frame can withstand the localized thermal environment imposed by the boost trajectory for the Ref. 18 vehicle. These tests are documented in Ref. 121.

SLOTTED RENE'41 HONEYCOMB EVALUATED IN LH_2/BOOST HEATING ENVIRONMENT

TEST SCHEMATIC

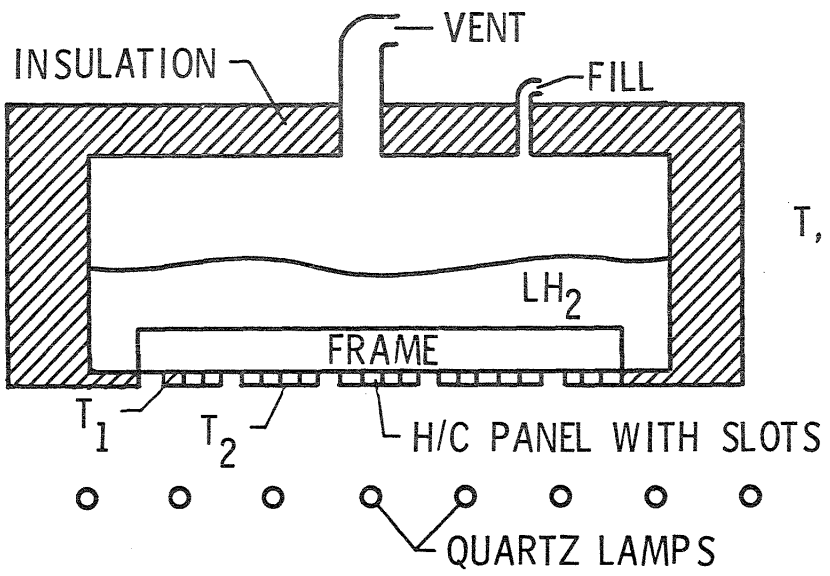

CRYOGENIC HOLD AND BOOST CYCLE

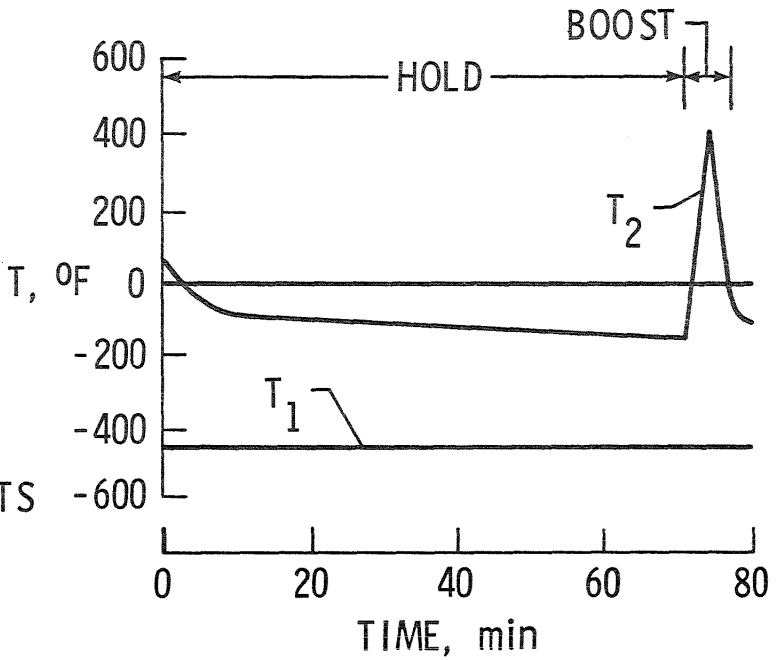

- 36 BOOST CYCLES
- CRYODEPOSITS IN SLOTS VENT WITHOUT PROBLEMS

Figure 85

MACH 7 AEROTHERMAL TESTS OF SLOTTED HONEYCOMB

A second slotted panel as tested to evaluate the effect of localized heating in the region of the slots during entry. The 22 X 34 x 1.2 in. panel shown in Figure 86 was designed to be exposed to a Mach 7 stream in the Langley Research Center 8-Ft High Temperature Tunnel (8' HTT). Two slot cover concepts were evaluated in addition to the open slot. The panel was instrumented with thermocouples on the inner face sheet directly beneath the slots and between slots so that the different cover concepts could be compared.

Preliminary results from these tests (completed in January 1983) indicate that no significant heating occurs in the slots since the thermocouples located directly beneath the slots showed no unusual temperature rise during exposure to the hypersonic flow. Infra-red camera data indicates that the temperatures at the surface of the slots were not higher than surface temperatures away from the slots. However, television cameras recorded greater brightness at the surface of the slots which suggests that the resolution of the infra-red camera (about 0.6 inches) may not be adequate to detect local heating at the slot which is designed to close from 0.030 inches to near zero when hot.

MACH 7 AEROTHERMAL TESTS OF SLOTTED HONEYCOMB

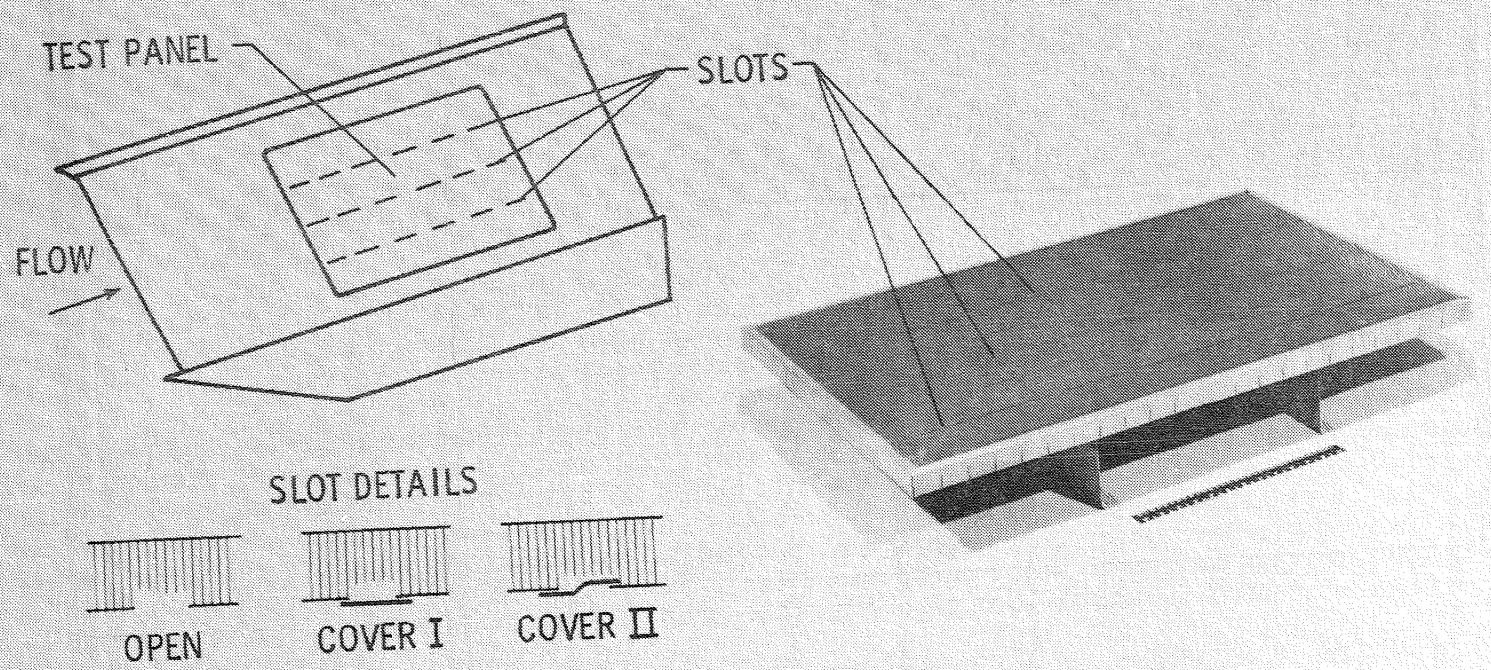

Figure 86

INTEGRAL AND NON-INTEGRAL CRYO TANK STRUCTURE/TPS CONCEPTS

Sections through the fuselage and tank walls of an aerospace plane type vehicle are shown in Figure 87. The packaged fibrous insulation is common to both tank concepts. However, the amount of fibrous insulation required varies depending on the temperature limit of the exterior tank surface. In both concepts, the tank walls are welded to provide leak-free containment of the cryogenic propellants.

The integral tank concept uses a near-art evacuated honeycomb core sandwich structure protected by a durable prepackaged TPS (Ref. 91). In this concept the honeycomb carries both tank and fuselage loads and provides the insulation for the cryogenic. The honeycomb sandwich structure has aluminum (or metal matrix composites) face sheets supported by ring frames but the core material is titanium to reduce conduction between the honeycomb faces. In this concept, the core thickness is varied to provide the required insulation function. The aluminum faces are compatible with the propellants or LOX and the honeycomb structure is more efficient than a more conventional Z-stiffened structure.

The non-integral structure is a more advanced concept using a welded metal-matrix composite tank with a 400°F closed-cell organic foam providing the cryogenic insulation and an organic composite fuselage structure. The foam thickness is varied to meet the insulation function. The foam may be on the interior of the tank wall, which is acceptable for LH_2. However, the organic foams are sensitive to LOX; that is, they burn in the presence of LOX with very little ignition energy. Therefore, for LOX tanks the foam insulation is required to be on the exterior tank wall. Additional details of these designs are given in References 122 and 123.

INTEGRAL AND NON-INTEGRAL TANK STRUCTURE TPS CONCEPTS

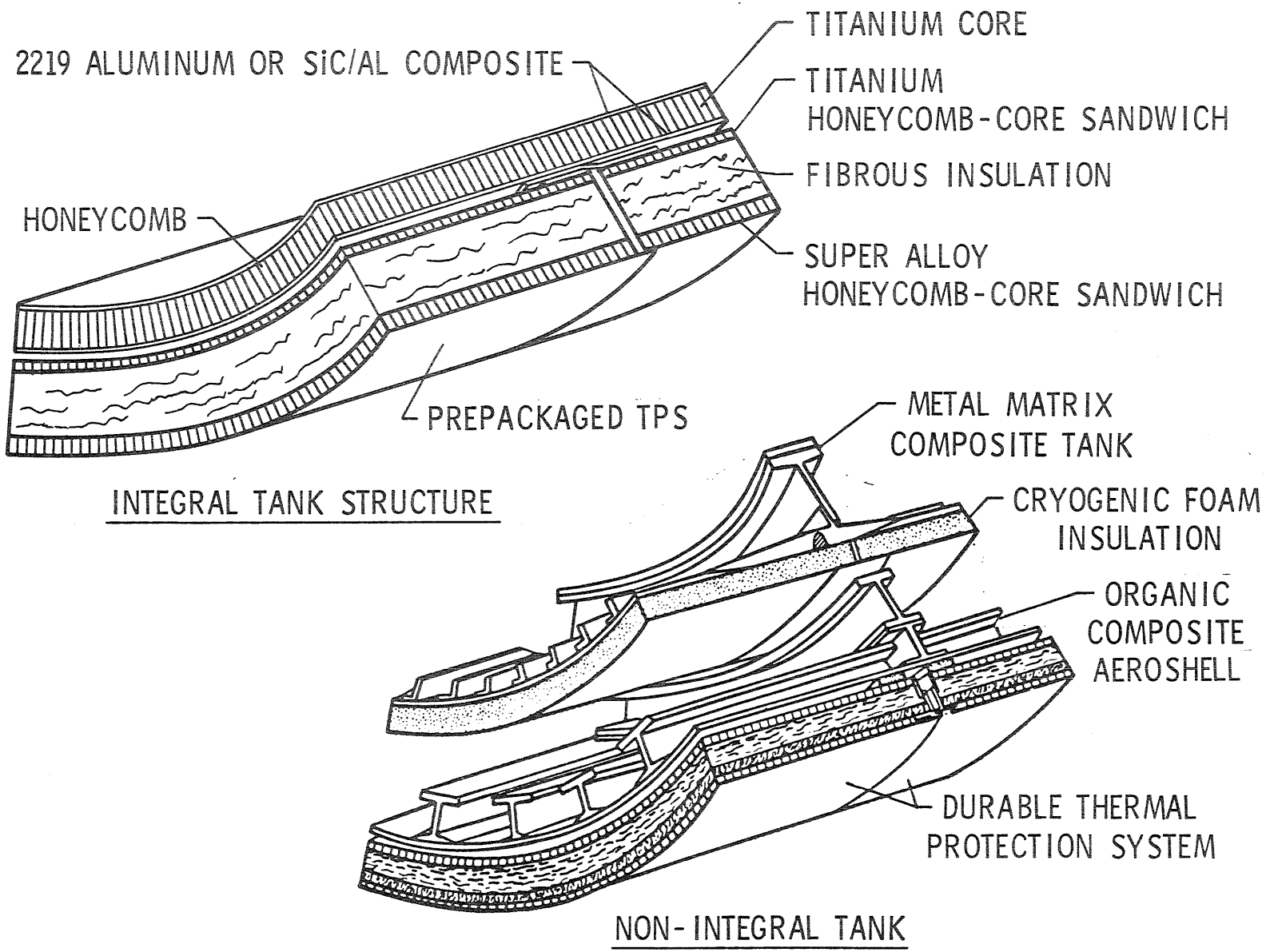

Figure 87

CRYOGENIC FOAM TEST PROGRAM

Analysis indicates that an exterior 175°F foam system (the max temperature limit used in previous studies of LN_2 fueled subsonic aircraft (Ref. 125) requires four times the total insulation thickness (the sum of fibrous insulation TPS and cryogenic foam) for a LH_2 tank than an internal foam system. Were a 400°F reuse temperature foam available, it would require half the total insulation thickness that a 175°F foam requires. This internal 400°F foam has potentially the minimum total insulation thickness for single wall aluminum LH_2 tanks. Thus current efforts are focused on developing a materials/system with a max use temperature of 400°F with a goal of 500 thermal-cycle-life.

The high temperature cyrogenic foam system (Fig. 88) is proposed to consist of 40 inch square tiles which contain 16 ten inch square blocks of Rhoacell WF110 grade foam adhesively bonded together. The 40 inch square tile is encapsulated within a Kapton-Aluminum-Kapton (KAK) cover to minimize permeation of gases. These tiles are in turn bonded to the surface of the cryogenic tank and the joints between the individual tiles are sealed with another layer of KAK over the joints.

A 10 inch square tile has been fabricated and tested as an exterior insulation using the cryogenic test apparatus shown in Figure 89. The thermal structural load histories represent the loads on a high speed aircraft LH_2 tank. This specimen has been tested for 10 cycles at LH_2 temperatures and 100 cycles at LOX temperatures with no apparent degradation of the cryogenic insulation function. Future tests are prosposed using lower density foams and larger tile arrays with joints. Also tests are planned to determine the conductivity, permeability and compatibility of the various Rohacell foams in partial pressure environments that simulate the actual anticipated use condition for the foam systems.

CRYOGENIC FOAM TEST PROGRAM

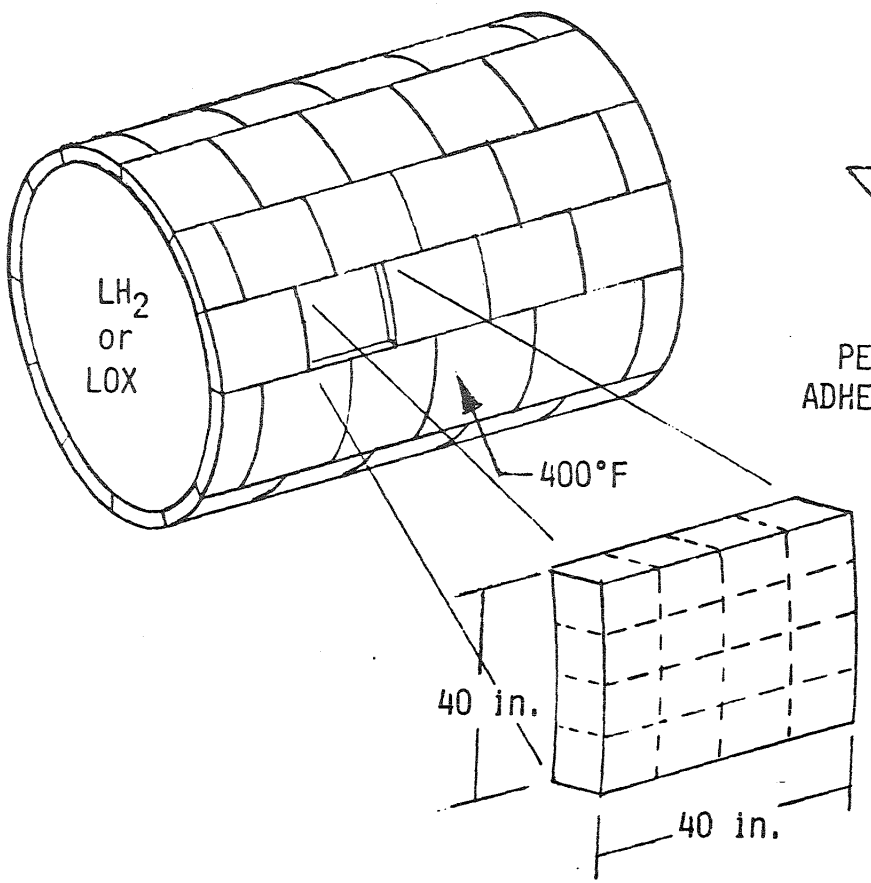

FLIGHT VEHICLE CRYOGENIC TANK

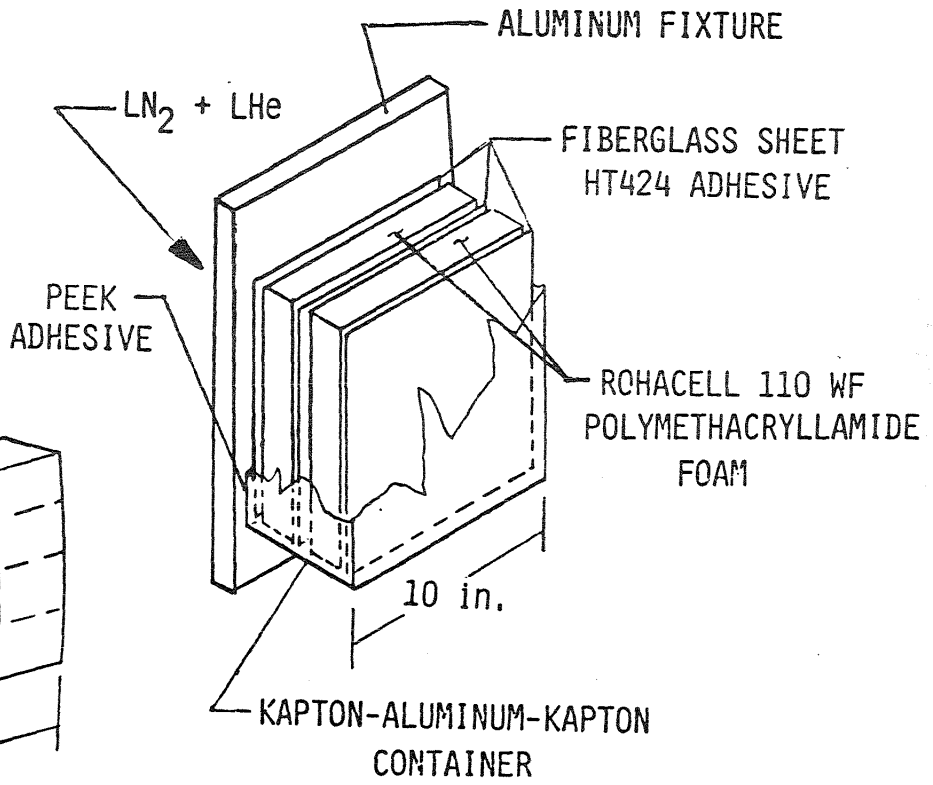

PRELIMINARY SCREENING
100 CYCLES

Figure 88

Page Missing in Original Document

HIGH TEMPERATURE CRYOGENIC FOAM CYCLIC TEST

PRELIMINARY SCREENING

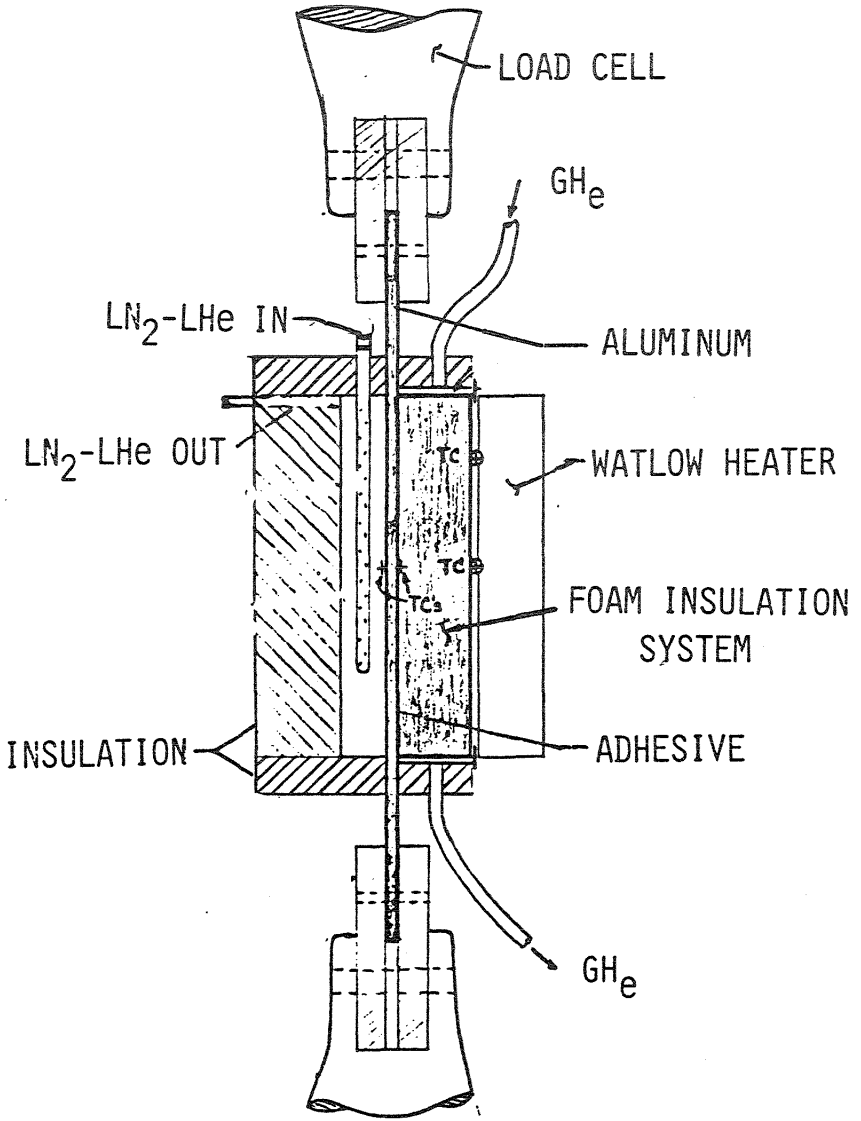

TEST APPARATUS

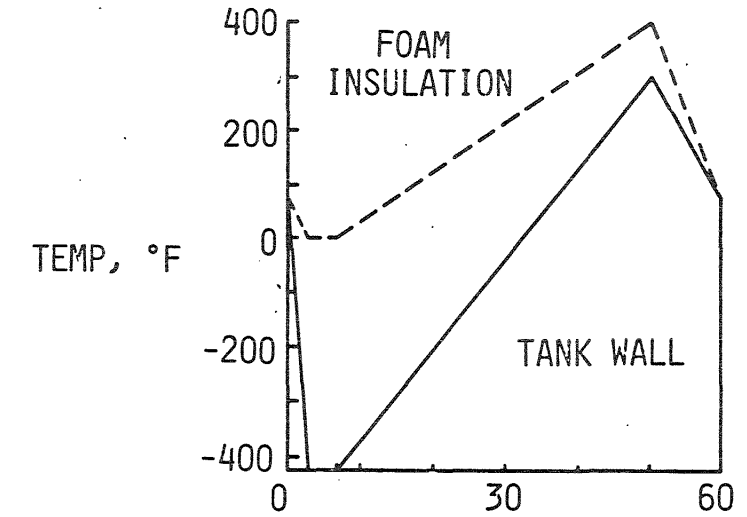

● GOAL - 500 THERMAL CYCLES

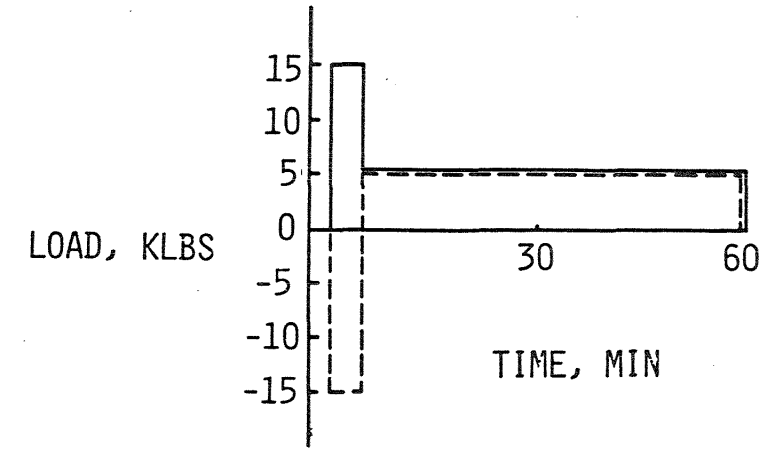

TEST PARAMETERS

Figure 89

SUMMARY - REUSABLE CRYOGENIC TANK TECHNOLOGY

Highlights of recent work on reusable cryogenic tank concepts was presented in Figures 82 to 89. Most work involving hardware in the past 10 years has been on a hot integral tank concept the uses evacuated Rene' 41 honeycomb structure. Panels 6 x 1 ft. were successfully subjected to 500 cycles of ascent and entry thermal and mechanical loading; for ascent cycles liquid nitrogen was used instead of LH_2 but external heating was adjusted to keep the thermal gradients and hence thermal stresses at the proper values. Slots in the outer skin to alleviate circumferential thermal stresses were a concern and panels were built and tested to determine performance during ground-hold ascent cycles and aerothermal tests at Mach 7 true temperature conditions. In these ascent test LH_2 was used. There were no structural problems or augmented heating in the gaps, but ice and LOX could form during ground hold which could be an operational problem. This concept is limited to max temperatures of about 1400°-1600°F and hence is not applicable to some aerospace plane missions currently under study.

A number of paper studies have been done for TPS/structure/tank concepts which could be required for the higher temperature missions. A wide variety of concepts have been studied only a few of which were reviewed herein. If the concept needs a cryogenic insulation, development of a reusable, high temperature (> 175°F) material is a high priority technology need. Composite tanks could be very attractive but some difficult problems such as internal liners for organic matrix composite tanks or for internal insulation must be solved. In addition, flaw-size crack-growth criteria for aircraft applications could impose big weight penalties on some cryogenic tank designs and a reassessment of the criteria is needed.

SUMMARY OF REUSABLE CRYOGENIC TANK TECHNOLOGY

- HOT STRUCTURE CONCEPT LOOKS PROMISING FOR LOW TEMPERATURE TRAJECTORIES
  - T_{MAX} LIMITED TO ABOUT 1600°F FOR CURRENT EVACUATED HONEYCOMB TECHNOLOGY
  - COULD HAVE OPERATIONAL PROBLEMS: ICE, LOX FROM CRYOPUMPING

- TPS/STRUCTURE/TANK CONCEPTS REQUIRED FOR HIGHER TEMPERATURE APPLICATIONS
  - REUSABLE CRYO INSULATION BIGGEST TECHNOLOGY NEED
  - HIGH T_{MAX} OF CRYO INSULATION DESIRABLE
  - COMPOSITE TANKS ATTRACTIVE, MAY NEED INTERNAL LINER
  - FLAW-SIZE CRACK-GROWTH POTENTIAL BIG DRIVER; NEED TO REASSESS CRITERIA

Figure 90

COMPOSITE AFT BODY FLAP FOR SPACE SHUTTLE

The aft body flap for the Space Shuttle Orbiter is 21 ft. x 7 ft. and was selected as the structural component to demonstrate the feasibility and benefits of using graphite/polyimide rather than the baseline aluminum structure. In the baseline design, the aluminum body flap is not permitted to exceed 350°F whereas the graphite/polyimide structure was designed to withstand 600°F. The aluminum body flap has a total weight of approximately 1300 pounds and the graphite/polyimide body flap is estimated to weigh approximately 950 pounds, for a weight savings of about 27 percent (Ref. 126). A study was conducted to demonstrate the capability to fabricate aerospace quality components with both C6000/PMR-15 and C6000/LaRC-160 graphite/polyimide material systems. Preliminary design allowables were developed for use in the design of a segment of the aft body flap. A 60 in. x 54 in. segment of the body flap was fabricated and tested to verify the performance potential of graphite/polyimide for future spacecraft structures.

COMPOSITE AFT BODY FLAP FOR SPACE SHUTTLE

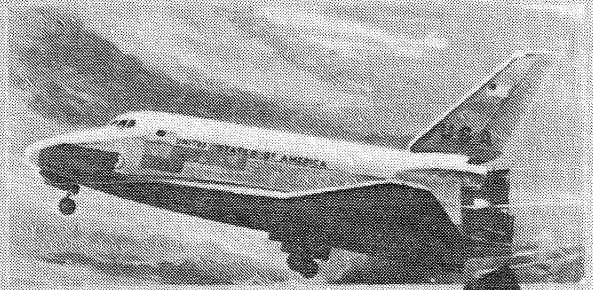

AFT BODY FLAP

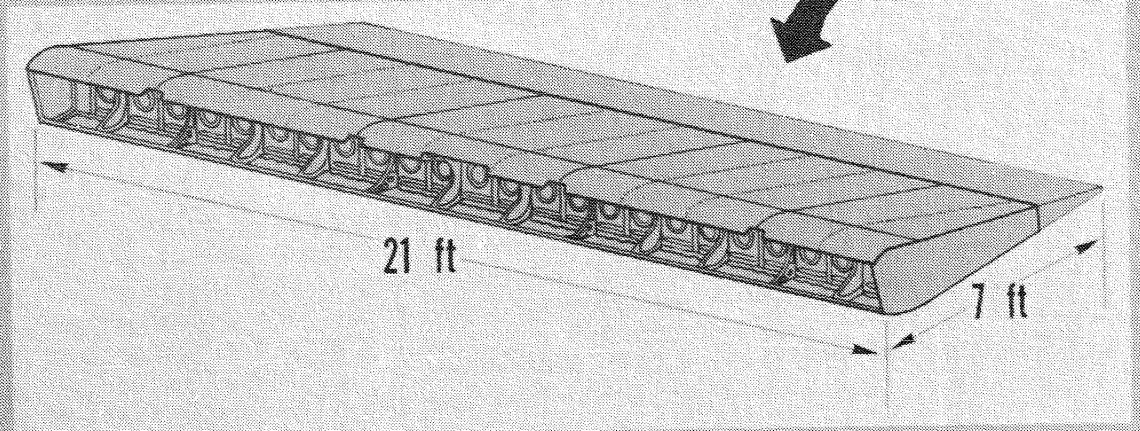

MATERIAL	STRUCTURAL WEIGHT, lb	TPS WEIGHT, lb
ALUMINUM	430	860
Gr/Pi	340	607

Figure 91

CELION/LARC-160 FABRICATION DEMONSTRATION COMPONENT

The LaRC-160 polyimide system that was developed at NASA Langley Research Center was selected as the material to demonstrate the performance potential of graphite/polyimide for future spacecraft structures. A segment of the Space Shuttle Orbiter aft body flap 60 in. long x 54 in. wide was designed, fabricated, and tested. The Technology Demonstration Segment (TDS) is bonded except for the front spar and upper leading edge, which are mechanically fastened to allow access to the torque box interior.

The cover panels for the TDS have 5-ply celion 6000/LaRC-160 skins on 0.70-inch thick glass/polyimide honeycomb cove. The stability ribs have 3-ply skins on 0.5 inch thick honeycomb core. The rear spar, rib caps, and shear clips are 8-ply quasi-isotropic solid laminates. The TDS was subjected to the following tests: RT ultimate load, 500°F ultimate load, 400 limit load cycles at 500°F, 125 thermal cycles between -160°F to 600°F, and a secondary ultimate load test at 500°F. Extensive ultrasonic and visual NDE did not find any evidence of structural failure as a result of the above tests. The results verified that a representative graphite/polyimide structure could be designed and fabricated to withstand thermal extremes representative of 100 Space Shuttle Orbiter missions. More detailed discussion is given in References 127 and 128.

CELION/LARC-160 FABRICATION DEMONSTRATION COMPONENT

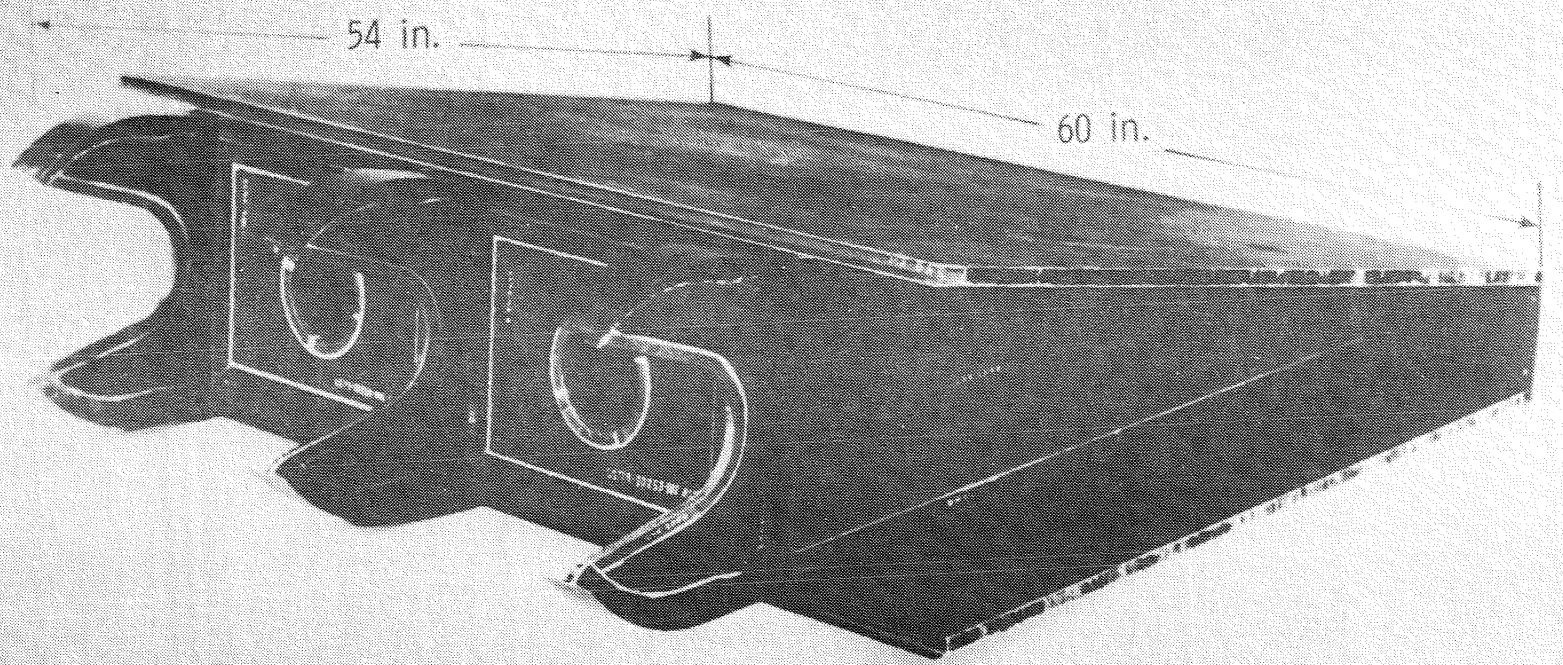

Figure 92

EFFICIENT PRIMARY-STRUCTURE CONCEPTS DEVELOPMENT CHRONOLOGY

Considerable effort has gone into the development of structural concepts for high-temperature applications that employ curved elements to provide axial stiffness while alleviating transverse thermal stresses. These concepts, which are highly efficient, were conceived in 1965 as part of a hypersonic aircraft study (Ref. 129). The concepts have undergone subsequent development, including design optimization and concept verification testing at both the elemental and component levels (Refs. 130, 131). The latter, which were completed late in 1978, includes tests of both beaded and tubular panels as part of a hot wing structure that was tested in the Flight Loads Research Facility at Dryden Flight Research Facility. During these tests the wing was subjected to combined thermal and structural loads, including temperatures up to 1340°F and loads up to the maximum design conditions. Although analysis of the data is incomplete, preliminary results indicate that the structures performed as expected and it may be concluded that curved-element hot structures represent a mature technology ready for flight demonstration.

EFFICIENT PRIMARY STRUCTURE CONCEPTS
DEVELOPMENT CHRONOLOGY

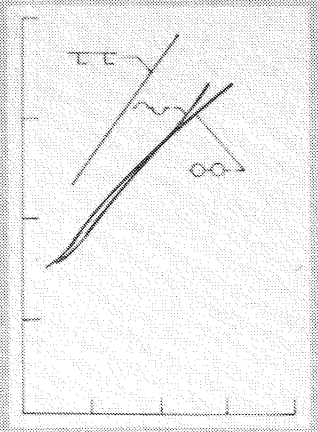

LOAD
DESIGN STUDIES
1965

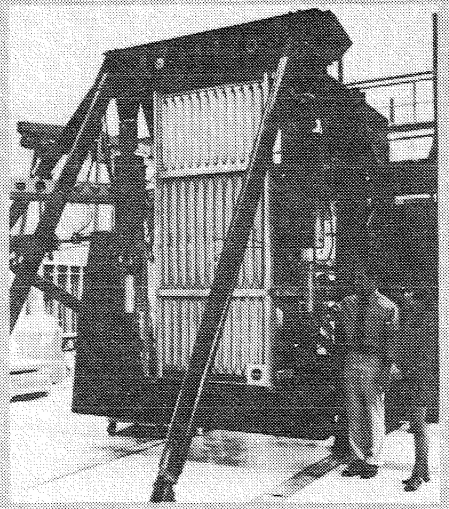

CONCEPT DEVELOPMENT

- ALLEVIATES THERMAL STRESS
- PROVIDES HIGH STRUCTURAL EFFICIENCY
- REQUIRES SMOOTH AERODYNAMIC SURFACE

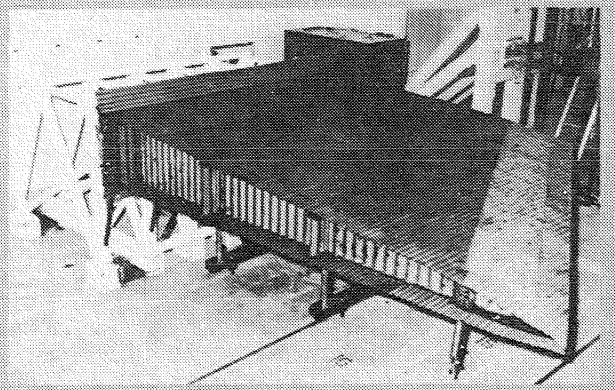

COMPONENT TESTS
1978

Figure 93

HYPERSONIC WING TEST STRUCTURE

Figure 94 shows various phases of a study of hot structure for an hypothetical M = 8 vehicle carried out by NASA Dryden that illustrates their capability for hot structure testing and thermal-structural analysis. A segment of wing structure 85 FT2 in area was built of the TPS and structural concepts described in Reference 129 (beaded panels and corrugation stiffened TPS). Reference 130 describes the design and fabrication of the actual test hardware. The picture in the lower left shows the structure being radiantly heated to a temperature of about 1800°F. The tests confirmed the performance of this structural concept. The sketch on the lower right shows the good correlation of measured and calculated temperatures for a segment of the test model. Additional details of this test program are given in Reference 131. The model is currently being reinstrumented in preparation for additional tests where emphasis will be given to detailed temperature and stress measurements for verification of current thermal-structural analysis codes.

HYPERSONIC WING TEST STRUCTURE

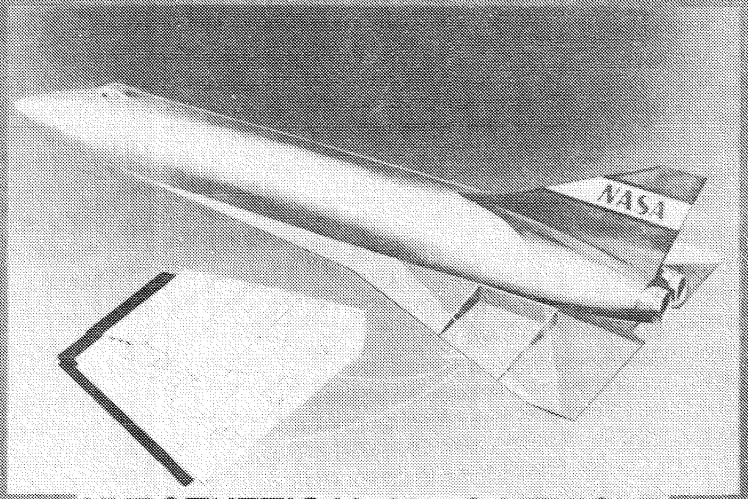

HYPOTHETICAL M = 8 VEHICLE

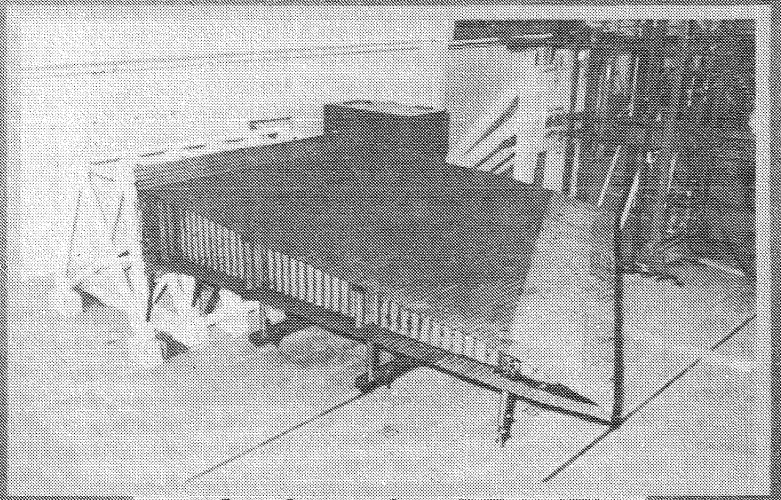

TEST STRUCTURE WITH HEAT SHIELDS INSTALLED

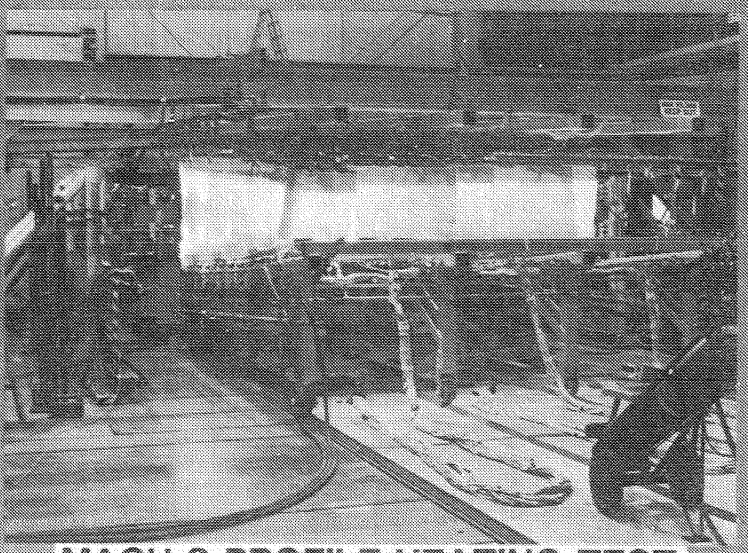

MACH 8 PROFILE HEATING TEST

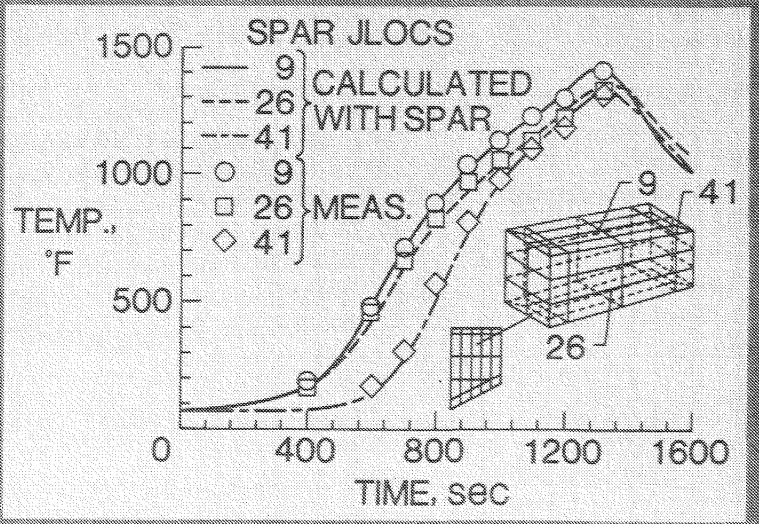

COMPARISON OF TEST AND ANALYSIS

Figure 94

PANEL EFFICIENCY R&T

The evolution of improvements in panel efficiency resulting from Langley R&T is shown from left to right in Figure 95. On the left is a tubular stiffened panel, then a beaded web corrugation, and finally a truss-core web corrugation. Comparative weights are listed for these panels for two materials. As indicated, the more efficient material, graphite/polyimide composite material, is lower weight for each panel type.

A factor effecting efficiency other than material selection is the geometry of the panel cross section. Geometric efficiency factors resulting from the studies are listed. For a structural panel to have maximum geometric efficiency, the principal load-bearing area (caps) should be symmetrical about the neutral axis, have a high local buckling coefficient (curved caps and clamped edges), have a low density web between the caps (low core density), and have its core material supporting load. The three panel geometries shown have improved geometries from left to right. The tubular panel satisfies three of these factors, but not the low core density. The beaded web corrugation does not have a load-bearing core, whereas the truss-core web corrugation satisfies all four geometry efficiency factors. More detailed results are given in References 132 and 133.

PANEL EFFICIENCY R&T

TUBULAR	BEADED WEB CORRUGATION	TRUSS-CORE WEB CORRUGATION
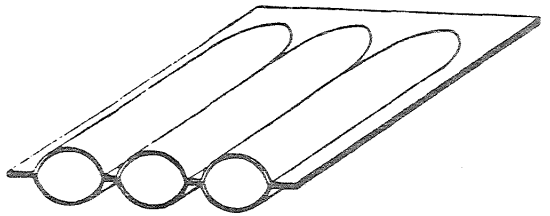	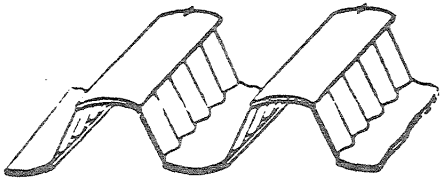	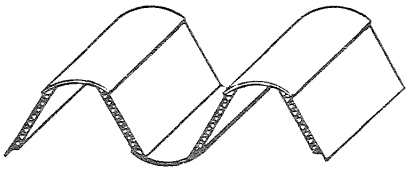

UNIT WEIGHTS - LBS/FT^2

(FOR L = 20 INCHES, N_x = 3000 LBS/IN.)

TITANIUM	.68	TITANIUM	.37	TITANIUM	.29
GR/POLYIMIDE	.37	GR/POLYIMIDE	.21	GR/POLYIMIDE	.13

GEOMETRIC EFFICIENCY FACTORS

- o SYMMETRY ABOUT CENTROID
- o HIGH LOCAL BUCKLING COEFFICIENT
- o LOW CORE DENSITY
- o LOAD BEARING CORE

Figure 95

SPF/WB BEADED WEB COMPRESSION PANEL DESIGNED FOR HIGH STRUCTURAL EFFICIENCY

Reference 134 describes an investigation of the feasibility of superplastically forming corrugated panels with beaded webs. The test panels in the study consisted of superplastically formed titanium alloy 6Al-4V half-hat stiffner elements that were joined by weld-brazing to titanium alloy 6Al-4V caps to form either single corrugation stiffened compression panels or multiple corrugation stiffened compression panels (Fig. 96). The panels were tested in end compression at room temperature and the results compared with analysis. Stretching of the titanium sheet during superplastic forming was reduced by approximately 35 percent using a shallow half-hat male die concept instead of a deep male die concept resulting in a uniform thickness across the beaded webs. The heavily loaded panels failed at strains approaching the yield strength of the titanium material. At maximum load the caps wrinkled accompanied with localized separation of the weld-braze joint in the wrinkle. None of the panels tested exhibited catastrophic failure of the weld-braze joint. Experimental results were in good agreement with structural analysis of the panels.

SPF/WB BEADED WEB COMPRESSION PANEL DESIGNED FOR HIGH STRUCTURAL EFFICIENCY

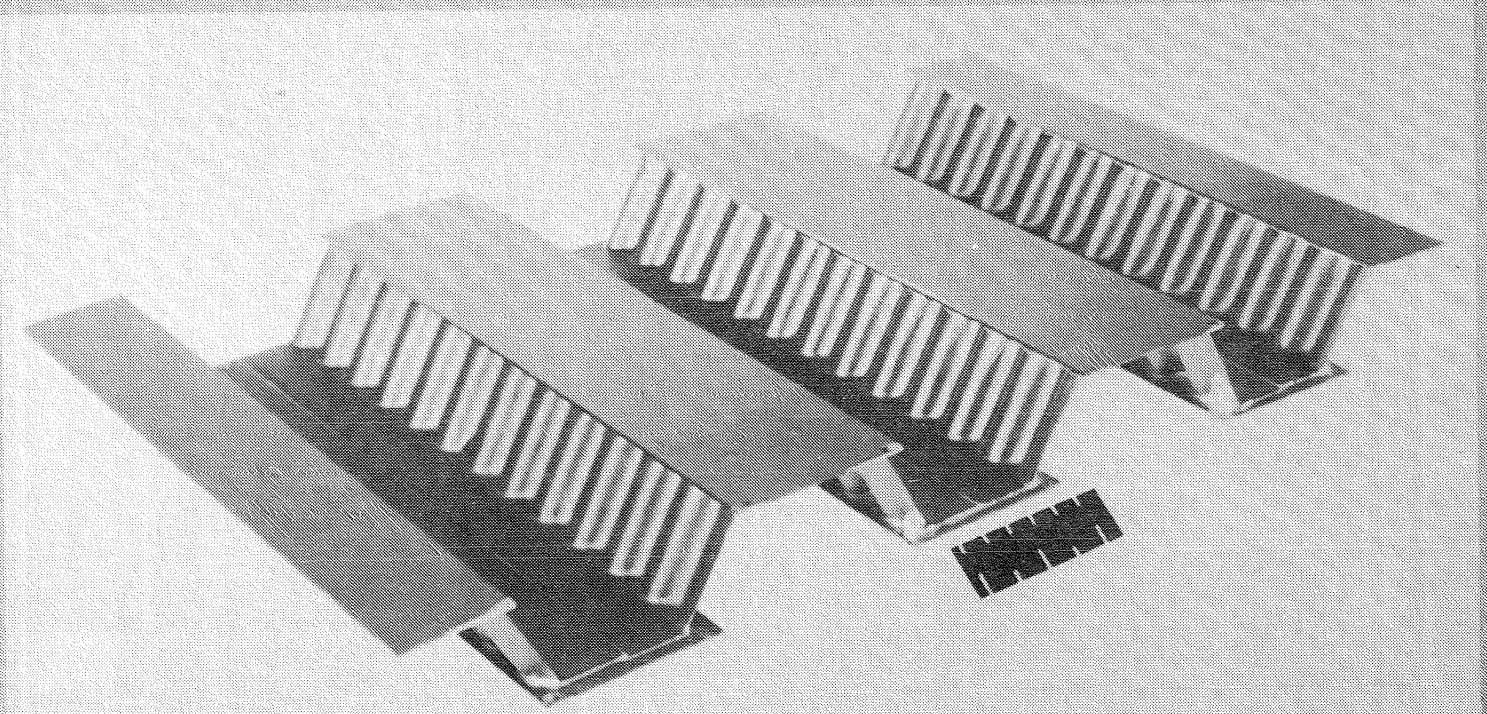

Figure 96

APPLICATION OF CARBON-CARBON ON SPACE SHUTTLE ORBITER

Innovative design concepts will be required to develop efficient structures for future space transportation systems. A class of materials class "carbon-carbon" has attractive features for such applications. These materials retain their strength at high temperatures (up to 3000°F or higher) and have a lower density than aluminum. Carbon-carbon is currently used as a load-bearing heat shield on the nose cap and wing leading edges of the Space Shuttle orbiter (Fig. 97). Carbon-carbon hot strutures potentially save weight when compared to convetional insulated aluminum structures used for the orbiter control surfaces because most of the insulation, which makes uip almost 70 percent of the weight, is eliminated. The material currently used on the orbiter is called Reinforced Carbon-Carbon (RCC). Newer carbon-carbon materials are stronger than RCC and appear attractive for replacement structure for control surfaces on the present orbiter.

The body flap on the Shuttle orbiter was selected for a conceptual design study to determine the feasibility of using carbon-carbon hot structure for light loaded control surfaces. Previous designs of carbon-carbon body flaps concepts employ combinations of metal and carbon-carbon components. The present design, however, uses only carbon-carbon components to reduce weight and to eliminate the inherent thermal expansion mismatch between metallic and carbon-carbon structures.

APPLICATION OF CARBON-CARBON ON SPACE SHUTTLE ORBITER

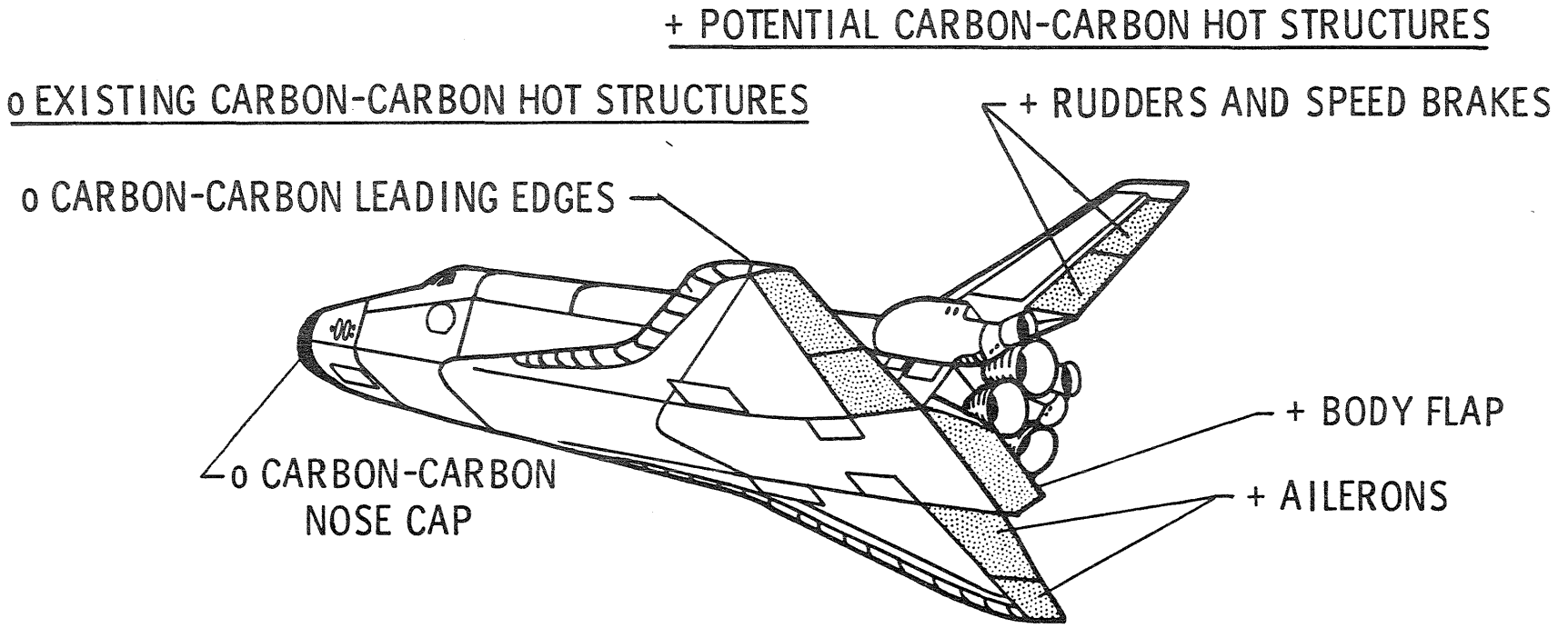

WEIGHT REDUCTION - 5000 lb (OPEN-FACE AILERONS, BODY FLAP)

Figure 97

TYPICAL-STRESS-FREE FASTENER CONFIGURATIONS

A theoretical basis has been developed for the design of fasteners which are free of thermal stress. (Ref. 135). A fastener can be shaped to eliminate the thermal stress which would otherwise result from differential thermal expansion between dissimilar fastener and sheet materials for many combinations of isotropic and orthotropic materials. The resulting joint remains snug, yet free of thermal stress at any temperature, if the joint is uniform in temperature, if it is frictionless, and if the coefficients of thermal expansion of the materials do not change with temperature. In general, such a fastener has curved sides; however, if both materials have isotropic coefficients of thermal expansion, a conical fastener is free of thermal stress.

Assumptions made in the analysis are as follows: the coefficients of thermal expansion of both materials are independent of temperature, both materials are uniform in temperature, and the interface between the materials is frictionless. In an actual joint, these requirements are unlikely to be fully satisfied. However, the resulting thermal interferences using a fastener shape defined by the analysis should be significantly smaller than those of a snug-fitting cylindrical fastener.

Typical thermal-stress-free fastener configurations utilizing the derived thermal-stress-free boundaries are shown on Figure 98. For values of the parameter p between 0 and 1, the fastener has a concave shape, whereas, for p greater than 1 it has a convex shape. A value of p equal to 1 results in a conical shaped fastener. Exprimental results for a conical fastener are given in Reference 136. The fastener configurations shown for p greater than zero appear practical to use for making joints. Note that if the diameter of the cylindrical portion of the fastener is maintained fixed as for the configuration shown the washer thickness varies widely depending on the value of p. A clearance between the washer and the shank of the fastener must be maintained at all temperatures. For values of p less than zero, the thermal-stress-free boundaries do not result in a compact joint configuration. The figure shows one possible thermal-stress-free configuration for the case where p is less than zero. The configuration shown is rather inefficient as the joint shear load would have to be carried in bending of the bolt. However, the joint is thermal-stress-free and may be the only joint configuration possible for certain combinations of materials. An example of high temperature materials that would require such a fastener is G/PI materials being joined together by a high temperature metal fastener. The negative value of p is due to the large difference in inplane and through-the-thickness CTE for G/PI which results in the CTE for the fastener being between the two values for G/PI. Other high temperature composite materials and metal fastener combinations have positive values of p which result in more practical thermal-stress-free configurations.

TYPICAL-STRESS-FREE FASTENER CONFIGURATIONS

$$y = cx^{p} \quad ; \quad \text{where } p = \frac{\alpha_{y1} - \alpha_{y2}}{\alpha_{x1} - \alpha_{x2}}$$

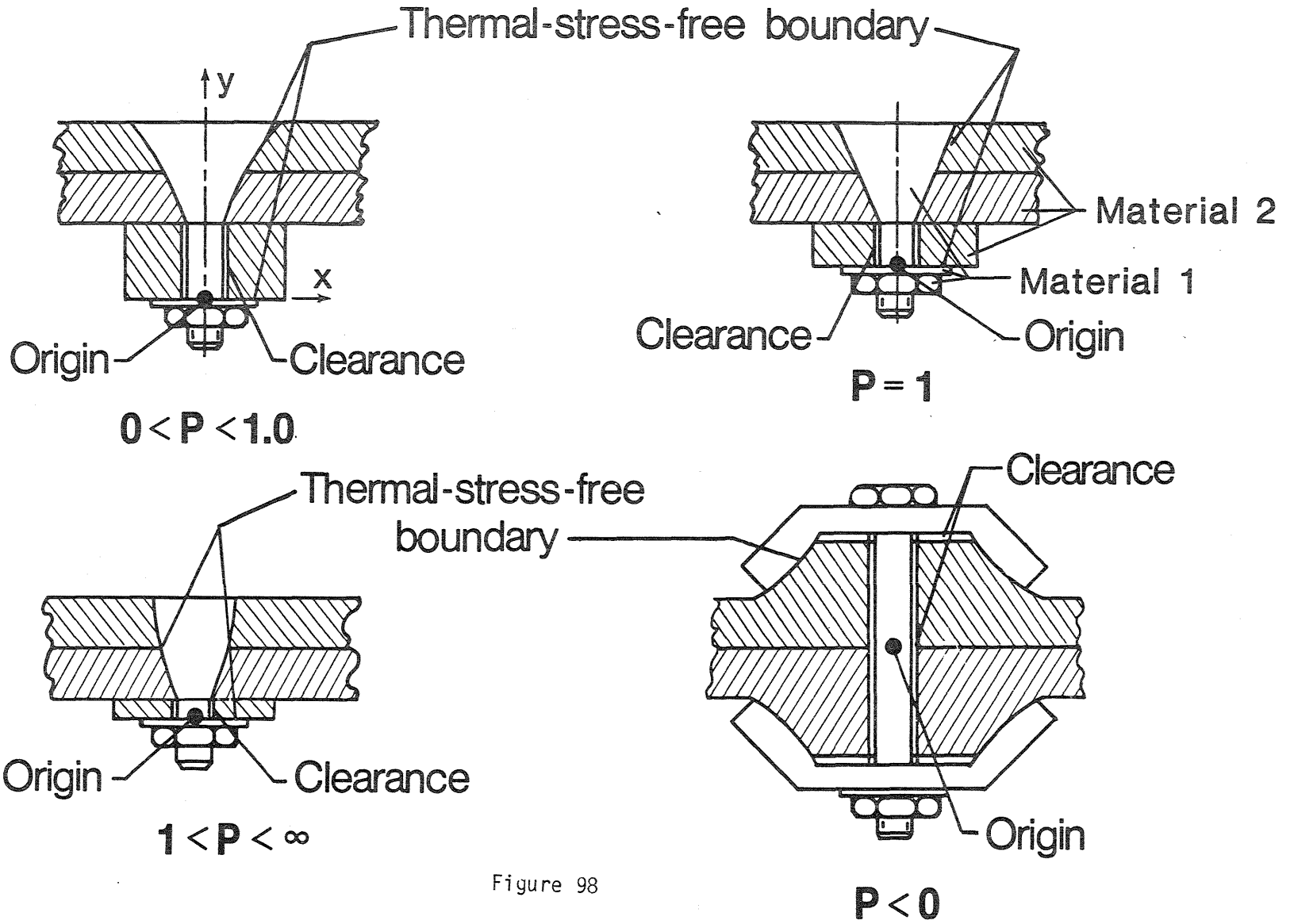

Figure 98

CONCEPTUAL DESIGN OF CARBON-CARBON BODY FLAP

The Shuttle Orbiter aft body flap is approximately 21 feet wide, 7 feet long, and 20 inches deep. The body flap is connected to the Shuttle at four actuator attachment points. A section of the baseline body flap and that of the carbon-carbon flap are shown in the lower left of Figure 99. The baseline design consists of upper and lower honeycomb core panels which are supported by aluminum ribs every 20 inches and connected to a full depth honeycomb core sandwich trailing edge. The aluminum structure is protected from entry heating by thick reusable surface insulation (RSI) tiles on both the lower and upper surfaces.

The carbon-carbon body flap design concept consists of a torque box and tapered, flanged ribs which support the continuous lower skin. Each rib extends into the torque box to form a bulkhead. Because the leading edge of the body flap is sealed, no significant air flow passes over the upper surface of the flap, and therefore the upper skin was removed to save weight. Removal of the upper surface also allows more heat to be radiated from the lower skin, thereby reducing peak temperatures. The hot structure design eliminates the RSI tiles except those left on the leading edge of the flap, which, along with the fibrous insulation indicated on the figure, are required to help prevent overheating of the aluminum structure of the orbiter.

There are several key considerations for the body flap design. The body flap is subjected to high acoustic loads from the main engines during liftoff. The structure is lightly loaded by aerodynamic pressure, but is subject to high entry heating. Another practical design consideration is the ease of retrofitting the replacement body flap.

The concept has been sized for static loads and the predicted weight is 610 pound, 850 pounds less than the current insulated aluminum body flap weight of 1460 pounds. Structural finite element analysis shows the carbon-carbon body flap to be stiffer than the baseline body flap. Thermal finite element analysis predicts that the carbon-carbon body flap will have a peak temperature of 2370°F, 330°F less than the baseline body flap. Moreover, thermal stresses are acceptable in the carbon-carbon body flap due to the low coefficient of thermal expansion of carbon-carbon. However, there may be potential problems with impact sensitivity as indicated by preliminary results given in Reference 59. More detailed information on the body flap design is given in Reference 137.

CONCEPTUAL DESIGN OF CARBON-CARBON BODY FLAP

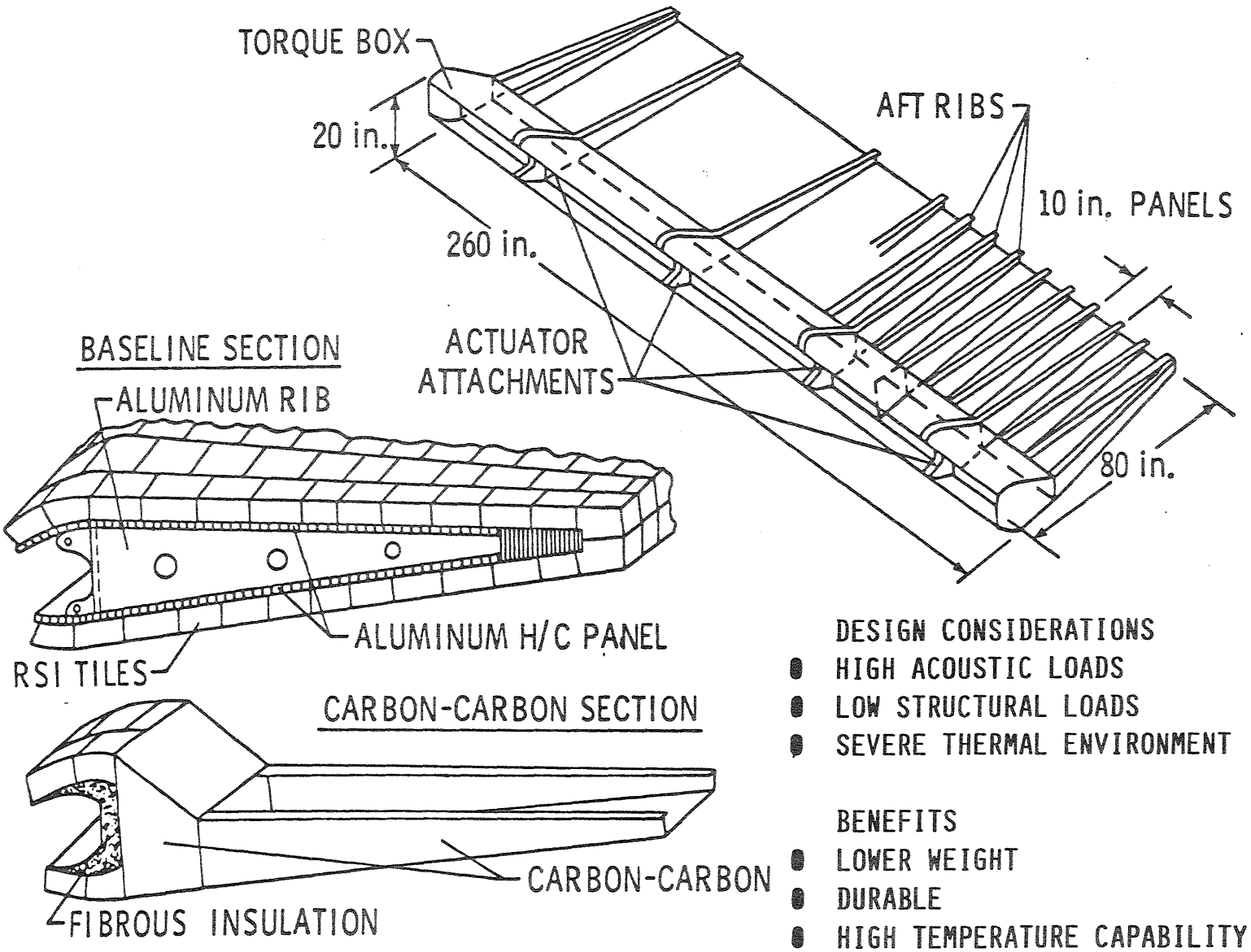

DESIGN CONSIDERATIONS

- HIGH ACOUSTIC LOADS
- LOW STRUCTURAL LOADS
- SEVERE THERMAL ENVIRONMENT

BENEFITS

- LOWER WEIGHT
- DURABLE
- HIGH TEMPERATURE CAPABILITY

Figure 99

SUMMARY - UNCOOLED STRUCTURES

Highlights of recent work on GR/PI composite, titanium, Rene' 41 and advanced carbon-carbon (ACC) structures are given in Figures 91-99. The NASA Composites for Advanced Space Transportation Systems (CASTS) program focused only on GR/PI but was broad in that many fiber and matrix materials within that class were studied as well as elevated temperature test techniques for material allowables, fabrication methods, stiffened and honeycomb structural panels, etc., culminating in the design, fabrication and test of a Technology Demonstrator Component (TDC) which was a 60 in. by 54 in. segment of a space shuttle orbiter body flap. Although the tests of the TDC were successful, the maximum temperature was 500°F compared to the original program goal of 600°F. Additional work is needed on GR/PI for airframe structural applications. In addition, little work has been done on metal matrix composites for airframe applications, and such materials could hold much promise for aerospace plane vehicles.

The superplastic forming (SPF) technology along with diffusion bonding (DB) or weld-brazing (WB) methods offer the structures designer many opportunities for more efficient geometries for structural panels. Geometric efficiency factors were identified and both paper and hardware concepts were highlighted. These new concepts can lead to new forms of old problems. An example, not presented herein, was the lid bonding of efficient box stiffeners to a panel that resulted in unanticipated stress concentrations due to the very small fillet associated with lid bonding.

Hot structures, in particular Rene' 41 structure, has been brought to a good level of maturity. A large component of a wing structure consisting of beaded or tubular panels has been extensively tested and analyzed. Much work has been done in the last 10 years on Rene' 41 honeycomb sandwich structures; in this paper this work was presented for application to a hot integral cryogenic tank. There is still concern about the state-of-the-art in predicting thermal stresses, and current high temperature test techniques and instrumentation are far from satisfactory. The aerospace community has neglected this area testing of large components. Requirements for certification of structure subjected to combined thermal and mechanical loads are not firm, and the impact of such requirements on the development of an aerospace plane is not understood. There is also a need to develop a better understanding of the performance of structure subjected to repeated thermal stresses that exceed the elastic range; plastic deformations that reduce thermal stresses may be acceptable, which could allow the designer to wring out more performance from his structure.

ACC is an attractive material for high temperature structural applications such as control surfaces and the other "Jackson Aeroshell" studied for Orbit-on-Demand vehicles. Work on stress-free fasteners and impact sensitivity is under way, but much more hardware development is required to truly assess the potential of this new material option to the structural design for airframe applications.

SUMMARY - UNCOOLED STRUCTURES

- COMPOSITES NEEDED TO MEET STRUCTURAL WEIGHT REDUCTION GOALS
  - CASTS BROUGHT GR/PI TO A FAIR LEVEL OF MATURITY, BUT MORE WORK NEEDED
  - LITTLE WORK ON METAL MATRIX COMPOSITES FOR AEROSPACE PLANE APPLICATIONS

- SPF/DB AND SPF/WB TITANIUM PERMITS FAB OF EFFICIENT STRUCTURAL GEOMETRIES
  - GEOMETRIC EFFICIENCY FACTORS IDENTIFIED
  - NEW CONCEPTS LEAD TO NEW FORMS OF OLD PROBLEMS - STRESS CONCENTRATIONS

- HOT STRUCTURE BROUGHT TO A GOOD LEVEL OF MATURITY
  - NEED TO VERIFY ANALYTICAL DESIGN TOOLS
  - NEED TO DEVELOP TEST TECHNIQUES/INSTRUMENTATION
  - NEED TO UNDERSTAND STRUCTURAL PERFORMANCE FOR σ_T IN PLASTIC RANGE

- CARBON-CARBON ATTRACTIVE FOR HIGH TEMPERATURE STRUCTURAL APPLICATIONS
  - CONTROL SURFACE STRUCTURE FEASIBLE NOW, BUT IMPACT SENSITIVITY IS A CONCERN
  - OTHER INTERESTING CONCEPT PROPOSED - JACKSON AEROSHELL
  - STRESS-FREE FASTENERS UNDER DEVELOPMENT
  - MORE HARDWARE DEVELOPMENT REQUIRED

Figure 100

HYDROGEN COOLED ENGINE STRUCTURES

Work on hydrogen-cooled engine structures at the Langley Research Center began with the Hypersonic Research engine (HRE) Program of the 1960's which culminated, from a thermal/structural standpoint, in tests of a complete flight-weight hydrogen-cooled engine assembly in the 8-Foot High Temperature Structures Tunnel (Fig. 101, upper left). These tests (Ref. 138) and others (Ref. 139) confirmed the suitability of the basic approach for research purposes. However, two major thermal/structural problems were uncovered that must be solved before a hydrogen-cooled scramjet can become a practical reality: (1) the coolant requirements must be reduced (the HRE required almost three times as much hydrogen for coolant as for fuel) and (2) the thermal fatigue life must be increased (HRE had an anticipated fatigue life of only 135 operational cycles). Both of these problems stemmed, at least in part, from the annular design and high compression ratio of the engine which resulted in large areas being exposed to an intense heating environment. A fundamental goal of the continuing research program was to develop an engine concept which required only a fraction of the total fuel heat sink for engine cooling.

Studies of airframe-integrated scramjets with high potential performance led to the sweptback, fixed-geometry, hydrogen-fueled, rectangular scramjet module shown in Figure 101. Two inner scramjet modules are shown; the sidewall of one module is removed to reveal the internal engine surfaces. The scramjet modules are integrated with the airframe and use the entire under surface of the aircraft to process engine airflow. The aircraft forebody serves as an extension of the engine inlet, and the afterbody serves as an extension of the engine nozzle. A number of aerodynamic/propulsion advantages are obtained with this concept. (Ref. 140) Structural advantages include the fixed geometry and reduced wetted surface area and heating rates. Surface area is reduced by the non-annular configuration and by the multiple fuel injection planes which promote fuel mixing and combustion and thereby reduce the combustor length. Heat transfer rates are reduced by the lower inlet compression ratio and by the large combustor exit-to-entrance area ratio which reduce pressures.

By 1971 propulsion technology for the airframe integrated scramjet had advanced sufficiently to warrant development of the thermal/structural technology. A preliminary thermal/structural design analysis study (Ref. 141) based on HRE technology indicated viability from both an engine structural mass and coolant requirement standpoint. This study revealed a number of critical areas (e.g., panel-to-panel seals, fuel injection struts) and reemphasized the need for advances in fabrication and materials technology to obtain reasonable structural life.

A more detailed study (Ref. 142) of this scramjet concept was undertaken by a major engine manufacturer while the effort at Langley concentrated on the fuel-injection strut.

Fabrication studies to improve thermal fatigue life were successful, and a major engine manufacturer is currently building a fuel injection strut for testing at NASA Langley. This test will be followed by tests of a flight-weight module, as indicated on the figure.

HYDROGEN COOLED ENGINE STRUCTURES

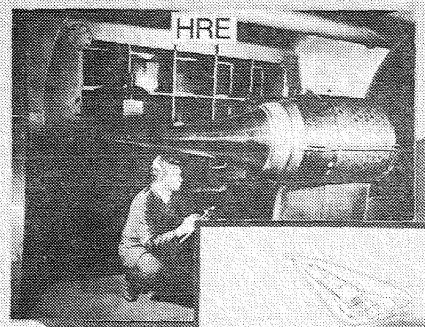

AIRFRAME INTEGRATED SCRAMJET

PRACTICAL
HYDROGEN COOLED
ENGINE-STRUCTURES

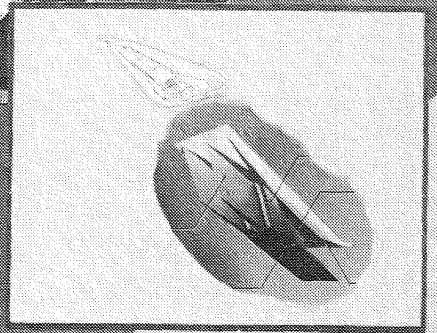

LANGLEY SUPERSONIC
COMBUSTION RAMJET

THERMAL/STRUCTUAL DEVELOPMENT

THERMAL/STRUCTUAL

DESIGN STUDY

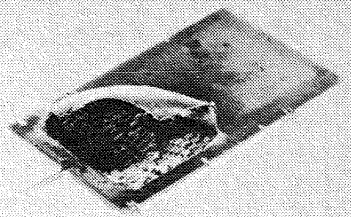

FABRICATION

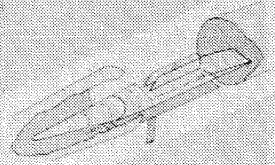

THERMAL STRUCTURAL
PERFORMANCE

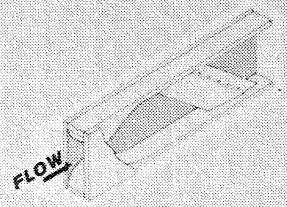

COOLING PERFORMANCE

Figure 101

COOLED SCRAMJET STRUCTURE

All engine surfaces wetted by the airstream are regeneratively cooled by circulating the hydrogen fuel through a cooling jacket before injecting the fuel into the combustor. The cooling jacket, which is brazed to the primary structure, consists of the aerodynamic skin and multiple straight-fin or pin-fin coolant passages; straight-fin passages are shown as part of Figure 102.

Three basic engine shell concepts were investigated: two frame-stiffened honeycomb-core sandwich panels and a deep-core honeycomb sandwich panel. All three concepts have approximately the same mass per unit capture area of about 84% of the value for the HRE; the HRE was heavier in spite of the more structurally efficient circular shell construction. The deep-core honeycomb concept was selected as shown in Figure 102 as the baseline design primarily because it exhibits the least deflection in the sidewall and nozzle areas and is the least complex structure. The deep-core honeycomb concept has a core thickness which varies from 0.24 to 1.97 in. and has two vertical frames. Analytical results indicate relative displacements between adjoining components are generally small which permits the panel corners to be rigidly joined allowing the use of a simple static seal or even a welded corner.

The results indicate that the basic shell concepts have a significant temperature gradient through the thickness during thermal transients (e.g., maneuvers, combustion shutdown) which may significantly impact the final design of both the seals and basic shell structure.

The fuel-injection struts presented the most formidable cooling and structural problems. The struts must simultaneously support a large side load, contain high-pressure hydrogen at two temperature extremes, and withstand the high thermal stresses resulting from complex aerodynamic heating as well as convective heating from the hot hydrogen in the internal manifolds. To compound these problems the cross sectional area and contour cannot be altered without significantly changing the engine propulsion performance.

The struts have a maximum thickness of 1 in. and chords of 10 in. (center strut) and 12 in. (side struts), a span of 18 in. and are swept back 42°. Each strut is subdivided internally into four longitudinal compartments. The fore and aft compartments serve as coolant inlet and outlet manifolds respectively and the central compartments serve as fuel manifolds for the strut trailing edge (parallel to airflow) and wall (perpendicular to airflow) fuel injectors. Coolant in the inlet manifold is injected through a slot, impinges on the leading edge, and splits (unequally) to flow along each wall to the trailing edge, where it is collected in the outlet manifold. This quadrilateral manifold configuration was selected over a more structurally efficient (high pressure containment) tubular configuration because the former has a greater volumetric efficiency which results in larger fuel and coolant flow areas and thus lower pressure losses.

COOLED SCRAMJET STRUCTURE

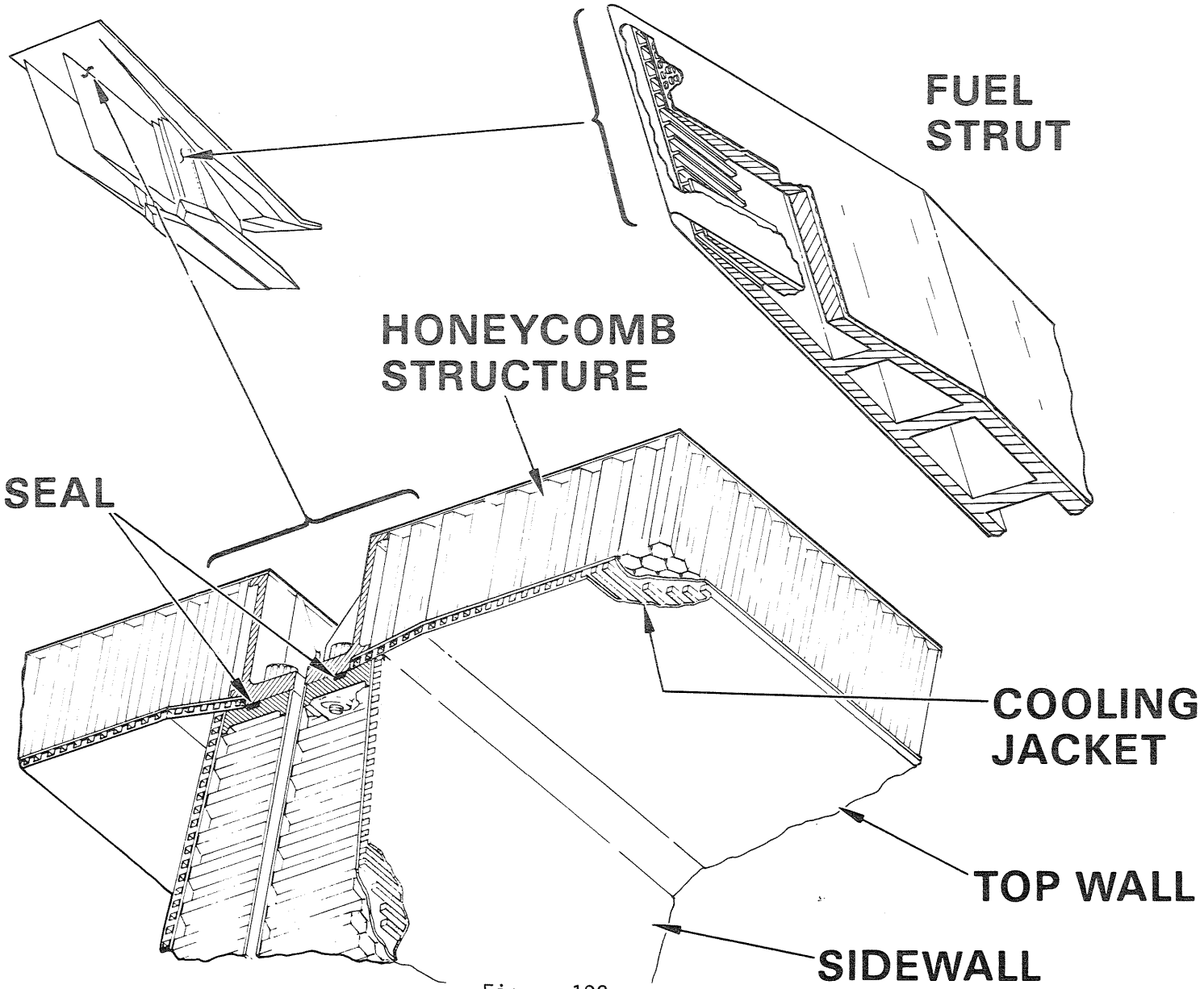

Figure 102

HYDROGEN COOLANT ROUTING

Although a fundamental design goal was the minimization of coolant requirements, the coolant routing scheme, depicted in Figure 103, results primarily from requirements to minimize thermal stresses and deflections to yield the least complex thermal/structural and seal concepts. In general, the coolant enters each component leading and trailing edge (low heat load areas) and flows longitudinally toward the component center (highest heat load area), where it is collected in manifolds and routed to a fuel plenum. (Leading edge stagnation heating is intense but the heat-load is low because of the small area). From there it is dispersed to the fuel manifolds in each strut and injected into the airstream. This routing scheme reduces the temperature variation transverse to the flow direction, the temperature differential through the cooling jacket, and to a lesser extent the total aerodynamic heat load thereby reducing the cooling requirements. Two coolant circuits per component were necessitated by the fuel pressure requirements, as frictional pressure losses with only one circuit would be excessive.

All leading edges exposed to stagnation heating from the airflow are impingement cooled. The coolant is injected through a slot in the coolant inlet manifold and impinges on the inside surface of the leading edge, which then turns the coolant around to flow along the component surface. This technique permits the use of the total sidewall coolant flow for impingement cooling. Even though the impingement cooling technique augments the coolant heat transfer characteristics along the stagnation line by a factor of two to three, the total circuit flow is required because of the high stagnation line heating.

A unique feature of the coolant routing scheme is the commonality of the cooling circuits for the sidewalls of adjoining modules. This scheme minimizes temperature gradients across the sidewall component and thus reduces thermal stresses and warpage in the sidewall. However, the primary structure is not common to the adjoining module sidewalls in that the frames are split to relieve top wall and cowl thermal stress by allowing the sidewalls to translate laterally relative to each other. The seal design is also simplified as the lateral expansion of only one module need be accommodated. In addition, module cowls are independent and allowed to slip relative to one another. The leading- and trailing-edge sections of the sidewall remain integral between adjoining scramjet modules; however, since these sections are near ambient temperature, the thermal stresses are acceptable (Refs. 141 and 142). The design features expansion joints and seals at the top and bottom of the sidewall and a sliding seal between the cowls. This overall freedom to expand precludes any thermal stress due to the absolute temperature change from ambient; however, thermal stresses caused by the nonlinear temperature profiles can be relieved only by minimizing the thermal gradients.

HYDROGEN COOLANT ROUTING

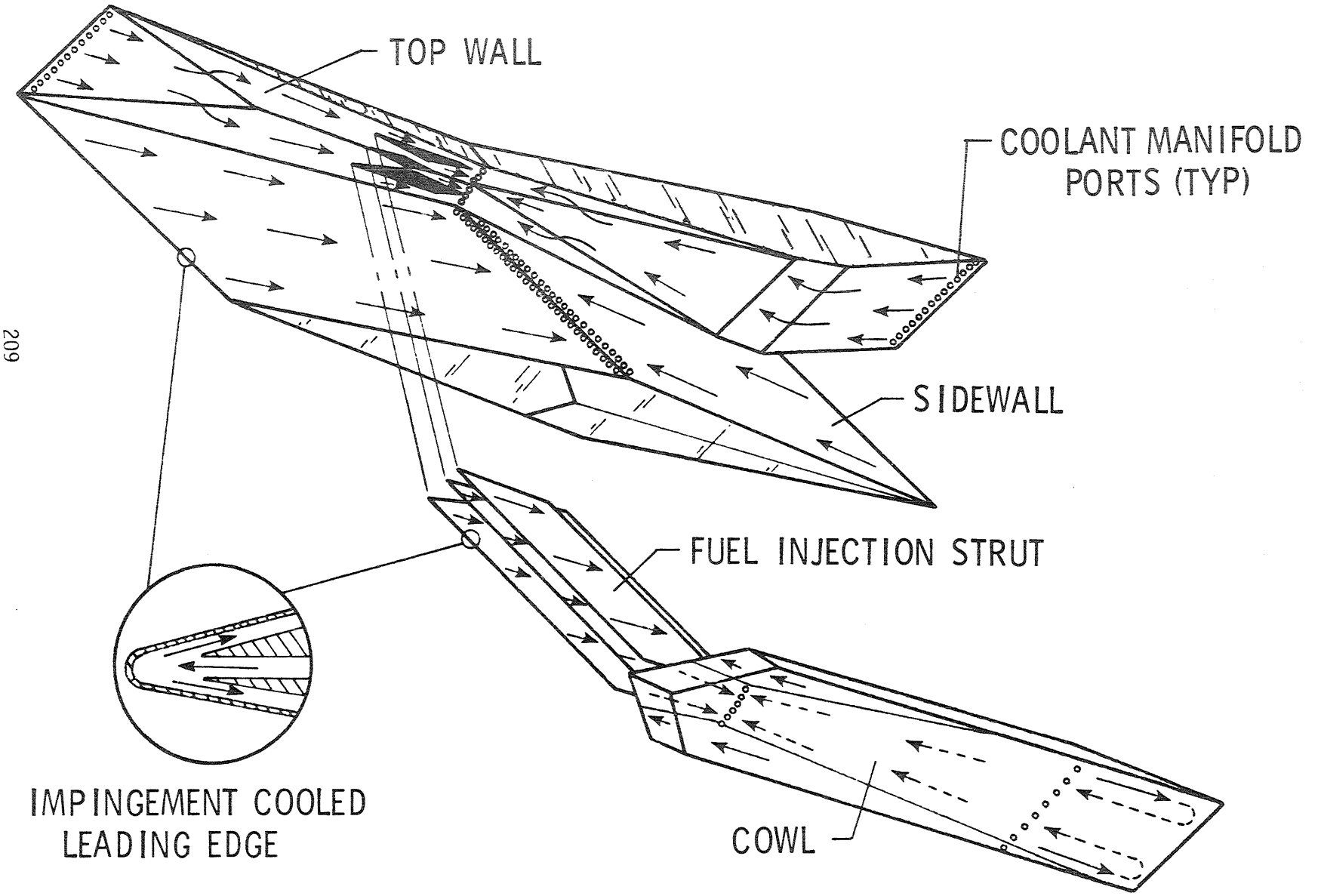

Figure 103

HEAT PIPE SANDWICH PANEL CONCEPT

A research program to develop hydrogen-fueled airframe-integrated scramjet engines has been underway for sometime (Ref. 143). The present engine design uses full-depth (1.8 in.) honeycomb sandwich walls whose heated surfaces are cooled regeneratively by the circulation of hydrogen fuel through a cooling jacket. During transient engine operation (e.g., maneuvers, combustion or shutdown) large temperature differences across the sandwich walls (1200°F) cause excessive thermal stresses in the facesheets (over 200ksi) and greatly reduce engine life.

The heat-pipe sandwich panel was conceived as a simple and efficient solution to the engine thermal stress problem. The heat-pipe concept can drastically reduce maximum temperature differences across the honeycomb walls, and, hence, reduce thermal stresses with potentially only a modest increase in mass, over the original, unacceptable nonheatpipe design. This exceptional performance may be possible because the integral heat-pipe sandwich panels synergistically combine the thermal efficiency of heat pipes with the structural efficiency of honeycomb sandwich construction. Several panels were fabricated and tested to verify feasibility of the concept (Refs. 144-146).

The goal was to develop a sandwich panel, similar in structural integrity to the original nonheat-pipe sandwich panel design, which could reduce maximum temperature differences, hence, stresses, by 50% and make the design feasible.

The heat-pipe sandwich panel, shown schematically in Figure 104, consists of a wickable honeycomb core, internally wickable facesheets, and a suitable working fluid. The term "wickage" is defined as porous and capable of wicking a working fluid by capillary pumping. For application to the scramjet engine, the working fluids considered are cesium, potassium, and sodium. During operation heating is absorbed at the heated face by the evaporation of working fluid. The heated vapor flows (see inset) due to a pressure differential, to the cooler face where it condenses and gives up its stored heat. The cycle is completed with the return flow of liquid condensate back to the heated face by the capillary pumping action of the wickable core. The core is perforated to allow intracellular vapor flow and is notched at both ends to allow intracellular liquid flow along the internally wicked faces.

HEAT PIPE SANDWICH PANEL CONCEPT

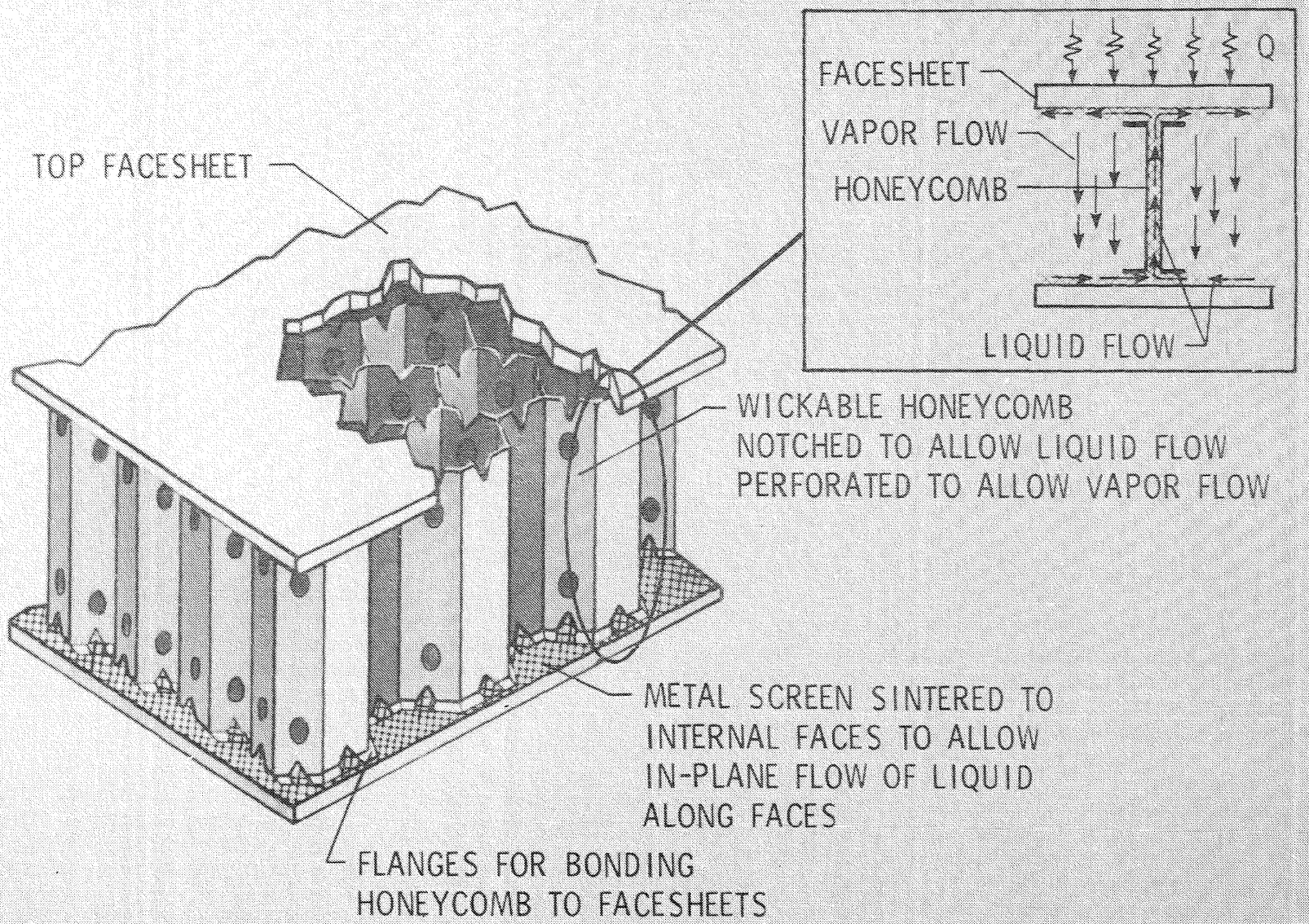

Figure 104

INITIAL TESTS VERIFY FEASIBILITY OF HEAT PIPE SANDWICH PANEL CONCEPT

Preliminary checkout tests of the heat pipe sandwich panels (Fig. 105) indicate that stainless-steel heat-pipe sandwich panels can be fabricated and operated successfully using cesium, potassium or sodium working fluids, at temperatures ranging from 1030°F to 1569°F. The reduction in maximum ΔT attainable at design loads by using a heat-pipe panel is 31 percent for sodium working fluid, 46 percent for potassium working fluid and 60 percent with cesium working fluid. The panels are durable and can withstand internal pressures over 500 psi at room temperatures and result in only a 10 percent increase in mass over the current, unacceptable non-heat pipe design for a scramjet engine sidewall. Additional details of the tests are given in References 144 and 146.

Low-temperature applications (using different materials and working fluids) of the concept include: cooling electronic components or circuit cards, limiting thermal distortions in large space structures (e.g., antennas, laser mirrors, or other optical systems), and serving as radiators for space stations or space transportation systems. A radiator application which has the potential of reducing mass of other heat-pipe or fluid loop systems by over 50% and increasing efficiency from 0.8 to approximately 1 is currently being investigated (Ref. 147).

INITIAL TESTS VERIFY FEASIBILITY OF HEAT PIPE SANDWICH PANEL CONCEPT

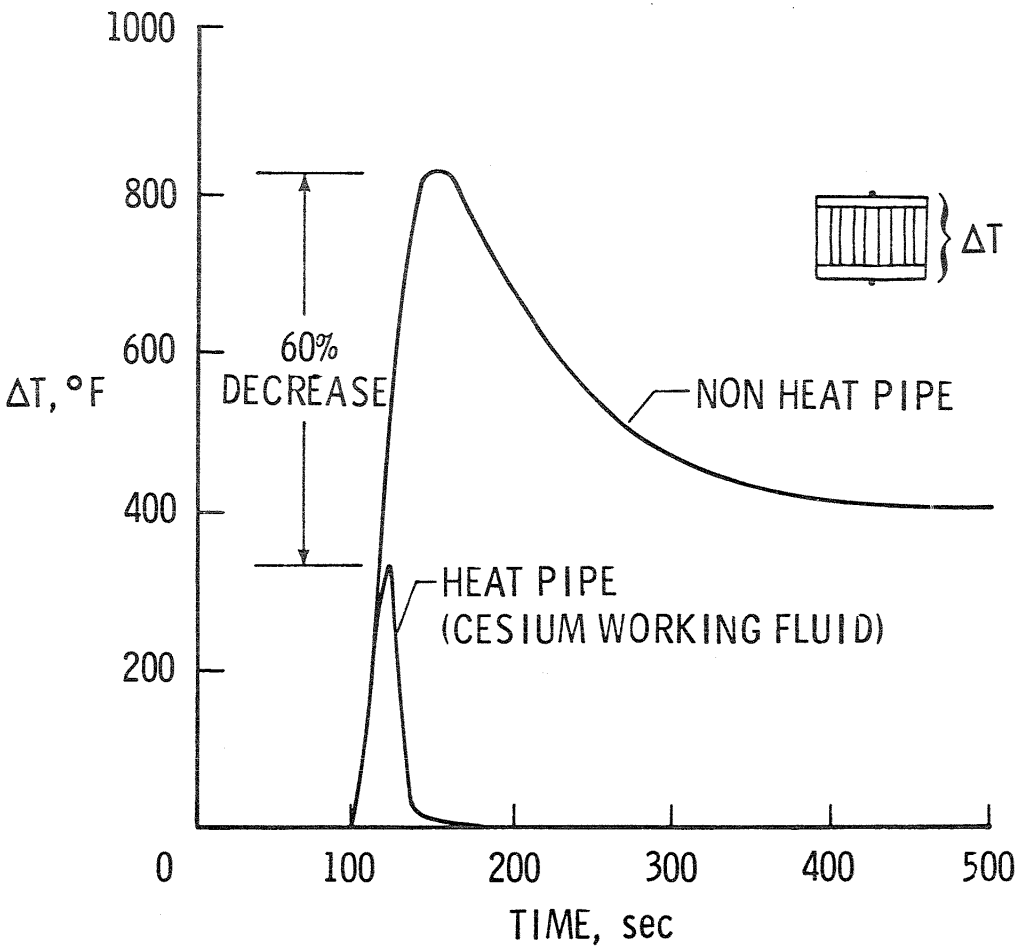

Figure 105

THERMAL FATIGUE LIFE

The fabrication and material technology required to obtain reasonable thermal fatigue life for the cooling jacket was developed and experimentally validated (Ref. 4). The goal for the airframe-integrated scramjet is 1000 hours and 10,000 cycles of hot operation which represents an improvement of two orders of magnitude over the HRE. Analytical predictions of the fatigue life as a function of the temperature difference between the hot aerodynamic skin and the back surface are presented in Figure 106. The life goal appears attainable through a number of factors such as engine design, fabrication, and material selection. The improvements attributable to these factors are graphically illustrated in the figure. The bottom curve indicates the anticipated life of the Hastelloy X coolant jacket for the HRE. The solid symbol at the right denotes the HRE design point and the open symbols indicate experimental data. A fundamental change in engine design to decrease the heat flux intensity and thus the temperature difference, as indicated by the horizontal arrow, is the first factor to increase the life of the airframe-integrated scramjet. An additional increase, as indicated by the vertical arrow, is obtained through and advanced fabrication technique. In this technique the fin coolant passages are photo-chemically etched into the aerodynamic skin which eliminates the strain concentration caused by local thickening of the skin by the fin and eliminates the hot skin to fin braze joint present in the HRE configuration. (The braze joint to the cooler primary structure remains, however.) The two candidate configurations fabricated by this process are shown in the figure. Finally, another increment in life is attained through the selection of a material with high thermal conductivity which decreases the temperature difference, and with high ductility which increases the fatigue life directly. To date Nickel 201 and Inconel 617 or 718 appear to be the most attractive materials.

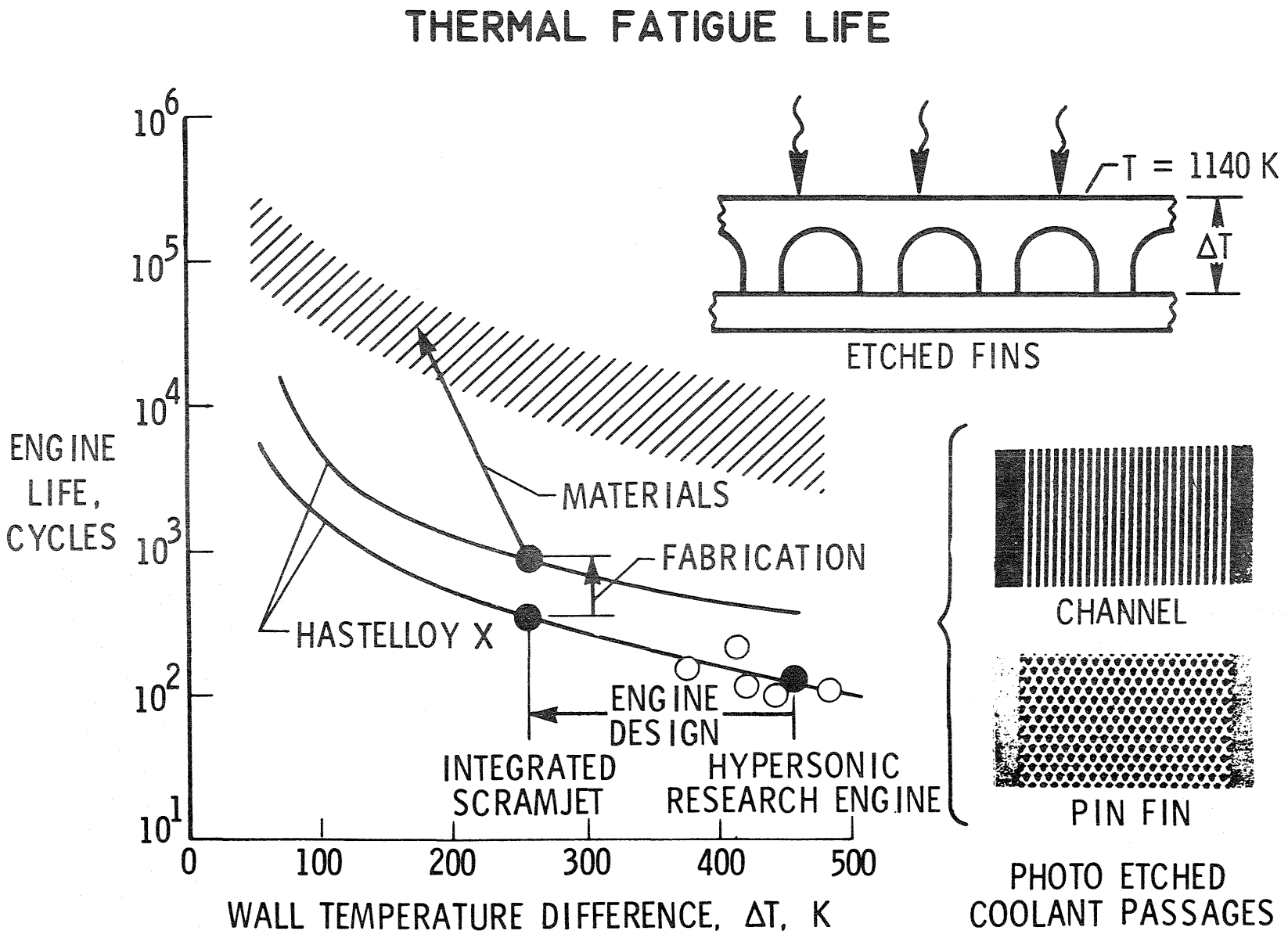
THERMAL FATIGUE LIFE
ENGINE LIFE, CYCLES
10^6
10^5
10^4
10^3
10^2
10^1
MATERIALS
FABRICATION
HASTELLOY X
ENGINE DESIGN
INTEGRATED SCRAMJET
HYPERSONIC RESEARCH ENGINE
0
100
200
300
400
500
WALL TEMPERATURE DIFFERENCE, ΔT, K
T = 1140 K
ΔT
ETCHED FINS
CHANNEL
PIN FIN
PHOTO ETCHED COOLANT PASSAGES

Figure 106

ADVANCED FABRICATION DEVELOPMENT COMPLEMENTS DESIGN STUDY

Figure 107 shows two struts, the orignal concept based on HRE technology and an improved strut, where the improvements are based on either advanced fabrication developments or design studies. Life is increased by use of a Nickel 201 pin fin cooling jacket rather than a Hasteloy X offset fin concept. Strut strength is increased by use of Inconel 718 structure rather than Hastelloy X, a result of the design study (Ref. 142). The integral manifold provides improved flow distribution compared to tube manifolds. Finally, the design study of Reference 141 revealed large temperature differences and thermal stresses in the strut primary structure caused by internal convective heating from the hot hydrogen in the manifolds. The internal heating, which is normally negligible compared to the aerodynamic heating, is increased significantly by the higher velocities caused by the restricted flow area. Attempts to reduce these stresses by rearranging the fuel and cooling manifolds as well as the coolant circuitry proved fruitless. However, the addition of a metallic plate-fin thermal buffer in the hot manifolds reduced primary structure thermal stresses by approximately 64 percent. The thermal buffer fins are oriented transverse to the fuel flow direction to restrict flow and provide essentially stagnant hydrogen in the passages between the shield and the strut wall, thereby eliminating direct convective heating to the strut wall.

ADVANCED FABRICATION DEVELOPMENT COMPLEMENTS DESIGN STUDY

ORIGINAL CONCEPT

COMPONENT VERIFICATION

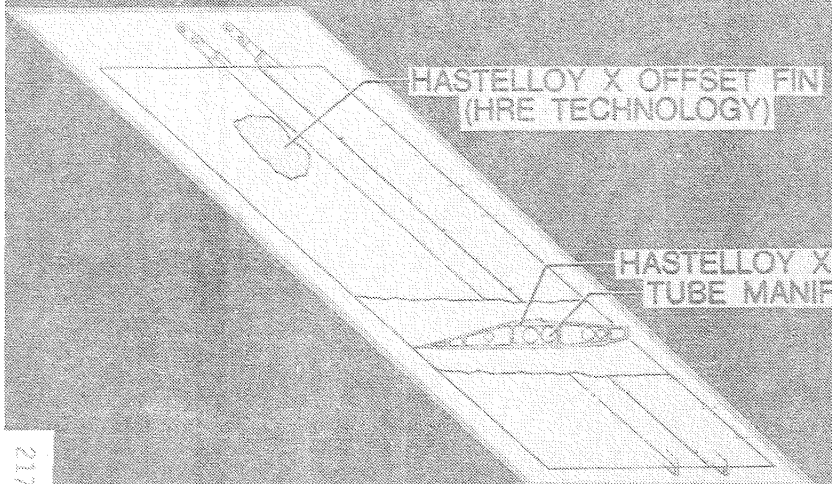

IMPROVED CONCEPT

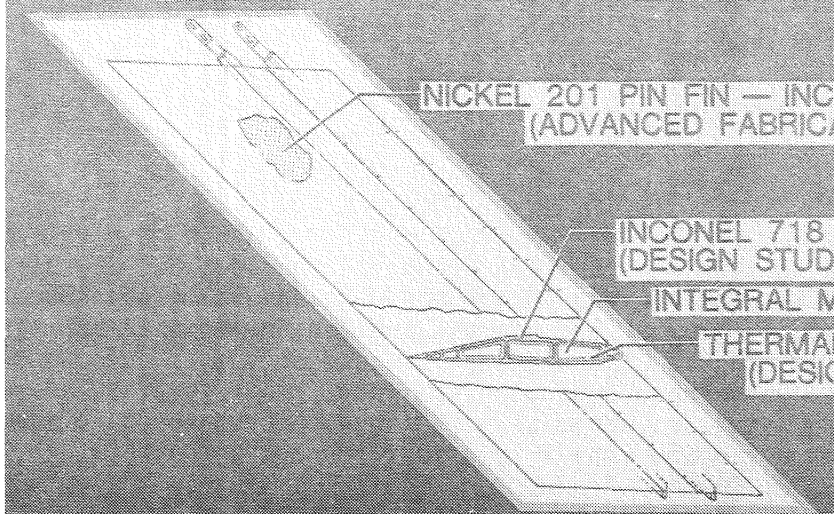

Figure 107

STRUT THERMAL EVALUATION

Figure 108 shows a sketch of a fuel injection side strut mounted in the NASA LaRC combustion and mixing research apparatus. The strut is currently being fabricated by a major engine manufacturer (NASA contract NAS1-16097) and should be completed by the last quarter of FY85. The strut will be tested to determine 1) the combustion efficiency of a strut of flightweight structure and 2) the performance of the flightweight structure and its cooling jacket. Other tests, still in the planning stage, will be conducted to verify the accuracy of the thermal and structural design analyses and possibly the creep life of the impingement cooled leading edge that is subjected to severe stagnation heating rates.

STRUT THERMAL EVALUATION

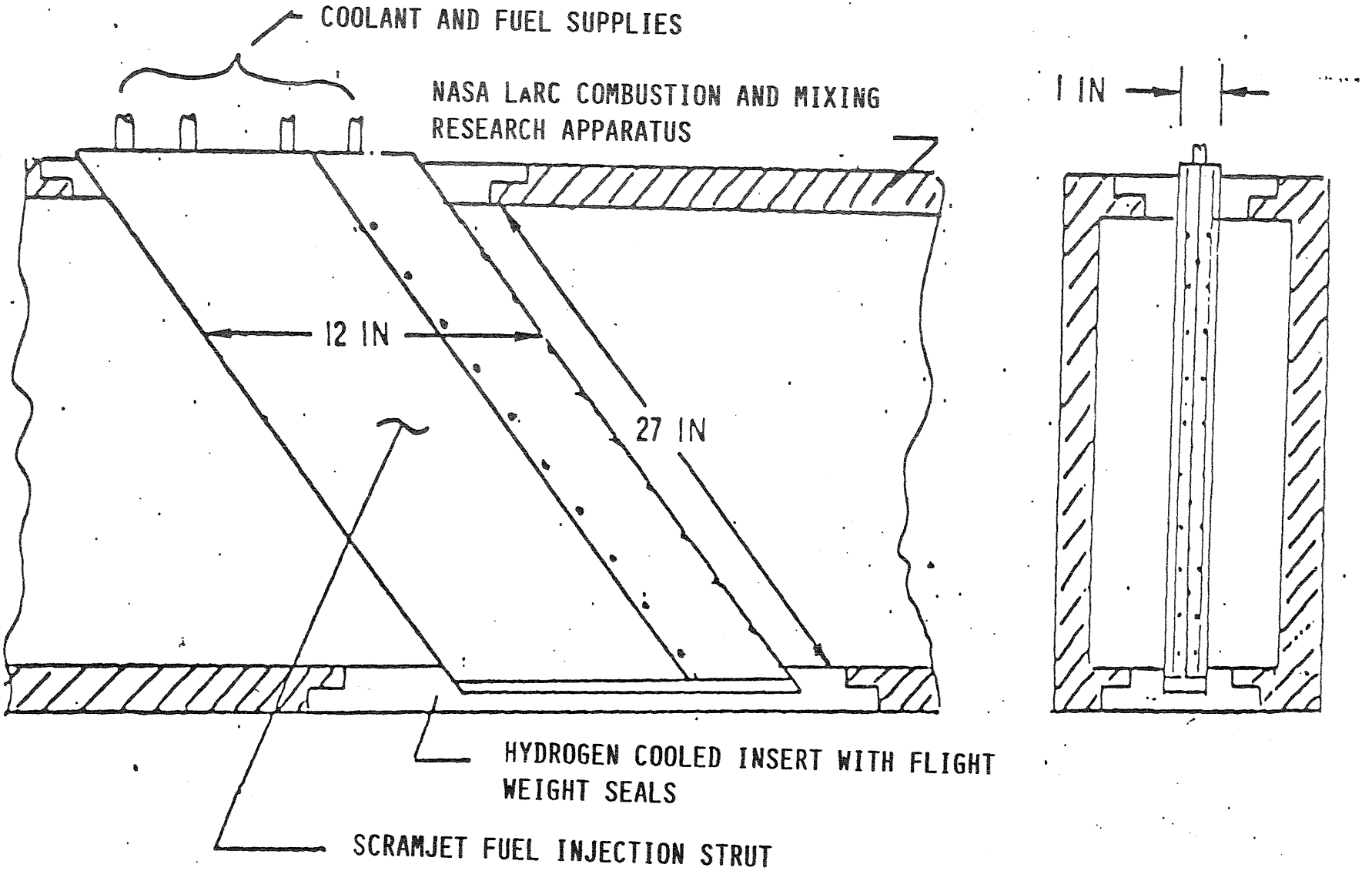

Figure 108

OPERATIONAL ENVELOPES FOR PROPULSION FACILITIES

Current facility capabilities for testing propulsion or missile systems at high Mach numbers are severely limited. The Marquardt Company, the Chemical Systems Division of United Technology Corporation, and Air force facilities at Arnold Engineering Development Center (Aero Propulsion Test Unit and Aero Propulsion System Test facility) can accommodate full-scale ramjets and missiles up to about Mach 4. Other test facilities (for example, those at NASA Langley and General Applied Science Laboratories) can simulate flight Mach numbers up to 7, but they are small and can only accommodate incomplete subscale engines or engine components. No existing facility in the U.S. can provide both true-temperature, high-Mach-number flow and a large scale.

The NASA Langley 8-Foot High Temperature Tunnel (8' HTT) has many of the attributes desirable for a propulsion test facility, in particular, size and true temperature simulation for Mach 7 flight; however, the high energy level required to simulate Mach 7 flight is obtained by burning high pressure methane and air and the resulting products of combustion are used as the test medium. Thus the test stream is oxygen depleted and will not support combustion. In addition it would be highly desirable to be able to test at lower Mach numbers nearer the range where transition from turbojet or rocket to ramjet or scramjet mode of operation is anticipated.

Reference 148 describes a planned modification of the 8' HTT to make it a unique national research facility for hypersonic air-breathing propulsions systems and discusses some of the ongoing supporting research for that modification. The modification involves: (1) the addition of an oxygen-enrichment system which will allow the methane-air combustion-heated test stream to simulate air for propulsion testing; and (2) supplemental nozzles to expand the test simulation capability from the current nominal Mach number of 7.0 to include Mach numbers 4.0 and 5.0. The modified facility will retain the present capability for aerothermostructural and aerothermal loads research for high speed vehicles and aerospace re-entry vehicles.

The modified facility will complement the two large scale Air Force facilities at the Arnold Engineering Development Center. As illustrated by Figure 109 in which the operating envelopes of the three facilities are superimposed on projected operating range of air-breathing propulsion systems, the Aero Propulsion Test Unit and Aero Propulsion System Test facility appear completely adequate for propulsion research for Mach numbers below approximately 4.5. The modified 8' HTT will extend that range to Mach 7 and provide coverage in the ramjet to scramjet transition region.

The large, approximately 8' diameter by 12-1/2' long, open jet test section will enable the modified facility to support both NASA sponsored research on scramjet engines and development tests of DOD missiles.

OPERATIONAL ENVELOPES FOR PROPULSION FACILITIES

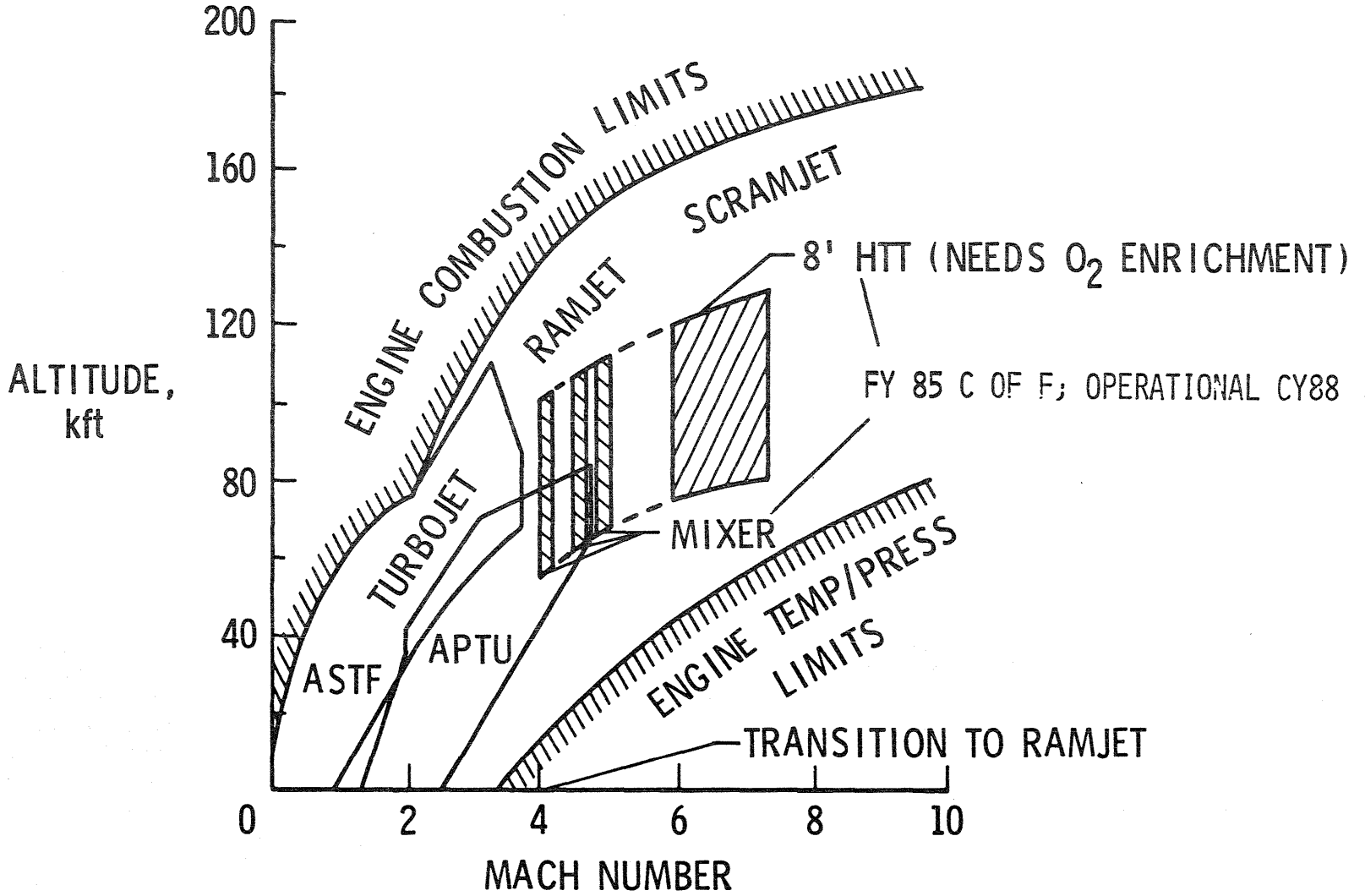

Figure 109

MULTIPLE MODULE SCRAMJET TEST CONFIGURATION

As shown in Figure 110 the facility can accommodate multiple modules of an airframe-integrated concept that includes a vehicle forebody/inlet, combustor, and vehicle/afterbody nozzle. Previously LaRC efforts to develop a technology base for hydrogen and hydrocarbon scramjets have been successful, but have been limited by facility size to the testing of single modules including only the inlet and combustor. The larger facility will permit the investigation of (1) potentially critical interactions between multiple engine modules at angles-of-attack and yaw, (2) the effects of engine scale on performance, and (3) the effects on performance of the integrated afterbody/nozzle, configurations for which the airframe provides up to 50-percent of the total thrust. The large scale will also permit the thermal/structural evaluation of flight-weight, fuel-cooled engine structures. Such tests must be made with essentially full-scale components since scaling of structure components is generally not applicable because of the adverse effects on fabrication and manufacturing techniques.

MULTIPLE MODULE SCRAMJET TEST CONFIGURATION

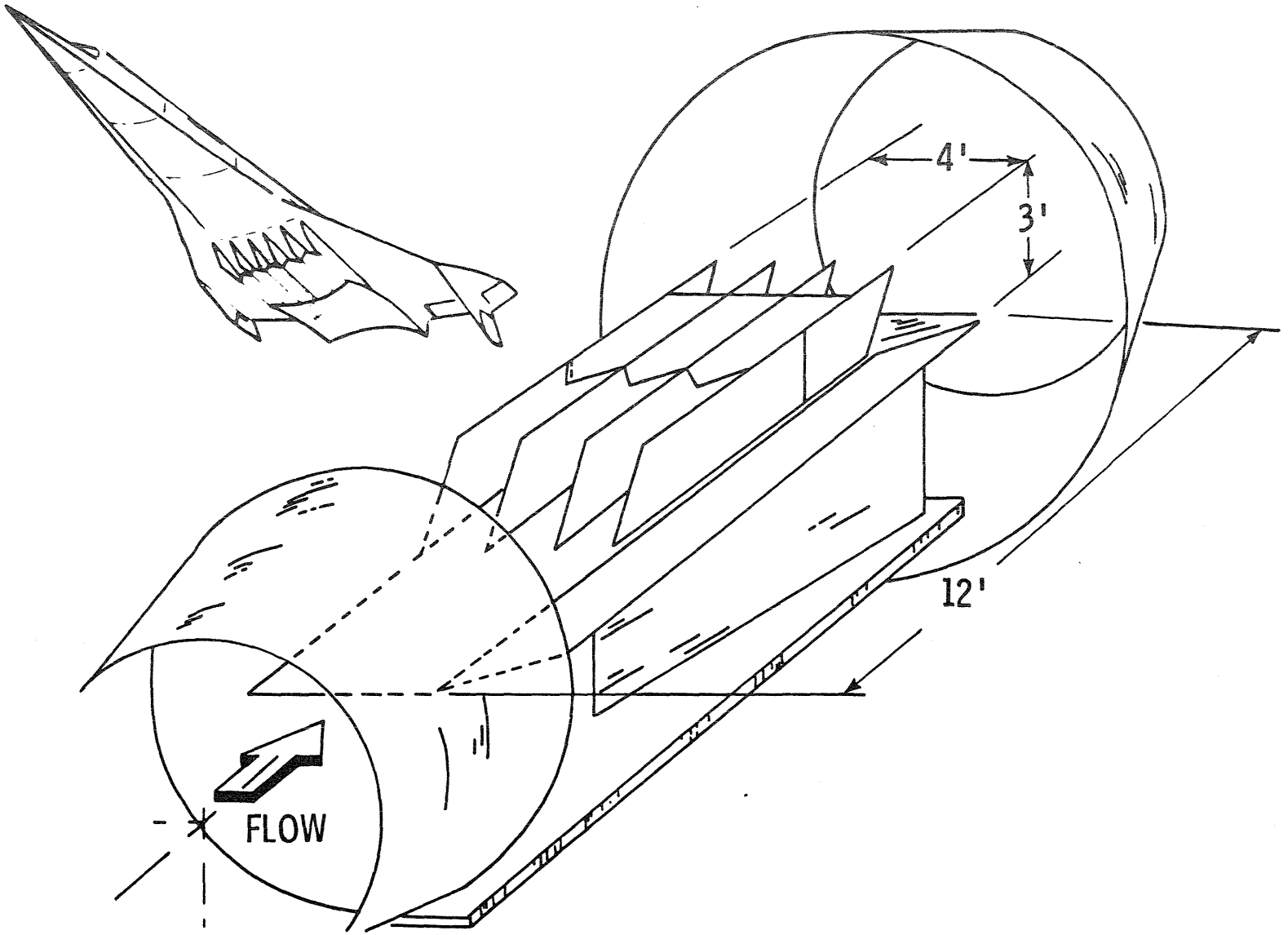

Figure 110

RAM/SCRAMJET STRUCTURES TECHNOLOGY DEVELOPMENT-SUMMARY

Figure 111 shows a summary of Ram/Scramjet structures technology development. Although not shown in this paper, basic transient unstart phenomena have been characterized (Ref. 149) and these pressure loads are particularly critical for the slender fuel injection struts. Again, although not shown in this paper, extensive finite element methodology for thermal-structural analysis of convectively cooled structures has been developed (Refs. 150).

Conceptually feasible cooled structure designs and fabrication techniques have been developed and a side fuel injection strut is being fabricated. Although not shown in this paper, work on thermal-structural concepts for hydrocarbon fueled ramjet engines have recently been defined (Ref. 151.)

In the future, the strut needs to be subjected to a variety of tests to verify thermal and structural design analyses, structural performance and life. Concepts for intersecting (and for some configurations moving) surfaces such as cowls and combustor walls need to be designed, fabricated and tested. Finally, prior to flight tests, large scale model tests should be conducted in the NASA Langley 8-Ft. HTT.

RAM/SCRAMJET STRUCTURES TECHNOLOGY DEVELOPMENT

WHERE WE HAVE BEEN

- CHARACTERIZED BASIC TRANSIENT UNSTART PHENOMENA
- DEVELOPED FINITE ELEMENT METHODOLOGY FOR THERMAL ANALYSIS OF CONVECTIVELY COOLED STRUCTURES
- DEFINED CONCEPTUALLY FEASIBLE THERMAL/STRUCTURAL CONFIGURATION FOR LARC SCRAMJET
- DEVELOPED FABRICATION TECHNIQUES

WHERE WE ARE

- FABRICATING A FUEL INJECTION STRUT
- DEVELOPING THERMAL/STRUCTURAL CONCEPTS FOR ALTERNATE FUELS/ENGINES

WHERE WE NEED TO GO

- EXPERIMENTALLY EVALUATE THE STRUT THERMAL/STRUCTURAL PERFORMANCE
- DEVELOP THERMAL/STRUCTURAL CONCEPTS FOR INTERSECTING AND MOVING SURFACES
- LARGE SCALE TESTS IN 8-FT. HTT

Figure 111

CONCLUDING REMARKS

Remarkable progress has been made in all technologies pertinent to the development of an aerospace plane type vehicle. The developments in CFD and the flight data obtained from the Space Shuttle provide a quantum leap from the state-of-the-art of the mid 1960's for high speed aerodynamics and aerothermodynamics. Significant progress has been made in the disciplines required for control configured vehicles, again including valuable data from the orbiter flights. In propulsion, the development of the space shuttle main engines (SSME), although plagued with problems, is a remarkable success considering the skepticism of some experts of meeting the original very challenging design goals for these reusable rocket engines. Also, progress is being made in solving the problems of the SSME. There is renewed interest in hypersonic airbreathing propulsion due in part to the significant progress made in that area over the last 5 years.

In the area of structures and materials, the progress is not as great but is still remarkable considering the resources provided this area during the last 20 years. The ceramic and carbon-carbon thermal protection systems (TPS) on the orbiter are working and could be used for an aerospace plane application provided they can be made to meet the durability requirements. Metallic TPS have received considerable attention and are beginning to reach maturity, at least from a R&T point of view. Significant progress has been made in hot structures for both wing and cryogenic tank/fuselage applications. This technology is at the point that fabrication of large test specimens is the next logical step for certain materials such as Rene' 41. For other materials such as GR/PI, metal matrix composites and ODS iron base materials, work on materials and small test specimens is required. Some progress including fabrication and testing of hardware has been made for actively cooled and heat-pipe cooled airframe and regeneratively cooled engine structure, and major problems for future research have been documented. However, much remains to be done for this class of structure. A good start has been made in developing an aerothermal loads data base and thermal-structural analysis methods, and these disciplines should mature in a timely manner if continued at their current level of effort.

In spite of such remarkable progress, much remains to be accomplished. Research in high payoff areas of materials and structures has barely scratched the surface. One of the most exciting areas is the development and use of advanced carbon-carbon materials for acreage TPS and structural applications. Little has been done for cryogenic tanks (other than the work on the Rene' 41 concept) especially composite tanks, and cryogenic insulations. Also, the area of high temperature test facilities, techniques and instrumentation has been largely neglected by the aerospace community, and work in these areas must begin if high temperature structures are to be considered for aerospace plane applications.

Finally, in those areas where progress has been made, work must continue, probably at an increased level in most areas, to bring the technology to maturity in a timely manner.

CONCLUDING REMARKS

- REMARKABLE PROGRESS MADE IN ALL PERTINENT TECHNOLOGIES FOR AEROSPACE PLANE TYPE VEHICLES SINCE 1970
  - AERODYNAMICS AND AEROTHERMODYNAMICS
    - * CFD DEVELOPMENTS
    - * SHUTTLE FLIGHT DATA
  - CONTROL-CONFIGURED VEHICLES
  - MATERIALS AND STRUCTURES
    - * METALLIC TPS
    - * HOT INTEGRAL TANK/FUSELAGE AND WING STRUCTURE
    - * ACTIVELY COOLED AIRFRAME CONCEPTS
    - * REGENERATIVELY COOLED AIRBREATHING ENGINE CONCEPTS
    - * AEROTHERMAL LOADS DATA BASE
    - * THERMAL-STRUCTURAL ANALYSIS METHODS
    - * HEAT-PIPE-COOLED STRUCTURE
  - PROPULSION
    - * SSME
    - * AIRBREATHING SCRAMJETS

- MUCH REMAINS TO BE ACCOMPLISHED
  - BARELY SCRATCHED THE SURFACE OF MANY HIGH PAYOFF MATERIALS AND STRUCTURES AREAS
    - * CARBON-CARBON FOR TPS AND STRUCTURE
    - * CRYO TANKS/INSULATION
    - * COMPOSITE TANKS/STRUCTURE
    - * HIGH TEMPERATURE TEST FACILITIES/TECHNIQUES
  - NEED TO BRING OTHER EFFORTS TO MATURITY IN A TIMELY MANNER

Figure 112

REFERENCES

1. Heldenfels, Richard R.: Historical Perspectives on Thermostructural Research at the NACA Langley Aeronautical Laboratory from 1948 to 1958. NASA TM 83266, Feb. 1982.

2. Heldenfels, R. R.: Structural Prospects for Hypersonic Air Vehicles. Presented at the 5th Congress of the International Council of the Aeronautical Sciences (ICAS), London, England, Sept. 1966.

3. Hearth, Donald P., and Preyss, Albert E.: Hypersonic Technology - Approach to an Expanded Program. Astronautics & Aeronautics, Vol. 14, No. 12, Dec. 1976, pp 20-37.

4. Kelly, H. Neale; Wieting, Allan R.; Shore, Charles P.; and Nowak, Robert J.: Recent Advances in Convectively Cooled Engine and Airframe Structures for Hypersonic Flight. Presented at the 11th Congress of the International Council of the Aeronautical Sciences (ICAS), Lisbon, Portugal, Sept, 1978.

5. Jones, Robert A.; and Huber, Paul W.: Airframe Integrated Propulsion System for Hypersonic Vehicles. Presented at the 11th Congress of the International Council of the Aeronautical Sciences (ICAS), Lisbon, Portugal, Sept. 1978.

6. Kelly, H. N.; Rummler, D. R.; and Jackson, L. R.: Research in Structures and Materials for Future Space Transportation Systems - An Overview. J. Spacecraft and Rockets, Vol. 20, No. 1, Jan.-Feb., 1983, pp. 89-96.

7. Kelly, H. Neale; and Gardner, James E.; Compilers: Advances in TPS and Structures for Space Transportation Systems. NASA CP 2315, Dec. 1983.

8. Howe, John T.: Introductory Aerothermodynamics of Advanced Space Transportation Systems. J. Spacecraft and Rockets, Vol. 22, No. 1, Jan.-Feb. 1985.

9. Martin, J. A.: Hydrocarbon Rocket Engines for Earth-to-Orbit Vehicles. J. Spacecraft and Rockets, Vol. 20, No. 3, May-June 1983, pp. 249-256.

10. Adelman, Howard M.; Compiler: Computational Aspects of Heat Transfer in Structures. NASA CP 2216, 1982.

11. Beasly, Gary P.; Compiler: NASA Aircraft Controls Research 1983. NASA CP-2296, Oct. 1983.

12. Sobieski, Jaroslaw; Compiler: Recent Experiences in Multidisciplinary Analysis and Optimization. NASA CP 2327, April 1984.

13. Arrington, James P.; and Jones, Jim J.; Compilers: Shuttle Performance: Lessons Learned. NASA CP 2283, March 1983.

14. Chaffee, Norman; Compiler: Space Shuttle Technical Conference. NASA CP-2342, 1985.

15. Eldred, Charles H.: Shuttle for the 21st Century. Aerospace America, Vol. 22, No. 4, April 1984. pp. 82-86.

16. Martin, James A.: Orbit on Demand; In This Century if Pushed. Aerospace America, Vol. 23, No. 2, Feb. 1985. pp. 46-48.

17. Haefeli, Rudolf C.; Littler, Ernest G.; Hurley, John B.; and Winter, Martin G.: Technology Requirements for Advanced Earth-Orbital Transportation Systems. Summary Report. NASA CR-2867, June 1977.

18. Hepler, A. K.; and Bangsund, E. L.: Technology Requirements for Advanced Earth Orbital Transportation Systems. Volume 2: Summary Report. NASA CR 2878, July 1978.

19. Freeman, D. C., Jr.; and Powell, R. W.: Impact of Far-Aft Center-of-Gravity Location for a Single-Stage-To-Orbit Vehicle. J. Spacecraft and Rockets, Vol. 17, No. 5, July - Aug. 1980, pp. 311-315.

20. Robinson, James C.; Bailey, James P.; and Wurster, Kathryn E.: Overview of a Preliminary Aerothermostructural Design of a Tip Fin Controller for Space Shuttle Orbiter. Advances in TPS and Structures for Space Transportation Systems. NASA CP-2315, Dec, 1983, pp. 573-593.

21. Powell, Richard W.; and Freeman, Delma C., Jr.: Evaluation of the Aerodynamics and Control of the Space Shuttle Orbiter with Tip-Fin Controllers. AIAA Paper No. 84-0488, 1984.

22. Weilmuenster, K. James; and Hamilton, H. Harris, II: A Method for Computation of Inviscid Three-Dimensional Flow Over Blunt Bodies Having Large Embedded Subsonic Regions. AIAA Paper No. 81-1203, June 1981.

23. Hamilton, H. Harris, II: Calculation of Laminar Heating Rates on Three-Dimensional Configurations Using the Axisymmetric Analogue. NASA TP 1698, Sept. 1980.

24. Davis, R. T.: Numerical Solutions of the Hypersonic Viscous Shock-Layer Equations. AIAA Journal, Vol. 8, May 1970, pp. 843-851.

25. Szema, K. Y.; and Lewis, C. H.: Three-Dimensional Viscous Shock-Layer Flows Over Lifting Bodies at High Angles of Attack. AIAA Paper No. 81-1146, June 1981.

26. Thareja, R. R., Szema, K. Y., and Lewis, C. H.: Space-Shuttle Windward Surface Laminar, Transitional and/or Turbulent Viscous Shock-Layer Flows in Equilibrium Air at High Angles of Attack (VSL81). Aerospace and Ocean Engineering Department, VPISU, January 1982.

27. Thompson, Richard A.: Three-Dimensional Viscous-Shock-Layer Applications for the Space Shuttle Orbiter. AIAA Paper 85-0246, January 1985.

28. Gnoffo, P. A.: Hypersonic Flow Over Biconics Using Variable Effective and Parabolized-Navier-Stokes Equations. AIAA Paper 83-1666, July, 1983.

29. Gnoffo, P. A.: Complete Flowfields Over Low and Wide Angle AOTV Conceptual Configurations. AIAA Paper 84-1695, June, 1984.

30. Siemers, P. M., III; and Larson, T. J.: Space Shuttle Orbiter and Aerodynamic Testing. J. Spacecraft and Rockets, Vol. 16, No. 4, July-Aug. 1979. pp 223-231.

31. Zoby, E. V., "Comparisons of Free-Flight Experimental and Predicted Heating Rates for the Space Shuttle," AIAA Paper 82-0002, Jan. 1982.

32. Zoby, E. V.: Analysis of STS-2 Experimental Heating Rates and Transition Data. AIAA Paper No. 82-0822, June 1982.

33. Zoby, E. V., "Approximate Heating Analysis for the Windward-Symmetry Plane of Shuttle-Like Bodies at Large Angle of Attack," AIAA Paper 81-1042, June 1981; see also, Thermophysics of Atmospheric Entry, Progress in Astronautics and Aeronautics, Vol. 82, 1982, pp. 229-247.24.

34. Hamilton, H. H., "Approximate Method of Predicting Heating on the Windward Side of Space Shuttle Orbiter and Comparisons with Flight Data," AIAA Paper 82-0823, June 1982.

35. Bertin, J. J., Hayden, T. E., and Goodrich, W. D., "Comparison of Correlations of Shuttle Boundary-Layer Transition Due to Distributed Roughness," AIAA Paper 81-8417, Jan. 1981.

36. Berkowitz, A. M., Kyriss, C. L., and Martellucci, A., "Boundary Layer Transition Flight Test Observations," AIAA Paper 77-125, Jan. 1977.

37. Beckwith, I. E., "Development of a High Reynolds Number Quiet Tunnel for Transition Research," AIAA Journal, Vol. 13, March 1975, pp. 300-306.

38. Harvey, W. D., "Some Anomalies Between Wind Tunnel and Flight Transition Results," AIAA Paper 81-1225, June 1981.

39. Moss, J. H.: Private Communication

40. Miller, C. G.; Gnoffo, P. A.; and Wilder, S. E.: Experimental Heating Distributions for Biconics at Incidence in Mach 10 Air and Comparison to Prediction. AIAA Paper 84-2119, August 1984.

41. Romere, P. O.; and Young, J. C.: Space Shuttle Entry Longitudinal Aerodynamic Comparisons of Flight 2 with Pre-Flight Predictions. J. Spacecraft and Rockets, Vol. 20, No. 6, Nov.-Dec., 1983, pp. 518-523.

42. Throckmorton, D. A.; and Zoby, E. L.: Orbiter Entry Leeside Heat-Transfer Data Analysis. J. Spacecraft and Rockets, Vol. 20, No. 6, Nov.-Dec., 1983, pp. 524-530.

43. Kim, M. D.; Swaminathan, S.; and Lewis, C. H.: Three Dimensional Nonequilibrium Viscous Shock-Layer Flow Over the Space Shuttle Orbiter. J. Spacecraft and Rockets, Vol. 21, No. 1, Jan.-Feb., 1984, pp. 29-35.

44. Rakish, J. L.; Vehkatarathy, E.; Tannehill, J. C.; and Prabhu, D.: Numerical Solution of Space Shuttle Orbiter Flow Field. J. Spacecraft and Rockets, Vol. 21, No. 1, Jan.-Feb., 1984, pp. 9-15.

45. Kerr, J. R.; and Haskins, J. F.: Time-Temperature-Stress Capabilities of Composite Materials for Advanced Supersonic Technology Application. Phase 1. NASA CR 159267, April 1980.

46. Davis, J. W.; and Cramer, B. A.: Predictions and Verification of Creep Behavior in Metallic Materials and Components for the Space Shuttle Thermal Protection System. NASA CR-2685, July 1976.

47. Klarstrom, D. L.: Thermomechanical Processing of Haynes Alloy No. 188 Sheet to Improve Creep Strength. NASA CR-3013, Aug. 1978.

48. Schaffer, John W.; Tong, Henry; Clark, Kimble J.; Suchsland, Kurt E.; and Neuner, Gary J.: Analytical and Experimental Evaluation of Flowing Air Test Conditions for Selected Metallics in a Shuttle TPS Application. NASA CR-2531, Aug. 1975.

49. Shore, Charles P.; and Weinstein, Irving: Aerothermal Performance of a Radiatively and Actively Cooled Panel at Mach 6.6. NASA TP-1595, 1979.

50. Shore, Charles P.; Nowak, Robert J.; and Kelly, H. Neale: Flightweight Radiantly and Actively Cooled Panel-Thermal and Structural Performance. NASA TP-2074, 1982.

51. Standard Methods of Tension Testing of Metallic Materials. E8-81, 1982 Annual Book of ASTM Standard, Part 10.

52. Clark, Ronald K.; Webb, Granville L.; and Dries, Gregory A.: Mechanical/Radiative Performance of Rene' 41 in TPS Applications. Advances in TPS and Structures for Space Transportation Systems, NASA CP 2315, 1983. pp 361-380.

53. Norris, Brian: High Temperature (1366 K (2000°F)) Sheet Material Selection for Use for Thermal Protection Systems. ROHR Industries Inc., Report No. RHR 80-017, April 1980.

54. Cunnington, G. R.; Fretter, E. F.; and Clark, R. K.: Radiative Properties of a Nickel Based Superalloy-Inconel 617 - After Simulated Earth Reentry. AIAA Paper No. 82-0898, St. Louis, MO, June 1982.

55. Cunnington, G. R.; Funai, A. I.; and McNab, T. K.: Radiative Properties of Advanced Spacecraft Heat Shield Materials. NASA CR-3740, November 1983.

56. Lowell, Carl E.; Deadmore, Daniel L.; and Whittenberger, J. Daniel: Long-Term High-Velocity Oxidation and Hot Corrosion Testing of Several NiCrAl and FeCrAl Base Oxide Dispersion Strengthened Alloys. Oxidation of Metals, Vol. 17, No. 3/4, 1982.

57. Clark, Ronald K.; Cunnington, George R.; and Robinson, John C.: Vapor Deposited Emittance/Catalysis Coatings for Superalloys in Heat Shield Applications. AIAA 23rd Aerospace Sciences Meeting, Reno, Nevada, January 14-17, 1985. AIAA Paper No. 85-0403.

58. Advanced Materials Technology. NASA CP-2251, Nov. 1982.

59. Sawyer, J. W.; and Moses, P. L.: Effects of Holes and Impact Damage on Tensil Strength of Two-Dimensional Carbon-Carbon Composites. NASA TM 86337, Jan. 1983.

60. Weinstein, Irving; Avery, Don E.; and Chapman, Andrew J.: Aerodynamic Heating to the Gaps and Surfaces of Simulated Reusable-Surface-Insulation Tile Arrays in Turbulent Flow at Mach 6.6. NASA TM X-3225, 1975.

61. Avery, Don E.: Aerodynamic Heating in Gaps of Thermal Protection System Tile Arrays in Laminar and Turbulent Boundary Layers. NASA TP-1187, 1978.

62. Avery, Don C.: Experimental Aerodynamic Heating to Simulated Space Shuttle Tiles in Laminar and Turbulent Boundary Layers. NASA TP-2307, 1985.

63. Avery, Don E.; Ballard, Gary K.; and Wilson, Maywood L.: Electroless-Plating Technique for Fabricating Thin-Wall Convective Heat-Transfer Models. NASA TP-2349, 1984.

64. Martin, F. W.; and Albertson, C. W.: Aerothermal Environment of a Blunted Three-Dimensional Nonaxisymmetric Body at Mach 6.8. AIAA 19th Thermophysics Conference, Snowmass, Colorado, June 25-28, 1984. AIAA Paper No. 84-1698.

65. Hunt, L. Roane: Aerothermal Environment in Chordwise Gaps Between Solid Elevons at Mach 6.8. NASA TP-1783, 1980.

66. Curry, Donald M.; and Tillian, Donald J.: Space Shuttle Orbiter Thermal Protection System Flight Experiences Advances in TPS and Structures for Space Transportation Systems. NASA CP 2315, 1983, pp 130-165.

67. Deveikis, William D.: Effects of Flow Separation and Cove Leakage on Pressure and Heat-Transfer Distribution Along a Wing-Cove-Elevon Configuration at Mach 6.9. NASA TP-2127, 1983.

68. Wieting, A. R.; Walsh, J. L.; and Bey, K. S.: Aerothermal Environment in Control Surface Gaps in Hypersonic Flow--An Overview. AIAA 18th Thermophysics Conference, Montreal, Canada, June 1-3, 1983. AIAA Paper No. 83-1483.

69. Bey, K. S.; Thornton, E. A.; Dechaumphai, P.; and Ramakruhnan, R.: A New Finite Element Approach for Prediction of Aerothermal Loads-Progress in Inviscid Flow Computations. To be presented at the 7th AIAA Computational Fluid Dynamics Conference, Cincinnati, OH, July 15-17, 1985. AIAA Paper No. 85-1533-CP.

70. Hunt, L. Roane: Aerothermal Analysis of a Wing-Elevon Cove with Variable Leakage. NASA TP-1703, 1980.

71. Fields, Roger A.: Dryden Flight Research Center Hot Structures Research. Recent Advances in Structures for Hypersonic Flight. NASA CP 2065, 1978. pp. 707-756.

72. Thornton, E. A., Dechaumphai, P., and Weiting, A. R.: Integrated Finite-Element Thermal-Structural Analysis with Radiation Heat Transfer. Paper presented at the AIAA/ASME/AHS 23rd Structures, Structural Dynamics, and Materials Conference, New Orleans, LA, May 10-12, 1982. AIAA Paper 82-0703-CP.

73. Thornton, Earl A.; and Dechaumphai, Pramote: Adaptive Refinement for Effective Finite Element Thermal-Structural Analysis. International Conference on Accuracy Estimates and Adaptive Refinements in Finite Element Computation (ARFEC). Lisbon, Portugal, June 19-22, 1984.

74. Thornton, E. A. and Dechaumpahai, P.: A Hierarchical Finite-Element Approach for integrated Thermal-Structural Analysis. AIAA/ASME/ASCE/AHS 25th Structures, Structural Dynamics, and Materials Conference, Palm Springs, CA, May 14-16, 1984. AIAA paper 84-0939.

75. SPAR Thermal Analysis Processors Reference Manual, System Level 16. NASA CR-159162, Oct. 1978. Also, SPAR Structural Analysis System Reference Manual, Vol. 1, NASA CR 158970-1, Dec. 1978.

76. Adelman, Howard M.: Preliminary Design Procedure for Insulated Structures Subjected to Transient Heating. NASA TP 1534, Dec. 1979.

77. Ransone, Philip O.; Rummler, Donald R.: "Microstructural Characterization of the HRSI Thermal Protection System for Space Shuttle, NASA TM-81821, May 1980.

78. Prabhakaran, R.; Cooper, Paul A.: Photoelastic Tests on Models of Thermal Protection System for Space Shuttle Orbiter, NASA TM-81866, August 1980.

79. Cooper, Paul A.; Holloway, Paul F.: The Shuttle Tile Story, Astronautics and Aeronautics, Vol. 19, No. 1, January 1981, pp. 24-34,36.

80. Korb, L. J.; Clancy, H. M.: "Shuttle Orbiter Thermal Protection System: A Material and Stuctural Overview." 26th National Symposium Society for the Advancement of Materials and Process Engineering, April 28-30, 1981.

81. Sawyer, James Wayne: Mechanical Properties of the Shuttle Orbiter Thermal Protection System Strain Isolator Pad. Presented at the AIAA/ASME/ASCE/AHS 23rd Structures, Structural Dynamics, and Materials Conference, New Orleans, Louisiana, May 10-12, 1982. AIAA Paper No. 82-0789.

82. Cooper, Paul A., et.al.: Assessment of the Shuttle Orbiter Thermal Protection System Undensified Tiles Under Mission Dynamic Loads. Presented at the AIAA 23rd Structures, Structural Dynamics and Materials Conference, May 10-12, 1982. AIAA Paper No. 82-0790.

83. Morita, W. H.; and Graves, S. R.: The Shuttle Orbiter Structural Weight Reduction Potential with Advanced Composites Application. 40th Annual Conference, Society of Allied Weight Engineers, Dayton, Ohio, May 1981.

84. Morita, W. H.: Graphite/Polyimide State-of-the-Art Panel Discussion. NASA Conference Publication 2079 Graphite Polyimidate Composites, Mar. 1979, pp. 441-444.

85. Morita, W. H.: Direct-Bond RSI Tile on GR/PI Structure. Advances in TPS and Structure for Space Transportation Systems. NASA CP 2315, Dec. 1983. pp. 207-222.

86. Sawyer, James W.: Aerothermal and Structural Performance of a Cobalt-Base Superalloy Thermal Protection System at Mach 6.6. NASA TN D-8415, May 1977.

87. Avery, Don E.: Performance of a Haynes 188 Metallic Standoff Thermal Protection System at Mach 7. NASA TP-1802, April 1981.

88. Jackson, L. Robert; and Dixon, Sidney C.: A Design Assessment of Multiwall, Metallic Stand-off, and RSI Reusable Thermal Protection Systems Including Space Shuttle Application. NASA TM-81780, April 1980.

89. Blair, W.; Meany, J. E.; and Rosenthal, H. A.: Re-Design and Fabrication of Titanium Multiwall Thermal Protection System (TPS) Test Panels. NASA CR-172247, 1984.

90. Blair, W.; Meany, J. W.; and Rosenthal, H. A.: Fabrication of Prepackaged Superalloy Honeycomb Thermal Protection System (TPS) Panels. NASA CR-3755, 1984.

91. Shideler, J. L.; Webb, G. L.; and Pittman, C. M.: Verification Tests of Durable TPS Concepts. AIAA 19th Thermophysics Conference, Snowmass, CO, June 24-28, 1984. AIAA Paper No. 84-1767.

92. Anon: Lightning Test Waveforms and Techniques for Aerospace Vehicles and Hardware. Report of SAE Committee AE for L, June 20, 1978.

93. Deveikis, W. D.; Bruce, W. E., Jr.; and Karns, J. R.: Techniques for Aerothermal Tests of Large, Flightweight Thermal Protection Panels in a Mach 7 Wind Tunnel. AIAA 8th Aerodynamic Testing Conference, Bethesda, MD, July 8-10, 1974. AIAA Paper No. 74-617.

94. Shideler, J. L.; Kelly, H. N.; Avery, D. E.; Blosser, M. L.; and Adelman, H. M.: Multiwall TPS - An Emerging Concept. J. Spacecraft & Rockets, Vol. 19, No. 4, July-August 1982, pp. 358-365.

95. Avery, D. E.; Shideler, J. L.; and Stuckey, R. N.: Thermal and Aerothermal Performance of a Titanium Multiwall Thermal Protection System. NASA TP-1961, 1981.

96. Pittman, C. M.; Brown, R. D.; and Shideler, J. L.: Evaluation of a Non-Catalytic Coating for Metallic TPS. NASA TM 85745, January 1984.

97. Blair, W.: Fabrication of Titanium Mulitwall Thermal Protection System (TPS) Curved Panel. NASA CR 165754, August 1981.

98. Shideler, John L.; and Blair, Winford: Design and Fabrication of Curved Superalloy Honeycomb Prepackaged TPS. Advances in TPS and Structures for Space Transportation Systems. NASA CP-2315, Dec. 1983, pp. 329-344.

99. Kelly, H. N.; and Webb, G. L.: Assessment of Alternate Thermal Protection Systems for the Space Shuttle Orbiter, Entry Vehicle Heating and Thermal Protection Systems: Space Shuttle, Solar Starprobe, Jupiter Galileo Probe, edited by P. E. Bauer and H. E. Collicott., Vol. 85 of Progress in Astronautics and Aeronautics, 1983.

100. While, D. M.: Development of Advanced Carbon-Carbon (ACC) Composites, Volume II - ACC Cover Panel Feasibility Study. NASA CR 165842-2, July 1982.

101. Matza, E. C.; and While, D. M.: Advanced Carbon-Carbon (ACC) Test Article Design and Fabrication. Vought Report No. 221RPTA018, May 1983.

102. Camarda, C. J.: Analysis and Radiant Heating Tests of a Heat-Pipe-Cooled Leading Edge. NASA TN D-8468, Aug. 1977.

103. Camarda, Charles J.: Aerothermal Tests of a Heat-Pipe-Cooled Leading Edge at Mach 7. NASA TP-1320, Nov. 1978.

104. Peeples, M. E.; Reeder, J. C.; and Sontage, K. E.: Thermostructural Applications of Heat Pipes. NASA CR-150906, June, 1979.

105. Henry, John R., and Anderson, Griffin Y., "Design Considerations for the Airframe-Integrated Scramjet." Presented at the 1st International Symposium on Air Breathing Engines, Marseille, France, June 19-23, 1972 (Also NASA TMX-2895, Dec. 1973).

106. Becker, J. V., "New Approaches to Hypersonic Aircraft," Presented at the Seventh Congress of the International Council of the Aeronautical Sciences (ICAS), Rome, Italy, Sept. 1970.

107. McConarty, W. A., and Anthony, F. M., "Design and Evaluation of Active Cooling Systems for Mach 6 Cruise Vehicle Wings," NASA CR-1916, 1971.

108. Helenbrook, R. G., McConarty, W. A., and Anthony, F. M., "Evaluation of Active Cooling Systems for a Mach 6 Hypersonic Transport Airframe," NASA CR-1917, 1971.

109. Helenbrook, R. G., and Anthony, F. M., "Design of a Convective Cooling System for a Mach 6 Hypersonic Transport Airframe," NASA CR-1918, 1971.

110. Anthony, F. M., Dukes, W. H., and Helenbrook, R. G., "Internal Convective Cooling Systems for Hypersonic Aircraft," NASA CR-2480, 1974.

111. Brewer, G. D., and Morris, R. E., "Study of Active Cooling for Supersonic Transports," NASA CR-132573, 1975.

112. Pirrello, C. J., Baker, A. H., and Stone, J. E., "A Fuselage/Tank Structure Study for Actively Cooled Hypersonic Cruise Vehicles-Summary," NASA CR-2651, 1976.

113. Nowak, Robert J., and Kelly, H. Neale, "Actively Cooled Airframe Structures for High-Speed Flight," Presented at the AIAA/ASME/SAE 17th Structures, Structural Dynamics and Materials Conference, King of Prussia, PA, May 5-7, 1976. (Also J. Aircraft, Vol. 14, No. 3, March 1977, pp. 244-250).

114. Koch, L. C., and Pagel, L. L., "High Heat Flux Actively Cooled Honeycomb Sandwich Structural Panel for a Hypersonic Aircraft," NASA CR-2959, 1978.

115. Pirrello, C. J., and Herring, R. L., "Study of a Fail-Safe Abort System for an Actively Cooled Hypersonic Aircraft-Volume I, Technical Summary," NASA CR-2652, Jan. 1976.

116. Herring, R. L., and Stone, J. E., "Thermal Design for Areas of Interference Heating on Actively Cooled Hypersonic Aircraft," NASA CR 2828, December, 1976.

117. Ellis, D. A., Pagel, L. L., and Schaeffer, D. M., "Design and Fabrication of a Radiative Actively Cooled Honeycomb Sandwich Structural Panel for a Hypersonic Aircraft," NASA CR 2957, March, 1978.

118. Deriugin, V.; Brogren, E. W.; Jaeck, C. L.; Brown, A. L.; and Clingan, B. E.: Thermal-Structural Combined Loads Design Criteria Study, NASA CR-2101, Oct. 1972

119. Hepler, A. K. and Swegle, A. R.: Design and Fabrication of Brazed Rene 41 Honeycomb Sandwich Structural Panels for Advanced Space Transportation Systems. NASA CR-165801, Dec. 1981.

120. Shideler, J. L.; Swegle, A. R.; and Fields, R. A.: Honeycomb Sandwich Structure for Future Space Transportation Systems With Integral Cryogenic Tankage. J. Spacecraft and Rockets. Vol. 21, No. 3, May-June 1984. pp 246-252.

121. Hepler, A. K. and Swegle, A. R.: Cryogenic Performance of Slotted Brazed Rene 41 Honeycomb Panels. NASA CR-3525, 1982.

122. Taylor, A. H.; and Jackson, L. R.: Structural Concepts for a Mach 5 Cruise Airplane LH_2 Fuselage Tank. J. Aircraft, Vol. 18, No. 8, August 1981, pp. 655-662.

123. Taylor, A. H.; MacConochie, J. O.; Jackson, L. R.; and Martin, J. A.: The FSTS Study-Structures and Subsystems. Astronautics and Aeronautics, Vol. 21, No. 6, June 1983, pp. 50-56, 62.

124. Taylor, A. H.; Cerro, J. A.; and Jackson, L. R.: An Analytical Study of Reusable Flight-Weight Cryogenic Propellant Tank Designs. AIAA/ASME/ASCE/AHS 25th Structures, Structural Dynamics and Materials Conference, Palm Springs, CA, May 14-16, 1984. AIAA Paper No. 84-0865.

125. Sharpe, Ellsworth L.; and Helenbrook, Robert G.: Cryogenic Foam Insulation for LH_2 Fueled Subsonic Transports. AIAA/ASME 2nd Thermophysics and Heat Transfer Conference, Palo Alto, CA, May 24-26, 1978, AIAA Paper No. 78-875.

126. Davis, John G., Jr.: Composites for Advanced Space Transportations Systems (CASTS). Graphite/Polyimide Composites. NASA CP-2079, March 1979, pp. 5-18.

127. Graves, S. R.; and Morita, W. H.: Analysis, Design and Test of a Graphite/Polyimide Shuttle Orbiter Body Flap Segment. 14th National Technical Conference, Society for the Advancement of Materials and Process Engineering, Oct. 1982.

128. Morita, H. W.; and Graves, S. R.: Graphite/LARC-160 Technology Demonstration Segment Test Results. NASA CR 172123, June 1983.

129. Plank, P. P.; Sakata, J. F.; Davis, G. W.; and Richie, C. C.: Hypersonic Cruise Vehicle Wing Structure Evaluation. NASA CR-1568, May 1970.

130. Plank, P. P. and Penning, F. A.: Hypersonic Wing Test Structure Design, Analysis and Fabrication. NASA CR-127490, August 1973.

131. Shideler, John L.; Fields, Roger A.; and Reardon, Lawrence F.: Tests of Beaded and Tubular Structural Panels. Recent Advances in Structures for Hypersonic Flight. NASA CP-2065, Sept. 1978. pp 539-576.

132. Shideler, J. L.; and Bohon, H. L.: Evaluation of Bead-Stiffened Metal Panels. J. Spacecraft and Rockets, Vol. 13, No. 3, March 1976, pp. 144-149.

133. Davis, Randall C.; and Mills, Charles T.: Structural Efficiency Studies of Advanced Compression Panels with Curved Elements. Advances in TPS and Structures for Space Transportation Systems. NASA CP-2315, Dec. 1983, pp. 559-571.

134. Royster, Dick M.; Davis, Randall; Shinn, Joseph M., Jr.; and Bales, Thomas T.: Fabrication and Evaluation of Superplastically Formed/Weld-Brazed Corrugated Compression Panels with Beaded Webs. Proposed NASA TP, 1985.

135. Blosser, Max L.; and McWithey, Robert R.: Theoretical Basis for Design of Thermal-Stress-Free Fasteners. NASA TP-2226, Dec. 1983.

136. Sawyer, James Wayne: Experimental Evaluation of Thermal Stress-Free-Fastening Techniques for Two-Dimensional Carbon-Carbon Structures. Advances in TPS and Structures for Space Transportation Systems. NASA CP-2315, Dec. 1983. pp 613-626.

137. Blosser, Max L.: Design Studies of Carbon-Carbon Shuttle Body Flap. Advances in TPS and Structures for Space Transportation Systems. NASA CP-2315, Dec. 1983, pp.595-612.

138. Wieting, Allan R.: Aerodynamic and Thermal Analysis of Results of Tests of a Hydrogen-Cooled Scramjet Engine (HRE-SAM) at Mach 6.3, NASA TMX-2767, May 1973.

139. Staff of Langley Research Center and AiResearch Manufacturing Co., The Garrett Corp.: Hypersonic Research Engine Project Technological Status 1971, NASA TM X-2572, 1972.

140. Jones, Robert A.; and Huber, Paul W.: Airframe Integrated Propulsion System for Hypersonic Vehicles. To be presented at the Eleventh Congress of the International Council of the Aeronautical Sciences (ICAS), Lisbon, Protugal, Sept. 10-16, 1978.

141. Wieting, Allan R.; and Guy, Robert W.: Preliminary Thermal-Structural Design and Analysis of an Airframe-Integrated Hydrogen-Cooled Scramjet, AIAA Paper 75-137, Pasadena, CA, 1975 (Also J. of Aircraft, Vol. 13, March 1976, pp. 192-197).

142. Killackey, J. J.; Katinsky, E. A.; Tepper, S.; and Vuigner, A. A.: Thermal-Structural Design Study of an Airframe-Integrated Scramjet, Interim Summary Report, NASA CR-145368, 1978.

143. Buchmann, O. A.: Thermal Structural Design Study of an Airframe - Integrated Scramjet, NASA CR 3141, Oct. 1979.

144. Basiulis; A.; and Camarda, C. J.: Design, Fabrication, and Test of Liquid Metal Heat-Pipe Sandwich Panels, AIAA Paper 82-0903, St. Louis, Mo., June 1982.

145. Tanzer, H. J.: Fabrication and Development of Several Heat-Pipe Honeycomb Sandwich Panel Concepts, NASA CR 165962, June 1982.

146. Camarda, C. J.; and Basiulis, A.: Radiant Heating Tests of Several Liquid-Metal Heat-Pipe Sandwich Panels, AIA Paper 83-0319, Reno, NV, Jan. 1983.

147. Tanzer, H. J.: High-Capacity Honeycomb Panel Heat Pipes for Space Radiators, AIAA Paper 83-1430, Montreal, Canada, June 1983.

148. Kelly, H. N.; and Wieting, A. R.: Modification of NASA Langley 8-Foot High Temperature Tunnel to Provide a Unique National Research Facility for Hypersonic Air-Breathing Propulsion Systems, AIAA Paper No. 84-0602. NASA TM-85783, May 1984.

149. Wieting, Allan R.: Exploratory Study of Transient Unstart Phenomena in a 3-Dimensional Fixed-Geometry Scramjet Engine. NASA TN D-8156, March 1976.

150. Thornton, Earl A.; and Wieting, Allan R.: Finite-Element Methodology for Transient Conduction/Forced Convection Thermal Analysis. Heat Transfer, Thermal Control and Heat Pipes, edited by Walter B. Olstad, Vol. 70, of Progress in Astronautics and Aeronautics.

151. McWithey, R. R.; and Jackson, L. R.: Structures for Mach 5 Reusable, Hydrocarbon Fueled Ramjet Engines. 1985 JANNAF Propulsion Meeting, San Diego, CA, April 9-12, 1985.

1. Report No.	2. Government Accession No.	3. Recipient's Catalog No
NASA TM-86429		

4. Title and Subtitle	5. Report Date
NASA R&T FOR AEROSPACE PLANE VEHICLES - PROGRESS AND PLANS	May 1985
	6. Performing Organization Code 506-53-33-07
7. Author(s) S. C. DIXON	8. Performing Organization Report No.
	10. Work Unit No.
9. Performing Organization Name and Address LANGLEY RESEARCH CENTER HAMPTON, VIRGINIA 23665	11. Contract or Grant No.
	13. Type of Report and Period Covered Technical Memorandum
12. Sponsoring Agency Name and Address NATIONAL AERONAUTICS AND SPACE ADMINISTRATION WASHINGTON, DC 20546	14. Sponsoring Agency Code

15. Supplementary Notes

This paper presented at the SAE Aerospace Vehicle Requirements Conference, Aerospace Plane Technology Session, Arlington, Va., May 20-23, 1985.

16. Abstract

The U. S. had extensive programs in the late 1950's and 1960's aimed at various vehicles/missions requiring flight at hypersonic speeds. Due to accelerating costs and formidable technical challenges most of these programs were terminated, and except for the NASA Space Shuttle program R&T for aerospace plane-type vehicles has been a low priority effort. In spite of this limited activity, mainly conducted by NASA, significant progress has been made in key technologies such as materials, structures, aerothermodynamics, hypersonic aerodynamics, and hypersonic airbreathing propulsion. In addition, advances have been made in more generic, but essential, areas such as active controls, flight computer hardware and software, and interdisciplinary analytical design methodology. These technology advancements coupled with the development of and experiences with the Space Shuttle now make feasible aerospace plane-type vehicles that meet the more demanding requirements of various DOD missions and/or an all-weather Shuttle II with reduced launch costs.

This paper will review studies of technology needs and high payoff technologies, and the technology advancements in propulsion, control-configured-vehicles, aerodynamics, aerothermodynamics, aerothermal loads, and materials and structures. The emphasis will be placed on the highest payoff technologies of materials and structures including thermal-structural analysis and high temperature test techniques. Since a whole session is devoted to the high priority technology of propulsion, this area will be only briefly discussed. Plans, in the sense of what remains to be done rather than firm program commitments, will also be briefly discussed.

17. Key Words (Suggested by Author(s))	18. Distribution Statement
Space Transportation Systems Transatmospheric Vehicles Aerothermodynamics Structures and Materials	Unclassified - Unlimited Subject Category - 16

19. Security Classif. (of this report)	20. Security Classif. (of this page)	21. No. of Pages	22. Price
Unclassified	Unclassified	241	A11

For sale by the National Technical Information Service, Springfield, Virginia 22161

End of Document